ONLINE ABSTRACT BOOK

SCR'24

JUNE 20–22, 2024 | PALEXPO, GENEVA

THE SWISS MEETING FOR MEDICAL IMAGING SPECIALISTS

DIAGNOSIS AND TREATMENT

www.myscr.ch

Dear Colleagues!

The Swiss Society of Radiology (SGR-SSR), the Swiss Society of Nuclear Medicine (SGNM-SSMN) and the Swiss Association of Radiographers (SVMTRA-ASTRM) are delighted about the high quality of abstracts which were submitted for presentation at the annual Swiss Congress of Radiology.

The continuous excellent work of all authors is highly appreciated as it makes the congress a very prestigious scientific meeting.

This "Online Abstract Book of the Swiss Congress of Radiology" is the 13th issue which is solely published online. It represents a cost efficient, durable platform independent documentation of scientific abstracts. Integration of the abstract data on the Congress' web page as well as permanent accessibility all over the world is the purpose.

The "Online Abstract Book of the Swiss Congress of Radiology" will be accessible on the Congress' web page at www.myscr.ch. It includes all the abstracts of the scientific talks and posters presented at the annual Swiss Congress of Radiology 2024 in Geneva.
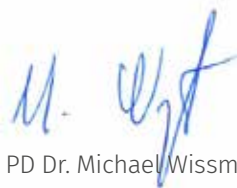
Proper citation of scientific abstracts is however important, especially in case of online-only web publications. The Swiss Society of Radiology thereof recommends the use of the following structure to cite abstracts from the "Online Abstract Book of the Swiss Congress of Radiology":

> "Author1 A, Author2 B, …, Author last X. Title of the abstract (abstr.).
> Swiss Congress of Radiology 2024, Geneva. Online Abstract Book, www.myscr.ch"
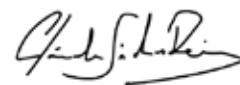
We look forward to welcoming you to the Swiss Congress of Radiology 2025 in St. Gallen.

Prof. Dr. Dr. J. Heverhagen
President of the Swiss Congress
of Radiology SGR-SSR

PD Dr. Michael Wissmeyer
President of the Swiss Congress
of Radiology SGNM-SSMN

Prof. Dr. Cláudia Sá dos Reis
President of the Swiss Congress
of Radiology SVMTR-ASTRM

SWISS CONGRESS OF RADIOLOGY 2024, GENEVA

Congress Presidents

PRESIDENT OF THE SWISS CONGRESS OF RADIOLOGY SGR-SSR
Prof. Dr. Dr. J. Heverhagen, Bern

PRESIDENT OF THE SWISS CONGRESS OF RADIOLOGY SGNM-SSMN
PD Dr. M. Wissmeyer, Zurich

PRESIDENT OF THE SWISS CONGRESS OF RADIOLOGY SVMTR-ASTRM
Prof. Dr. C. Sá dos Reis, Lausanne

Scientific Committee

REGULAR MEMBERS
Prof. Dr. H. Alkadhi, Zurich (Scientific Committee President)
Prof. Dr. Dr. J. Heverhagen, Bern (SGR-SSR Congress President)
PD Dr. A. Hötker, Zurich
Prof. Dr. K.O. Loevblad, Geneva
Prof. Dr. S. Schmidt Kobbe, Lausanne
Prof. Dr. H. Thoeny, Fribourg
Prof. Dr. H. von Tengg-Kobligk, Bern

EX-OFFICIO MEMBERS
Prof. Dr. F. Del Grande, Lugano (SSSR)
Prof. Dr. J. Geiger, Zurich (SGPR-SSRP)
Ms. I. Gremion, Epalinges (SVMTR-ASTRM)
Ms. A. Landsmann, Aarau (SGR-SSR Resident representative)
Prof. Dr. A. Platon, Geneva (SSER)
Prof. Dr. P-A. Poletti, Geneva (local representative)
Prof. Dr. S. D. Qanadli, Lausanne (SSVIR)
Prof. Dr. A. Rominger, Bern (SGNM-SSMN)
Dr. M. Sans Merce, Geneva (SSRMP)
PD Dr. M. Wissmeyer, Zurich (SGNM-SSMN Congress President)
Prof. Dr. C. Zech, Basel (SSVIR)

Swiss Radiological Conventions AG

Weggismattstrasse 11
6004 Luzern
E-Mail   info@radiologiekongress.ch

Congress Services

Education Congress Research GmbH
Wolfgang Duchek/Agathe Milliken
Am Gestade 1
1010 Vienna/Austria
E-Mail   info@radiologiekongress.ch
Phone   +43 1 5350599
www.myscr.ch

SGR-SSR Standing Abstract Reviewer Committee

Prof. Dr. H. Alkadhi, Zurich
Dr. M. Behe, Villigen
Dr. Robyn Benz, Fribourg
PD Dr. C. Brendle, Tübingen
Dr. J. Brendle, Scherzingen
Prof. Dr. Andreas Christe, Bern
Dr. S. Dellas, Basel
PD Dr. T. Dietrich, St. Gallen
Dr. T. Dobrocky, Bern
Prof. Dr. O. Donati, Zurich
Prof. Dr. C. Dromain, Lausanne
Dr. V. Dunet, Lausanne
PD Dr. M. Eberhard, Zurich
PD Dr. A. Falkowski, Winterthur
Prof. Dr. phil. M. Fani, Basel
Prof. Dr. J. Geiger, Zurich
Prof. Dr. R. Guggenberger, Zurich
Dr. Céline Habre, Geneva
Dr. D. Harder, Basel
PD Dr. N. Kawel-Böhm, Chur
PD Dr. K. Kinkel, La Chaux-de-Fonds
Dr. Patrick Knüsel, Chur
Prof. Dr. R. Kubik-Huch, Baden
PD Dr. F.P. Kuhn, Zurich
Prof. Dr. S. Leschka, St. Gallen
PD Dr. M. Marcon, Zurich
Dr. R. Menz, Basel
Prof. Dr. J-Y. Meuwly, Lausanne
Dr. phil. L. Mu, Zurich
Prof. Dr. T. Niemann, Baden
Prof. Dr. T. Pfammatter, Zurich
Prof. Dr. A. Platon, Geneva
Prof. Dr. P-A. Poletti, Geneva
PD Dr. Thomas Ruder, Bern
Prof. Dr. Salah D. Qanadli, Rennaz
Prof. Dr. S. Schindera, Aarau
Dr. F. Schmaranzer, Bern
Prof. Dr. S. Schmidt Kobbe, Lausanne
PD Dr. G. Sommer, Lucerne
Dr. M. Straub, Lausanne
Prof. Dr. H. Thöny, Fribourg
Assoc. Prof. F. Verdun, Lausanne
Dr. S. Wälti, St. Gallen
Dr. L. Wissmann, Münsterlingen
Prof. Dr. R. Wyttenbach, Bellinzona
Prof. Dr. C. Zech, Basel

SGNM-SSMN Standing Abstract Reviewer Committee

Dr. C. Antonescu, Fribourg
Prof. Dr. phil. M. Fani, Basel
Prof. Dr. Dr. F. Forrer, St. Gallen
Prof. Dr. V. Garibotto, Geneva
Prof. Dr. P. Kaufmann, Zurich
Dr. S. Kneifel, Chur
Prof. Dr. E. Nitzsche, Aarau
Prof. Dr. Dr. J. Prior, Lausanne
Prof. Dr. A. Rominger, Bern
Prof. Dr. N. Schaefer, Lausanne
Prof. Dr. R. Schibli, Zurich
Prof. Dr. K. Strobel, Lucerne
Prof. Dr. D. Wild, Basel
PD Dr. M. Wissmeyer, Zurich

SVMTR-ASTRM Standing Abstract Reviewer Committee

C. Bruguier, Lausanne
S. Dziergwa, Basel
E. Fleury, Geneva
I. Gremion, Lausanne
S. Ghotra, Lausanne
S. Scherz, Bern

A1

Quantitative T2 Mapping for the Assessment of Acute Pancreatitis: A Prospective Study

F. Porões[1,2], N. Vietti Violi[2], E.Uldry[2], T. Hilbert[2,3,4], F. Schütz[5], S. Schmidt Kobbe[2,5]; [1] HFR – Hôpital fribourgeois, Fribourg, Switzerland, [2] CHUV – Centre Hospitalier Universitaire Vaudois, Lausanne, Switzerland, [3] Siemens Healthineers, Lausanne, Switzerland, [4] EPFL – Ecole Polytechnique Fédérale de Lausanne, Lausanne, Switzerland, [5] UNIL – University of Lausanne, Lausanne, Switzerland

Purpose: To evaluate MR-derived pancreatic T2 mapping values in acute pancreatitis (AP) and correlate them with parameters of disease severity.

Methods and Materials: In a single-center study, we prospectively included 76 consecutive patients with suspected AP between December 2020 and November 2022. The severity of AP was assessed clinically, biologically, and by contrast-enhanced CT (CECT) performed 48-72 h after symptom onset. MRI was also performed at ≤24h after CT. Two radiologists blinded to any clinical information independently evaluated the T2 values by placing three regions of interest inside the pancreatic head, body, and tail on the T2 mapping MR sequence. Results were compared with corresponding CECT images as the gold standard; patient parameters, such as age, gender, and body mass index (BMI); and clinical severity parameters. Inter-reader reliability was determined by calculating the interclass coefficient (ICCs).

Results: Seventy-six patients (mean age, 52 years ± 18, 39 women) were evaluated. T2 values significantly correlated with the length of hospital stay ($P = 0.01$), CT severity index ($P < 0.001$), ICU admission ($P < 0.05$) and presence of organ failure ($P < 0.05$). T2 values did not depend on age, gender, BMI, anatomical location (pancreatic head, body, and tail) or main pancreatic duct dilatation. Interreader agreement was good (ICC = 0.85, 95% confidence interval: 0.77–0.90).

Conclusion: T2 mapping is useful for assessing the severity of AP enabling differentiation between mild and moderate/severe cases, and, thus, predicting patients at risk of complications and long hospital stays. T2 values are reproducible and do not depend on patients' parameters, such as age, gender and BMI. Compared with current gold standards, T2 mapping offers a non-invasive, non-ionizing, contrast-free alternative.

A2

What is the optimal strategy for initial staging of esophageal cancer? Comparison of standard staging procedures (EUS, CT and FDG- PET/CT) and MRI.

V. Levy[1], M. Jreige[1], L. Haefliger[1], C. Du Pasquier[2], D. Wagner[1], S. Mantziari[1], M. Schäfer[1], Vietti-Violi[1], C. Dromain[1]; [1] CHUV – Centre Hospitalier Universitaire Vaudois, Lausanne, Switzerland, [2] HRC – Hôpital Riviera-Chablais, Rennaz, Switzerland

Purpose: To compare diagnostic performance of MRI, CT, endoscopic ultrasound (EUS), PET/CT and different combinations for the initial staging of esophageal cancer.

Methods and Materials: In this prospective study we included 60 patients between 10.2017 and 12.2021 (M/F 50/10, mean age 66 ± 9 y.o.) with newly diagnosed esophageal cancer. Written informed consent was obtained for all participants. Each patient underwent a 3T MRI in addition to the standard staging procedures (EUS, CT and FDG-PET/CT) for initial tumor staging. Two independent readers (except for EUS) were asked to determine T-stage using MRI, CT and EUS, N-stage using MRI, CT, PET/CT and EUS, M-stage using MRI, CT and PET/CT. Consensus was obtained in case of discordance using a third reader. The reference standard was the histopathology of the surgical specimen or TNM-staging established during the tumor board meeting considering all available imaging and endoscopic data. Diagnostic performance of each procedure was analyzed separately and in combination.

Results: For T-stage, sensitivities and specificities for classifying non-advanced tumors (T1-T2) versus advanced tumors (T3-T4) were 98% and 80% for MRI, 92.5% and 100% for CT and 91.3% and 90% for EUS, respectively. For N-stage, sensitivities and specificities for classifying N0 versus N+ were 87.5% and 69.2% for MRI, 94.4% and 55.6% for CT, 67.4% and 100% for PET/CT and 89.1% and 66.7% for EUS, respectively. For M-stage, sensitivities and specificities for classifying M0 versus M+ were 100% and 100% for MRI and PET/CT and 40% and 100% for CT. Combination of MRI+PET/CT to differentiate T1-2N0M0 from T3-4N1-3M0-1 showed sensibility of 88% and specificity of 96% versus 58% and 98% for EUS+CT+PET/CT.

Conclusion: MRI is highly accurate for the initial TNM staging enabling the optimal discrimination between early-stage and advanced-stage esophageal cancer. The combination of PET-CT and MRI is the most effective combination for guiding therapeutic choices.

A3

Evaluating Treatment Response in GEJ Adenocarcinoma: The Role of Pre- and Post-Therapeutic Iodine mapping

M. Graf, J. Gawlitza, M. Makowski, F. Meurer, T. Huber, S. Ziegelmayer; MRI TUM – School of Medicine & Klinikum rechts der Isar, Department of Diagnostic and Interventional Radiology, Munich, Germany

Purpose: The purpose of this retrospective study is to assess the potential of pre- and post-therapeutic Spectral-CT iodine density (IoD) in predicting histopathological response to neoadjuvant chemotherapy in patients diagnosed with adenocarcinoma of the GEJ.

Methods and Materials: In this retrospective cohort study, a total of 62 patients with GEJ carcinoma were studied. Patients received a multiphasic CT scan at diagnosis and preoperatively. Iodine-density maps were generated based on spectral CT data. All tumors were histopathologically analyzed and the tumor regression grade (TRG) according to Becker et al. was determined. Two experienced radiologists blindedly placed 5 defined ROIs in the tumor region of highest density, and the maximum value was used for further analysis. After assessing inter-rater reliability, the correlation of IoD values with treatment response and with histopathologic TRG was evaluated.

Results: The ΔIoD (IoD at Diagnosis - IoD after neoadjuvant treatment) and the IoD after neoadjuvant treatment correlated significantly with the TRG. For the detection of responders and non-responders, the ROC curve for ΔIoD yielded the highest AUC of 0.96 and achieved a sensitivity and specificity of 92.1% and 92.3%, respectively. IoD after neoadjuvant treatment achieved an AUC of 0.86 and a sensitivity and specificity of 76.3% and 84.6% (cut-off 1.67mg/ml). IoD at diagnosis showed no significant differences for TGR and did not provide information to distinguish responders from non-responders (AUC: 0.42). Using the cut-off value for IoD after neoadjuvant treatment, a reliable classification of responders and non-responders was achieved for both readers in a test set of 11 patients. Intraclass correlation coefficient (ICC) revealed excellent inter-rater reliability (ICC > 0.9).

Conclusion: Changes in IoD after neoadjuvant treatment of GEJ-cancer may be a potential surrogate for therapy response.

A4

Optimization of Mesenteric Vascular CT Mapping

J. Heeb[1], H. Najberg[1], E. Kalogiannis[2], H. Thoeny[2,1], L. Widmer[2,1]; [1] University of Fribourg, Fribourg, Switzerland, [2] HFR – Hôpital fribourgeois, Fribourg, Switzerland

Purpose: Colorectal cancer complete mesocolic excision is technically challenging due to colonic vascularization variations. This study aims to optimize preoperative vascular mapping in CTA of mesenteric vessels by comparing contrast opacification between three cohorts, employing different injection protocols: fixed trigger delay, patient-individualized split-bolus injection, and slow contrast media injection.).

Methods and Materials: This IRB-approved, single-center prospective study included 162 consecutive patients (mean age: 55.3±20.5 years; 41% were female) recruited from January 2022 to October 2023. The participants were divided into three cohorts with distinct CT vascular mapping protocols, with 54 participants per cohort determined through a priori statistical power analyses. Objective image quality was assessed by one reader, and subjective image quality by two readers. A one-way ANOVA tested differences in attenuation values and image quality.

Results: The split-bolus protocol had the most extreme attenuation values. The fixed trigger delay and the slow injection protocols had more similar mean values, with the slow injection protocol showing higher attenuation values for arteries and veins. Artery attenuation values in the fixed trigger delay were significantly lower than in the other protocols (F[2,159] = 49.5, p <0.001) and vein attenuation values in the split-bolus were significantly lower than in the other protocols (F[2,159] = 37.8, p <0.001). All protocols had similar image noise (all Cohen's d <0.3; F[2,159] = 1, p = 0.37). Contrat-to-noise ratio was smaller in the fixed trigger delay than in the other protocols (F[2,159] = 19.8, p <0.001). Subjective image quality was significantly higher in the split-bolus protocol than in the other protocols (F[2,159] = 19.6, p <0.001).

Conclusion: Slow contrast media injection improves opacification in CTA of mesenteric vessels, providing enhanced vascular mapping for surgery.

A5

Computed tomography for evaluation of abdominal wall hernias – what is the value of the Valsalva maneuver?

S. Stocker[1], A. Tognella[2], A.T. Hoppe[1], M. Lange[1], K. Lehmann[1], M. Bueter[1], H. Alkadhi[1], D. Stocker[1]; [1] USZ – Universitätsspital Zürich, Zurich, Switzerland, [2] University of Zurich, Zurich, Switzerland

Purpose: To evaluate the influence of the Valsalva maneuver on detection rate, visibility, and size of abdominal wall hernias in computed tomography (CT).

Methods and Materials: This single-center retrospective study included consecutive abdominal CTs performed with Valsalva maneuver between January 2018 and January 2022. Inclusion criteria was availability of additional, non-Valsalva CT within 6 months. A combined reference standard including clinical and surgical findings was used. Two independent, blinded radiologists measured the hernia sac size and rated hernia visibility on CTs with and without Valsalva maneuver. Differences were tested with a Wilcoxon signed rank test and McNemar's test.

Results: The final population included 95 patients (16 women; mean age 46 ± 11.6 years) with 205 hernias. The median time between Valsalva CT and non-Valsalva CT was 57 days (interquartile range: 33, 91). Median hernia sac size on Valsalva CT was 31 mm compared with 24 mm on non-Valsalva CT (p<0.001). In 72.7% and 82.4% of cases the hernias were better visible on CT with Valsalva as compared to that without. 13.6% and 16.5% of hernias were only visible on the Valsalva CT. Hernia visibility on non-Valsalva CT varied according to subtype, with only 0% and 3% of umbilical hernias not being visible compared with 42.5% and 42.5% of femoral hernias.

Conclusion: Abdominal CT with Valsalva maneuver has a higher hernia detection rate than CT without Valsalva maneuver. The hernias are better visible, larger, and some hernias are only visible on the Valsalva CT. Therefore, this method should be preferred for the evaluation of abdominal wall hernias.

A6

Prostate MRI at 7T using high performance gradients and a 8Tx/16Rx RF array: a clinical feasibility study

T. de Perrot[1], *D. Wenz*[2], *I. Aslam*[1], *G.F. Piredda*[3,4,5], *R. Martuzzi*[5], *L. Mattera*[5], *J-F. Deux*[1], *P-A. Poletti*[1], *C. Glessgen*[1], *A. Delattre-Klauser*[3,4,5], *T. Hilbert*[3,6,7], *M. Valerio*[1], *S. Schmitter*[8], *A. Bitz*[9], *S. Wildenberg*[9], *A. Nagel*[10], *Nico Egger*[10], *S. Nagelstrasser*[10], *T. Lanz*[11], *R. Kimmlingen*[3], *J. Herrler*[3], *L. Xin*[2], *J-P. Vallee*[1]; [1] HUG – Hôpitaux universitaires de Genève, Geneva, Switzerland, [2] EPFL – Ecole Polytechnique Fédérale de Lausanne, Lausanne, Switzerland, [3] Siemens Healthineers, Erlangen, Germany, [4] CIBM – Center for Biomedical Imaging, Geneva, Switzerland, [5] FCBG – Fondation Campus Biotech, Geneva, Switzerland, [6] CHUV – Centre Hospitalier Universitaire Vaudois, Lausanne, Switzerland, [7] Ecole Polytechnique Fédérale de Lausanne, Lausanne, Switzerland, [8] PTB – Physikalisch-Technische Bundesanstalt, Berlin, Germany, [9] FH Aachen, Aachen, Germany, [10] Universitätsklinikum Erlangen, Erlangen, Germany, [11] RAPID Biomedical Biomedizinische Geräte GmbH, Rimpar, Germany*

Purpose: To investigate the clinical feasibility of prostate MRI at 7T using the latest generation of whole-body 7T MRI scanners incorporating enhanced gradient performance, advanced deep learning based image reconstruction and an 8Tx/16Rx torso array.

Methods and Materials: Healthy volunteers (n=5, 47 ±10 y.o.) were scanned on a Siemens 7T (MAGNETOM Terra.X, Siemens Healthcare, Erlangen, Germany) using gradient strength of 130 T/m and 8Tx/16Rx RF coil array (Rapid Biomedical, Germany), as well as on a 3T MR scanner (MAGNETOM Prisma, Siemens Healthcare, Erlangen, Germany) with an 18-channels Rx only coil. The following sequences were acquired at 7T: T2-TSE (TE=87 ms, TR=12100 ms, 0.2x0.2x3 mm3 after interpolation, axial 10:40 min, sagittal/coronal 6:12 min), segmented resolve SE-DWI (TE 54 ms, TR 5740 ms, 5 shots, 1x1x3 mm3, 9:58 min) and water excitation T1 3D-GRE (TE 4.5 ms, TR 12 ms, 1x1x2 mm3, 4:05 min). Corresponding MR sequences were applied at 3T using the standard clinical parameters and resolution with time matching acquisition for the axial T2-TSE. To compare 7T and 3T images, qualitative blinded image analysis was performed by 4 radiologists. SNR was calculated in transition and peripheral zone.

Results: High image quality was successfully obtained in all the volunteers at 7T. Homogeneous signal intensity was obtained for the T1- and T2-weighted images in the prostate. No significant distortions were observed in DWI. Using a 5 points Likert scale (1=worst, 5=best), signal homogeneity of T2 images was graded 5 at 3T and 4.2 at 7T and image quality 3.3 at 3T and 4.2 at 7T. The SNR for 3T clinical T2, 3T matched T2 and 7T T2 images in the transition zone, respectively the peripheral zone was 3.9 ±1.2, 5.3 ±1.8 and 8.4 ±4.1, respectively 7.2 ± 2.5, 7.3 ±0.9 and 9.3 ±2.3.

Conclusion: This work demonstrates for the first time that high-quality prostate MRI using a dedicated RF array and a 7T Terra.X system is feasible. Such achievement supports further clinical studies.

A7

Risk Factors for Prostate Cancer in Men with False-Negative mpMRI: A Retrospective Single Center Cohort Study of Image Quality Scores and Clinical Parameters

A. Pausch, S. Ghafoor, J. Kluckert, N.J. Rupp, D. Eberli, A. Hötker; USZ – Universitätsspital Zürich, Zurich, Switzerland

Purpose: To identify predictors of prostate cancer (PCa) and clinically significant prostate cancer (csPCa) in men with prior false-negative multiparametric MRI (mpMRI), focusing on image quality scoring systems and clinical parameters.

Methods and Materials: In this IRB-approved retrospective single-center study, patients with a negative mpMRI (PI-RADS score ≤ 2) and subsequent prostate biopsies were included. Histopathological results served as reference standard. Welch's t-Test was conducted to identify significant differences in image quality scores (PI-QUAL and PSHS) between patients with and without PCa/csPCA. In addition, clinical parameters (age, BMI, PSA density) and image quality scores (PI-QUAL and PSHS) were examined as potential predictors of PCa/csPCa detection after a false-negative mpMRI in uni- and multivariate analyses.

Results: Among 96 patients with negative mpMRI results, 44.8% had PCa and 16.7% had csPCa upon biopsy with histopathological confirmation. PI-QUAL scores were significantly lower in patients with PCa (p = 0.03) and csPCa (p = 0.005). PSHS scores were lower in patients with csPCa, but the difference was not statistically significant (p = 0.1). Higher age (p = 0.035) and a lower PI-QUAL score (p < 0.004) were predictors of subsequent csPCa detection upon biopsy, however, a lower PI-QUAL score was the only independent predictor of missed csPCa in false-negative mpMRIs.

Conclusion: Lower image quality scores were associated with missed PCa/csPCa in patients with false-negative mpMRIs, with PI-QUAL being an independent predictor of failed csPCa detection. This highlights the importance of image quality for prostate MRI and advocats the inclusion of its measurement into the standardized report.

A8

To iMAR or not to iMAR: impact of energy and metal artifact reduction algorithms on image quality with a multi-insert phantom

D. Cester, H. Alkadhi; USZ – Universitätsspital Zürich, Zurich, Switzerland

Purpose: CT images in presence of metal implants suffer from artifacts caused by the presence of high density material. The effect is less pronounced for high-energy X-rays; moreover, dedicated Metal Artifacts Reduction (MAR) algorithms have been developed to further improve the image quality.

This work aims at quantifying the effects of using high energy Virtual Monoenergetic Images (VMI) as well as an iterative MAR algorithm (iMAR) in a pelvic phantom with inserted high-density metal rods.

Methods and Materials: A multi-energy elliptical CT pelvic phantom was imaged in five different configurations to simulate metal implants during a abdominopelvic examination. Images were acquired with a clinical photon counting detector CT (PCD-CT) scanner at fixed kV and radiation dose settings, to match a corresponding clinical protocol. Image reconstructions were performed with the same kernel at different VMI energies, with and without iMAR.

For each reconstruction the image quality was assessed in terms of HU values, noise properties and Root Mean Square Difference (RMSD) referred to the image at low VMI without inserts.

Results: Increasing the VMI energy from 70 keV to at least 110 keV significantly improves the noise properties and the RMSD, and also reduces the standard deviation of the HU values of selected ROIs. VMI increases up to 140 keV provide only smaller improvements.

The use of iMAR results in noise levels and RMSD lower than the high-energy VMI images, already at 70 keV VMI. The improvement is stronger in presence of one steel insert, or with bilateral inserts of any metal.

The combination of energy increase and iMAR does not lead to significant improvements compared to iMAR alone.

Conclusion: Even at low-energy VMI the use of iMAR can lead to similar image quality compared to high-energy VMI alone, and performs significantly better when the phantom included bilateral inserts or one single steel insert.

A9

Depth dependence of ultrasound Shear Wave Speed and Shear Wave Dispersion in liver measurements of healthy volunteers

C. Paverd[1], S. Kupfer[1], L. Ruby[1,2], A. Martin[1], F. Huber[1], M. Rominger[1], T. Frauenfelder[1]; [1] USZ – Universitätsspital Zürich, Zurich, Switzerland, [2] Memorial Sloan Kettering, New York, United States

Purpose: Ultrasound elastography is important in early detection of liver disease, including fibrosis (assessed with Shear Wave Speed, SWS) and inflammation (assessed with Shear Wave Dispersion, SWD). Confounders of SWS have previously been studied, however confounders of SWD have only been studied in phantoms, where depth was significant. Here we investigate the depth dependency of SWS and SWD in healthy volunteers.

Methods and Materials: A board-certified radiologist measured 20 healthy volunteers using a Canon Aplio i800. Nine elastography videos were obtained at three different acquisition box depths, starting 1 cm below the liver capsule. A trained operator was blinded to on-screen SWS and SWD values, and selected 40 circular Regions Of Interest (ROIs, diameter 1 cm) per person. ROIs were placed where the propagation map showed stable, parallel lines. Absolute ROI depth (measured at ROI centres) was restricted to 2.5 - 6.5 cm. Linear mixed effects models with varying slopes and intercepts were fitted for analysis.

Results: Both SWS and SWD showed significant depth dependency, with SWS increasing at 0.06 m/s per cm (p<0.001) and SWD increasing at 0.98 m/s/kHz per cm (p<0.001). Changes in clinical staging with depth were more pronounced for SWD; comparing measurements in superficial ROIs (2.5 - 3.5 cm) to deep ROIs (5.5 - 6.5 cm) showed that fibrosis staging (SWS) increased from F0/F1 to F2 in one volunteer, whereas inflammation staging (SWD) increased from A0/A1 to A2 in thirteen volunteers.

Conclusion: Depth is a significant confounder of SWS and SWD, which is important when assessing obese patients, evaluating deep liver areas, or when performing time-based follow-up examinations. The limitation of this study is that a healthy European cohort was assessed, but results may vary in other demographic cohorts or patient populations.

A10

Whole-Body Composition Features by Computed Tomography in Ovarian Cancer: Pilot Data on Survival Correlations

G. Raia[1], M. Del Grande[2], I. Colombo[2], M. Nerone[2], L. Manganaro[3], M.L. Gasparri[4,5], A. Papadia[4,5], F. Del Grande[1,6], S. Rizzo[1,7]; [1] EOC – Ente Ospedaliero Cantonale, IIMSI – Imaging Institute of Southern Switzerland, Lugano, Switzerland, [2] EOC – Ente Ospedaliero Cantonale, Service of Medical Oncology, Oncology Institute of Southern Switzerland, Bellinzona, Switzerland, [3] University of Rome Sapienza, Department of Radiological, Oncological and Pathological Sciences, Rome, Italy, [4] EOC – Ente Ospedaliero Cantonale, Department of Gynecology and Obstetrics, Lugano, Switzerland, [5] USI – Università della Svizzera Italiana, Facoltà di Scienze Biomediche, Lugano, Switzerland, [6] Università della Svizzera Italiana, Facoltà di Scienze Biomediche, Lugano, Switzerland, [7] USI – Università della Svizzera Italiana, Faculty of Biomedical Sciences, Lugano, Switzerland

Purpose: The primary objective of this study was to assess the associations of computed tomography (CT)-based whole-body composition values with overall survival (OS) and progression free survival (PFS) in epithelial ovarian cancer (EOC) patients. The secondary objective was the association of body composition with chemotherapy-related toxicity.

Methods and Materials: Thirty-four patients (median age 64.9 years; interquartile range 55.4–75.4) with EOC and thorax and abdomen CT scans were included. Clinical data recorded: age; weight; height; stage; chemotherapy-related toxicity; and date of last contact, progression and death. Automatic extraction of body composition values was performed by dedicated software. Sarcopenia was defined according to predefined cutoffs. Statistical analysis included univariate tests to investigate associations of sarcopenia and body composition with chemotoxicity. Association of body composition parameters and OS/PFS was evaluated by log-rank test and Cox proportional hazard model. Multivariate models were adjusted for FIGO stage and/or age at diagnosis.

Results: We found significant associations of skeletal muscle volume with OS (p = 0.04) and PFS (p = 0.04); intramuscular fat volume with PFS (p = 0.03); and visceral adipose tissue, epicardial and paracardial fat with PFS (p = 0.04, 0.01 and 0.02, respectively). We found no significant associations between body composition parameters and chemotherapy-related toxicity.

Conclusion: In this exploratory study, we found significant associations of whole-body composition parameters with OS and PFS. These results open a window to the possibility to perform body composition profiling without approximate estimations.

A12

Imaging assessment of pancreatic transplant complications

J. Grossmann, A. Platon, P-A. Poletti; HUG – Hôpitaux universitaires de Genève, Geneva, Switzerland

Purpose: To assess the imaging pattern of postoperative complications in patients undergoing pancreatic transplantation in our institution.

Methods and Materials: Retrospective analysis of radiological reports of patients with pancreas transplantation undergoing emergency imaging over a period of 12 years. Patients 'demographics, surgical technique, and presence and type of complications at imaging were retrieved and analyzed.

Results: Fifty-nine patients (41 men, mean age: 44.7 years) received a pancreatic transplant during the study period: 44 (75%) simultaneous pancreatic-kidney transplantation, 8 (13%) pancreas after kidney transplantation, and 7 (12%) pancreas-alone transplantation.

Imaging analysis revealed that 30 of the 59 patients (60%) developed one or several postoperative complications: 25/30 (83%) were found at CT scan, 5/30 (17%) at sonography only. Vascular complications were found in 13 (43%) patients. Ten (33%) of them exhibited venous graft thrombosis: 3 (10%) with associated arterial thrombosis, 1 (3%) with associated arterial thrombosis and active bleeding and 1(3%) with graft pancreatitis. An arterial thrombosis was found in 3 (10%) patients (one of them with associated peripancreatic collections). Intraabdominal collections were described in 7 (23%) patients (including one with associated small bowel occlusion), and acute pancreatitis in 4 (13%) cases (including one with peripancreatic collections). Active bleeding was diagnosed in 3 (10%) cases. Isolated intraabdominal hematoma was found in 2 (6%) patients and small bowel occlusion in 1(3%) patient.

Conclusion: Vascular thromboses were the most frequent complications after pancreas transplantation, followed by intraabdominal collections. Association of different complications was common occurrence; this finding must raise awareness among radiologists when interpreting follow-up imaging of pancreatic transplantation.

A16

Diagnosis of periprosthetic hip joint infection using new-generation 0.55T MRI

J. Plesniar[1,2], H-C. Breit[1], M. Clauss[1], R. Donners[1]; [1] USB – Universitätsspital Basel, Basel, Switzerland, [2] University of Basel, Basel, Switzerland

Purpose: To assess the accuracy of 0.55T MRI in diagnosing periprosthetic joint infection (PJI) in patients with symptomatic total hip arthroplasty (THA).

Methods and Materials: 0.55T MRI of hip and pelvis (May 2021-July 2023) in patients with THA PJI (infection group) and non-infected THA (control group) were analysed retrospectively by two musculoskeletal radiologists with respect to literature-derived system of PJI signs in MRI. Presence of changes within bone (oedema, periosteal reaction, osteolysis), joint (effusion, capsule oedema and thickening) and soft tissue (fluid collection, oedema, bursitis, inguinal adenopathy, abductor tear) was reported. The diagnostic accuracy of MRI discriminators between PJI and non-PJI was evaluated for statistically significant features (p<0.05) and inter-rater variance was determined.

Results: 61 THA patients (34 female; median age 68) were identified, of which nine had THA PJI (4 female; median age 69, age range 56-82) and fifty-two were the control group (30; 67.5, 41-93). Periosteal reaction, capsule oedema, joint effusion, subcutaneous oedema, intramuscular oedema, fluid collection, and inguinal adenopathy were all significant discriminators for PJI diagnosis (p≤0.037). The best performance was found for capsule oedema (sensitivity 89%, specificity 92%, accuracy 92%), intramuscular oedema (89%, 83%, 84%), joint effusion (89%, 73%, 75%) and subcutaneous oedema (78%, 79%, 79%). Combining these parameters in parallel testing yielded 100% sensitivity and 44% specificity for the identification of PJI.

Conclusion: New generation 0.55T MRI may aid the detection of PJI in symptomatic PJI patients. The presence of oedema of joint capsule, adjacent muscles, and subcutis as well as joint effusion were significant indicators of the PJI.

A17

Radiopalmar ganglion cysts: Prevalence, morphology and clinical implications in 1053 wrist MR examinations

S. Goller, G.W. Kajdi, R. Sutter; Balgrist University Hospital, Department of Radiology, Zurich, Switzerland

Purpose: Radiopalmar ganglion cysts (RPG) are a common finding on MRI. However, their significance in symptomatic patients is poorly understood. This study aimed to assess the prevalence and morphology of RPG, associated findings, and radiopalmar complaints.

Methods and Materials: This retrospective study included patients who underwent wrist MRI during a two-year interval. MRI examinations were evaluated by two radiologists for the presence of RPG, and if present, for characteristic features including diameter, loculation, debris, contact to adjacent structures, and related symptoms. Mann-Whitney-U-test and Chi-square test were applied.

Results: 1053 wrists in 909 patients (mean age 43.4 ±15.5 years, 602 females) were included. Of the 308 RPGs (Group 1;29.2%), 49 were unilocular, 95 polylocular, and 164 multilocular; 745 wrists had no RPG (Group 2;70.8%). 126 RPGs showed internal debris. Mean RPG size was 8.5 ±5.6 mm (cranio-caudal), 8.0 ±4.1 (medio-lateral), and 3.7 ±2.3 mm (dorso-palmar). In group 1, significantly more patients showed either a partial (82/308, 26.6%) [group 2: 45/745, 6.0%, P < .001] or complete scapholunate ligament rupture (22/308, 7.1%) [group 2: 20/745, 2.7%, P < .001]. From the patients with RPGs, 47/308 (15.3%) had radiopalmar symptoms, while 261/308 (84.7%) did not. Neither direct contact with adjacent structures, nor the evidence of debris or the RPG loculation were shown to discriminate between patients with and without radiopalmar complaints (area under the curve (AUC) 0.53-0.61). The dorso-palmar RPG extension positively correlated with radiopalmar complaints with P = .024/.044 (reader 1/2, R of .113/.97, respectively). Inter-reader agreement was almost perfect for imaging characteristics (Kappa: 0.90-0.95) and size measurements (Intraclass correlation coefficient: 0.95-0.98).

Conclusion: RPG can be found in 29% of patients who undergo wrist MRI and are mostly asymptomatic. The dorso-palmar RPG extension positively correlates with radiopalmar complaints.

A18

Inflammatory knee synovitis: Evaluation of an accelerated deep learning-based FLAIR sequence

G. Feuerriegel[1], S. Goller[1], C. von Deuster[2,1], R. Sutter[1]; [1] Balgrist University Hospital, Zurich, Switzerland, [2] Siemens Healthineers, ACIT – Advanced Clinical Imaging Technology, Zurich, Switzerland

Purpose: To assess the diagnostic value and accuracy of a Deep learning (DL)-reconstructed fluid attenuated inversion recovery (FLAIR) sequence with fat saturation (FS) in patients with inflammatory synovitis of the knee.

Methods and Materials: Patients with suspected knee synovitis were retrospectively included between January and September 2023. All patients underwent a 3T knee MRI including a DL-accelerated non-contrast FLAIR FS sequence (acquisition time: 1 min 38 sec) and a contrast-enhanced (CE) T1-weighted FS sequence (acquisition time: 4 min 50 sec), which served as reference standard. All knees were scored by two radiologists using the semiquantitative modified knee synovitis score, effusion synovitis score and Hoffa synovitis score. Diagnostic confidence, image quality and image artifacts were rated on separate Likert scales. Wilcoxon signed rank test was used to compare the semiquantitative scores. Inter- and intra-reader reproducibility were calculated using Cohen's kappa.

Results: 55 patients (mean age 52 ± 17 years, 28 females) were included in the study. 27 patients (49%) had mild to moderate synovitis (synovitis score 6-13) and 17 patients (31%) had severe synovitis (synovitis score >14). No signs of synovitis were detected in 11 patients (20%) (synovitis score <5). A scan time reduction of 66% was achieved with the FLAIR FS sequence compared to the CE T1-weighted FS sequence. Semiquantitative assessment of the whole knee synovitis score showed no significant difference between the DL-accelerated FLAIR sequence and the CE T1-weighted sequence (mean FLAIR score: 10.69 ± 8.83, T1 TSE FS: 10.74 ± 10.32, P = 0.521). Both inter- and intra-reader reproducibility were excellent (range Cohen's κ (0.82 - 0.96)).

Conclusion: Assessment of inflammatory knee synovitis using a DL-accelerated non-contrast FLAIR FS sequence was feasible and equivalent to CE T1-weighted FS imaging, with a 66% reduction in acquisition time.

A19

Comparison of CT and dual-energy CT for the detection of crystals in gout and calcium crystal deposition diseases: a task-based phantom study

M. Khorsi[1,2], J. Damet[1,3,4], L. Gallego Manzano[1], P. Monnin[1], F. Becce[5], A. Viry[1]; [1] CHUV – Centre Hospitalier Universitaire Vaudois, Institute of Radiation Physics, Lausanne, Switzerland, [2] UNIL – University of Lausanne, Lausanne, Switzerland, [3] CERN – European Organization for Nuclear Research, Geneva, Switzerland, [4] University of Otago, Christchurch, New Zealand, [5] CHUV – Centre Hospitalier Universitaire Vaudois, Department of Diagnostic and Interventional Radiology, Lausanne, Switzerland

Purpose: CT imaging is playing an increasingly important role in the diagnosis and classification of patients with gout and calcium pyrophosphate deposition diseases. Here, we aimed to compare the diagnostic performance of conventional CT (single-energy, SECT) and dual-energy CT (DECT) for the detection of monosodium urate (MSU), calcium pyrophosphate (CPP) and hydroxyapatite (HA) crystal deposition using phantoms and advanced metrics.

Methods and Materials: We used two dedicated CT phantoms: the first containing synthetic crystals of increasing concentration (MSU: 200-600 mg/ml; CPP and HA: 50-150 mg/ml) suspended in a background mimicking soft tissue, the second to assess noise and spatial resolution. Phantoms were scanned successively using SECT (100 kVp) and DECT (80/140 kVp) at 7 mGy. Virtual monoenergetic images (VMIs) were reconstructed from 40 to 140 keV. Noise power spectrum and modulation transfer function were inserted into a non-prewithening with eye filter model observer (MO) to assess the detectability of 2, 1, and 0.5 mm diameter crystal deposits. The area under the curve (AUC) was used as a figure of merit, with an AUC ≥0.90 representing good diagnostic performance.

Results: For 1 mm diameter crystal deposits, SECT showed AUC values of 0.75 (MSU), 0.88 (CPP), and 0.89 (HA) at the highest concentrations, while DECT (40 keV VMI) identified all three crystals with AUCs of 1. For the highest HA concentration, SECT AUC values decreased from 1 to 0.89 to 0.53 as the crystal deposit diameter decreased from 2 to 1 to 0.5 mm, respectively. In comparison, DECT provided corresponding AUCs of 1, 1, and 0.75. DECT images showed more noise than SECT, but higher spatial resolution. Detectability increased with decreasing VMI-energy and increasing crystal concentration and diameter.

Conclusion: Despite higher noise, DECT outperforms SECT, especially at low-keV VMIs, for the detection of small MSU and calcium crystal deposits.

A20

Detection of degenerative and inflammatory changes of hands and wrists with MRI: T2- weighted Dixon fat-only images can replace T1-weighted images

C. Obermüller, K. Pawlus, F. Ensle, E. Deininger-Czerniak, J. Saraiva Alexandre, R. Guggenberger, USZ - Universitätsspital Zürich, Zurich, Switzerland

Purpose: To show that additional T1-weighted sequences in coronal plane can be waived when using a coronal T2-weighted (w) Dixon sequence including fat-only images in MR imaging of the hands and wrists for the detection of inflammatory and degenerative changes.

Methods and Materials: Two radiologists retrospectively reviewed 46 MRI studies (at 1.5 T or 3 T) of hands and wrists (each both right and left side) in 46 patients suspected of rheumatoid arthritis. Two protocols were separately analyzed: a standard protocol (T1-w, T2-w Dixon in-phase and water-only images, contrast material–enhanced fat-suppressed T1-w sequences) and a simplified protocol (exchanging T1-w by fat-only images of T2-w Dixon sequence). Four items (subchondral sclerosis, ganglions and erosions, osteophytes and joint space narrowing) were analyzed in each of the 5 articulation groups (radiocarpal and ulnocarpal joints, intracarpal joints and II- IV. carpometacarpal joints, I. carpometacarpal joint, I-V. metacarpophalangeal joints, interphalangeal joints).

Results: A decrease in interobserver agreement of ≥ 5% when one reader used the simplified protocol compared with when both readers used the standard protocol was considered clinically significant. Interreader and intrareader agreement were assessed using kappa statistics. Rates of findings with each protocol were compared using odds ratios. The standard and simplified protocols were interchangeable (range of upper bound of the 95%CI of individual equivalence index = 0.25 to 1.38%). Intraprotocol and interprotocol interreader kappa values were similar (0.253–0.671 vs. 0.236–0.723, respectively). Rates of findings were not statistically significantly different (p ≥ 0.074), or were higher with the simplified protocol (p ≤ 0.036).

Conclusion: Single coronal T2-w Dixon MRI sequence including fat-only images may obviate additional T1-w images, allowing for comparable diagnostic confidence in detection of inflammatory and degenerative changes of the hands and wrists.

A21

Morphological and quantitative parametric MRI follow-up of cartilage changes before and after intra-articular injection therapy in patients with mild to moderate knee osteoarthritis: A randomized, placebo-controlled trial

A.B. Rosskopf[1,2], M. Tschopp[1], J. Galley[1], C. Stern[1], S.F. Fucentese[1], F. Brunner[1], R. Sutter[1], S. Catanzaro[1], N. Kühne[1], C.W.A. Pfirrmann[1,2]; [1] Balgrist University Hospital, Zurich, Switzerland, [2] MRI TUM – School of Medicine & Klinikum rechts der Isar, Zurich, Switzerland

Purpose: To detect and compare knee cartilage changes after intraarticular injection of glucocorticoid, hyaluronic acid, or platelet-rich plasma (PRP) to placebo using quantitative and morphological MRI parameters in patients with mild or moderate osteoarthritis.

Methods and Materials: In a double-blinded, placebo-controlled single-center trial, knees with mild or moderate osteoarthritis (Kellgren Lawrence grade 1-3) were randomly assigned to an intraarticular injection with one of these substances: glucocorticoid, hyaluronic acid, PRP, or placebo. Cartilage degeneration in 14 knee compartments was assessed by two readers on baseline and follow-up MRIs (after 3 and 12 months) using quantitative (T2- and T2*-times (ms)) and morphological parameters (modified Outerbridge grading, subchondral bone marrow edema and cysts, osteophytes).

Results: 120 knees (30 knees per treatment group) were analyzed with a median patient age of 60 years (IQR: 54.0, 68.0). Interreader reliability was good for T2- (ICC=0.76;IQR 0.68–0.83) and T2*- (ICC=0.83;IQR 0.76–0.88) measurements. Morphological parameters showed no significant changes between all groups after 3 and 12 months. T2 mapping after 12 months showed the following significant (P=0.001–0.03) changes between groups in 6 of 14 compartments: Values after PRP injection decreased compared to glucocorticoid in 4 compartments (complete medial femoral condyle and central part of lateral condyle) and compared to placebo in 2 compartments of the medial tibial plateau. No significant changes were seen for T2 and T2* times after 3 months and T2* times after 12 months.

Conclusion: PRP has a positive long-term effect on cartilage quality compared with glucocorticoid injection, resulting in significantly improved T2-values at the medial femoral condyle after 12 months. Morphological cartilage parameters did not change significantly after the injections compared to placebo.

A22

Correlation of weight-bearing CT and MRI findings in Flatfoot Deformity

M. Seng[1], L. Andres[2], C. Nüesch[1], D. Harder[1], N. Krähenbühl[1], R. Donners[1]; [1] USB – Universitätsspital Basel, Basel, Switzerland, [2] Schulthess Klinik, Zurich, Switzerland

Purpose: The presence of sinus tarsi impingement in flatfoot deformity (FFD) can be assessed via weight-bearing computed tomography (WBCT) and serve as guidance for recommendations on realignment fusion surgery. Because WBCT is not always available, we aimed to assess whether significant correlation exists between WBCT and magnetic resonance imaging (MRI) findings.

Methods and Materials: In this retrospective study, 24 patients presenting with various stages of FFD (51 ± 18 years; 12 women) underwent WBCT (Multitom Rax, Siemens Healthineers) and MRI. In addition to signs of sinus tarsi impingement, four commonly used 3D measurements were assessed with dedicated postprocessing software (DISIOR 2.1) on the WBCT datasets. Sinus tarsi obliteration, spring and tibiospring ligament (SL, TSL) integrity, as well as tibialis posterior tendon (TP) degeneration, were evaluated on MRI. Statistical analysis was performed to assess whether there was significant (P < 0.05) correlation between WBCT and MRI findings.

Results: A total of 35% of patients with evidence of sinus tarsi impingement on WBCT scans did not show sinus tarsi obliteration on MRI. SL rupture was evident in 43% of patients without sinus tarsi impingement on WBCT. Of note, 24% of patients with sinus tarsi impingement on WBCT did not show SL rupture on MRI. No patient without sinus tarsi impingement on WBCT showed TSL or TP rupture on MRI. However, 59% and 76% of patients with sinus tarsi impingement did not show TSL or TP rupture, respectively. An increased Meary's angle and talocalcaneal overlap, assessed on WBCT, were associated with TSL and TP rupture (P < 0.05).

Conclusion: The sinus tarsi was obliterated in most but not all ankle MRI studies in patients with WBCT evidence of sinus tarsi impingement. MRI diagnoses of ligament and tendon injuries showed only limited correlation with the WBCT diagnosis of sinus tarsi impingement.

A23

Patients with Hip Dysplasia can Present with Femoral Torsion Deformities and with Combined Acetabular version and Femoral Torsion Deformities on Hip MRI

T. Lerch[1], E. Grigoriou[2], Y-J. Kim[2], E. Novais[2]; [1] Inselspital – Universitätsspital Bern, Department of Diagnostic, Interventional and Paediatric Radiology, Bern, Switzerland, [2] Boston Children's Hospital, Boston, United States

Purpose: The effect of femoral torsion(FT) is unclear for patients with hip dysplasia. Increased FT was associated with hip dysplasia. The purpose of this study was to investigate frequency of increased or decreased FT or acetabular version (AV) and combined version on preoperative MRI of patients with hip dysplasia.

Methods and Materials: A retrospective comparative study that involved 419 hips of symptomatic patients with hip dysplasia undergoing periacetabular osteotomy was performed. Mean age was 28 years, 88% were female patients and mean preoperative LCE angle was 11°. Preoperative MRI was performed for all patients in clinical routine for evaluation of cartilage and labrum lesions and for dGEMRIC. Preoperative hip MRI was evaluated for assessment of FT, AV and combined version on axial T1-weighted images. Combined version equals the sum of FT and AV. FT was measured by one radiology resident with 5 years of experience in musculoskeletal imaging according to the Reikeras method. Field of view of the CT scan and MRI included pelvis and knee.

Results: Mean FT of 419 hips was 16° (range -20-57°), and mean central AV was 19° (3-35°) and mean combined version was 35° (-8-78°). 44% of hips had FT between 10-25°, 24% had FT>25° and 32% had FT<10°. FT>35° was found in 6% and FT<0° was found in 8%. The combination of normal FT and AV was present in 36%, while 19% have increased FT>25° and normal AV and 27% have decreased FT<10° and normal AV. Decreased combined version <20° was present in 12%, increased combined version >50° was present in 14%.

Conclusion: One third of patients with hip dysplasia have normal FT combined with normal AV. Almost a third of patients have decreased FT<10°, while 23% have increased FT>25°. Patients with hip dysplasia can exhibit combined deformities. This is important for preoperative planning of hip preservation surgery.

A24

Assessing Lateral Posterior Meniscal Root Insertion Variations of the Knee on a Clinical 7 Tesla MRI in an Asymptomatic Cohort

R. Marcus, A. Marth, S. Zimmermann, R. Sutter; Balgrist University Hospital, Zurich, Switzerland

Purpose: To assess variations of posterolateral meniscal root insertions using a high-resolution sequence on a clinical 7 Tesla (T) MRI scanner.

Methods and Materials: 58 knees of healthy subjects were examined on a clinical 7 T MRI scanner (Magnetom Terra, Siemens Healthineers). Multiplanar reconstructions of a sagittal isotropic 0.24 mm double echo steady state 3D-sequence were used. Number of root insertion reins and insertion localizations were recorded for the lateral meniscus by two radiologists.

Results: Majority consisted of double root insertion rein (66.7%), followed by single (31.6%) and triple insertion reins (1.8%). The majority of single posterior lateral rein roots inserted into the intercondylar area (77.8%) and the remaining 22.2% inserted into the posterior slope of the posteromedial tubercle. The majority of double reins inserted with a major rein along the intertubercular area to the posteromedial insertion of the ACL and a minor rein to the lateral tubercle (78.9%). The inverted variant (major rein inserts into the lateral tubercle and the minor rein inserts next to the tibial ACL-insertion) was reported in 5.3%. The remaining double reins inserted into the posterolateral slope of the medial and lateral eminence. Interrater reliability for describing the meniscal root reins was perfect (κ = 1) and identifying the insertion sites was strong (κ = 0.808).

Conclusion: Posterolateral meniscal roots have a single, double or triple rein insertion in five possible locations.

A25

Development of a Deep Learning Model for Automated Detection of Calcium Pyrophosphate Deposition on Hand Radiographs

E. Rosoux[1], T. Hügle[1], T. Manigold[2], G. Fahrni[1], D. Markham[3], F. Becce[1];
[1] CHUV – Centre Hospitalier Universitaire Vaudois, Lausanne, Switzerland,
[2] Inselspital – Universitätsspital Bern, Bern, Switzerland, [3] University of Oxford, Oxford, United Kingdom

Purpose: Identifying the presence of calcium pyrophosphate deposition (CPPD) on large radiograph datasets is labor-intensive and limited by moderate inter- and intra-observer reliability. Here, we aimed to develop a deep learning approach for automatically and reliably detecting CPPD on hand radiographs in patients with various rheumatic diseases, focusing on the triangular fibrocartilage complex (TFCC) and 2nd and 3rd metacarpophalangeal joints (MCP-2, MCP-3) according to the 2023 ACR/EULAR classification criteria.

Methods and Materials: Two radiologists independently labeled a dataset of 630 hand radiographs, yielding 177 CPPD positive and 453 CPPD negative cases across the three sites of interest. CPPD presence was then predicted using a convolutional neural network. The model performance was assessed using the area under the receiver operating characteristic (AUROC) and area under the precision-recall (AUPR) curves, with heatmaps (Grad-CAM) aiding in case discrimination.

Results: The algorithm for combined TFCC, MCP-2, and MCP-3 classification showed robust performance with a mean AUROC of 0.81 and AUPR of 0.60, sensitivity of 0.89, specificity of 0.70, and precision of 0.53. The TFCC-alone model had a mean AUROC of 0.84 with a slightly higher mean AUPR of 0.64. In contrast, the MCP-2-alone and MCP-3-alone models exhibited mean AUROCs of 0.79-0.80, with lower mean AUPRs of 0.29-0.38. Heatmap analysis revealed activation in the regions of interest for positive cases (true and false positives), but unexpected highlights were encountered possibly due to correlated features in different hand regions.

Conclusion: This study highlights the potential of an automated model for CPPD detection on hand radiographs with high performance in the combined and TFCC-alone models. MCP-2-alone and MCP-3-alone models showed less accuracy due to class imbalance. Future work includes dataset expansion, threshold optimization, preprocessing refinement, and validation with an external dataset.

A26

Metal Artifact Reduction Strategies for Clinical Photon Counting Computed Tomography of Total Hip Arthroplasty – a Volumetric Quantitative and Qualitative Phantom Study

R. Marcus, G. Feuerriegel, A. Marth, D. Nanz, R. Sutter, Balgrist University Hospital, Zurich, Switzerland

Purpose: To systematically evaluate the impact of various scanning and reconstruction modes on both metal artifact volume and overall image quality within the context of a hip prosthesis phantom acquired on a 1st generation clinical photon-counting detector computed tomography (PCCT).

Methods and Materials: A total hip prosthesis phantom was scanned on a PCCT (Naeotom Alpha, Siemens Healthineers) employing four distinct modes at 140 kV and constant dose of 7 mGy: Quantumplus (Q+), UHR-Quantumplus (UHR-Q+), QuantumSn (Q-Sn) and UHR-QuantumSn (UHR-Q-Sn); Sn = tin filter. Polychromatic and virtual monoenergetic images (VMI) were reconstructed with and without iterative metal artifact reduction (iMAR, Siemens Healthineers). Artifacts were quantified using a 3D printing software and image quality was evaluated by two radiologists.

Results: Tin filter reduced artifact volume in polychromatic reconstructions by 14% (298 ml (Q-Sn) vs. 347 ml (Q+) and 310 ml (UHR-Q-Sn) vs. 360 ml (UHR-Q+)). iMAR reduced the metal artifact volume by 46 – 57% with UHR-Q+ images achieving the lowest artifact volume at 150 ml. In VMI, the smallest total artifact volume was quantified at 130 keV with Q+ (150 ml) and UHR-Q+ (164 ml), at 120 keV with Q-Sn (169 ml) and UHR-Q-Sn (172 ml). iMAR reduced artifact volume in VMI: 130 ml in Q+ (150 keV), 140 ml in UHR-Q+ (160 keV), 134 ml in Q-Sn (150 keV) and 140 ml (UHR Q-Sn at 190 keV). Best subjective image quality was achieved for VMI Q+ with iMAR (65 keV), polychromatic UHR-Q+ with iMAR, VMI Q-Sn with iMAR (100 keV), polychromatic Q-Sn with iMAR, VMI UHR-Q-Sn (100 keV) and polychromatic UHR Q-Sn.

Conclusion: VMI or polychromatic images using tin filter, UHR and iMAR achieve the strongest artifact reduction and best image quality.

A27

Metal Artifact Reduction at 0.55T Outperforms 1.5T MRI in Patients with Posterior Spinal Fusion – Results from a Scanner-Comparison-Study

A. Seifert, H-C. Breit, F. Schlicht, R. Donners, D. Harder, J. Vosshenrich; USB – Universitätsspital Basel, Department of Radiology, Basel, Switzerland

Purpose: To assess image quality and metal artifact reduction capabilities of 0.55T MRI of the spine compared with 1.5T MRI in patients following posterior fusion surgery.

Methods and Materials: 50 consecutive patients (mean age: 69±12 years, 16 men) who underwent MR imaging at 0.55T and 1.5T following posterior fusion surgery of the lumbar (n=42) or thoracolumbar spine (n=8) were included. Examinations included routine follow-up imaging, as well as scans to assess for postoperative complications, using metal artifact reduction protocols from clinical routine.

Images were rated by two fellowship-trained MSK radiologists for signal/contrast, resolution, assessability of the spinal canal and the neural foramen on a 5-point Likert scale (range: 1 = non-diagnostic to 5 = perfect image quality). Implant-related susceptibility artifacts were scored from 1 (minimal) to 5 (non-diagnostic), and effects of posterior fusion length (1-level vs. 2-level vs. > 2-level) on image quality and artifact severity were assessed.

Results: Even though overall image quality at 0.55T was rated lower than at 1.5T in terms of signal/contrast (mean: 4.0±0.3 vs. 4.4±0.6; p<.001) and resolution (3.8±0.5 vs. 4.2±0.7; p<.001), assessability of spinal canal (4.4±0.5 vs. 4.2±0.9; p=.69) and neural foramen (3.8±0.5 vs. 3.8±0.9; p=.19) were rated equal at both field strengths with excellent interrater agreement (range: 0.84-0.91). Implant-related susceptibility artifacts were rated lower at 0.55T, both overall (1.82±0.52 vs. 3.03±0.64; p<.001) and for distinct pulse sequences. In the presence of multi-segment implants, assessability of spinal canal and neural foramen was deemed superior to 1.5T MRI (4.4±0.5 vs. 3.6±1.1; p<.001).

Conclusion: 0.55T MRI of the spine outperforms 1.5T MRI with regard to metal artifact severity. In patients with multi-level implants, low-field MRI allows to reliably assess near-metal anatomy, where 1.5T MRI reaches diagnostic limitations.

A44

Synthetic hematocrit from virtual non-contrast images for the assessment of myocardial extracellular volume with photon-counting detector CT

V. Mergen[1], N. Ehrbar[1], J. Harmes[1], L. Moser[1], H. Alkadhi[1], M. Eberhard[1,2];
[1] USZ – Universitätsspital Zürich, Department of Diagnostic and Interventional Radiology, Zurich, Switzerland, [2] Spitäler fmi AG – Spital Interlaken, Department of Radiology, Unterseen, Switzerland

Purpose: To assess the value of a synthetic hematocrit derived from virtual non-contrast images to compute the myocardial extracellular volume (ECV) with photon-counting detector (PCD) CT.

Methods and Materials: In this IRB-approved study, consecutive patients undergoing a PCD-CT including a coronary CT angiography (CCTA) and a late enhancement scan (LE) and having a blood hematocrit test were included. In the first 75 patients, CCTA and LE scans were reconstructed as virtual non-iodine images (VNI) at 60, 70, and 80keV and virtual non-contrast images (VNC) with quantum iterative reconstruction (QIR) strengths 2, 3, and 4. Mean blood pool attenuation (BPmean) calculated by placing regions-of-interest in the left ventricle, ascending and descending aorta, and blood hematocrit were evaluated using linear regression and Pearson correlation analyses. In the next 50 patients, synthetic hematocrit was calculated using the reconstruction with the highest previously determined Pearson R2. Synthetic myocardial ECV was computed using the synthetic hematocrit and then compared with the ECV using the blood hematocrit as the reference.

Results: In the first 75 patients (49 men, age 79±8 years), the correlation between BPmean and blood hematocrit ranged from poor (R2=0.12) for VNI of CCTA at 80keV with QIR 2 to moderate for VNI of LE at 60keV with QIR 4, 70keV with QIR 3 and 4, and VNC of LE with QIR 3 and 4 (all, R2=0.58). In the next 50 patients (29 men, age 75±14 years), synthetic hematocrit was calculated from VNC with QIR 3 applying the following regression analysis formula: hematocrit = -0.053 + 0.0093 * mean attenuation. The median ECV was 26.9% (interquartile range (IQR) 25.5-28.8%) using the blood hematocrit and 26.9% (IQR, 25.6-29.8%) using the synthetic hematocrit (VNC, QIR 3; mean difference, 0.2%; limits of agreement, -2.5%, 2.0%; p=0.23).

Conclusion: Synthetic hematocrit from VNC images enables accurate calculation of myocardial ECV with PCD-CT, potentially obviating the need for a blood hematocrit test.

A45

A novel reconstruction technique to reduce stair-step artifacts in sequential mode coronary CT angiography

L.J. Moser[1], V. Mergen[1], M. Robert[1], M. Eberhard[1,2], H. Alkadhi[1];
[1] USZ – Universitätsspital Zürich, Department of Diagnostic and Interventional Radiology, Zurich, Switzerland, [2] Spitäler fmi AG – Spital Interlaken, Department of Radiology, Unterseen, Switzerland

Purpose: To evaluate a novel reconstruction algorithm to reduce the occurrence and severity of stair step artifacts in sequential coronary CT angiography.

Methods and Materials: In this IRB-approved, retrospective study, 50 consecutive patients were included who underwent coronary CT angiography on a dual-source photon-counting detector CT in the sequential mode (collimation 120x0.2mm). Each scan was reconstructed without (hereafter called standard) and with a novel ZeeFree algorithm, which aims to minimize stair-step artifacts. The presence and extent of stairstep artifacts was rated by two independent, blinded readers. The relationship of artifacts was correlated with the average and variability of heart rate and with patient characteristics.

Results: In standard reconstructions, reader 1 reported stair-step artifacts in 40/504 (7.9%) segments, from which 12/504 led to non-diagnostic image quality (2.4% of all segments). Reader 2 reported 56/504 (11.1%) stair-step artifacts, from which 11/504 lead to non-diagnostic image quality (2.2%). With ZeeFree, 9/12 (75%) and 8/11 (73%) of the non-diagnostic segments improved to diagnostic quality for the readers, respectively. ZeeFree significantly reduced the frequency and extent of stairstep artifacts compared to standard reconstructions (p<0.001, each). Heart rate variability and body mass index were significantly related to the occurrence of stair-step artifacts (p<0.05).

Conclusion: Our results demonstrate the feasibility and effectiveness of a novel reconstruction algorithm fsignifican't reduction of stair-step artifacts and hence, a reduction of coronary segments with a non-diagnostic image quality in sequential ultra-high resolution coronary CT angiography.

A46

Simultaneous Bright- and Black-Blood Whole-Heart (BOOST) MRI to demarcate left atrial ablated tissue immediately after radiofrequency catheter ablation without administered intravenous contrast media

M. Kassai[1], J-F. Deux[1], C.G. Glessgen[1], L.A. Crowe[1], K. P. Kunze[2], M. Schmidt[3], R. Botnar[4], C. Prieto[4], V. Breguet[1], D. Adamopoulos[1], D. Shah[1], J-P. Vallée[1];
[1] HUG – Hôpitaux universitaires de Genève, Geneva, Switzerland, [2] Siemens Healthcare AG, Erlangen, Germany, [3] Siemens Healthineers, Erlangen, Germany, [4] King's College London, London, United Kingdom

Purpose: Cardiac MR imaging is used to assess the effectiveness of left atrium radio-frequency catheter ablation (RFA) with Late gadolinium enhancement imaging (LGE). One of its limitations is the blood-lesion contrast. Our study aimed to evaluate free-breathing, simultaneous Bright- and Black-Blood Whole-Heart (BOOST) research sequence with alternating 2-HB preparation scheme iT2prep-BOOST to detect post-ablation left atrial myocardial lesions without contrast media; generating Bright Blood and co-registered, T1-weighted Black Blood datasets

Methods and Materials: Ten patients with atrial fibrillation underwent left atrial RFA procedure, followed by a clinical cardiac MRI (IMRIS 3T MAGNETOM Skyra, Siemens Healthineers Ag, Erlangen, Germany) including pre-contrast, free-breathing iT2prep-BOOST 3D imaging and a post-contrast free-breathing 3D LGE sequence. Both research sequences used a Dixon-GRE readout in combination with image navigators (iNAV) leading to 100% respiratory scan efficiency and predictable scan time. After water-fat separation, water images of both research sequences were aligned using 3D Slicer software (slicer.org). Acute necrosis zones appearing as low signal intensity (SI) lesions on LGE and high SI zones from the proposed BOOST sequence were segmented manually. Pearson correlation test was used to compare volumes.

Results: High-quality images with dark area on LGE and bright area on BOOST with a distribution corresponding to RF ablation points were obtained in 9/10 patients. Lesions SI normalized to the blood pool on BOOST were hyper-intense compared to necrosis on LGE (2.176 +-0.45 and 0.53 +- 0.11 respectively, p<0.001). Volumes of low SI regions on the LGE correlated significantly with hyperintense BOOST SI volumes (n=9, r2=0.58, p=0.027).

Conclusion: High-quality images with dark area on LGE and bright area on BOOST with a distribution corresponding to RF ablation points were obtained in 9/10 patients. Lesions SI normalized to the blood pool on BOOST were hyper-intense compared to necrosis on LGE (2.176 +-0.45 and 0.53 +- 0.11 respectively, p<0.001). Volumes of low SI regions on the LGE correlated significantly with hyperintense BOOST SI volumes (n=9, r2=0.58, p=0.027).

A47

Clinical applicability of highly accelerated 2D kat-ARC Cine in patients with arrythmia

M. Polacin[1], T. Hünermund[1], M. Lohezic[2], H. Alkadhi[1], R. Manka[1];
[1] USZ – Universitätsspital Zürich, Institute of Diagnostic and Interventional Radiology, Zurich, Switzerland, [2] GE HealthCare, Advanced Technology, Science and Technology Organization, Zurich, Switzerland

Purpose: Acquisition of short-axis cine stack for evaluation of volumes and function during a cardiac MRI scan can be challenging in patients with arrhythmia. The aim of this study was to compare 2D cine imaging during a single breath hold using the kat ARC (k- and adaptive-t autocalibrating reconstruction for Cartesian sampling) technique with conventional multi-breath hold 2D cine in 20 patients with arrythmia.

Methods and Materials: 2D multi-breath hold cine short axis stack as well as 2D kat-ARC single breath-hold cine short-axis stack were acquired in 20 patients on a 1.5 T MRI (GE Signa Arist). Two readers independently evaluated image quality, acquisition time as well as end-diastolic left- and right-ventricular volumes, ejection fraction and left-ventricular myocardial mass in both sequences.

Results: The 2D kat-ARC cine had significantly shorter acquistion time (20.2 ± 9.1 s vs. 100.4 ± 16.7 s; p < 0.0001). Image quality was not inferior using 2D kat-ARC compared to 2D SSFP cine (p = 0.6) and the two sequences demonstrated no significant differences in end-diastolic left- and right-ventricular volumes (p =0.2 and 0.4), ejection fraction (p= 0.2) and left-ventricular myocardial mass (p = 0.5).

Conclusion: One breath-hold 2D kat-ARC cine is a reliable technique that could be used in clinical evaluation of ventricular volumes and function without impairment in image quality and remarkably reduced acquisition time.

A147

Fully Automated Artificial Intelligence-based Coronary Artery Disease Diagnosis from SPECT Myocardial Perfusion Imaging

G. Hajianfar[1], O. Gharibi[2], M. Sabouri[3,4], M. Mohebi[5], M. Amini[1], M. J. Yasemi[5], M. Chehreghani[2], M. Edalat-Javid[2], S. Valavi5, A.B. Rajabi[2], Y. Salimi[1], H. Arabi[1], A. Rahmim[3,4], I. Shiri[1,6], H. Zaidi[1]; [1] HUG – Hôpitaux universitaires de Genève, Division of Nuclear Medicine and Molecular Imaging, Geneva, Switzerland, [2] RCMRC – Iran University of Medical Sciences, Rajaie Cardiovascular Medical and Research Center, Tehran, Iran, Islamic Republic of, [3] University of British Columbia, Department of Physics and Astronomy, Vancouver, Canada, [4] BC Cancer Research Institute, Department of Integrative Oncology, Vancouver, Canada, [5] RCMRC – Iran University of Medical Sciences, Tehran, Iran, Islamic Republic of, [6] Inselspital – Universitätsspital Bern, Department of Cardiology, Bern, Switzerland

Purpose: While the gold standard method for the diagnosis of obstructive coronary artery disease (CAD) is invasive coronary angiography (ICA), SPECT myocardial perfusion imaging (MPI) has diagnostic value in the assessment of CAD. As such, it is conventionally used as a non-invasive tool for pre-ICA-diagnosis. In this study, we developed a robust automated diagnosis method of obstructive CAD from SPECT-MPI polar maps using deep learning (DL).

Methods and Materials: A total of 940 patients who underwent SPECT-MPI were enrolled, of which 281 were accompanied with ICA (#1), and 659 without ICA (#2). In #2, patients with a sum score >=4 (based on nuclear medicine physician (NMP) report) were considered abnormal. Three different scenarios (SCs) were pursued; 1) using only #1 for training/validation and testing the models; 2) adding #2 to the training cohort only; 3) using both datasets but only using the NMPs report as ground truth. Both stress and rest polar maps were used as input for the models. DensNet201 network with spatial pyramid pooling (SPP) aggregation model was utilized. We evaluated our models for the left anterior artery (LAD), left circumflex artery (LCX), and right coronary artery (RCA).

Results: The following results are obtained for LAD, RCA, and LCX, respectively. In the SC1, an AUC of [0.61, 0.62, 0.69], sensitivity (SEN) of [0.70, 0.72, 0.88], and specificity (SPE) of [0.42, 0.49, 0.47] were achieved. In the SC2, AUC was [0.60, 0.63, 0.71], SEN was [0.72, 0.59, 0.58], and SPE was [0.53, 0.62, 0.74]. In the SC3, AUC was [0.87, 0.90, 0.92], SEN was [0.93, 0.83, 0.85], and SPE was [0.73, 0.78, 0.82].

Conclusion: Overall, the results for all SCs were superior for LCX. The SC2 did not improve SEN but enhanced SPE. The SC3 showed outstanding outcomes. This study demonstrated the potential of SPECT-MPI for predicting ICA diagnosis. The use of an expanded dataset might improve the performance of the model.

A30

RoentGen: Vision-Language Model for Chest X-Ray Generation

C. Blüthgen[1,2], P. Chambon[2], J-B. Delbrouck[2], R. van der Sluijs[2], M. Polacin[1], J. MZ Chaves[2], T.M. Abraham[3,4], S. Purohit[4], C. Langlotz[2], A. Chaudhari[2]; [1] USZ – Universitätsspital Zürich, Zurich, Switzerland, [2] AIMI – Center for Artificial Intelligence in Medicine and Imaging, Stanford, United States, [3] UC Davis – University of California, Davis, United State, [4] Stability AI, London, United Kingdom

Purpose: New generative AI models allow the flexible creation of high-quality images but fail to produce radiologically plausible samples. The purpose was(1)to adapt a text-to-image model (Stable Diffusion, SD) to be able to generate chest X-rays (CXR) based on radiological descriptions;(2)To evaluate the use of synthetic CXR for training deep learning (DL) models and beyond.

Methods and Materials: MIMIC-CXR, a dataset of 337k real CXR and corresponding reports was used to fine-tune SD. Synthetic CXR were created using the impression sections of real CXR reports as input and evaluated in multiple categories: (1)human assessment of image quality and alignment of text and generated CXR by 2 radiologists; (2)quantitative image quality (Fréchet inception distance,FID) and generative diversity(MS-SSIM); (3)the impact of using synthetic CXR when training DL models for classification tasks.

Results: Synthetic CXR were realistic and had decent text-image alignment. Synthetic CXR outperformed SD samples in terms of fidelity (FID of 3.6 vs. 19.5) and diversity (MS-SSIM 0.29 vs. 0.36). Training on a blend of real and synthetic CXR slightly improved classification performance (up to +3% AUC) over training on real CXR alone.

Conclusion: Domain-adapted generative models allow the flexible creation of high-quality synthetic CXR, that can improve or partially replace real training data. This may reduce the need to share real medical data and – through the flexibility granted by text-conditioning – allow the creation of tailored datasets, e.g., to counter imbalances.

A31

Comparison of deep learning-based CAD systems regarding pulmonary nodule detection, localization and classification: A multi-reader study

A. Peters, N. Wiescholek, J. Klaus, F. Strodka, A. Macek, E. Primetis, D. Dionysios, J. Heverhagen, A. Christe, L. Ebner; Inselspital – Universitätsspital Bern, Bern, Switzerland

Purpose: To evaluate and compare the performance of two DL-based CAD systems regarding detection, localization and classification of pulmonary nodules.

Methods and Materials: The study population consisted of a cohort provided by the local lung cancer center containing proven T1 tumors of the lung (n=122) extended by 83 additional cases (subsolid, n=13; solid<6mm, n=40; controls, n=30). Five independent blinded readers with different experience levels (residents, n=3; seniors, n=2) performed two readouts, first without and then with access to the results of the DL-CAD. Two readers used software 1 and the three readers used software 2. Readers had to score nodule size, density and localization.

Results: The final cohort consisted of 198 patients with 221 pulmonary nodules. Residents' mean detection rate increased from 64% to 77% (p<0.001) using the respective DL-CAD (table 2). Senior radiologists' mean detection rate did not improve (85% vs. 86%; p=0.25). The rates of the residents for lobar (73% vs. 77%) and segmental (64% vs. 68%) localization both improved significantly (p<0.001). The senior radiologists had no significant benefit, neither for lobar (90% vs. 91%; p=0.63) nor segmental (78% vs. 80%; p=0.243) localization.

Software 2 lead to a slightly higher increase in detection rates (software 1, 80% to 86% and software 2, 67% to 77%; both p<0.001). Both systems showed no significant effect on the rate of correct LungRADS classification (Software 1, 68% vs. 69%; p=0.754 and Software 2, 60% vs. 57%; p=0.190).

Conclusion: Less experienced readers have more benefit from using DL-CAD systems regarding detection and localization of pulmonary nodules. For most readers, there is no effect on correct tumor classification. The two systems performed comparably in the current study, hereby software 2 lead to a slightly higher increase in detection rates.

Influence of CT dose reduction on AI-driven malignancy estimation of incidental pulmonary nodules

A. Peters[1], J. Solomon[2], O. von Stackelberg[3], E. Samei[2], N. Alsaihati[2], W. Valenzuela[1], M. Debic[3], C. Heidt[3], A. Huber[1], Andreas Christe[1], J. Heverhagen[1], H-U. Kauczor[3], C.P. Heussel[3], L. Ebner[1], M. Wielpütz[3]; [1] Inselspital – Universitätsspital Bern, Bern, Switzerland, [2] Duke University Medical Center, Carl E. Ravin Advanced Imaging Laboratories, Durham, United States, [3] Universitätsklinikum Heidelberg, Heidelberg, Germany

Purpose: The purpose of this study was to determine the influence of dose reduction on a commercially available lung cancer prediction convolutional neuronal network (LCP-CNN).

Methods and Materials: CT scans from a cohort provided by the local lung cancer center with confirmed pulmonary malignancies and their corresponding reduced dose simulations (25%- and 5%-dose) were subjected to the LCP-CNN. The resulting LCP scores (scale 1-10, increasing malignancy risk) and the proportion of correctly classified nodules were compared. The cohort was divided into a low-, medium- and high-risk group based on the respective LCP scores, shifts between the groups were studied to evaluate the potential impact on nodule management. Two different malignancy risk score thresholds were analyzed; a higher threshold of ≥9 ("rule-in"-approach) and a lower threshold of >4 ("rule-out"-approach).

Results: 169 patients with 196 nodules were included (mean age±SD, 65±9y; 49% females). Mean LCP scores for original, 25%- and 5%-dose levels were 8.5±1.7, 8.4±1.7 (p>0.05 vs. original dose) and 8.2±1.9 (p<0.05 vs. original dose), respectively. The proportion of correctly classified nodules with the "rule-in"-approach decreased with simulated dose reduction from 58% to 56% (p=0.34) and to 52% for the respective dose levels (p=0.01). For the "rule-out"-approach the values were 96%, 96% and 94% (p=0.12). When reducing the dose to 25%/5%, eight/twenty-two nodules shifted to a lower, five/seven nodules to a higher malignancy risk group.

Conclusion: CT dose reduction may affect the analyzed LCP-CNN regarding the classification of pulmonary malignancies and potentially alter pulmonary nodule management.Utilization of a "rule-out" approach with a lower malignancy risk threshold prevents underestimation of the nodule malignancy risk for the analyzed software.

Potential of Photon-counting detector CT for radiation dose reduction in pulmonary nodule detection and feasibility of AI-based detection systems at different ultra-low dose levels

L. Jungblut[1], A. Euler[2], A. Landsmann[3], V. Englmaier[1], V. Mergen[3], M. Sefirovic[1], T. Frauenfelder[1]; [1] USZ – Universitätsspital Zürich, Institut für Diagnostische und Interventionelle Radiologie, Zurich, Switzerland, [2] KSB – Kantonsspital Baden, Institut für Radiologie, Baden, Switzerland, [3] USZ – Universitätsspital Zürich, Department of Diagnostic and Interventional Radiology, Zurich, Switzerland

Purpose: To evaluate the potential of PCD-CT for dose reduction in pulmonary nodule detection.

Methods and Materials: A chest-phantom containing pulmonary nodules of different sizes/densities was imaged on a PCD-CT with standard low-dose protocol as well as with 1/2, 1/4 and 1/40 dose (eff. dose ranging from 0.2mSv to 0.01mSv) by adapting the reference tube current. Dose-matched scans were performed on a third-generation energy-integrating detector CT (EID-CT). Nodule detection was performed by two blinded radiologists. Subjective image quality was rated on a five-point-likert-scale. AI-based nodule detection was performed using a commercially available AI-CAD system. Parametric tests were performed.

Results: Highest image noise was found at the lowest dose setting of 1/40 radiation dose (eff. dose=0.01mSv) with 166.1±18.5 HU for PCD-CT and 351.8±53.0 HU for EID-CT. Overall sensitivity was 100% vs. 93% at standard low-dose protocol (eff. dose=0.2 mSv) for PCD-CT and EID-CT, respectively. At 1/40 radiation dose sensitivity for nodule detection was 100% for solid/subsolid and 75% for ground-glass nodules in PCD-CT and 80% for solid, 60% for subsolid and 25 vs. 0% (reader 1 vs. 2) for ground-glass nodules in EID-CT. AI-CAD-system delivered a sensitivity of 93% at the lowest radiation dose level in PCD-CT.

Conclusion: At an eff. dose of 0.01mSv all nodules requiring follow-up imaging could be detected. The use of AI-based CAD software is feasible at ultra-low-dose levels in PCD-CT.

Optimization of CT pulmonary angiography using task-based image quality assessment and diagnostic reference levels

V. Vitzthum, D. Racine, P. Monnin, D. Rotzinger, A. Viry; CHUV – Centre Hospitalier Universitaire Vaudois, Lausanne, Switzerland

Purpose: It is important that frequent CT protocols like computed tomography pulmonary angiography (CTPA) for the detection of pulmonary embolism (PE) are controlled and optimized regularly. The comparison of the radiation dose to the diagnostic reference levels (DRLs) alone does not consider patient corpulence nor image quality. The purpose of this study is to establish size specific DRLs for PE based on patient CT examinations and to assess the task-based image quality (IQ) with phantom studies for each device.

Methods and Materials: 1051 CT pulmonary angiography dose data were collected from 74 CT devices. Two categories of patient sizes (medium and large) were established from the distribution of the thoracic perimeters. DRLs were calculated as the 75th percentile of CT dose index (CTDI). IQ was assessed with two thoracic phantom sizes using local acquisition parameters and three other dose levels. The area under the ROC curve (AUC) of a 2mm low perfused vessel was assessed with a non-prewhitening with eye-filter model observer. The optimal IQ-dose relationship was mathematically assessed from the fitted curve between IQ and dose. The variability across different CTs before and after applying the proposed optimization were described.

Results: The DRLs of CTDIvol were 6.4 mGy and 10 mGy for the two patient categories. 75th percentiles of phantom CTDIvol were 6.3 mGy and 10 mGy with inter-quartile AUC values of 0.047 and 0.066, respectively. After the optimization, 75th percentiles of phantom CTDIvol decreased to 5.9 mGy and 7.55 mGy and the interquartile AUC values were reduced to 0.025 and 0.057 for the two phantom sizes.

Conclusion: DRLs for PE were proposed as a function of patient thoracic perimeters. Phantom measurements could be used to establish an individual optimization process for each CT leading to a global harmonization of dose and IQ.

BI-RADS category assignments by GPT-3.5, GPT-4, and Google Bard: A multilanguage study

A. Cozzi[1], *K. Pinker*[2], *A. Hidber*[6], *T. Zhang*[3,4,5], *L. Bonomo*[1], *R. Lo Gullo*[2], *B. Christianson*[2], *M. Curti*[1], *S. Rizzo*[1,6], *F. Del Grande*[1,6], *R. Mann*[7,4], *S. Schiaffino*[1]; [1] EOC – Ente Ospedaliero Cantonale, IIMSI – Imaging Institute of Southern Switzerland, Lugano, Switzerland, [2] Memorial Sloan Kettering, New York, United States, [3] Netherlands Cancer Institute, Department of Radiology, Amsterdam, Netherlands, [4] Radboud University Medical Center, Department of Diagnostic Imaging, Nijmegen, Netherlands, [5] GROW – School for Oncology and Reproduction, Maastricht, Netherlands, [6] USI – Università della Svizzera Italiana, Faculty of Biomedical Sciences, Lugano, Switzerland, [7] NKI – Netherlands Cancer Institute, Department of Radiology, Amsterdam, Netherlands

Purpose: To assess and compare the agreement between human readers and large language models (LLMs) in Breast Imaging Reporting and Data System (BI-RADS) category assignments across three languages, also evaluating the rate of discordant assessments changing patient management.

Methods and Materials: This exploratory prospective study involved three referral centers in Switzerland, USA, and The Netherlands. In each center, 800 reports (40 for each BI-RADS category 1-5 for MRI, mammography, US, mammography+US), written in Italian, English, and Dutch, were collected up to October 1, 2023. After deleting patient data and conclusions, findings described by radiologists were entered into GPT-3.5, GPT-4, and Bard, asking for BI-RADS category assignments with standardized prompts, and then separately reviewed by board-certified breast radiologists. Gwet's agreement coefficients (AC1) and McNemar's tests were used to assess and compare human and LLMs agreement in the five BI-RADS categories and according to macro-categories defining patient management (BI-RADS 0, BI-RADS 1/2, BI-RADS 3, BI-RADS 4/5).

Results: Across 2400 reports, human-human agreement was significantly higher (AC1 0.91, 95% CI 0.90-0.92; p<0.001) than the moderate human-GPT-4 (0.52, 95% CI 0.51-0.53), human-GPT-3.5 (0.48, 95% CI 0.47-0.48) and human-Bard (0.42, 95% CI 0.39-0.43) agreements. Human-LLM disagreements changed patient management significantly more often (Bard: 611/2400, 25.5%; GPT-3.5: 573/2400, 23.9%; GPT-4: 435/2400, 18.1%) than human-human disagreements (118/2400, 4.9%, p<0.001), the latter negatively impacting patient management significantly less often (37/118, 31.4%, p<0.001) than LLMs (Bard: 435/611, 71.2%; GPT-3.5: 344/573, 60.0%; GPT-4: 255/435, 58.6%).

Conclusion: LLMs achieved only moderate agreement with human-assigned BI-RADS categories across three languages. The high percentage of disagreements negatively impacting patient management highlights the potential consequences of unwarranted and unrestricted LLMs use.

Tumor involvement of the nipple at preoperative contrast-enhanced mammography (CEM): preliminary results of a multicenter diagnostic accuracy study

A. Cozzi[1], *T. van Nijnatten*[2,3], *R. Alcantara*[4], *G. Della Pepa*[5], *J. James*[6], *C. Depretto*[5], *G. Scaperrotta*[5], *S. Schiaffino*[1]; [1] EOC – Ente Ospedaliero Cantonale, IIMSI – Imaging Institute of Southern Switzerland, Lugano, Switzerland, [2] Maastricht University Medical Center, Department of Radiology and Nuclear Medicine, Maastricht, Netherlands, [3] GROW – School for Oncology and Reproduction, Maastricht, Netherlands, [4] Hospital del Mar, Barcelona, Spain, [5] IRCCS – Fondazione Istituto Nazionale dei Tumori, Milan, Italy, [6] Nottingham University Hospital, Nottingham, United Kingdom

Purpose: To assess the diagnostic accuracy of contrast-enhanced mammography (CEM) in the prediction of pathologic nipple involvement, also comparing CEM diagnostic accuracy with contrast-enhanced breast MRI.

Methods and Materials: This retrospective multicenter study included patients with biopsy-proven breast cancer who underwent preoperative CEM in three referral centers (Italy, Spain, The Netherlands), between April 2013 and June 2023. Patients were included if they did not undergo neoadjuvant therapy and if they underwent either mastectomy or central lumpectomy. After local image review by board-certified breast radiologists (5-to-10 years of experience) the diagnostic performance of CEM in predicting nipple involvement was calculated taking surgical pathology as the reference standard and compared with MRI (McNemar's test) in a subset of patients.

Results: A total 70 patients (median age 64 years, interquartile range 51-73 years) with breast cancer (50/70 invasive ductal carcinoma, 16/70 invasive lobular carcinoma, 4/70 pure DCIS) were included in the analysis, 59/70 also having undergone MRI. Nipple involvement at surgical pathology was found in 25/70 cases (35.7%). Considering all 70 patients, CEM had a 72.0% sensitivity (95% CI 50.6-87.9%) and an 88.9% specificity (95% CI 76.0-96.3%) for the prediction of pathological nipple involvement. All 7 false negative cases presented as non-mass enhancement lesions without peri-areolar skin thickening. Among the 59 patients with both CEM and MRI, CEM had a 65.0% sensitivity (95% CI 44.1-85.9%), significantly lower (p=0.014) than the 95.0% sensitivity of MRI (95% CI 85.4-100%), whereas no significant differences (p=0.179) were found between CEM specificity (97.4%, 95% CI 92.5-100%) and MRI specificity (89.7%, 95% CI 80.2-99.3%).

Conclusion: Preoperative CEM showed moderate sensitivity and high specificity in assessing nipple involvement. Compared to MRI, CEM had significantly lower sensitivity and non-significantly higher specificity.

Motion Blur Detection in Digital Mammography: Combining reciprocal space features with deep learning

S. Nowakowska[1], *V. Vescoli*[2], *T. Schnitzler*[3], *C. M. Ruppert*[1], *K. Borkowski*[2], *C. Rossi*[1], *B. Wein*[4], *A. Ciritsis*[1]; [1] USZ – Universitätsspital Zürich, Zurich, Switzerland, [2] b-rayZ AG, Schlieren, Switzerland, [3] KSA – Kantonsspital Aarau, Aarau, Switzerland, [4] RWTH Uniklinik Aachen, Aachen, Germany

Purpose: Development of a model for the automatic detection of motion blur in diagnostically relevant areas within digital mammography

Methods and Materials: A collection of 152 examinations obtained using mammography machines from three distinct vendors was employed. Radiologists specializing in breast imaging delineated the blurry regions. Wiener Spectra (nWS) were then extracted from each mammogram using a sliding window approach. These spectra were used as input for a Convolutional Neural Network (CNN), which calculated the likelihood of the spectra originating from a blurred region. By applying a threshold to the generated blur probability mask, the mammograms could be classified as either blurred or sharp.

Results: The model demonstrated concordance with Reader 1 in 81% and with Reader 2 in 78% of mammograms identified as blurred. In sharp mammograms, the model achieved accord in 76% with Reader 1 and in 72% with Reader 2.

Conclusion: A model for generalizable blur detection was developed and assessed, indicating that a robust approach to blur detection, based on feature extraction in frequency space and tailored to radiologist expertise regarding clinical relevance, can eliminate subjectivity associated with visual assessment. The motion blur detection model, when implemented in clinical practice, can offer instantaneous feedback to technicians, enabling prompt retakes and ensuring the utilization of only high-quality mammograms for diagnostics.

Image quality assessment in screening mammography: How subjective is PGMI really and can AI software help?

T. Santner[1], C. Ruppert[2], S. Gianolini[3], J-G. Stalheim[4], S. Frei[5], M. Hondl[6], V. Fröhlich[7], L. Gruber[1], S. Hofvind[8], G. Widmann[1]; [1] Medical University Innsbruck, Innsbruck, Austria, [2] USZ – Universitätsspital Zürich, Department of Diagnostic and Interventional Radiology, Zurich, Switzerland, [3] Hirslanden Klinik, Zurich, Switzerland, [4] Evidia, Bergen, Norway, [5] Unisanté, Programmes vaudois de dépistage du cancer, Lausanne, Switzerland, [6] Klinik Ottakring, Vienna, Austria, [7] University of applied sciences Wiener Neustadt, Vienna, Austria, [8] Cancer Registry of Norway, Oslo, Norway

Purpose: The purpose of this study was to evaluate human inter-reader agreement of the PGMI (perfect-good-moderate-inadequate) quality assessment in screening mammography and explore the role of artificial intelligence (AI) as an alternative reader.

Methods and Materials: Five independent readers from three European countries (Austria, Norway, Switzerland) performed the PGMI quality assessment of 520 anonymized screening mammograms randomly selected from representative subsets from 13 imaging centres within two European countries (Austria, Switzerland). As a sixth reader, a dedicated AI software (b-rayZ AG, Switzerland) was used. Accuracy, Cohen's Kappa, and confusion matrices were used to compare the predictions of the AI software against the individual assessment of the readers, as well as potential discrepancies between them.

Results: Significant inter-reader variability among human readers with poor to moderate agreement (κ=-0.018 to κ=0.41) was observed, with some showing more homogenous interpretations of quality features and overall quality than others. In comparison, the AI software surpassed human inter-reader agreement in detecting glandular tissue cuts, mammilla deviation, pectoral muscle detection, and pectoral angle measurement, while remaining features and overall image quality exhibited comparable performance to human assessment.

Conclusion: Notably, human inter-reader disagreement of PGMI assessment in screening mammography is considerably high. AI software may reliably categorize quality. Its potential for standardization and immediate feedback for achieving and monitoring high levels of quality for screening programs needs to be further evaluated.

Breast DCE-MRI: Generalizable segmentation of breast tissue and constrast uptake with attention U-Net

S. Nowakowska[1], K. Borkowski[2], C.M. Ruppert[1], A. Landsmann[1], M. Marcon[1], N. Berger[1], A. Boss[1], A. Ciritsis[1], C. Rossi[1]; [1] USZ – Universitätsspital Zürich, Zurich, Switzerland, [2] b-rayZ AG, Schlieren, Switzerland

Purpose: Development of automated segmentation models enabling standardized volumetric quantification of fibroglandular tissue from native volumes and Background Parenchymal Enhancement from subtraction volumes of Dynamic Contrast Enhanced breast MRI. Subsequent assessment of the developed models in the context of FGT and BPE BI-RADS compliant classification.

Methods and Materials: For the training and validation of attention U-Net models, data coming from a single 3.0 T scanner was used. For testing, additional data from 1.5 T scanner and data acquired in a different institution with a 3.0 T scanner was utilized. The developed models were used to quantify the amount of FGT and BPE in 80 DCE-MRI examinations and a correlation between these volumetric measures and the classes assigned by radiologists was performed.

Results: To assess the model performance using application-relevant metrics, the correlation between the volumes of breast, FGT, and BPE calculated from ground truth masks and predicted masks was checked. Pearson correlation coefficients ranging from 0.963 ± 0.004 to 0.999 ± 0.001 were achieved. The Spearman correlation coefficient for the quantitative and qualitative assessment, i.e., classification by radiologist, of FGT amounted to 0.70 (p < 0.0001), whereas BPE amounted to 0.37 (p = 0.0006).

Conclusion: Generalizable algorithms for FGT and BPE segmentation were developed and tested. Our results suggest that when assessing FGT, it is sufficient to use volumetric measures alone. However, for the evaluation of BPE, additional models considering voxels' intensity distribution and morphology are required. A standardized assessment of FGT density can rely on volumetric measures, whereas in the case of BPE the volumetric measures constitute, along with voxels' intensity distribution and morphology, an important factor.

Standardized Recommendation for Clinical Actions in Breast Ultrasound: Lesion Detection and Classification using a dCNN

C. Ruppert[1], A. Landsmann[1], K. Borkowski[1], P. Hejduk[1], L. Jungblut[1], T. Schnitzler[2], C. Rossi[1], A. Boss[1], M. Bonmarin[3], A. Ciritsis[1]; [1] USZ – Universitätsspital Zürich, Department of Diagnostic and Interventional Radiology, Zurich, Switzerland, [2] KSA – Kantonsspital Aarau, Department of Radiology, Aarau, Switzerland, [3] ZHAW – Zurich University of Applied Sciences, Zurich, Switzerland

Purpose: This study investigated the potential of a deep convolutional neural network (dCNN) to detect, segment, and classify lesions in breast ultrasound images in accordance with the Breast Imaging Reporting and Data System (BI-RADS).

Methods and Materials: 3278 breast ultrasound images from 1078 patients depicting lesions were annotated according to the BI-RADS standard. A U-Net-based multiclass segmentation network was trained with 2510 images and validated with 768 images. We quantified the network's performance compared to human readers with standard metrics for detection and segmentation and evaluated classification using interrater agreement (Cohen's Kappa) and receiver operating characteristics (ROC) analysis on a test dataset consisting of 154 images.

Results: The dCNN detected and segmented lesions with a precision of 80.7% (70.7%), recall of 63.8% (69.5%), and an intersection over union (IoU) of 75.1% (74.5%) with respect to the annotating radiologist 1 (2). The interrater agreement for lesion classification between the dCNN and radiologist 1 (2) was substantial (moderate) for three classes and almost perfect (substantial) for binary classification. The diagnostic performance of the dCNN to classify detected lesions exhibited an area under the curve (AUC) of 0.962 (95% CI: 0.9151, 1).

Conclusion: In this study, we demonstrated that the performance of the dCNN was comparable to the performance of experienced radiologists. Thus, our dCNN can serve as an observer-independent guide for subsequent clinical procedures. Furthermore, it can contribute to the standardization of lesion classifications preventing unnecessary biopsies.

Learning curve over three years after implementation of an automated breast ultrasound system in an academic radiology department.

E. Nikolova, J. Weber, G. Zanetti, J. Wieler, T. Frauenfelder, M. Marcon; USZ – Universitätsspital Zürich, Zurich, Switzerland

Purpose: To investigate the learning curve after implementation of an automated breast ultrasound system (ABUS) over three years

Methods and Materials: In this IRB-approved retrospective study we included all women undergoing ABUS examination in our department between Oct2015-Oct2018, who have undergone a follow-up of at least 24 months after ABUS examination or with BI-RADS category 4 or 5, who have undergone histological evaluation. Number of additional handheld ultrasound exams (AHHUS) for better definition of an ABUS finding and number of false positive (FP) cases were noted. FP were defined as cases classified BI-RADS 3, 4 or 5 in ABUS who have shown to be benign lesions during follow-up/after biopsy. AHHUSs and FPs were compared in the first 6 months versus second 6 months, yearly over the three years and considering presence/absence of previous ultrasound exam (UE). Chi-square test was applied.

Results: A total of 1223 women (mean age±SD, 51.9±11.0 years) were included: 346(28.3%), 597(48.8%) and 280(22.9%) exams were performed respectively in the year 1,2 and 3. 288/1223(23.5%) had no previous UE. FP cases were 13/45 (28.9%) in the first 6 months and 70/301 (23.3%) in the second 6 months (p=.454). Cases with AHHUS were 16/45 (35.6%) in the first 6 months and 66/301 (21.9%) in the second 6 months (p=.038). Over three years FP were 83/346 (24.0%), 76/597 (12.7%) and 14/280 (5.0%) for year 1,2 and 3 respectively (p<.001). AHHUS were 82/346(23.7%), 57/597(9.5%) and 19/280(6.8%) for year 1,2 and 3, respectively (p<.001). FP and AHHUS were more frequent in women without previous ultrasound exam (FP:21.2% versus12.0%, p<.001 and AHHUS:17.7% versus 11.4%, p<.001).

Conclusion: After ABUS implementation FP and AHHUS gradually reduced, especially after the first year; FP and AHHUS are more frequent in women without previous ultrasound exam.

Quantitative MRI method for characterising endometriomas

U. Shah[1], A. Bagur[1], H. Curwen[1], M. Brady[1,2], S. Collins[1,2], A. Herlihy[1], M. Pansini[1,3]; [1] Perspectum Ltd, Oxford, United Kingdom, [2] University of Oxford, Oxford, United Kingdom, [3] EOC – Ente Ospedaliero Cantonale, IIMSI – Imaging Institute of Southern Switzerland, Lugano, Switzerland

Purpose: Endometriosis, affecting 1 in 10 women, often results in long-term pain and infertility, with an average diagnostic delay of 8 years. Traditionally, laparoscopy has been the gold standard for diagnosis, but recent advances in AI-enhanced medical imaging have led to calls for new imaging methods, such as by the European Society of Human Reproduction and Embryology (ESHRE), to improve early detection. While Transvaginal ultrasound (TVU) is useful, it has limitations in scope, comfort, and requires expert interpretation. MRI, an alternative to TVU, lacks quantitative metrics for pelvic structures. Quantitative multiparametric MRI (qMRI) could improve the characterization of endometriomas, which are non-malignant masses characterized by varying levels of iron and fibrotic content.

Methods and Materials: The aim of this study was to evaluate the utility of qMRI for detecting endometriomas in the female pelvis. The study involved 106 participants undergoing pelvic MRI scans, using LiverMultiScan protocols with adjusted field of view and resolution. Tissue metrics from parametric maps were extracted, including T1 MOLLI, T2*, and PDFF values for identified endometriotic lesions and other tissues.

Results: Results showed that endometriomas have distinct qMRI metrics compared to other pelvic tissues, with PDFF values <5%, T1 values ranging 200-600ms, and T2* values 10-100ms. The study demonstrates that endometriomas exhibit a unique signature when considering these metrics collectively, enabling differentiation from other tissues.

Conclusion: In conclusion, quantitative multiparametric MRI is promising for detecting endometriomas, offering potential improvements in early diagnosis and AI-based imaging for endometriosis management.

MRI of pelvic endometriosis: Evaluation of the mr#Enzian Classification and the Importance of Adenomyosis Subtypes

A. Pausch, V. Filleböck, M. Benli, I. Witzel, A. Hötker; USZ – Universitätsspital Zürich, Zurich, Switzerland

Purpose: This study aimed to investigate the utility of the #Enzian classification in magnetic resonance imaging (MRI) for endometriosis assessment, focusing on inter-reader agreement, diagnostic accuracy, and the correlation of adenomyosis with deep endometriosis (DE).

Methods and Materials: This IRB- approved retrospective single-center study included 412 women who underwent MRI evaluation for endometriosis between February 2017 and June 2022. Two experienced radiologists independently analyzed MRI images using the #Enzian classification and assessed the type of adenomyosis, if any. The surgical #Enzian classification served as the gold standard for evaluating preoperative MRI results. Statistical analysis was performed to assess inter-reader agreement and diagnostic accuracy.

Results: Inter-reader agreement was substantial to excellent (Cohen's kappa 0.75 – 0.96) for most compartments except peritoneal involvement (0.39). The preoperative MRI showed mostly substantial to excellent accuracy (0.84 – 0.98), sensitivity (0.62 – 1.00), specificity (0.87 – 1.00), positive (0.58 – 1.00) and negative predictive values (0.86 – 1.00) for most compartments, except for peritoneal lesions (0.36, 0.17, 1.00, 1.00, 0.26 respectively). A trend with a higher prevalence of concordant DE in women with external compared to those with internal adenomyosis was visible (p = 0.067).

Conclusion: The mr#Enzian showed mostly high inter-reader agreement and diagnostic accuracy for various endometriosis compartments. MRI's role is particularly significant in the context of the current paradigm shift towards medical endometriosis treatment. The inclusion of information about the type of adenomyosis in the mr#Enzian classification could enhance diagnostic accuracy and inform treatment planning.

Efficacy of gadopiclenol in contrast-enhanced MRI of the breast: A post-hoc analysis

C. Kuhl, D. Cereghetti; Universitätsklinikum RWTH Aachen, Department of Diagnostic and Interventional Radiology, Aachen, Germany

Purpose: This post-hoc analysis aimed to evaluate specifically the efficacy of gadopiclenol (Elucirem™, Guerbet), a high relaxivity macrocyclic gadolinium-based contrast agent, in breast contrast-enhanced MRI.

Methods and Materials: The subgroup of patients with breast lesions (N=70) included in the prospective phase III PROMISE study (conducted between 08/2019 and 12/2020) were analyzed. In the PROMISE study, 277 patients underwent two separate MRI examinations of different body regions, one with gadopiclenol (0.05 mmol/kg) and one with gadobutrol (0.1 mmol/kg). Lesion visualization parameters (border delineation, internal morphology and contrast enhancement) were qualitatively assessed by 3 independent blinded readers, through a qualitative scoring (1 to 4) of up to 3 most representative lesions in each patient. Percentage of enhancement (E%) and lesion to background ratio (LBR) were measured. To assess differences between gadopiclenol and gadobutrol in terms of qualitative and quantitative lesion visualization, a generalized linear mixed model with a two-sided paired t-test was used.

Results: For all readers, and all lesion visualization parameters, the difference in mean of scores showed the non-inferiority of gadopiclenol to gadobutrol for breast lesions (lower limit of 95%CI between -0.21 and -0.05, above the non-inferiority margin [-0.35], p <0.0001). Regarding quantitative measurements, E% was higher with gadopiclenol for all 3 readers (least square [LS] mean [standard error (SE)] of the difference: 28.1 [9.4] % to 46.8 [19.6] %, p≤0.02), while there were no significant differences between the two contrast agents for LBR (LS mean of the difference (SE): -1.0 [0.05] to 0.3 [0.04], p≥0.01).

Conclusion: Gadopiclenol at 0.05 mmol/kg is non-inferior to gadobutrol at 0.1 mmol/kg for breast contrast-enhanced MRI. The reduction in gadolinium dose achieved with gadopiclenol may be particularly important in high-risk women undergoing multiple contrast-enhanced MRI examinations for breast cancer screening.

Thermal ablation of benign thyroid nodules in patients with multinodular goiter

L. Szabo[1], C. Zech[2], M. Takes[2], O. Dudeck[1]; [1] Hirslanden Klinik, Zentrum für Mikrotherapie, Zurich, Switzerland, [2] USB – Universitätsspital Basel, Radiologie und Nuklearmedizin, Basel, Switzerland

Purpose: Radiofrequency ablation (RFA) has been shown to be an alternative to surgery in the treatment of benign thyroid nodules, which is best suited to treat uninodular goiter. The purpose of this study was to evaluate the efficacy of RFA in patients with extensive multinodular goiter in whom total thyreoidectomy would normally be indicated.

Methods and Materials: A total of 438 patients with benign thyroid nodules were treated at our institute between 7/2017 and 11/2021 whose data were prospectively recorded in an institutional register. We conducted a subgroup analysis of 40 patients (mean age 60 years ±12.0 years) who presented with at least 3 nodules in bilobar location, were either unwilling or ineligible to undergo total thyroidectomy and had a follow-up interval of at least 2 years. Clinical, laboratory, and ultrasound evaluations were scheduled at baseline, and after 3, 12 months, and yearly afterwards. The number and size of nodules were assessed. Particularly, we evaluated the completeness of ablated nodules and the appearance of new nodules.

Results: In 40 patients a total of 190 nodules (average 4.7 ± 2.1; range 3-11) were treated in 1 (n= 24), 2 (n= 15), or 3 (n=1) sessions. At the most recent follow up time point (average follow up interval of 40 ±13 months) complete ablation rate was 98.4 % (incomplete ablation in 3 of 190 nodules in 3 patients). The mean size reduction of the treated nodules was 85 %. In 7 patients initially small nodules increased in size – only in one of them to such an extent that repeat RFA was required. In another 3 patients a total of 4 new nodules were discovered at follow up of which only one nodule required repeated RFA. In result, in none of the patients thyroid disease could not be controlled by the strategy of RFA and – if needed – repeated RFA.

Conclusion: RFA is a minimally invasive organ- and function preserving technique which can be applied repetitively also in patients with multinodular goiter.

Mild hyperthermia induced by MRgHIFU as adjuvant to radiation therapy in bone metastases: preliminary results of a phase I study

O. Lorton[1], Y. M'rad[1], P.C. Guillemin[1], M. Gau[2], P. Tsoutsou[3], T. Zilli[4], P-A. Poletti[2], R. Salomir[5,6], S. Boudabbous[7,8]; [1] University of Geneva, Faculty of medicine, Geneva, Switzerland, [2] HUG – Hôpitaux universitaires de Genève, Geneva, Switzerland, [3] HUG – Hôpitaux universitaires de Genève, Radiooncology, Geneva, Switzerland, [4] EOC – Ente Ospedaliero Cantonale, IOSI – Oncology Institute of Southern Switzerland, Bellinzona, Switzerland, [5] HUG – Hôpitaux universitaires de Genève, Radiology department, Geneva, Switzerland, [6] University of Geneva, Faculty of Medicine, Geneva, Switzerland, [7] HUG – Hôpitaux universitaires de Genève, Department of Radiology, Geneva, Switzerland, [8] HUG – Hôpitaux universitaires de Genève, Faculty of medicine, Geneva, Switzerland

Purpose: Radiotherapy (RT) is one of the most common palliative treatment for bone metastases (BM). Combination of hyperthermia (HT) and RT may increase the treatment efficiency. We present the first case of a palliative treatment combining MR-guided high intensity focused ultrasound (MRgHIFU) induced local HT and RT in BM.

Methods and Materials: A 48-year-old patient with a cortex discontinuity in a lytic mass in posterior right acetabulum (4.8cm) was indicated for a palliative course of RT. Adjuvant ultrasound was generated by an MR-compatible transducer maintained posteriorly (dimensions 9.3x12.6cm^2, focal 10cm). MRgHIFU targeting in BM used a 3D T1-w sequence acquired with a flexible 18-channel and a 12-element spine coil in a 3T Siemens MR scanner (1.25x1.25 x1.3mm^3). The temperature was monitored in near real-time by merging magnitude images with temperature maps acquired using the proton resonance frequency shift in 3 crossing planes centered on the target (2x2x5mm^3, refresh rate 4.5s). The target temperature was set to 43°C for 30min. The delivered power ranging 19-39W was manually adjusted by the radiologist every 60s. For the RT, the planning target volume including the radiologically visible BM with a 7mm isotropic margin was delineated on a previously acquired CT scan. Just after the HT, the patient received a single 8Gy fraction of palliative RT.

Results: The HT session lasted 90min. The average power was 22W and the HT lasted 30min54s. The 25min between the end of the HT and RT demonstrated the technical feasibility and workflow in this first patient. No adverse events were self-reported. The mean temperature elevation was 6.01°C as compared to prescribed value of 6.00°C inside an effective volume of 1.8x1.4x1.2cm^3.

Conclusion: We report the first adjuvant HT induced by MRgHIFU before RT in one BM. The safe and successful intervention, or absence of adverse events confirmed the technical feasibility.

Bleomycin-Electrosclerotherapy (BEST): A Promising Minimally-Invasive Image Guided Treatment Option for Vascular Malformations in Children

R. Gnannt[1], T. Pfammatter[2], L. Weibel[3], K. Neuhaus[4], M. Theiler[3], C. Kellenberger[1]; [1] Kinderspital Zürich, Department of Diagnostic and Interventional Paediatric Radiology, Zurich, Switzerland, [2] USZ – Universitätsspital Zürich, Department of Diagnostic and Interventional Radiology, Zurich, Switzerland, [3] Kinderspital Zürich, Paediatric Dermatology, Zurich, Switzerland, [4] Kinderspital Zürich, Division of Plastic and Reconstructive Surgery, Zurich, Switzerland_

Purpose: To describe the short-term outcome and side-effects of a promising minimally invasive treatment option for vascular malformations in children.

Methods and Materials: Retrospective review of eight patients between 3 and 16 years of age with a vascular malformation at the head and neck area (n=1), trunk (n=2) and extremities (n=5). All patients underwent BEST either with the hexagonal- or a finger-probe. Prior and after treatment tumor volume was calculated and pain was assessed on a visual analogue scale (VAS) from 0 to 4. Side effects and complications were documented.

Results: Six patients with a venous malformation and two patients with a lymphatic malformation were treated. Mean Bleomycin amount injected during the procedure was 4500IU (range 3000IU to 6000IU). Mean tumor size prior to treatment was 132cm^3 (range 24cm^3 to 375cm^3) and mean pain score 2.3 (range 1 to 4). Mean tumor size after treatment was 87cm^3 (range 15cm^3 to 210cm^3) which corresponds to a volume reduction of 35% after one single treatment cycle. Pain score improved to a mean of 0.5 (range 0 to 2). No Bleomycin typical side-effect and no severe complication were noted. Mean follow-up was 5months (range 3 to 6 months).

Conclusion: BEST seems to be a promising and safe alternative treatment option in children to conventional sclerotherapy, but long-term follow-up is still lacking.

Risk reduction by preoperative transjugular intrahepatic portosystemic shunt (TIPS) placement in cirrhotic patients undergoing surgery

A. Kobe, G. Puippe, T. Pfammatter; USZ – Universitätsspital Zürich, Zurich, Switzerland

Purpose: Cirrhotic patients have a significant risk of decompensation and mortality following surgery. The purpose of this study was to investigate the outcome of patients undergoing TIPS placement upfront surgery.

Methods and Materials: Between 2012 und 2022 14 patients underwent preoperative TIPS (mean age 61.8±9.3years, 79% male). Alcoholic cirrhosis was encountered in seven (50%), viral in two (14%), NAFLD in one (7%) and other etiologies in four patients (29%). Most of the patients presented with esophageal varices (10/14, 71%), a history of upper GI-bleeding (4/14, 29%) and ascites (7/14, 50%). Child A, B and C cirrhosis was found in eight (57%), five (36%) and one patient (7%). Mean MELD score was 10.6±4.

Results: Technical success rate of TIPS was 100% without complications. Pre- and Post-TIPS mean HPVG was 22.6±6.8mmHg and 7.9±3.1mmHg. Mean time between TIPS and surgery was 58±78 days. Major abdominal surgery was performed in nine (64%), hernial repair in three (21%) and endoscopic mucosectomy in two patients (14%). Mean calculated postoperative mortality at 30, 90 and 180 as well as 90 days decompensation risk according to the VOCAL-Penn score was 2.2±2.9%, 4.4±5.8%, 7.1±8.1% and 13.6±10.7%. Encountered mortality rate at 30 and 180 days was 7% (1/14) and 14% (2/14). Only one patient (7%) developed liver decompensation three months after hernial repair.

Conclusion: TIPS placement in cirrhotic patients for preoperative risk reduction is feasible. Postoperative decompensation risk and mortality appear to be rather low.

Safety of Percutaneous Transmesenteric and Transsplenic Access for Portosystemic Shunt Creation in Patients with Portal Vein Obstruction: Single-Center Experience and Review of Literature

D. Steffen, A. Najafi, C. Binkert; KSW – Kantonsspital Winterthur, Winterthur, Switzerland

Purpose: To evaluate the safety of ultrasound-guided percutaneous mesenteric vein access compared to transsplenic portal vein access for portosystemic shunt placement in patients with portal vein obstruction.

Methods and Materials: Eight patients underwent portosystemic shunt creation through either a transsplenic (n = 4) or transmesenteric (n = 4) approach. The superior or inferior mesenteric vein was percutaneously accessed under ultrasound guidance using a 21G needle and a 4F sheath. Hemostasis at the mesenteric access site was achieved with manual compression. For transsplenic access, sheath sizes between 6 and 8F were used and tract embolization with gelfoam was performed.

Results: Portosystemic shunt placement was successful in all patients. While there were no bleeding complications with transmesenteric access, hemorrhagic shock requiring splenic artery embolization occurred in one patient in which the transsplenic approach was used.

Conclusion: Ultrasound-guided mesenteric vein access seems feasible and a valid alternative to the transsplenic access in case of portal vein obstruction.

Endovascular Management of Acquired Uterine Vascular Anomalies

S. Kupfer; USZ – Universitätsspital Zürich, Institute of Diagnostic and Interventional Radiology, Zurich, Switzerland

Purpose: To evaluate clinical presentation, imaging features, embolization techniques and their outcome for acquired uterine vascular anomalies (UVA) related to obstetric events.

Methods and Materials: 11 women (mean age = 34 yrs; range = 20 to 40) who had undergone interventional radiological treatment of UVA's between 2013 and 2023 were retrospectively worked-up. They presented with ongoing vaginal blood losses (n=10) or with a pulsating uterine mass (n=1). Fertilization had been performed by intractyoplasmatic sperm injection in 3/11 w. 7 out of 11 w had delivered healthy babies. C-section had been performed in 1 out these 7 w. The other 4 w had surgical, drug-induced or missed abortions. Postpartal curettage was performed for retained products of conception in 2 w. UVA's were diagnosed by TVUS. The delay between the obstetric event and the embolization ranged from 19 to 193 days (median=49 d). A uterine artery branch pseudoaneurysm was detected by catheter angiography in 5/11 patients, whereas arterio-venous malformation type of lesions were found in 6/11 w. Primary unilateral selective transcatheter or direct glue (Histoacryl®, Braun/D) embolization was performed in 8/11 w. In 3/11 w bilateral gelatin sponge slurry or calibrated trisacryl gelatin spheres were utilized as embolic agents.

Results: Primary clinical embolization success was achieved without complications in 10/11 interventions. The only failed embolization had been performed with gelatin sponge slurry. Re-embolization with glue was successful. Long-term FU information was available in 9/11 women. The pregnancy rate in that group was 7/9 with a birth rate of 5/9.

Conclusion: Embolization of acquired UVAs, and in particular by means of glue, is an effective and safe treatment. The post-interventional pregnancy and live birth rates are within the range of the general population.

Induced pain on interventional Radiology: A large cohort with focus on epidemiologic and multiparametric analyses on CT interventions under local anesthesia

S. Boudabbous, H. Bouredoucen, D. Ferreira Branco, P. Challande, P-A. Poletti; HUG – Hôpitaux universitaires de Genève, Geneva, Switzerland

Purpose: Resources on anesthesia are limited in radiologic centers. Local anesthesia is used in majority of cases with more and more awareness of intensity of pain induced by procedures under imaging guiding. The purpose of this study is to analyze parameters interfering with induced pain with focus on CT guided interventions.

Methods and Materials: A register of induced pain collected for 6 years (2017-2022) on Radiology section on Geneva University Hospital was analyzed (EC n°: 2017-02326). Only interventions under local anesthesia on CT sector were collected and subdivided on soft tissue (abdomen, pelvis, thorax) biopsies and drainage and bone and limb soft tissue interventions (including biopsies and infiltrations). Age (≤40, 40-64 and > 64 years old), sex, size of material (+/- 10 French for drainage and +/- 14 Gauge for biopsy) were correlated to the severity of pain measured on analogic visual scale (AVS). Three categories were defined: 0-3: mild pain, 4-6: moderate pain and 7-10. Severe pain.

Results: A total of consecutive 25436 interventions were available for analyses. 17.6 % was excluded as pain data was not curried out. 2252 interventions were performed under CT guiding and from them 1858 (82.50%) under local anesthesia. Interventions included: 34.12% of abdomino-pelvic interventions, 24.46% soft tissue and bone interventions and 29.08 % thorax interventions. Regarding abdomino-pelvic and thoracic interventions, severe pain (15.05%) was correlated with sex (p=0.016), age (p= 0.0039) and material size (p≤0.00001). For limbs soft tissue and bone interventions, severe pain (10.1%) was correlated with age (p ≤0.05), sex (p= 0.001) and for material size only needles > 12G were used in this category.

Conclusion: Severity of induced pain under local anesthesia is observed on a minority of cases (10-15%) for CT guided procedures with correlation with sex, age, and size of material. This study on Radiologic center allows an adjustment and an objective request of anesthetic resources.

Postinterventional Patient Comfort After Uterine Artery Embolization and Superior Hypogastric Nerve Block

D. Steffen, A. Najafi, C. Binkert; KSW – Kantonsspital Winterthur, Winterthur, Switzerland

Purpose: To evaluate the duration and effect of superior hypogastric nerve block (SHNB) with ropivacaine and clonidine on postinterventional pain levels and opioid requirements in patients undergoing uterine artery embolization.

Methods and Materials: Postinterventional pain levels (numeric rating scale, NRS 0-10) and opioid doses were retrospectively analyzed in 53 patients undergoing transfemoral uterine artery embolization and intraprocedural superior hypogastric nerve block during 24 h. A mixture of 150 mg of ropivacaine and 150 µg of clonidine was used for the block.

Results: Postinterventional pain averaged between 1.4 and 2.0 during the first 9 h, after which a small but significant increase was observed (NRS 1.7 ± 1.6 vs. NRS 2.6 ± 2.2, p < 0.001). 70% of patients did not exceed a tolerable pain threshold of NRS 4 during the first 9 h after the intervention. Thirty-three patients (62%) did not require any opioid medication. Mean iv morphine dose was 3.1 ± 4.7 mg, whereas 71% of opioid doses were administered after 9 h.

Conclusion: Superior hypogastric nerve block using a mixture of ropivacaine and clonidine provides good pain relief for 9 h after uterine artery embolization requiring only very low amounts of additional opioids.

Can ChatGPT reduce the time required for administration/ documentation in interventional radiology?

W.A. Bosbach[1], J.F. Senge[2,3], M.T. McMurray[1], F. Haupt[1], C. Beisbart[4,5], P.S. Breiding[6], K. Daneshvar[1], A. Komarek[1], G. Nöldge[1], F. Mosler[1]; [1] Inselspital – Universitätsspital Bern, DIPR – Department of Diagnostic, Interventional and Pediatric Radiology, Bern, Switzerland, [2] University of Bremen, Department of Mathematics and Computer Science, Bremen, Germany, [3] Max-Planck Dioscuri Centre for Topological Data Analysis, Warsaw, Poland, [4] University of Bern, Institute of Philosophy, Bern, Switzerland, [5] University of Bern, Center for Artificial Intelligence in Medicine, Bern, Switzerland, [6] Inselspital – Universitätsspital Bern, University Institute of Diagnostic and Interventional Neuroradiology, Bern, Switzerland

Purpose: All stakeholders of interventional radiology would benefit from a reduction of resources required for the necessary administration and documentation processes. This is true from the perspective of patients, doctors, and also hospital administrators. Chatbots based upon large language models, including ChatGPT, might provide relevant future AI solutions for this.

Methods and Materials: We defined a set of cases for peripherally inserted central catheter line insertion, based on the current RSNA template. ChatGPT was tasked with writing adequate radiology reports. Output texts were rated by human radiologists and compared using a similarity analysis.

Results: Overall, the output texts generated by ChatGPT received a positive review in the score card assessment by human radiologists. A need for edits before sending was still identified by the reviewers. The reviewers did not consider the output texts as clearly identifiable as AI-produced.

Conclusion: With potentially increasing economic pressure on the healthcare system, large language models might increase the efficiency of work in radiology without compromising central variables such as quality of treatment and patient outcome. It remains to be seen to what extent they will find their way into clinical practice. If proven to be more economical, questions about trust and decision making in human-machine hybrid processes will have to be answered.

Application of post-mortem MRI (PMMRI) in the forensic routine work.

C. Egger[1], C. Bruguier[2,3], V. Magnin[2], S. Grabherr[4,2], P. Genet[2];
[1] _CHUV – Centre Hospitalier Universitaire Vaudois, Unit of Forensic Medicine and Imaging, University Center of Legal Medicine Lausanne, Geneva, Switzerland,_ [2] _University Center of Legal Medicine of Lausanne-Geneva, Unit of Forensic Imaging and Anthropology, Lausanne, Switzerland,_ [3] _CHUV - Centre Hospitalier Universitaire Vaudois, Department of Diagnostic and Interventional Radiology, Lausanne, Switzerland,_ [4] _University Center of Legal Medicine of Lausanne-Geneva, Unit of Forensic Medicine and Imaging, Geneva, Switzerland_

Purpose: To present indications and contra-indications of post-mortem MRI (PMMRI) in the forensic routine work and show its difficulties and possibilities.

Methods and Materials: Forensic imaging is already well established in many medico-legal centres, especially post-mortem CT (PMCT), which is routinely used. In contrast, PMMRI is not yet used standardly, although it can be useful in treating forensic cases, permitting an optimal analysis of soft tissues and CNS. To best use PMMRI, its advantages compared to other radiological techniques and autopsy, as its difficulties and contraindications in a forensic setting must been known.

At our institute, PMMRI has already been integrated in the routine work. Our protocols are based on clinical-radiological protocols which are adapted to post-mortem conditions.

Results: We determined that PMMRI is of great help in cases where brain analysis is crucial, as e.g. in inflammatory diseases or ischaemic/hypoxic lesions. It's a big advantage in trauma cases of the spine, as fractures which are difficult to detect by PMCT can be identified as also lesions of the spinal cord. Moreover, it permits a better evaluation of the organs/soft tissues compared to PMCT, which is fundamental in paediatric deaths. In cases of strangulation/hanging it allows to find haemorrhagic infiltrations and fractures. In sudden cardiac deaths signal abnormalities in the myocardium can be visible, which can help the forensic pathologist to target samples.

Conclusion: PMMRI is an important asset to forensic cases, as alterations of tissues/structures can be visible by signal changes, which aren't always visible macroscopically at autopsy. It prepares the forensic pathologist for autopsy, guides the samples and can be relevant for the determination of further examinations. However, it cannot be used the same way as in clinical radiology, certain parameters must be adapted, and contraindications must be known.

Investigating the role of peripheral blood mononuclear cells (PBMCs) in gadolinium deposition in the brain

D. Parakkattel[1,2], N. Ruprecht[3,2], H. von Tengg-Kobligk[3,2], B. Engelhardt[4], J. Heverhagen[5,6]; [1] _Inselspital – Universitätsspital Bern, Department of Diagnostic, Interventional, and Pediatric Radiology, Bern, Switzerland,_ [2] _University of Bern, Department of BioMedical Research, Bern, Switzerland,_ [3] _Inselspital – Universitätsspital Bern, DIPR - Department of Diagnostic, Interventional and Pediatric Radiology, Bern, Switzerland,_ [4] _University of Bern, Theodor Kocher Institute, Bern, Switzerland,_ [5] _Inselspital – Universitätsspital Bern, Department of Diagnostic, Interventional and Paediatric Radiology, Bern, Switzerland,_ [6] _Inselspital – Universitätsspital Bern, Department of BioMedical Research, Bern, Switzerland_

Purpose: This study is aimed at understanding gadolinium (Gd) deposition in the brain by investigating gadolinium based contrast agent (GBCA) permeability across the blood-brain barrier (BBB) and how GBCA uptake affects immune cell migration across the BBB post GBCA exposure.

Methods and Materials: As an in vitro model of the human BBB, we used human induced pluripotent stem cells (hiPSCs), and differentiated those employing the extended endothelial cell culture method (EECM) to human brain microvascular endothelial cell (BMEC) like cells. EECM-BMEC-like cells show good barrier properties and a mature immune phenotype. The excellent barrier properties of EECM-BMEC-like cells were confirmed by our observation that EECM-BMEC-like cells did not allow for diffusion of any of the GBCAs - Dotarem, ProHance, Gadovist and Omniscan- across the cellular monolayer.

Results: According to our previous observations, we observed that peripheral blood mononuclear cells (PBMCs) take up GBCAs. Using flow cytometry, we found that GBCA uptake by PBMCs does not affect cell surface expression of adhesion molecules. Next, we investigated if GBCA uptake would affect the extravasation of PBMCs across EECM-BMECs under physiological flow. To this end, we observed the dynamic behaviour of PBMCs loaded or not with GBCA on EECM-BMECs under physiological flow by in vitro live cell imaging. We did not observe any effect of GBCA uptake on the arrest and post-arrest crawling or probing of PBMCs on EECM-BMECs under flow _in vitro_.

Conclusion: Our study therefore confirms that GBCA cannot freely pass the BBB. However, PBMCs can take up GBCA and migrate across the BBB in vitro. This suggests that GBCA loaded PBMCs cross the brain barriers in vivo and could contribute to the permanent deposition of GBCA in the brain.

Evaluation of 3D MRI for early detection of periapical lesions and associated maxillary sinus pathologies

E. Burian[1], M. Probst[2], A. Lutz[3], M. Folwaczny[4], G. Andreisek[3]; [1] Kantonsspital Frauenfeld, Department of Nuclear Medicine, Frauenfeld, Switzerland, [2] MRI TUM – School of Medicine & Klinikum rechts der Isar, Munich, Germany, [3] Kantonsspital Frauenfeld, Department of Radiology, Frauenfeld, Switzerland, [4] LMU München, Department of Restorative Dentistry and Periodontology, Munich, Germany

Purpose: To detect and evaluate early signs of periapical lesions and associated mucosa thickening in the maxillary sinus using MRI based on a 3D short-tau-inversion-recovery (STIR) sequence compared to conventional panoramic radiography (OPT) and dental radiographs (DR).

Methods and Materials: Patients with clinical evidence of periodontal disease were enrolled prospectively and received OPT as well as MRI of the viscerocranium including a 3D-STIR sequence. The MRI sequences were assessed for the occurrence and extent of bone changes associated with periapical lesions including: bone edema, periradicular cysts, and associated mucosa thickening. OPTs and dental radiographs, if available, were assessed for corresponding periapical radiolucencies using the periapical index (PAI).

Results: In total, 232 teeth of 37 patients (mean age 62±13.9 years, 18 women) were assessed. In 69 cases reactive bone edema was detected on MRI with corresponding radiolucency according to OPT. In 105 cases edema was detected without corresponding radiolucency on OPT. The overall extent of edema measured on MRI was significantly larger compared to the radiolucency on OPT (p=0.01). The overall PAI score was significantly higher on MRI compared to conventional OPT (p=0.02).
In 16 patients, 21 maxillary sinuses were affected with associated periapical lesions of premolars and molars (58 teeth). Using the STIR sequence, a significant association of PAI score > 1 and the presence of mucosal swelling in the maxillary sinus was detected (p=0.03).

Conclusion: Early detection and assessment of bone changes of periapical lesions using MRI was feasible while the extent of bone edema measured on MRI exceeded the radiolucencies measured on OPT. Radiologically concealed maxillary mucositis could be visualized using STIR imaging.
This may allow for initial disease detection and primary prevention.

Internal carotid artery dissection due to Eagle-Syndrome: Can the toothpick in your neck cause a stroke?

T. Klail[1], L. Sachs[2], L. Panos[3], O.Y. Urban[3], T. Siller[3], W. Almiri[1], S. Pilgram-Pastor[1], R. Giger[4], F. Wagner[1]; [1] Inselspital – Universitätsspital Bern, Universitätsinstitut für Diagnostische und Interventionelle Neuroradiologie, Bern, Switzerland, [2] Inselspital – Universitätsspital Bern, Universitätsklinik für Hals-, Nasen- und Ohrenkrankheiten (HNO), Bern, Switzerland, [3] Inselspital – Universitätsspital Bern, Universitätsklinik für Neurologie, Bern, Switzerland, [4] Inselspital – Universitätsspital Bern, Universitätsklinik für Hals-, Nasen- und Ohrenkrankheiten, Bern, Switzerland

Purpose: Internal carotid artery dissection is a common cause of stroke, especially in patients under the age of 50. It is a complex vascular condition, and while the etiology is well understood in many cases, a significant number of patients present with what is termed a "spontaneous dissection". This term underscores the fact that, despite our knowledge of certain predisposing conditions, there remains a subset of individuals for whom the exact cause of carotid artery dissection is unknown. Eagle syndrome encompasses a range of symptoms resulting from the compression of adjacent structures by an elongated styloid process of the temporal bone, with a typical criterion for elongation being a length exceeding 3 cm. This condition affects approximately 4% of the population and its clinical manifestations vary according to the structures being compressed.

Methods and Materials: We intend to offer a comprehensive overview of the existing literature pertaining to this matter and provide an intricate account of the diagnostic and treatment modalities employed for the patients under our care, with the primary aim of enhancing awareness of this diagnosis among physicians.

Results: Recent research has unveiled a noteworthy association between the contact of the styloid process tip and the carotid artery vessel wall, potentially serving as a precipitating factor in cervical segment carotid artery dissection. In our institute, ongoing investigations have also identified several patients with spontaneous or traumatic carotid artery dissections related to Eagle-Syndrome, prompting us to consider the possibility of underdiagnosis of Eagle-Syndrome as potential cause of an internal carotid artery dissection.

Conclusion: In conclusion, Eagle Syndrome emerges as a plausible causative factor in internal carotid artery dissection. In cases where the etiology of the dissection remains unclear, especially in emergency scenarios, it is imperative to include an assessment of the stylohyoid process.

A63

Detection of intracranial hemorrhage on unenhanced cerebral CT: performance of an AI-based software in emergency settings

Q. Pedrini, C. Chrysostomou, R. Meyer, P-A. Poletti, A. Platon;
HUG – Hôpitaux universitaires de Genève, Geneva, Switzerland

Purpose: To evaluate the performance of a commercial artificial intelligence (AI) software in detecting intracranial hemorrhage (ICH) in emergency settings.

Methods and Materials: All consecutive unenhanced cerebral CT-scans performed over a 3-months period of time in emergency, initially interpreted by the radiology residents on-call and subsequently verified and approved by a board-certified radiologist, were analyzed by an AI software for the presence of ICH. Images labelled as positive by the AI software were stored in a separate PACS partition and were unavailable to the radiologist for the case reading. We assessed the diagnostic performance of the AI software and of the radiology residents in detecting ICH. The reference standard was the final report of the board-certified radiologist.

Results: 2153 CT-scans were analyzed; the prevalence of ICH was 15.2%. Sensitivity was 83.8% (79.5-87.4 CI) for the AI software and 96.3% (93.7-97.9 CI) for the residents; specificity was 94.2% (93.1-95.2 CI) for the AI software and of 99.4% (98.9-99.7 CI) for the residents, respectively.
The sensitivity for detecting ICH was 97.7 % for the AI and 98.5% for the residents when CT examinations displayed an association of multiple hemorrhagic types. The sensitivity for detecting ICH was 95.2% for AI and 98.4% for radiology residents in the presence of multiples ICH sites.

Conclusion: Radiology residents demonstrated a better performance in detecting ICH compared to the AI software. The AI exhibits very good diagnostic performance in identifying ICH, particularly in the presence of multiple hemorrhagic sites or an association of multiple hemorrhagic types.

A13

Dual-Energy CT of Acute Bowel Ischemia – Influence on diagnostic accuracy and reader confidence

M. Oberparleiter, J. Vosshenrich, H-C. Breit, B. Friebe, D. Harder, D. Boll, C. Zech, M. Obmann; USB - Universitätsspital Basel, Clinic for Radiology and Nuclear Medicine, Basel, Switzerland

Purpose: Initial experimental studies suggested Dual-Energy CT (DECT) to be a powerful tool to increase diagnostic accuracy in diagnosing acute mesenteric ischemia. However, current guidelines do not recommend the usage of DECT for suspected acute mesenteric ischemia due to a lack of clinical studies. This study aimed to investigate the diagnostic accuracy, reader confidence and reading time of DECT compared to conventional CT.

Methods and Materials: Twenty-five patients with surgically proven acute mesenteric ischemia and 25 gender- and age-matched controls who underwent arterial and portal venous phase DECT of the abdomen were included in this retrospective study. Two fellowship-trained abdominal radiologists evaluated all cases with and without using DECT-derived virtual non-contrast images and iodine maps for mesenteric ischemia. Reading time was recorded, and diagnostic confidence was rated on a 10-point Likert scale. The inter-reader agreement was assessed using Cohen's kappa. Sensitivity and specificity were compared using McNemar's test, reading time and reader confidence with the Wilcoxon rank-sum test.

Results: Inter-reader agreement was good (κ = 0.72). Sensitivity and specificity for diagnosing acute mesenteric ischemia were 78% and 100%, respectively, using conventional image data alone. Utilizing additional DECT data, sensitivity was significantly higher at 94% (p = 0.02), while specificity remained at 100% (p = 1.00). Diagnostic confidence increased significantly from 8 (IQR, 7-10) to 9 (IQR, 8-10) (p < 0.01). Mean reading time per case increased significantly from 154 to 183s (p = 0.02) using additional DECT images.

Conclusion: DECT should be considered when examining scans for suspected acute mesenteric ischemia, using supplementary iodine maps and virtual-non-contrast images, as DECT increased reader diagnostic accuracy and confidence for mesenteric ischemia, with only a moderate increase in reading time.

A43

Revised 2022 ACC/AHA Guidelines: Impact on Uncomplicated Type B Aortic Dissection Management

M. Polacin[1], G. Mistelbauer[2], D. Mastrodicasa[2], A. Sriprachyakul[2], V. Hinostroza[2], K. Bäumler[2], D. Craig Miller[2], D. Fleischmann[2];
[1] USZ – Universitätsspital Zürich, Institute of Diagnostic and Interventional Radiology, Zurich, Switzerland, [2] Stanford University School of Medicine, Department of Radiology, Stanford, United States

Purpose: This study aims to evaluate the impact of the 2022 ACC/AHA aortic disease guidelines on the management of uncomplicated Type B aortic dissection (TBAD), with a focus on the frequency of high-risk imaging features as per the new guidelines and the actual rate of interventions.

Methods and Materials: A retrospective cohort analysis was conducted on 60 patients with uncomplicated TBAD between 2013-2017. We specifically assessed the prevalence of high-risk imaging features defined by the guidelines: aortic diameter > 40 mm, false lumen diameter > 20 mm, entry tear > 10 mm, entry tear at the lesser aortic curvature, imaging-only evidence of malperfusion, aortic growth and hemorrhagic pleural effusion.

Results: Of the 60 patients with uncomplicated TBAD, 48 (80%) had at least one high-risk imaging feature on initial imaging. At a 2-year follow-up, 7 additional patients without initial high-risk imaging features showed significant aortic growth, totaling 55 (92%) patients potentially benefiting from early TEVAR. However, only 15 patients (27%) eventually required TEVAR or other interventions due to secondary complications.

Conclusion: The study indicates a substantial increase in the number of patients eligible for preemptive TEVAR under the revised 2022 ACC/AHA guidelines. However, the actual clinical benefit of this approach is uncertain, given the gap between guideline recommendations and clinical practice, and the limited evidence on the predictive value of high-risk features. This necessitates a prospective trial to better understand the benefits of early TEVAR and to refine the role of imaging in risk stratification.

A14

Implementing AI for Fracture Detection: Accuracy and Impact Assessment

A. Dumitrescu[1], C. Buitrago Tellez[2]; [1] soH – Kantonsspital Olten, Olten, Switzerland, [2] soH – Kantonsspital Olten, Solothurn, Switzerland

Purpose: This study aims to assess the impact of AI analysis tools on the radiologist's workflow in the context of radiographic imaging used to rule out traumatic bone lesions. The primary objectives include evaluating the accuracy and usability of these tools in fracture detection and understanding their influence on the radiologist's workflow. The findings can serve as guidance on how to evaluate, select, and implement AI tools for medical imaging.

Methods and Materials: Bone radiographs from our institution underwent fracture evaluation using two AI algorithms over a two-month period. AI assessments integrated into PACS were accessible to radiologists during report dictation. Radiologists completed a feedback form within PACS, assessing AI accuracy. The resulting data were categorized and used to calculate performance metrics (sensitivity, specificity, PPV, NPV, F1 Score, and Youden's Index). Perceived helpfulness was also evaluated using qualitative questionnaire-based assessment among participating radiologists.

Results: The first AI tool demonstrated a sensitivity of ~0.582, specificity of ~0.815, PPV of ~0.891, NPV of ~0.429, an F1 Score of ~0.696, and Youden's Index of ~0.397. The second algorithm showed a sensitivity of ~0.376, specificity of ~0.838, PPV of ~0.844, NPV of ~0.407, an F1 Score of ~0.518, and Youden's Index of ~0.214. Radiologists' questionnaire responses indicated positive perceptions for both AI tools regarding integration and perceived usefulness.

Conclusion: The introduction of AI analysis tools proved to be an easily implementable and beneficial addition to the radiologist's workflow. Despite variations in accuracy, both algorithms demonstrated a positive impact. The insights gained from this study provide a framework for algorithm evaluation and selection when integrating AI into medical imaging workflows.

A78

Comparison of two different AI solution in the detection of fractures

S. Sintzoff, O. Segall, M. Shin; ImageRive – Unilabs company, Geneva, Switzerland

Purpose: To evaluate the accuracy of 2 different AI software for the detection of fractures.

Methods and Materials: A prospective study was performed, including 110 consecutive cases of CR performed for post-traumatic skeletal indications, processed in real-time by AI solutions 1 & 2. The gold standard for the positive diagnosis was the interpretation of the CR by a senior MSK radiologist, confirmed by the follow-up and additional imaging when performed.

Results: For solution 1, we observed a sensitivity of 96,4%, specificity of 75.6%, negative predictive value of 98.4%, positive predictive value of 57.4% and accuracy of 80.9%. For AI solution 2, we had a sensitivity of 75%, specificity of 93.9%, negative predictive value of 91.7%, positive predictive value of 80.8% and accuracy of 89.1%. These results show that the performance of AI solutions designed for the detection of fractures may be quite different. In our situation, as solution 1 offered the highest sensitivity, it was preferred as and aid for the first reading by the emergency room team. In other settings, solution 2 could be preferred, if the goal is to obtain the best accuracy, specificity, as a second reading tool in a teaching environment for instance.

Conclusion: This study shows that the performance of AI solutions designed for the fracture detection can be quite different in a clinical setting. Based on our results, we recommend that the choice of an AI fracture detection solution be based on a real-time simultaneous trial of at least two competitors to define which is best suited to local clinical specifications.

A29

CT for Acute Pulmonary Embolism: Diagnostic Performance of an AI algorithm in an Academic Emergency Department

P.C. Chrysostomou, R. Meyer, P-A. Poletti, A. Platon; HUG – Hôpitaux universitaires de Genève, Geneva, Switzerland

Purpose: To compare the diagnostic performance of a commercial artificial intelligence (AI) software and of radiology residents in diagnosing acute pulmonary embolism (PE) in the emergency department.

Methods and Materials: All consecutive pulmonary CT-scans performed in emergency for PE, over a 3 month period, initially interpreted by the radiology residents on-call and subsequently approved and verified by the attending radiologists, were also analysed by a commercially available AI software for the presence of PE. Readings of the images by the attending radiologists, residents and the AI software were independent of each other. The results of the AI software were unavailable to the radiologists during the study period. The reference standard was the diagnosis of presence or absence of PE on the final report submitted by the attending radiologist.

Results: We included 624 CT-scans, of which 83 were considered positive for PE by the attending radiologist (prevalence 13.3%), 518 were negative, and 23 were indeterminate (the latter were excluded from further analysis). Sensitivity was 89.2% for the AI system and 97.2% for the residents. Specificity was 99% for the AI system and 99.2% for the residents. Agreement between the AI system and the residents was high (Cohen's kappa 0.86).

Conclusion: Both the AI software and the radiology residents performed well at diagnosing PE in the emergency room. The specificity was near perfect for both, but sensitivity was higher for radiology residents. In our emergency setting, radiology residents outperformed an AI based software for detecting acute PE.

Dynamic Contrast Magnetic Resonance Lymphangiography (DCMRL) in Neonates and Children: Categorizing imaging findings to predict outcome and to guide therapy

R. Gnannt[1], H. Dave[2], T. Pfammatter[3], E. Kühlwein[4], U. Moehrlen[5], C. Kellenberger[1]; [1] Kinderspital Zürich, Department of Diagnostic and Interventional Paediatric Radiology, Zurich, Switzerland, [2] Kinderspital Zürich, Paediatric Cardiac Surgery, Zurich, Switzerland, [3] USZ – Universitätsspital Zürich, Department of Diagnostic and Interventional Radiology, Zurich, Switzerland, [4] Kinderspital Zürich, Paediatric Intensive Care Unit, Zurich, Switzerland, [5] Kinderspital Zürich, Paediatric Surgery, Zurich, Switzerland

Purpose: To describe the technique and report our initial experience with the use of Dynamic intranodal contrast-enhanced magnetic resonance lymphangiography (DCMRL) in children.
Methods and Materials: Retrospective review of all patients between 0 and 18 years of age who underwent a DCMRL at our institution between January 2018 and December 2022. Needle placement into lymph nodes in each groin was performed by ultrasound guidance under general anesthesia. Gadolinium contrast was injected to acquire dynamic imaging. Technical success was defined as contrast enhancement of the thoracic duct. Patients were categorized into Pulmonary Lymphatic Perfusion Syndrome (PLPS), Central Lymphatic Flow Disorder (CLFD), and surgical leaks. Clinical outcome and therapy options were noted.
Results: 20 patients (7 females) were included in the analysis. Mean age at date of scan was 2yrs and 1 month (range 11d – 9yrs). Indication for DCMRL was congenital chylothorax (n=6), post-cardiac surgery chylothorax (n=12), and plastic bronchitis (n=2). 6 patients showed a lymphatic flow pattern of a PLPS, 7 patients of a CLFD, one patient a surgical complication, and 5 showed a normal flow pattern with anatomical variants. In one patient, the thoracic duct remained unenhanced (95% technical success rate). Additional Lipiodol embolization to close lymphatic leakage was used in 2 patients.
All 6 patients with a PLPS survived, 2 out of 6 with Lipiodol embolization. On the other hand, 4 out of 7 patients with a CLFD died, two of them despite surgical pleurodesis. Mean follow-up was 1 year and 8 months (range 4 months – 5 years).
Conclusion: DCMRL has evolved as a useful diagnostic tool for neonatal or post-operative high output chylothoraces. It may guide therapeutic decisions including Lipiodol based closure of lymphatic leakage as well to predict outcome.

Accelerated cardiac MRI using deep learning for volumetric cardiac assessment in children

M. Köchli[1], F. Callaghan[2], B. Burkhardt[3], M. Lohézic[4], X. Zhu[4], B. Rücker[3], E. Valsangiacomo Buechel[3], C. Kellenberger[1], J. Geiger[1]; [1] Kinderspital Zürich, Department of Diagnostic Imaging, Zurich, Switzerland, [2] Kinderspital Zürich, Center for MR research, Zurich, Switzerland, [3] Kinderspital Zürich, Department of Pediatric Cardiology, Zurich, Switzerland, [4] GE HealthCare, Zurich, Switzerland

Purpose: To assess the diagnostic performance of accelerated 3RR cine MRI sequences using deep learning (DL) reconstruction compared with standard two-dimensional (2D) cine balanced steady-state free precession (bSSFP) sequences for cardiac volumetry.
Methods and Materials: 29 consecutive patients (11±5 years) undergoing cardiac MRI were scanned with a short axis cine bSSFP and an accelerated DL cine 3RR acquisition on a 1.5 T scanner. Volumetric analysis was performed (semi-)automatically in both datasets retrospectively by two readers with a cloud-based postprocessing software. Two experienced readers visually assessed image quality using a four-point grading scale. Scan times and image quality were compared using a Wilcoxon rank sum test. Volumetrics were assessed with linear regression and Bland-Altmann analysis, measurement agreement with intraclass correlation coefficient (ICC).
Results: Mean acquisition time for a short axis stack was significantly shorter for the DL cine compared with the 2D cine sequence (45.5±13.8 s vs. 218.3±44.8 s; $p<0.001$). No significant differences in biventricular volumetric analysis were found. Left ventricular (LV) mass was increased in the DL cine compared with the 2D cine sequence (71.4±33.1 g vs. 69.9±32.5 g; $p<0.05$). All volumetric measurements had excellent agreement with ICC>0.9 except for ejection fraction (LVEF=0.81, RVEF=0.73). Image quality was decreased for end-diastolic and end-systolic contours, papillary muscles and valve depiction in the DL cine images (3.5±0.4 vs. 2.9±0.5; $p<0.05$).
Conclusion: DL cine volumetrics did not differ significantly from 2D cine results except for LV mass that was slightly overestimated with cine DL. Image quality rating of DL cine images was inferior to 2D cine images. DL cine may enable more patient comfort and decrease the need for anaesthesia by the significant reduction of scan time.

Implementation of Structured Reporting in Pediatric Radiology for a use case in Liver Transplantation Follow-up: Feasibility and Technical Challenges

C-M. Bitter, E. Katirtzidou, M. Laurent, P. Trolliard, P-A. Poletti, S. Toso; HUG – Hôpitaux universitaires de Genève, Geneva, Switzerland

Purpose: We assessed the feasibility and the technical challenges of initiating structured reporting with data mining capacity in our pediatric radiology department.
Methods and Materials: A multidisciplinary team was created including pediatric radiologists, informatics programmers, secretaries and department administration. Liver transplantation follow-up was defined as the use case. Key elements of the radiology report were identified in conjunction with known radiologic criteria and validated with our surgical and gastroenterological counterparts. With our programmers a "point and click" report was generated. This report was trialed within the team and modified as needed. The report was integrated into our RIS system and tested in clinical practice.
Results: A total of 10 days was necessary from generation of the team to creation of a workable, data-minable report. Testing demonstrated easy-of-use in the clinical setting. Report appearance was unchanged compared to existing reports. All data was extractable to excel database with ease. The processes and steps are further outlined. Technical challenges included clear communication amongst various team members
Conclusion: Though structured reporting appears to be very opaque and complicated, with correct and relatively accessible resources, the creation of structured reporting templates was relatively easy and well-integrated into everyday practice.

Assessing O-RADS utility in pediatric ovarian masses for effective imaging classification and histopathological correlation

E. Katirtzidou, B.M. Cipullo, M. Laurent, S. Toso; HUG – Hôpitaux universitaires de Genève, Geneva, Switzerland

Purpose: Ovarian masses are common tumours in paediatric population. Although there is data available on imaging characteristics of these masses in children, no standard imaging classification system. The Ovarian-Adnexal Reporting and Data System Ultrasound (O-RADS) classification system currently used for adults, has not been extensively applied and tested in children and adolescents.

Methods and Materials: In this retrospective mono-centric study, all children with ovarian tumours were included if they had undergone US. ORADs classification was applied to all US imaging and compared to radiological reports. The clinical radiologic diagnosis, ORADS diagnosis and histologic findings were compared, and agreement evaluated with the Kappa coefficient of agreement.

Results: A cohort of 35 female children (mean age 12.4 years ± 3years) with ovarian masses detected on ultrasound were identified. Of these 24 also had MRI. Among 35 patients, 21 had surgery (ORADS 2, 4 or 5) and in 19 cases a histopathological result was obtained. In these preliminary findings, among the 35 ovarian masses evaluated with ORADS, 2 were classified ORADS 1 (5.7%), 28 ORADS 2 (80%), 3 ORADS 4 (8.6%) and 2 ORADS 5 (5.7%). Of the 16 patients that did not have histology, all were considered ORADS 2. In our sample, all diagnoses between radiologist and ORADS were concordant (kappa 1.00). In all but one cases, the histopathological result was concordant with the ORADS classification/radiologic diagnosis. In one case, an ovarian mass classified as ORADS 4 (due to solid appearance and moderate flow in colour Doppler), was proved to be a dermoid cyst (Kappa 0.912).

Conclusion: Our preliminary study demonstrates an excellent correlation between ORADS ultrasound imaging classification, radiological assessment and histopathological results. Future prospective studies with larger cohorts are warranted to validate these findings, thereby optimizing clinical management and treatment decisions.

Preliminary Analysis of Ultrasound Derived Fat Fraction in Comparison to MR Derived Fat Fraction in Children

E. Katirtzidou, M. Laurent, S. Hanquinet, S. Toso; HUG – Hôpitaux universitaires de Genève, Geneva, Switzerland

Purpose: With the increase in obesity in children, measuring steatosis in the liver is becoming more important in prevention and lifestyle modification. Though liver biopsy was considered the gold standard for identify fatty liver, MRI has been found to be an adequate non-invasive adjunct modality for this diagnosis. However, MRI has limited accessibility, is expensive and is a long exam for some children. Adult research suggests the use of ultrasound to measure fatty liver, but little pediatric literature exists.

Methods and Materials: Children undergoing abdominal MRI for non liver indications were invited to participate in an additional ultrasound for UDFF and pSWE measurements. The mean UDFF and pSWE measurements were compared to the mean MR derived fat fraction (MRDFF).

Results: Ten children initially underwent both an abdominal MRI and ultrasound. Intra-observer measurements. A paired t-test was used to compare the mean UDFF to MRDFF in each participant. A kappa correlation demonstrated good reliability between UDFF and MR measurements of fat.

Conclusion: In our preliminary study, ultrasound derived fat fraction appears to be positively correlated with MR based fat fraction in normal children.

Association Between Radiographic Bubbly "Faecal Pattern" and Sonographic Findings in Suspected Necrotizing Enterocolitis

M. Schmidt, I. Altmann, C. Kellenberger; Kinderspital Zürich, Zurich, Switzerland

Purpose: In 1984, Patriquin et al. have introduced a bubbly "faecal pattern" on abdominal radiographs in newborns as a potential sign of intestinal pneumatosis in the first two weeks of life. This has not been correlated with sonographic findings so far. This study aimed to retrospectively assess the correlation between the presence of bubbly "fecal pattern" on radiographs and the occurrence of pneumatosis and portal venous gas on sonography in newborns undergoing evaluation for suspected necrotizing/ischemic enterocolitis.

Methods and Materials: Between January 2012 and November 2023, consecutive patients between the ages of 0 – 90 days with abdominal radiographs and sonographies from the neonatal/intensive care unit with suspected necrotizing/ischemic enterocolitis were included. Radiograph and sonography had to be performed within 24 hours, counting as one case.

Results: In total, 197 patients were included, 84 female and 113 male patients. Among these, 78 patients underwent sequential imaging, resulting in 322 cases (mean age 24 days). In total, on 161 radiographs a bubbly "faecal pattern" was identified (118 patients, 49 girls and 69 boys, mean age 26 days). Concomitant sonographic intestinal pneumatosis was found in 122 cases (74%). Concomitant sonographic portal venous gas only was found in 9 cases (6%). On 30 radiographs with bubbly "faecal pattern" neither intestinal pneumatosis nor portal venous gas was found on sonography (18%).

Conclusion: The radiographically evident bubbly "faecal pattern" in newborns undergoing evaluation for suspected necrotizing/ischemic enterocolitis is a valuable indicator of intestinal pneumatosis, especially in the initial 12 weeks of life.

Systematic Review of the Use of Artificial Intelligence in Pediatric Abdominal Imaging.

J. Namorado Stoffel Feria, M. Ndengera, E. Katirtzidou, M. Laurent, P-A. Poletti, S. Toso; HUG – Hôpitaux universitaires de Genève, Geneva, Switzerland

Purpose: To identify peer-reviewed articles addressing the use of artificial intelligence in pediatric abdominal imaging.

Methods and Materials: A systematic review of the literature was performed accessing PUBMED, Embase and Library of Congress using the following search criteria: artificial intelligence, pediatric, children, abdominal imaging. Of a total of 76 initial articles, 39 articles were retained based on title and abstract search. These articles were analyzed by two radiologists. Of these 10 were excluded (no AI, adult population clearly identified) and 29 were further evaluated. Conficts were resolved by consensus. Qualitative data are presented.

Results: Our systematic search yielded 76 articles, from which 39 were potentially relevant based on their titles and abstracts. Ten studies were excluded (adult, no AI). The 29 remaining studies were selected for analysis. Off these 9 corresponded to all criteria. Three articles addressed image optimization and synthesis, two pertained to automatic organ segmentation, two discussed ultrasound image classification and quality control and one discussed the use of AI in detection. We outline the details.

Conclusion: Though AI literature has rapidly increased in adult abdominal imaging, the pediatric remains sparse, mainly influenced by the absence of large datasets and accurate labelling. Insufficient economic incentives also play a role in resources allocation for these projects. Further work in this area is necessary and awareness in this domain will lead us closer towards important future initiatives.

Artificial intelligence-aided fracture detection in a paediatric emergency department: the end of misdiagnoses?

I. Altmann-Schneider, C.J. Kellenberger, F. Callaghan, M. Seiler;
Kinderspital Zürich, Zurich, Switzerland

Purpose: To retrospectively assess the effect of introducing artificial intelligence (AI)-based software for automated fracture detection on the incidence of misdiagnoses in identifying fractures by emergency paediatricians.

Methods and Materials: Consecutive radiographs of patients aged 2-18 years, who attended the emergency department for suspected fractures, were included. Diagnoses of emergency paediatricians were retrospectively compared to AI-software output (BoneView; Gleamer, Paris, France) and consensus paediatric radiology reference diagnoses. Radiographs of patients below two years of age, of the thorax and C-spine have been excluded as the software is not approved for these.

Results: Between 15 May and 04 July 2023, 1157 radiographs of 967 patients revealed 290 discrepancies between diagnoses made by emergency paediatricians or BoneView and the paediatric radiology consensus diagnoses. Mean age was 9.5 years (age range: 2-18 years) (61% male). Emergency paediatricians made 58 false negative diagnoses of which BoneView correctly identified 37 cases. Conversely, emergency paediatricians made 38 false positive diagnoses of which BoneView correctly identified 32 cases. In 70 true negative diagnoses made by emergency paediatricians BoneView yielded 56 misleading results. In 124 true positive diagnoses made by emergency paediatricians, BoneView showed 46 misleading results.

Conclusion: This retrospective review of AI software for automated fracture detection in a paediatric emergency department indicates its potential to reduce misdiagnoses made by emergency paediatricians. However, the output of the software included potentially misleading results. A prospective study is needed to further assess the effect of introducing such a software on the incidence of misdiagnoses and to evaluate the consequences of potentially misleading results.

Minimal Invasive Cryoablation for Aneurysmal Bone Cysts in Paediatric Patients: preliminary experience

M. Zellner[1], C. Kellenberger[1], S. Pistorius[1], T. Pfammatter[2], T. Dreher[3],
P. Knüsel[4], R. Gnannt[1]; [1] Kinderspital Zürich, Department of Diagnostic and Interventional Paediatric Radiology, Zurich, Switzerland,
[2] USZ – Universitätsspital Zürich, Department of Diagnostic and Interventional Radiology, Zurich, Switzerland, [3] Kinderspital Zürich, Paediatric Orthopedics and Traumatology, Zurich, Switzerland,
[4] Kantonsspital Graubünden, Chur, Switzerland

Purpose: To evaluate the outcome of aneurysmal bone cysts (ABC) in children using percutaneous cryoablation as the sole treatment.

Methods and Materials: This retrospective, single-centre study included 7 children mean age 8.7 years (range 3.0 to 11.9 years) who received at least one cryoablation for ABC. Dedicated cryoablation needles (Boston Scientific) were placed within the lesion, guided by computer tomography (CT) scan.

Imaging follow-up combined with clinical examination was performed by X-Ray 1 and 6 months and Magnetic Resonance Imaging (MRI) 3 and 12 months after the procedure. In case of recurrence seen on MR, additional cryoablation treatment were performed. Data was analysed by anatomical location, measurement of the whole lesion volume, numbers of intralesional cysts, grade of mineralization (5 point Likert scale), pain (0 none to 4 severe) and grade of fluid-fluid levels (FFL, 4 point Likert scale).

Results: 14 cryoablations were performed without any adverse events. All patients showed either complete (one out of 7) or partial (6 out of 7) response. Following treatment, there was a substantial reduction in lesion volume compared to the baseline, leading to an average volume decrease of 81.9% (ranging from 66.8% to 100%). The grade of mineralization (3.2 ± 1.2 after therapy vs 1.1 ± 0.3 at baseline), grade of FFL (1.6 ± 0.5 after therapy vs 3.4 ± 1.1 at baseline) and pain (0.29 +- 0.4 after therapy vs 1.86 +- 0.7 at baseline) significantly improved after therapy.

Conclusion: Our findings indicate that minimal invasive Cryoablation is a valuable treatment option of ABC in children.

Evaluation of the Clinical Impact of Beam Hardening Correction on Computed Tomography

T. Lima[1,2], *M. Gravinatti*[1], *R. Figueiredo Pohlmann Simoes*[3], *J. Fornaro*[1], *T. Gassenmaier*[1], *J.E. Roos*[1]; [1] LUKS – Luzerner Kantonsspital, Department of Radiology and Nuclear Medicine, Lucerne, Switzerland, [2] University of Lucerne, Faculty of Health Sciences and Medicine, Lucerne, Switzerland, [3] INCa – National Institute of Cancer, Section of Medical Physics, Rio de Janeiro, Brazil

Purpose: To quantify the effects of beam hardening correction (BHC) in Head exams compared to without BHC in computed tomography (CT) images and to evaluate the influence of these corrections on quantitative images.

Methods and Materials: This study was perfomed on five different CT devices (Siemens Healthineers® and GE Healthcare®) using a Catphan®604 phantom. The acquisitions protocols were set with and without kV modulation (fixed at 120 kVp) and 240 mAs additionally a low-dose acquisition protocol with fixed 120 kVp and 120 mAs. For each acquisitions three reconstructions were performed: one without the BHC and two with the BHC option (two for each model). The HU values of the different structures (Air, Teflon, DelrinTM, Bone20%, Acrylic, Polystyrene, LDPE, Bone50%, PMP) were measured and compared with the nominal values provided by the manufacturer in all reconstructions. Analyses included the evaluation of quantification of different material present in the phantom using CTQA_cp software and MicroDicom DICOMViewer. Additionally, we evaluated the clinical translation of these corrections using the Software CT CaScoring SyngoVia Siemens®.

Results: The largest deviations in HU values were found with the use of BHC ranging from 3% to 32%. Regarding to the clinical translation of the quantification uncertainties, the variations between protocols without and with BHC represented largest mean difference (-30.85% +/- 6.33%), for Delrin for all combinations, ranging from −36.65% to −6.54%. For the other materials an average mean difference of −10.54% +/- 10.62% was observed. No concrete deviations were found for the differences in acquisition protocols.

Conclusion: The differences found in this study highlight the importance to understand the impact of different protocols' parameters for the clinical evaluations. The results found significant quantitative difference introduced using BHC which could impact patient's clinical care.

Reduction of radiation burden due to MR-only treatment planning for prostate radiotherapy

M. Casiraghi[1], *J. Berg*[2], *L. Bellesi*[1], *S. Presilla*[1]; [1] EOC – Ente Ospedaliero Cantonale, IIMSI – Imaging Institute of Southern Switzerland, Bellinzona, Switzerland, [2] FOPH – Federal Office of Public Health, Health Protection Directorate – Radiation Protection Division, Bern, Switzerland

Purpose: The use of MR-based synthetic CT (sCT) for radiotherapy (RT) planning improves volume delineation and enhances patient safety by reducing the imaging dose. We aim to assess the decreased radiation burden on the Ticino population due to sCT planning for prostate RT.

Methods and Materials: Among 188 prostate cancer patients treated with RT at our center, the percentage undergoing MR-only RT was determined. The validity of sCT planning was previously assessed by comparing dose distributions for 50 patients calculated on both sCT and standard planning CT (pCT), with a 1% difference acceptance threshold. The Radimetrics application was used to assess the mean cumulative effective dose (CED) per patient from pCTs. From the Ticino cancer register and our center data, the annual number of prostate patients benefiting from MR-only RT was assessed. The total spared effective dose per year was calculated and the collective dose spare was obtained for the subgroup of males over 40 years in Ticino. The reduction of radio-induced tumors was estimated based on BEIR VII data for the same subgroup.

Results: 65% of patients could be treated with MR-only RT. The remaining had a pCT: 5% had contraindication to MR, and 30% required pCT due to sCT reconstruction failures due to metal implants or non-standard anatomy, or lack of rectum-bladder preparation. The mean CED/patient was 14.2 mSv with 16% of patients having more than one pCT due to preparation issues. The estimated dose sparing was 1.1 Sv/year, leading to a collective dose reduction in the subgroup of 11.4 µSv/year/male and a reduction of 0.1 induced tumors/year. Extrapolating to the Swiss population (males>40y) indicated a reduction of 2.6 tumors/year.

Conclusion: Although pCT dose is a fraction of the RT patient total dose, it affects the lifetime CED and population radiation burden. Broader MR-only RT adoption, beyond clinical benefits, can mitigate the medical exposure detriment.

Objective comparison of image quality for fluorcopy systems using a novel task-based image quality methodology

A. Viry, M. Nowak, V. Vitzthum, D. Racine, L. Gallego Manzano;
CHUV – Centre Hospitalier Universitaire Vaudois, Lausanne, Switzerland

Purpose: Interventional radiology procedures with fluoroscopy systems should be optimized to ensure the balance between image quality (IQ) and dose level. Model observers (MO) allow an objective assessment of IQ. This study aims to compare the IQ using a MO that includes the temporal resolution and the dose rate of different fluoroscopy systems.

Methods and Materials: A high contrast disc on a motorized mobile bench was placed on top of a 20cm thick solid water phantom. The phantom was imaged to assess the in-plane spatial resolution, the temporal resolution and the noise content. These metrics were introduced in a new spatiotemporal formulation of the non-prewhitening with eye filter MO to assess the detectability of moving objects at a speed of 10 mm/s. The dose rate was measured at the bottom of a 20cm thick solid water. Dose and IQ were assessed using local acquisition parameters for 7 fluoroscopy devices equipped with both fluoroscopy and fluorography modes. Medians and interquartile range (IQR) were used to synthetize the results.

Results: The median entrance dose rate was 4.5 mGy/min with an IQR of 3.1 mGy/min and 50 mGy/min with an IQR of 15.4 mGy/min for fluoroscopy and fluorography modes, respectively. The IQR of detectability values was 1.0 with a median of 1.3 for the fluoroscopy mode. For the fluorography mode, IQR was 4.1 with a median of 3.7. 70% of the systems show a relatively high detectability for a dose level close to the median for both modes. On the other hand, 30% of the systems reveal both a dose and a detectability lower than the medians.

Conclusion: A large heteregoneity of IQ and dose levels was observed. The use of MO opens the possibility of objectively benchmark and optimize the dose/IQ pair for various systems or protocols.

A145

Assessment of Lumbar Disc Degeneration using 23Na-MRI at 3T: Correlation with Pfirrmann score

M. Cavusoglu, A. Landsmann, A. Boss, C. Rossi; USZ – Universitätsspital Zürich, Zurich, Switzerland

Purpose: The objective of this work is to explore the correlation between sodium content of the lumbar intervertebral disks with degenerative grade based on Pfirrmann score at 3T MRI and thus to explore the potential utilization of 23Na-MRI in detecting early degenerative changes in the intervertebral disks in a clinical MRI setting.

Methods and Materials: One hundered lumbar intervertebral discs (L1-S1) from 20 volunteers (10 males, 10 females, mean age of 39.9±18.2 years, range, 21-88) were examined. Sagittal-weighted fast spin-echo and spin density-weighted gradient echo (GRE) sequences for 1H anatomical imaging protocol were performed for morphological imaging and image segmentation. Sagittal spin density-weighted 23Na-MRI images were acquired using a two-dimensional GRE pulse sequence that was optimized for sodium imaging. Morphological grading according to five-level Pfirrmann score was performed.

Results: The mean TSC was calculated as 158.8±49 mmol/L for AF and 269.6±46.6 mmol/L for NP from all disks. In the semi-quantitative image evaluation, 10 disks were classified as Pfirrmann grade I, 41 disks were classified as grade II, 33 disks were classified as grade III and 16 disks were evaluated as grade IV. The sodium concentrations exhibit a highly linear decreasing pattern with increasing Pfirmann grade both for annulus fibrosus and nucleus pulposus.

Conclusion: These results suggest that the measurement of tissue sodium concentration representing the proteoglycan content of the disk might provide a non-invasive, quantitative tool for assessment of disc degeneration at an early stage giving the possibility for prevention and monitoring treatment effects. 23Na-MRI can be utilized in establishing supportive biochemical schemes to existing morphological scoring.

A79

Large Language Model (LLM) Based Clinical Decision Support System (CDSS) Monitoring Pipeline

F. Burn, M. Weibel; KSA – Kantonsspital Aarau, Aarau, Switzerland

Purpose: There is emerging interest to implement CDSS into radiology workflows. Commercialized CDSS underwent high regulation hurdles prior to market access. AI applications are strongly regulated prior to certification but are much less observed during post-implementation. We developed a monitoring pipeline for AI solutions to analyze performance of CDSS and to track the performance of an implemented AI in radiology workflows.

Methods and Materials: To build this pipeline we fine-tuned an open source LLM that analyzes radiology reports and compares the findings to the AI fracture detection modelto display the discrepancy and trend evolution over time. The disagreements are compared with the ground truth coming from an expert radiology team. The results are stored in a database and are used for internal teaching or quality and security monitoring. For refining of the LLM and validation of the monitoring setup 524 conventional radiographs were processed with a train/test/validation split of 314/63/147.

Results: Preliminary validation results of the monitoring pipeline are based on a retrospective dataset (n=147) acquired after implementation of the AI fracture detection model into our radiology workflow. The LLM model shows an accuracy of 96.6% to correctly detect the radiologist's opinion concerning fracture out of the radiology reports.

Conclusion: Our LLM based monitoring solution for CDSS in radiology workflows can automatically detect with a very high accuracy the diagnostic decision in radiology reports and compare this information with the results of a commercialized CDSS. It displays the discrepancies between the radiologist's opinion and the CDSS prediction. By the implemented verification process using ground truth of the cases with disagreements, the system can show how a CDSS, and radiologist team performs during the daily workflow and provide important quality feedback with relevant information for safety and security reasons.

A15

Photon counting detector CT: Clinical utility of virtual monoenergetic imaging combined with tin prefiltration to reduce metal artifacts in the postoperative ankle

A. Marth, S. Goller, G. Kajdi, R. Marcus, R. Sutter; Balgrist University Hospital, Zurich, Switzerland

Purpose: To evaluate the effectiveness and clinical utility of virtual monoenergetic image (VMI) reconstructions combined with tin prefiltration on a photon-counting detector (PCD) CT system to reduce metal artifacts in the postoperative ankle.

Methods and Materials: This retrospective study included patients with internal fixation of the ankle scanned on a PCD CT scanner between March and July 2023. VMIs between 60 and 190 keV were reconstructed with a 10 keV increment and compared to polychromatic standard images. Noise measurements assessed artifact reduction in the most prominent near-metal image distortions. Three readers assessed the visibility of osseous healing along with image interpretability and artifact extent.

Results: This study included thirty patients (13 female; mean age 53.8±18.8 years). A significant reduction of artifacts was observed for VMI ≥120 keV compared to standard images (p≤0.01). For assessment of osseous healing, VMI120keV yielded higher ratings compared to standard images (p≤0.001). Image interpretability was rated better (p=0.023), and artifact extent was rated lower (p≤0.001) for VMI120keV compared to standard images.

Conclusion: VMI at 120 keV showed a significant artifact reduction compared to standard images, while visibility of osseous healing and image interpretability was improved. Therefore, VMI reconstructions may be a helpful complement to post-surgical CT imaging of the ankle in patients with metal implants.

A73

Photon-Counting Detector CT for Liver Lesion Detection – Optimal Virtual Monoenergetic Energy for Different Simulated Patient Sizes and Radiation Doses

D. Racine[1], V. Mergen[2], A. Viry[1], T. Frauenfelder[3], H. Alkadhi[4], V. Vitzthum[1], A. Euler[2,5]; [1] CHUV – Centre Hospitalier Universitaire Vaudois, Institute of Radiation Physics, Lausanne, Switzerland, [2] USZ – Universitätsspital Zürich, Department of Diagnostic and Interventional Radiology, Zurich, Switzerland, [3] USZ – Universitätsspital Zürich, Zurich, Switzerland, [4] USZ – Universitätsspital Zürich, Institute of Diagnostic and Interventional Radiology, Zurich, Switzerland, [5] KSB – Kantonsspital Baden, Department of Radiology, Baden, Switzerland

Purpose: To evaluate the optimal energy level of virtual monoenergetic images (VMI) from photon-counting detector CT (PCD-CT) for the detection of liver lesions as a function of phantom size and radiation dose.

Methods and Materials: An anthropomorphic phantom with liver parenchyma and lesions (diameter, 5-10 mm) was imaged on a PCD-CT. Five hypoattenuating lesions (-30HU and -45HU to the background) and three hyperattenuating lesions (+30HU and +90HU) were used. Medium- or large-sized patients were emulated. Radiation dose was 5, 2.5, 1.25 mGy for the medium and 5, 2.5 mGy for the large size, respectively. 40-80 keV at 5 keV-increments were reconstructed. Lesion detectability was measured using a channelized Hotelling model observer.

Results: Highest detectability was found at 65 and 70keV independent of radiation dose (AUC-range: 0.91-1.0 for the medium and 0.94-0.99 for the large phantom). Lowest detectability was found at 40keV irrespective of radiation dose and size (AUC-range: 0.78-0.99). A more pronounced reduction in detectability was apparent at 40-50keV as compared to 65-75keV when radiation dose was decreased. At equal radiation dose, detection as a function of VMI differed stronger for the large as compared with the medium size (12% versus 6%).

Conclusion: Detectability of hypo- and hyperattenuating liver lesions differed between VMI energies for different phantom sizes and radiation doses. VMI at 65 and 70 keV yielded highest detectability independent of phantom size and radiation dose.

A74

Cross-Domain Adaptation of Machine Learning-Based Whole-Body MRI Segmentation Framework for Brain Tumor Segmentation

S. Ramedani[1,2,3], J.T. Heverhagen[4], H. Von Tengg-Kobligk[5], K. Daneshvar Ghorbani[5]; [1] GCB - Graduate School for Cellular and Biomedical Sciences, Bern, Switzerland, [2] Inselspital – Universitätsspital Bern, Department of Diagnostic, Interventional and Pediatric Radiology, Bern, Switzerland, [3] Prokando GmbH, Ludwigsburg, Germany, [4] Inselspital – Universitätsspital Bern, Department of Diagnostic, Interventional and Paediatric Radiology, Bern, Switzerland, [5] Inselspital – Universitätsspital Bern, DIPR – Department of Diagnostic, Interventional and Pediatric Radiology, Bern, Switzerland

Purpose: The study aimed to assess the adaptability of a 3D attention U-Net-based Convolutional Neural Network (CNN) model, initially developed for whole-body MRI segmentation in muscle fat composition analysis, for the segmentation of brain tumors using the BraTS dataset. The primary objective was to evaluate its effectiveness in accurately identifying brain tumor lesions in MRI images.

Methods and Materials: The CNN model designed for whole-body MRI segmentation was adapted to the task of brain tumor segmentation using the BraTS dataset. Rigorous training and optimization of the model were conducted on a subset of the dataset, followed by evaluation on unseen data. The evaluation employed three main metrics—Dice Score, Sensitivity, and Specificity—to assess the model's ability to differentiate tumor from non-tumor tissues.

Results: The adapted model exhibited robust performance metrics in differentiating various tumor types from non-tumor tissues. Notably, it achieved Dice scores of 0.88, 0.76, and 0.81 for WT, ET, and TC tumor regions, respectively. Additionally, Sensitivity values were recorded at 0.95, 0.84, and 0.71, while Specificity values reached 0.99, 0.98, and 0.99 for WT, ET, and TC, respectively.

Conclusion: This study introduced an innovative methodology for precise brain tumor segmentation in MRI images by adapting a CNN model originally designed for whole-body MRI analysis. The adaptability of this approach from its original application to brain tumor segmentation demonstrates its versatility and potential for deployment in various medical imaging scenarios without compromising accuracy. The findings suggest promising prospects for improving patient care, optimizing clinical workflows, enabling quicker and more precise diagnoses, and ultimately enhancing healthcare delivery and outcomes.

A75

Image quality enhancement of 2.5-minute multi-contrast brain MRI using deep learning-based transformers

A. Sanaat[1,2], R. Hussein[2], M. Zhao[2], H. Zaidi[1], S. Skare[3], T. Deller[4], M. Moseley[2], G. Zaharchuk[2]; [1] HUG – Hôpitaux Universitaires de Genève, Division of Nuclear Medicine and Molecular Imaging, Geneva, Switzerland, [2] Stanford University School of Medicine, Radiological Sciences Laboratory, Palo Alto, United States, [3] Karolinska University Hospital, Department of Neuroradiology, Stockholm, Sweden, [4] GE HealthCare, PET/ MR Engineering, Waukesha, United States

Purpose: MRI, a non-invasive imaging method, is vital for detailed diagnostic images. Yet, its lengthy scanning process often causes discomfort and patient movement. Efforts to speed up MRI scans to match CT's pace have mostly led to lower image quality. This study aims to enhance the quality of rapidly acquired multi-contrast MR images using deep learning.

Methods and Materials: A deep learning-based Swin UNEtTRansformers (SwinUNETR) model was trained to improve the image quality of a fast MR multi-contrast scan protocol called NeuroMix which acquires five sequences in one single 2.5 min acquisition, using echo-planar imaging and fast spin echo readouts. 350 clinical studies include both T1w and T2w images acquired by NeuroMix and conventional methods were used for training. The train/validate/test set size was 245/35/70 patients. Standard signal processing metrics, including the structural similarity index (SSIM) and peak signal-to-noise ratio (PSNR), were obtained, using the high-quality MR images of the conventional scan were used as ground-truth.

Results: There was a significant (p-value<0.05) improvement in SSIM and PSNR using the network for both T1w and T2w images, with SSIM increasing by about 6% (0.82±0.05 to 0.87 ± 0.04) and 5% (0.85±0.05 to 0.89 ± 0.08) and PSNR increasing by about 33% (18.42±2.1 to 24.57 ± 3.1) and 20% (21.20±4.1 to 25.47 ± 2.1) for T1w and T2w images respectively. The visual quality assessment revealed that the SwinUNETR generates images with sharper edges, less noise, and higher quality. Additionally, our model eliminates common artifacts, such as motion, Herringbone artifact, inhomogeneity artifact, and RF overflow which exist in several cases in our test set.

Conclusion: The SwinUNETR model can be used to increase the quality of multi-contrast fast MR images and significantly reduce artifacts.

A76

Deep Learning Based Conversion of Ultrasound to CT Images: A Simulation Study

A. Aicher, D. Cester, A. Martin, F. Huber, T. Frauenfelder, C. Paverd; USZ – Universitätsspital Zürich, Zurich, Switzerland

Purpose: Diagnostic ultrasound (US) is affordable, portable, and does not require ionizing radiation. However US sensitivity in parenchymal lesion detection, such as hepatocellular carcinoma, is significantly lower than with cost- and radiation-intensive contrast-enhanced Computed Tomography (CT). We aim to address this problem by generating CT-like images from US data using a deep learning model. The goal of this in silico study is to demonstrate that our model output significantly improves lesion detection in phantoms.

Methods and Materials: Employing the k-Wave and Astra simulation toolkits, we generated two phantom datasets, each containing 1000 matched US and CT simulations. Phantoms were designed to have up to three inclusions, distinguished by varying densities and sound speeds. The pix2pix model, a conditional Generative Adversarial Network (cGAN), was trained on 800 samples from each dataset, with the remaining 200 samples reserved for testing. Model outputs were assessed using the generalized Contrast to Noise Ratio (gCNR) and the Structural Similarity Index (SSIM).

Results: Our model-synthesised CT images showed substantially improved gCNR when compared to the original US images across numerous phantom and inclusion types (from 0.57 ± 0.21 to 0.87 ± 0.16;). The SSIM between model-synthesised CT images and ground truth CTs ranged from 0.85 ± 0.08 to 0.88 ± 0.08, contingent on phantom and inclusion type. The model-synthesised CT images successfully show lesions that were undetectable in the original US images in multiple cases.

Conclusion: A deep learning model can effectively transform US images into CT-like images. In our in silico study, this improved overall image quality and subsequent detectability of previously unseen lesions and lesion details, which holds substantial potential for advancing diagnostic US. Future research will explore the application of the algorithm to real-world US and CT data.

A146

Deep Learning-powered Ultra-Low Dose CT for Anatomic Localization and Attenuation Correction in Whole-Body PET/CT

Y. Salimi[1], C. Sun[1,2], Z. Mansouri[1], A. Sanaat[1], H. Zaidi[1,3,4,5]; [1] HUG – Hôpitaux universitaires de Genève, Division of Nuclear Medicine and Molecular Imaging, Geneva, Switzerland, [2] Beijing University of Posts and Telecommunications, Beijing, China, [3] University of Geneva, Geneva University Neurocenter, Geneva, Switzerland, [4] University of Groningen, Department of Nuclear Medicine Groningen and Molecular Imaging, Groningen, Netherlands, [5] University of Southern Denmark, Department of Nuclear Medicine, Odense, Denmark

Purpose: In PET/CT examination procedures, the patient is exposed to two sources of external and internal radiation. The effective dose from the CT part increases regarding potential radiation hazards. This study aimed to improve the image quality of ultra-low dose whole-body CT images used for anatomic localization and attenuation correction using deep learning (DL).

Methods and Materials: Raw CT data of 28 whole-body CT scans (60.4±15 years, 62.9±10.9Kg) acquired as part of PET/CT examinations were included. The raw data were reconstructed using Admire reconstruction (Siemens Healthineers) once considering the full-dose (FD) data and again with low-dose (LD) data considering 1% of the acquired raw data. A UNET DL neural network was trained to improve the quality of LD images using FD images as a reference. Subsequently, the attenuation maps (µmap) were generated. Multiple organs were segmented to compare the DL and FD µmaps quantitatively on the unseen external group. The effective doses by NCICT software were compared.

Results: The average SSIM, PSNR, and mean error between LD and FD µmaps were 29.16±4.52, 15.82±0.94 dB, and 0.0155±0.0023 cm-1. These improved to 84.57±2.35, 26.21±1.08 dB, and 0.0029±0.0004 cm-1 in DL images. The average % error in µmaps (LD vs DL) in organs were 23.15±3.97 vs 2.11±0.50 (aorta),30.19±2.02 vs 3.06±0.73 (brain),26.57±2.57 vs 2.85±0.35 (liver),24.39±2.60 vs 2.14±0.41 (spleen),30.71±3.48 vs 3.81±0.66 (bladder), and 19.07±2.33 vs 4.21±0.25 (vertebrae). The effective dose for the LD scan decreased by 99% compared to the FD scan (4.1mSv).

Conclusion: We developed a DL-assisted solution to generate ultra-low dose µmaps with comparable image quality and quantitative accuracy as the FD µmap. This enables reducing the patient's radiation dose by 99 % with minimal compromise on µmaps quality.

A77

Safety of post-implantation MRI with Dixi microdeep electrodes in situ: An in vitro evaluation of MRI-related heating at 1.5T

R. Tuura[1], R. Luechinger2, R. Heule[1], R. Kottke[1], N. Krayenbühl[1], G. Ramantani[1]; [1] Kinderspital Zürich, Zurich, Switzerland, [2] USZ – Universitätsspital Zürich, Zurich, Switzerland

Purpose: Post-implantation assessment of the position of intracerebral EEG electrodes in patients with refractory focal epilepsy can be done with MRI or CT co-registered to a pre-implantation MRI. While both methods offer risks and advantages, MRI risks depend on the electrode heating under different conditions. We aimed to assess the MRI-related heating of the Dixi microdeep electrodes at 1.5T, in two different electrode configurations and with varying levels of radiofrequency (RF) power.

Methods and Materials: In vitro RF heating tests were performed according to the F2182-19e1 standard from the ASTM (American Society for Testing and Materials International), using the ASTM head torso tank filled with PAA gel. A 10-contact Dixi microdeep electrode was inserted into the torso region 3 cm from the right side of the phantom. Fluoroptic thermometry probes recorded the temperature of 3 electrode contacts before and during MRI, and a 4th probe recorded the background temperature in the gel. Tests were performed with the end of the electrode coiled or in a straight line. MRI was conducted on a 1.5T Philips Achieva scanner using the circular polarized transmit-receive body coil, with the specific absorption rate (SAR) ranging from 0.16-3.3 W/kg.

Results: With the electrode end coiled, the maximum temperature rise was 1.5 °C during a 3-minute scan with SAR=3.3 W/kg. With the electrode in a straight line the maximum temperature rise was 45 °C for SAR=3.3 W/kg, 7.8 °C for SAR=0.7 W/kg and 1.8 °C for SAR=0.16 W/kg. The peak heating was seen in the 10th electrode contact furthest from the tip.

Conclusion: Dixi microdeep electrodes show significant heating during MRI at 1.5T, particularly when the electrode is in a straight line. To keep heating within acceptable levels, a conservative SAR limit of 0.1 W/kg should be used. Coiling of the electrode wire outside the body appears to reduce the heating risk, but further tests are needed to establish safe limits for the diameter and orientation of the coiled wire.

Visual identification and clinical characterization of the LATE FDG-PET pattern in amnestic MCI

L. Knappe[1], C. Boccalini[2], F. Ribaldi[3], L. Mu[4], M. Scheffler[5], G. Frisoni[3], V. Garibotto[1,6,7]; [1] HUG – Hopitaux universitaires de Genève, Division of Nuclear Medicine and Molecular Imaging, Geneva, Switzerland, [2] University of Geneva, Laboratory of Neuroimaging and Innovative Molecular Tracers (NIMTlab) – Geneva University Neurocenter and Faculty of Medicine, Geneva, Switzerland, [3] HUG – Hopitaux universitaires de Genève, Memory Clinic, Department of Rehabilitation and Geriatrics, Geneva, Switzerland, [4] ETH – Center for Radiopharmaceutical Sciences, Paul Scherrer Institute, Zurich, Switzerland, [5] HUG – Hopitaux universitaires de Genève, Division of Radiology, Geneva, Switzerland, [6] University of Geneva, Neurocenter and Faculty of Medicine – NIMTlab Laboratory of Neuroimaging and Innovative Molecular Tracers, Geneva, Switzerland, [7] HUG – Hopitaux universitaires de Genève, CIBM – Center for Biomedical Imaging, Geneva, Switzerland

Purpose: Limbic age-related TDP-43 encephalopathy (LATE) is common in advanced age and an important differential diagnosis of Alzheimer's disease (AD). Aim of this study was to test the ability of visually detecting a characteristic medial temporal and limbic hypometabolic pattern of LATE at FDG-PET.

Methods and Materials: We selected all patients with amnestic Mild Cognitive Impairment for which FDG, amyloid and tau PET and cognitive evaluations were available (N=70). FDG-PET scans were analyzed visually with SPM and syngo.via single-subject maps and categorized as normal, AD, LATE or other neurodegenerative diseases, blinded from other data. Age, mini-mental state examination (MMSE), centiloid, tau SUVR, IMT (ratio inferior/medial temporal metabolism) and hippocampal volume (HPV) were compared between groups with Kruskal-Wallis test. Differences in cognitive trajectories were tested using linear mixed-effects models. Significance threshold was $p<0.05$.

Results: 16 scans were classified as normal, 36 as AD, 13 as LATE, and 5 as other. Patients with LATE pattern were significantly older than patients with AD, showed lower MMSE scores and lower HPV as subjects with normal scans. Patients with AD pattern had lower MMSE and IMT than subjects with normal or LATE patterns and higher centiloid values and global tau SUVR than subjects with normal scans. While global tau SUVR did not differ between AD and LATE subjects, there was a trend for higher tau values in AD in Braak IV stage and significantly higher values in Braak V and VI regions. Only subjects classified as AD showed a faster cognitive decline than negative subjects.

Conclusion: Our data show that an FDG-PET LATE pattern in amnestic MCI can identify a subgroup of subjects distinct from AD and from controls in terms of clinical severity, atrophy, cortical tau load and cognitive decline, supporting the utility of FDG-PET for the specific detection of LATE.

Validation of a topographic visual assessment method for 18F-Flortaucipir based on Subtype and Stage Inference Model (SuStaIn)

G. Mathoux[1], C. Boccalini[2], I. Hristovska[3], A. Annachiara[4], D.E. Peretti[4], M. Scheffler[5], J.W. Vogel[3], G.B. Frisoni[6,7], V. Garibotto[8,9,10]; [1] HUG – Hopitaux universitaires de Genève, Division of Nuclear Medicine and Molecular Imaging, Geneva, Switzerland, [2] University of Geneva, Laboratory of Neuroimaging and Innovative Molecular Tracers (NIMTlab) – Geneva University Neurocenter and Faculty of Medicine, Geneva, Switzerland, [3] Lund University, Department of Clinical Sciences Malmö, Faculty of Medicine, SciLifLab, Lund, Sweden, [4] University of Geneva, Laboratory of Neuroimaging and Innovative Molecular Tracers (NIMTlab), Geneva University Neurocenter and Faculty of Medicine, Geneva, Switzerland, [5] HUG – Hopitaux universitaires de Genève, Division of Radiology, Geneva, Switzerland, [6] HUG, Memory Clinic, Department of Rehabilitation and Geriatrics, Geneva, Switzerland, [7] University of Geneva, LANVIE – Laboratory of Neuroimaging of Aging, Geneva, Switzerland, [8] University of Geneva, Neurocenter and Faculty of Medicine – NIMTlab Laboratory of Neuroimaging and Innovative Molecular Tracers, Geneva, Switzerland, [9] HUG – Hopitaux universitaires de Genève, Geneva, Switzerland, [10] CIBM – Center for Biomedical Imaging, Geneva, Switzerland

Purpose: Our study aims to provide evidence for multiple tau accumulation patterns in a clinical setting by applying a novel topographic visual method for tau-PET, based on Subtype and Stage Inference algorithm (SuStaIn) staging, and to compare it with the algorithm classification.

Methods and Materials: We retrospectively included 245 participants who underwent 18F-flortaucipir-PET. Three physicians visually evaluated all scans for tau (T) status and SuStaIn subtypes (limbic [S1], medial temporal lobe-sparing[S2], posterior[S3], and lateral temporal [S4]). Subjects were classified into these different subtypes by the automated SuStaIn algorithm. Global tau burden was measured as Standardized Uptake Value ratio (SUVr) in a meta-region of interest. To test the agreement between visual and automated subtypes, we used Cohen's kappa (k). Chi-squared and Kruskal-Wallis tests were used to test the differences in clinical features, tau, and amyloid (Aβ) loads between subtypes. Differences in cognitive trajectories were tested using linear mixed-effects models.

Results: Our study showed substantial agreement in subtype attribution between different raters ($k>0.65$, $p<0.001$) and a fair agreement with the result of the automated SuStaIn algorithm ($k=0.393$, $p<0.001$). T+ individuals had a higher Aβ burden and performed worse on MMSE than T- independently from subtypes ($p<0.001$). Visually identified individuals with S2 subtype were younger than S1 and S3 ($p<0.001$) and had worse MMSE scores than S4 and S1 ($p<0.05$). Furthermore, T+ individuals demonstrated a higher global tau SUVr and significantly faster cognitive decline compared to the T- group ($p<0.001$), with the highest tau accumulation ($p<0.05$) and fastest decline observed in the visually defined S2 subtype.

Conclusion: Different subtypes of tau accumulation are visually distinguishable and exhibit differences in tau levels, clinical characteristics, and long-term outcomes, suggesting clinical usefulness for the detection of higher risk AD variants.

A93

Automated conclusion extraction from brain PET multi-tracer reports (Tau, Amyloid and FDG)

E. Teixeira Andrade[1], J-P. Goldman[1,2], J. Zaghir[3], D.E. Peretti[4], C. Lovis[3,2], V. Garibotto[1,4], P. Jané[1,4]; [1] HUG – Hôpitaux universitaires de Genève, Geneva, Switzerland, [2] University of Geneva, Department of Radiology and Medical Informatics, Geneva, Switzerland, [3] HUG – Hôpitaux universitaires de Genève, Division of Medical Information Sciences, Geneva, Switzerland, [4] University of Geneva, Geneva, Switzerland

Purpose: The purpose of this study is to develop and test a series of machine learning based text classification methods to interpret conclusions from brain PET reports from our clinic (FDG, Amyloid and Tau PET) in order to 1) identify positive or negative results in all three modalities, and 2) extract diagnostic impressions for Alzheimer's Disease (AD), Fronto-Temporal Dementia (FTD) , Lewy Bodies Dementia (LBD) or Undetermined Neurodegenerative Disorder (UND) based on metabolism or perfusion patterns.

Methods and Materials: First, train and test datasets were created by extracting anonymised conclusion texts from brain PET reports. These documents were manually annotated by two medical experts and in case of disagreement a third one would help deciding the final label. Second, a pre-processing step was applied to all texts prior to training. Third, different traditional machine learning models were trained and tuned with optimized hyperparameters using a 5-fold cross-validation scheme to assess their performance and generalisability on the text collection.

Results: 1435 conclusion texts from our Nuclear Medicine Division were annotated (311 Tau, 591 Amyloid, 650 Diagnostic impression.) Six models were trained and tested. (Support Vector Machine (Linear and Radial Basis function), Naive Bayes, Logistic Regression, Random Forrest, and K-Nearest Neighbors) The best classifiers showed the following accuracies: Tau (0.94), Amyloid (0.98), Oriented Diagnostic (0.91 for Neg vs. AD.

Conclusion: Automated medical text interpretation using these machine learning methods showed excellent results, paving the way for a change of paradigm in the field of large scale real world data analysis of imaging findings.

A94

A radiomics-based analysis of functional dopaminergic scintigraphic imaging for the diagnosis of dementia with Lewy bodies

J. Perriraz[1], D. Abler[1], N. Lejay[1], P. Salvioni Chiabotti[1], C. Hall[1], O. Rouaud[1], M. Nicod Lalonde[1], N. Schaefer[1], R. Schaer[2], G. Allali[1], A. Depeursinge[1], J.O. Prior[1], M. Jreige[1]; [1] CHUV – Centre Hospitalier Universitaire Vaudois, Lausanne, Switzerland, [2] HESAV/HES-SO – Haute Ecole de Santé Vaud, Institute of Informatics, Sierre, Switzerland

Purpose: Radiomics features can be used for capturing tissue and lesion characteristics. Using functional dopaminergic scintigraphy, we investigated the usefulness of radiomics features in predicting the diagnosis of dementia with Lewy bodies (DLB).

Methods and Materials: We retrospectively analyzed 74 patients (29 F and 45 M, mean age 72±9 y) investigated in the Leenaards Memory Center (CHUV) for DLB who underwent quantitative I-123-ioflupane SPECT/CT (DATscan™). All scanned examinations had xSPECT reconstruction, allowing SUV quantification. We segmented the right and left striatum using 3DSlicer and performed radiomic feature extraction and analysis on the QuantImage v2 platform (https://quantimage2.ehealth.hevs.ch/). The dataset was split into training (80%) and test (20%) sets, and various classification algorithms were used to predict the definitive clinical diagnosis of DLB. Receiver operating characteristic (ROC) curve analysis was performed to characterize the performance of the obtained models.

Results: In total, 33/74 (45%) patients were finally diagnosed with DLB using the 2017 revised consensus criteria for clinical diagnosis of DLB. The best obtained model was based on 10 non-correlated features from both striatal regions using a support vector machine (SVM) algorithm. This xSPECT/CT radiomics model showed a higher overall performance than SUVmax alone, with similar sensitivity, and significantly better specificity and AUC: 73% (95% CI: 71–77), 89% (87–91) and 0.891 (0.877–0.908) versus 74% (71–76, p=0.24), 45% (42–49, p<0.001) and 0.679 (0.651–0.701, p<0.001), respectively.

Conclusion: The radiomics model based on quantitative I-123-ioflupane xSPECT/CT showed good performance in predicting the definitive clinical diagnosis of DLB, using diverse features derived from striatal analysis. This tool may improve the diagnostic accuracy of I-123-ioflupane that is of major importance with the approval of disease-modifying therapies for Alzheimer's disease.

A87

Development of [^{18}F]F-MLN4760, a small molecule-based PET imaging agent for targeting ACE2

C. Vaccarin[1], D. Beyer[1], J. Wang[2], J. Bode[2], L. Mu[2], R. Schibli[1,3], C. Müller[1,2]; [1] ETH - Center for Radiopharmaceutical Sciences, Paul Scherrer Institute, Villigen, Switzerland, [2] ETH – Center for Radiopharmaceutical Sciences, Paul Scherrer Institute, Department of Chemistry and Applied Biosciences, Zurich, Switzerland, [3] ETH – Center for Radiopharmaceutical Sciences, Paul Scherrer Institute, Zurich, Switzerland

Purpose: The angiotensin converting enzyme-2 (ACE2) plays an important role in cardiovascular regulation and acts as the entry receptor for SARS-CoV-2. Recent studies highlighted a possible correlation between the ACE2 expression and Covid-19 susceptibility and severity. In this project, we developed a radiofluorinated analog of the ACE2 inhibitor MLN4760 and evaluated its potential use for the PET imaging of ACE2.

Methods and Materials: The radiofluorination concept involved replacing one of the chlorine of the MLN4760 structure with a fluorine atom. The maintenance of a high ACE2 affinity was evaluated by displacement assays performed with the non-radioactive compound F-MLN4760. The radiofluorination precursor was synthesized using a multi-step pathway before being subjected to radiolabeling. The resultant [^{18}F]F-MLN4760 was evaluated _in vitro_ using ACE2- and ACE-expressing HEK cells. Biodistribution and PET/CT imaging studies were carried out in HEK-ACE2/HEK-ACE xenografted mice.

Results: The IC_{50} values measured for F-MLN4760 and MLN4760 were in the same range (13 ± 2 nM and 21 ± 2 nM, respectively). The precursor was synthesized in 5 steps with an overall yield of 8%. The labeling process yielded [^{18}F]F-MLN4760 with a radiochemical purity ≥ 99% and molar activities up to 38 GBq/µmol. [^{18}F]F-MLN4760 showed uptake of 67 ± 9% in HEK-ACE2 cells after 3 h incubation, while <0.3% uptake was detected in HEK-ACE cells. In biodistribution studies, [^{18}F]F-MLN4760 selectively accumulated in the HEK-ACE2 xenografts (13 ± 2% IA/g, 1 h p.i.) with negligible uptake in HEK-ACE xenografts (<0.5%). Unspecific accumulation of activity was seen mainly in the intestinal tract.

Conclusion: Our preliminary data showed that [^{18}F]F-MLN4760 binds specifically to ACE2, making it a favorable candidate for further investigations aimed at verify its possible use to detect ACE2 at physiological levels.

A88

Pulmonary transit time measured using dynamic rubidium cardiac PET/CT is associated with right ventricular function

N. Spielhofer[1], B. Zhang2, J. Heimer[2], C. Popescu[1], U. Hufschmid[1], I. Burger[1], A.Sauter[1]; [1] KSB – Kantonsspital Baden, Baden, Switzerland, [2] ETH – Center for Radiopharmaceutical Sciences, Paul Scherrer Institute, Zurich, Switzerland

Purpose: Pulmonary transit time (PTT) represents the time needed for the circulation of blood from the right to the left ventricle. This parameter can be measured during dynamic acquisition of rubidium cardiac PET/CT (Rb-PET). We wanted to assess the association between PTT and parameters derived from echocardiography.

Methods and Materials: Patients underwent Rb-PET with rest/stress protocol on an integrated hybrid PET/CT system. For both rest and stress, a weight-adjusted dose of 82Rb-chloride was intravenously injected (7.5 MBq/Kg). Among other sequences, dynamic images were reconstructed with the following framesets: 1 s delay, 12 x 10 s, 2 x 30 s, 2 x 60 s, 1 x 120 s. VOIs were drawn in the left and right ventricle using the dynamic PET datasets. The peak time in each of the two time activity curves was analyzed and the time difference extracted as PTT. Statistical analysis included binomial regression modeling for rest PTT < versus >= 10 s).

Results: 58 patients were enrolled and the time difference between PET and echocardiography was 16.43 (23.21) days. 13 patients had a rest PTT of 0 s, 38 patients 10 s and 4 patients 20 s. Parameters derived from echocardiography: rest EF 51.95 (14.18), E/A ratio 0.87 (0.40), TAPSE 22.80 (4.38). Binomial regression revealed a significant association for: TAPSE (0.58026 Estimate Std., 0.0468 Pr(>|z|)), Heart Rate (-0.10340 Estimate Std., 0.0380 Pr(>|z|)). No association was found for: Rest EF (-0.06226 Estimate Std., 0.4240 Pr(>|z|)), E/A ratio (1.26208 Estimate Std., 0.4294 Pr(>|z|)).

Conclusion: PTT can be estimated with Rb-PET but smaller time frames than 10 s are needed. In a few cases the Rest PTT exceeded 20 s. Binomial regression indicates that TAPSE has a higher association with PTT than EF. Therefore, right ventricular function seems to have the highest contribution to PTT. In the next step, we will improve the time resolution of the acquisition.

New semiquantitative parameters to improve diagnostic accuracy of digital FDG-PET/CT in suspected endocarditis

C. Bregenzer[1], L. Knappe[2], C. Mingels[1], N. Gözlügöl[1], A. Rominger[3], F. Caobelli[1]; [1] Inselspital – Universitätsspital Bern, Universitätsklinik für Nuklearmedizin, Bern, Switzerland, [2] HUG – Hôpitaux universitaires de Genève, Médecine nucléaire et imagerie moléculaire, Geneva, Switzerland, [3] Inselspital – Universitätsspital Bern, Bern, Switzerland

Purpose: In the diagnostic workup of Infective endocarditis (IE), qualitatively evaluated FDG-PET is recommended in unclear cases. However, semiquantitative parameters may prove more accurate in the diagnostic work-up.

Methods and Materials: Patients with suspected IE in native and prosthetic valves underwent a [18F]FDG-PET/CT on a digital scanner. If a focal increased uptake was visually present, a semiquantitative evaluation was performed. Max/mean/peak standardized uptake values (SUV) and normalized values (to-liver/mediastinum/surrounding uptake) were calculated (isocontour-VOI 40% threshold). Surrounding activity was defined as homogenous, circumferential uptake around the focus. Final diagnosis was obtained by a multidisciplinary board.

Results: Eighty-two patients (64 males) aged 58.5±18.8 y/o were included (56 with prosthetic valves). In the multidisciplinary board, IE was confirmed in 28 patients and rejected in 54. At PET, visually detectable hypermetabolic foci were present in 32 subjects (in total 49 foci). Normalized semiquantitative values were different between patients with and without IE (p≤0.01): to-mediastinum SUVmax (3.4±1.6 vs 2.3±0.6), to-liver SUVmax (2.8±1.0 vs 1.6±0.5), to-mediastinum SUVpeak (2.8±1.1 vs 1.7±0.5), to-liver SUVpeak (2.3±0.8 vs 1.0±0.4), to-liver SUVmax/SUVmean (2.1±0.9 vs 1.2±0.4), to-mediastinum SUVmax/SUVmean (2.4±1.1 vs 1.4±0.5), SUVmax/SUVmean focus (3.3±1.5 vs 2.0±0.7), SUVpeak/SUVpeak surrounding (1.9±0.9 vs 1.2±0.2). All these values proved accurate in diagnosing IE (AUC always >0.8). Adding semiquantiative values to the qualitatively analysis increased sensitivity, specificity, PPV, NPV and accuracy compared to visual analysis only (86% vs 57%, 93% vs 83%, 86% vs 64%, 93% vs 79%, 90% vs 74%).

Conclusion: Our proposed semiquantiative parameters proved accurate and increased accuracy of FDG-PET in the diagnostic workup of IE and should be recommended in clinical practice.

Prognostic value of ^{99m}Tc-DPD quantitative SPECT/CT in patients with suspected and confirmed cardiac ATTR-Amyloidosis and preserved left ventricular function

F. Caobelli[1], N. Gözlügöl[2], A. Bakula[1], A. Rominger[1], R. Schepers[1], S. Stortecky[1], L. Hunziker Munsch[1], S. Dobner[1], C. Gräni[1]; [1] Inselspital – Universitätsspital Bern, Bern, Switzerland, [2] University of Bern, Bern, Switzerland

Purpose: Quantitative ^{99m}Tc-3,3-diphosphono-1,2 propanodicarboxyli-cacid (^{99m}Tc-DPD) Single Photon Emission Computed Tomography (SPECT) may be used for risk stratifying patients with transthyretin-related amyloidosis-cardiomyopathy (ATTR-CM). We aimed to analyse the predictive value of quantitative ^{99m}Tc-DPD SPECT/CT in suspected and confirmed ATTR-CM according to different disease stages

Methods and Materials: Consecutive patients with suspected ATTR-CM referred to a single tertiary center who underwent quantitative ^{99m}Tc-DPD SPECT/CT allowing standardized uptake values (SUVmax, SUVpeak) analysis were enrolled. Patients were divided into two groups according to left ventricular ejection fraction (LVEF) at baseline (i.e. LVEF≥50% and <50%). Correlations between clinical, laboratory, and echocardiographic parameters and major adverse cardiac events (i.e. all-cause death, sustained ventricular tachyarrhythmia, hospitalization for heart failure, implantation of a cardioverter defibrillator) to quantitative uptake values were investigated.

Results: A total of 144 patients with suspected ATTR-CM were included in the study (98 with LVEF≥50% and 46 with LVEF<50%), of whom 99 were diagnosed with ATTR-CM (68,75%; 69 with LVEF≥50% and 30 with LFEV<50%). Myocardial SUVmax≥7 was predictive of MACE at 21.9±13.0 months follow-up (HR 2.875, 95%CI 1.23 – 6.71, p=0.015) in suspected ATTR-CM and in patients with confirmed ATTR-CM (global X^2= 6.892, p=0.02) and LVEF≥50%. There was no predictive value for patients with LVEF<50% in suspected or confirmed ATTR-CM.

Conclusion: In patients with suspected or confirmed ATTR-CM and preserved LVEF, representing early disease stage, a myocardial SUV≥7 is a predictive marker for MACEs. Quantitative ^{99m}Tc-DPD SPECT should be considered for improved early stage risk stratification of patients with ATTR-CM.

A107

Quantification of [⁹⁹ᵐTc]Tc-HDP bone SPECT/CT: Can we improve the body weight based standardized uptake value with a more robust normalization?

T. Damian[1], N. Spielhofer[2], J. Heimer[3], A. Sauter[2,4], C. Popescu[2], J. L. Manser[5], I.A. Burger[2,6]; [1] KSB – Kantonsspital Baden, Department of Radiology, Baden, Switzerland, [2] KSB – Kantonsspital Baden, Department of Nuclear Medicine, Baden, Switzerland, [3] ETH – Center for Radiopharmaceutical Sciences, Paul Scherrer Institute, Department of Mathematics, Seminar for Statistics, Zurich, Switzerland, [4] Universitätsklinikum Tübingen, Department of Radiology, Tuebingen, Germany, [5] KSB – Kantonsspital Baden, Department of Informatics, Baden, Switzerland, [6] USZ – Universitätsspital Zürich, Department of Nuclear Medicine, Zurich, Switzerland

Purpose: The introduction of quantitative SPECT/CT offers the possibility for more objective assessment of SPECT tracer accumulation. For bone SPECT it is not clear, if body weight (BW) based standardized uptake values (SUV_{BW}) are reliable. A robust normalization and the use of quantitative measures, however, might be important for an objective assessment of e.g. painful lesions.

Methods and Materials: We retrospectively analyzed patients that received a quantitative [⁹⁹ᵐTc]Tc-HDP bone SPECT/CT scan of the lumbar spine. For an equal distribution in BW and gender, we selected 20 man and women in 4 BW categories (C1-4: <60kg, 60-80kg, 80-110kg and >110kg). Regular bone activity was measured in kBq/cc in a standard volume of interest in the fifth lumbar vertebra. Values where then normalized with BW (SUV_{BW}) or size (SUV_{Size}). Correlations between BW and tracer uptake, SUV_{BW} and SUV_{Size} were analyzed using a spearman test.

Results: A total of 120 patients were identified. C1 for males and C4 for women were incomplete. The mean activity decreased with increasing weight 114.2, 90.4, 73.0 and 61.3 kBq/cc for C1-4, respectively, while SUV_{BW} increased with 8.1, 9.3, 9.2 and 10.6. SUV_{Size} decrease with 25.2, 22.6, 18.0 and 15.9, respectively. The correlation indexes with BW were -0.44, 0.22, -0.38 for activity, SUV_{BW} and SUV_{Size}, respectively.

Conclusion: Interestingly, despite the bone dominant tracer distribution, the correlation of activity measured in L5 seems to be stronger with BW than with size. Therefore, a simple replacement of SUV_{BW} with SUV_{Size} might not lead to a more robust quantification.

A108

Quantitative bone SPECT/CT in symptomatic and asymptomatic foot and ankle osteoarthritis

M. Ulrich[1], K. Strobel[2], D. Lehnick[3], H. Grünig[4], L. Iselin[5], T. Leike[4], U. Bhure[2]; [1] Stadtspital Zürich Waid, Klinik für Orthopädie, Hand- und Unfallchirurgie, Zurich, Switzerland, [2] LUKS – Luzerner Kantonsspital, Department of Radiology and Nuclear Medicine, Lucerne, Switzerland, [3] University of Lucerne, Faculty of Health Sciences and Medicine, Lucerne, Switzerland, [4] LUKS – Luzerner Kantonsspital, Department of Nuclear Medicine and Radiology, Lucerne, Switzerland, [5] Hirslanden Klinik St. Anna, Orthopädische Klinik, Lucerne, Switzerland

Purpose: To evaluate and quantify the prevalence of increased uptake in bone SPECT/CT in symptomatic and asymptomatic foot and ankle joints in patients with suspected osteoarthritis

Methods and Materials: In 63 patients (27 women, 36 men, median age: 52 years, range: 23 - 84 years) with osteoarthritis (OA) the symptomatic foot (SF) and asymptomatic contralateral foot (AF) were imaged with quantitative bone SPECT/CT (Symbia Intevo Bold, Siemens Healthineers, Erlangen, Germany). Presence, localization, and SUVmax (maximum standardised uptake value) of active joints were assessed for SF and AF. On CT OA grade [grade 1: mild, grade 2: moderate, grade 3: severe] was evaluated. The statistical analysis was performed with Stata (StataCorp, College Station, Texas, USA). Approval of the local Ethics Committee was obtained and informed consent was waived due to the retrospective design.

Results: 32 (51%) patients showed increased uptake in the AF and 31 (49%) patients only in the SF. SF showed significantly more active joints (108 versus 45) and significantly higher mean SUVmax compared to the AF [13.9 ± 7.7 (range: 2.7 - 40.7) versus 9.9 ± 5.4 (range: 2.3 - 25.1)] ($P < 0.005$). CT OA grade showed significant positive correlation with SUVmax: grade 1: n=73 [mean SUVmax: 8.1 ± 3.9], grade 2: 42 [mean SUVmax: 13.6 ± 4.9], and grade 3: 34 [mean SUVmax: 22.0 ± 6.6] [Pearson's coefficient of correlation: 0.746, $P < 0.001$]. SF had more joints with moderate to severe OA (58%), whereas AF showed more joints with mild OA (65%). TMT joints were predominantly involved in AF whereas upper ankle, lower ankle, and TMT joints were predominantly involved in SF.

Conclusion: More than half of patients (51%) with symptomatic food have increased uptake in the asymptomatic contralateral foot in bone SPECT/CT. There is a strong correlation between SUV uptake and severity grade of osteoarthritis on CT.

The Imageable Genome

P. Jané[1,2], X. Xu[3], V. Taelman[3], E. Jané[4], K. Gariani[1,2], M. del Val Gómez[5], R.A. Dumont[6], M.A. Walter[3,7]; [1] HUG - Hôpitaux universitaires de Genève, Geneva, Switzerland, [2] University of Geneva, Geneva, Switzerland, [3] University of Lucerne, Lucerne, Switzerland, [4] Universidad Politécnica de Madrid, ETSIAE – Departamento de Matemática Aplicada a la Ingeniería Aeroespacial, Madrid, Spain, [5] Hospital Universitario Ramón y Cajal, Madrid, Spain, [6] UNIL – University of Lausanne, Lucerne, Switzerland, [7] Hirslanden Klinik St. Anna, Lucerne, Switzerland

Purpose: The purpose of this study was to identify all the genes in the human genome whose expression can be evaluated using nuclear medicine imaging modalities.

Methods and Materials: We developed a hybrid Human-Artificial Intelligence pipeline in order to analyse all publicly available abstract texts from the Medline/Pubmed database and search for radiotracer-protein associations in a systematic manner. In a second step all proteins were mapped to their coding genes. Once we had the list of genes that constituted The Imageable Genome, this genes were cross-referenced with large scale RNA-seq public datasets so that we could find new diagnostic, predictive and prognostic applications in the fields of cardiology, neurology and oncology.

Results: 6387 bibliographical references were identified containing 9285 radiotracer-to-gene associations. This data were cross-referenced with more than 60.000 patients RNA-seq samples, producing a large amount of new applications for these molecular imaging agents and thus significantly expanding the potential of nuclear medicine.

Conclusion: By connecting the fields of nuclear medicine, genomics and artificial intelligence based systematic review, The Imageable Genome promises not only to accelerate, but to revolutionise the way radiopharmaceutical developement and molecular imaging research are performed.

Deep learning-powered generation of 18F-FDG images from early-phase 18F-Florbetapir and 18F-Flutemetamol brain PET images

A. Sanaat[1,2], C. Boccalini[1,3,4], I. Shiri5, Y. Salimi[1], V. Garibotto[6,7,8], H. Zaidi[1]; [1] HUG – Hôpitaux universitaires de Genève, Division of Nuclear Medicine and Molecular Imaging, Geneva, Switzerland, [2] Stanford University School of Medicine, Radiological Sciences Laboratory, Palo Alto, United States, [3] University of Geneva, Laboratory of Neuroimaging and Innovative Molecular Tracers (NIMTlab) – Geneva University Neurocenter and Faculty of Medicine, Geneva, Switzerland, [4] UniSR – Università Vita-Salute San Raffaele, Milan, Italy, [5] Inselspital – Universitätsspital Bern, Department of Cardiology, Bern, Switzerland, [6] HUG – Hôpitaux universitaires de Genève, Geneva, Switzerland, [7] University of Geneva, Neurocenter and Faculty of Medicine – NIMTlab Laboratory of Neuroimaging and Innovative Molecular Tracers, Geneva, Switzerland, [8] CIBM – Center for Biomedical Imaging, Geneva, Switzerland

Purpose: Amyloid brain PET imaging can identify amyloid plaques years before cognitive decline, hence aiding early Alzheimer's disease (AD) diagnosis. Early-phase amyloid-PET images indicate cerebral perfusion, linked to neural dysfunction, while the 18F-FDG estimates cerebral glucose metabolism linked to synaptic dysfunction and neurodegeneration. Several studies showed a strong correlation between early-phase amyloid and FDG images in AD patients. Our goal is to evaluate a deep learning model's capability to generate synthetic FDG images from early-phase amyloid-PET images, with the aim to reduce radiation exposure, scanning time, and enhance patient comfort.

Methods and Materials: A clinical brain PET dataset including 122 FDG and early-phase amyloid-PET scans was used. Early-phase amyloid-PET started immediately after tracer injection to acquire 5 min (18F-Florbetapir) or 10 min (18F-Flutemetamol) static images. A Swin UNEtTRansformers (SwinUNETR) transformer model was employed. Qualitative and quantitative assessment was conducted using structural similarity index metrics (SSIM), root mean squared error (RMSE), and peak signal-to-noise ratio (PSNR) between pseudo-FDG and reference FDG PET images.

Results: Visual inspection indicated that the generated pseudo-FDG images closely resembled to reference FDG compared to early-phase amyloid across all individual cases, regardless of disease stage or severity. The quantitative assessment revealed 19.25% increase in PSNR, 2% increase in SSIM, and 40.25% reduction in RMSE between early-phase amyloid and FDG, and between pseudo-FDG and reference FDG.

Conclusion: Our deep learning-based model generates synthetic FDG images that exhibit higher similarity to actual FDG images than early-phase amyloid images. This could streamline the integration of dual-phase amyloid PET scans into clinical practice by providing pseudo-FDG images that closely resemble to standard FDG images.

The results from a national survey to characterise image quality in oncological [¹⁸F]FDG PET examinations across Switzerland

T. Lima[1,2], U. Bhure[1], H. Grünig[1], A. Zander[1], M. del Sol Pérez Lago[1], R. Guidnard[3], I.A. Burger[4,5], E. Nitzsche[6], M. Huellner[5], R. Linder[7], N. Stritt[7], K. Strobel[1]; [1] LUKS – Luzerner Kantonsspital, Department of Radiology and Nuclear Medicine, Lucerne, Switzerland, [2] University of Lucerne, Faculty of Health Sciences and Medicine, Lucerne, Switzerland, [3] Scintidoc – Nuclear Medicine and PET Center, Montpellier, France, [4] KSB – Kantonsspital Baden, Department of Nuclear Medicine, Baden, Switzerland, [5] USZ – Universitätsspital Zürich, Department of Nuclear Medicine, Zurich, Switzerland, [6] KSA – Kantonsspital Aarau, Department of Nuclear Medicine, Aarau, Switzerland, [7] Swiss Federal Office of Public Health, Radiation Protection Division, Bern, Switzerland

Purpose: This survey aimed to correlate known performance characteristics from individual PET devices to patient-based image quality (IQ) across devices and protocols in Switzerland.

Methods and Materials: All centres submitted 3-4 anonymised datasets (PET/CT or PET/MR) from [¹⁸F]FDG PET examinations for each device with the centre's standard protocol, without liver pathological uptake and body mass index in normal range (18.5-24.9). Anonymized images were stored in a dedicated workstation (MIM Software Inc., Ohio, USA) for scoring. IQ was evaluated by 8 expert nuclear medicine physicians with experience in the devices evaluated. Each image was scored blindly (no device or hospital info) by 4 randomly selected physicians focusing on parenchymal radiotracer homogeneity and border delineation of the liver and spleen, and MIP images. The IQ was ranked from 1 (non-diagnostic) to 5 (excellent). Result was grouped based on device vendor and model, injected activity (IA), and acquisition time (AT).

Results: Participation from 63% of installed devices: 2 PET/MR and 26 PET/CT. 86 patients' data were received with 1 to 3 reconstructions (192 datasets). Overall, the IQ was average to excellent (75 percentile of the physician scored: 4.0, 3.8, 3.7, 3.7, and 3.8, for liver delineation, liver uniformity, spleen delineation, spleen uniformity, and MIP, respectively). There was a wide range of IA (200 ± 65 MBq, mean ± stdev) and AT (2.25 ± 1.16 min per frame) but no correlation was found between statistics (IA and AT) and IQ showing the impact of reconstruction optimisation where similar devices got similar IQ score for different levels of statistics.

Conclusion: This survey benchmarked the image quality in oncological PET imaging across Switzerland. Some differences were linked with protocol optimisation allowing for a reduction in injected activity or acquisition time without image quality degradation.

Evolution of CT radiation dose in pediatric patients undergoing hybrid 2-[18F]FDG PET/CT between 2007 and 2021

S. Skawran[1,1], T. Sartoretti[1,1], A. Gennari[1,2], M. Schwyzer[1,1], E. Sartoretti[1,2], V. Treyer[1,1], A. Maurer[1,2], M. Huellner[1,2], S. Waelti[3,1,1], M. Messerli[1,2]; [1] USZ – Universitätsspital Zürich, Zurich, Switzerland, [2] University of Zurich, Zurich, Switzerland, [3] KSSG – Kantonsspital St. Gallen, St. Gallen, Switzerland

Purpose: To evaluate the evolution of CT radiation dose in pediatric patients undergoing hybrid 2-[18F]fluoro-2-deoxy-D-glucose (2-[18F]FDG) PET/CT between 2007 and 2021.

Methods and Materials: Data from all pediatric patients aged 0-18 years who underwent hybrid 2-[18F]FDG PET/CT of the body between January 2007 and May 2021 were reviewed. Demographic and imaging parameters were collected. A board-certified radiologist reviewed all CT scans and measured image noise in the brain, liver, and adductor muscles.

Results: 294 scans from 167 children (72 females (43%); median age: 14 (IQR 10-15) years; BMI: median 17.5 (IQR 15-20.4) kg/m²) were included. CT dose index-volume (CTDIvol) and dose length product (DLP) both decreased significantly from 2007 to 2021 (both $p < 0.001$, Spearman's rho coefficients -0.46 and -0.35, respectively). Specifically, from 2007 to 2009 to 2019-2021 CTDIvol and DLP decreased from 2.94 (2.14-2.99) mGy and 309 (230-371) mGy*cm, respectively, to 0.855 (0.568-1.11) mGy and 108 (65.6-207) mGy*cm, respectively. From 2007 to 2021, image noise in the brain and liver remained constant ($p = 0.26$ and $p = 0.06$), while it decreased in the adductor muscles ($p = 0.007$). Peak tube voltage selection (in kilovolt, kV) of CT scans shifted from high kV imaging (140 or 120kVp) to low kV imaging (100 or 80kVp) ($p < 0.001$) from 2007 to 2021.

Conclusion: CT radiation dose in pediatric patients undergoing hybrid 2-[18F]FDG PET/CT has decreased in recent years equaling approximately one-third of the initial amount.

A third of the radiotracer dose: two decades of progress in pediatric [18F]fluorodeoxyglucose PET/CT and PET/MR imaging

S. Waelti[1,2,2], S. Skawran[2,2], T. Sartoretti[2,2], M. Schwyzer[2,2], A. Gennari[2,3], C. Mader[2,3], V. Treyer[2,2], C. Kellenberger[4,3], I. Burger[2,3], T. Hany[3,5], A. Maurer[2,3], M. Huellner[2,3], M. Messerli[2,3]; [1] KSSG – Kantonsspital St. Gallen, St. Gallen, Switzerland, [2] USZ – Universitätsspital Zürich, Zurich, Switzerland, [3] University of Zurich, Zurich, Switzerland, [4] Kinderspital Zürich, Zurich, Switzerland, [5] MRI – Medizinisch Radiologisches Institut Bahnhofplatz, Zurich, Switzerland

Purpose: To assess the evolution of administered radiotracer activity for F-18-fluorodeoxyglucose (18F-FDG) PET/CT or PET/MR in pediatric patients (0-16 years) between years 2000 and 2021.

Methods and Materials: Pediatric patients (≤ 16 years) referred for 18F-FDG PET/CT or PET/MR imaging of the body during 2000 and 2021 were retrospectively included. The amount of administered radiotracer activity in megabecquerel (MBq) was recorded, and signal-to-noise ratio (SNR) was measured in the right liver lobe with a 4 cm³ volume of interest as an indicator for objective image quality. Descriptive statistics were computed.

Results: Two hundred forty-three children and adolescents underwent a total of 466 examinations. The median injected 18F-FDG activity in MBq decreased significantly from 296 MBq in 2000-2005 to 100 MBq in 2016-2021 ($p < 0.001$), equaling approximately one-third of the initial amount. The median SNR ratio was stable during all years with 11.7 (interquartile range [IQR] 10.7-12.9, $p = 0.133$).

Conclusion: Children have benefited from a massive reduction in the administered 18F-FDG dose over the past 20 years without compromising objective image quality.

Lung lesion detectability on decimated and CNN-based denoised ¹⁸F-FDG PET/CT

D. Faist[1], S. Gnesin[1], S. Medici[1], A. Khan[2], M. Nicod Lalonde[1], N. Schaefer[1], A. Depeursinge[1], M. Conti[3], J. Schaefferkoetter[3], M. Jreige[1], J.O. Prior[1]; [1] CHUV – Centre Hospitalier Universitaire Vaudois, Lausanne, Switzerland, [2] EPFL – Ecole Polytechnique Fédérale de Lausanne, Lausanne, Switzerland, [3] Siemens Medical Solutions USA, Knoxville, United States

Purpose: ¹⁸F-FDG PET/CT is fundamental for lung nodule (LN) characterization. We investigated the impact of PET decimation and AI image denoising on LN detectability at different noise levels simulating lower injected activity relevant for lung cancer screening conditions.

Methods and Materials: We retrospectively analyzed full statistics and decimated (30%, 10%, 5%, 2%, 1% of the full injected activity) ¹⁸F-FDG PET/CT simulating decreasing levels of injected activity in 10 patients presenting at least one LN. Full statistics data was acquired on a Biograph Vision (Siemens Medical Solutions, Knoxville TN). A CNN trained for denoising PET images generated output from the full statistics and the decimated PET reconstructions. Three readers assessed in consensus a LN detectability score varying from 0 (non-visible) to 3 (clearly visible) on a total of 12 randomized images per subject. SUV_{max} as a function of the decimation level was reported. LN detectability and quantitative measurements were compared between full statistics and the different decimation levels.

Results: We analyzed in total 20 lung lesions on 120 ¹⁸F-FDG PET/CT reconstructions (60 with denoising). Overall, the mean LN SUVmax and size were 6.7± 9.3 and 20.3±22mm. LN score (0,1,2,3) was: 15/15/17.5/52.5%, 27.5/2.5/15/55%, 30/17.5/7.5/45%, 30/22.5/10/37.5%, 45/20/15/20%, 52.5/25/10/12.5% for 100, 30, 10, 5, 2 and 1%, decimations, respectively. We found significant differences in LN scores in 2 and 1% decimations (p=0.007 and p=0.000), but not with 30, 10 and 5% in comparison to full statistics (p=0.162, p=0.272, p=0.220, respectively). There was no significant difference of the SUV_{max} across decimation levels (p=0.099).

Conclusion: We found comparable lesion score detectability on different decimated images until 5% of the full injected activity. This result encourages the possibility of the implementation a low-dose ¹⁸F-FDG PET/CT in perspective of lung cancer screening.

A141

Characterisation of CNN-based image denoising for lesion detection in lung cancer screening with F-18-FDG PET/CT

S. Gnesin[1], A. Khan[1], S. Medici[1], P. Monnin[1], D. Faist[2], M. Conti[3], J. Schaefferkoetter[3], M. Jreige[2], J.O. Prior[2]; [1] CHUV – Centre Hospitalier Universitaire Vaudois, Institute of Radiation Physics, Lausanne, Switzerland, [2] CHUV – Centre Hospitalier Universitaire Vaudois, Department of Nuclear Medicine and Molecular Imaging, Lausanne, Switzerland, [3] Siemens Medical Solutions USA, Knoxville, United States

Purpose: Artificial intelligence (AI), including convolutional networks (CNNs) has been introduced to improve image quality (IQ) and signal recovery in challenging image noise conditions, while preserving clinical image information. We characterize the impact of CNN denoising on the detectability of lung nodules with ^{18}F-FDG PET at different noise levels simulating reduced injected activity such as used in lung cancer screening.

Methods and Materials: CNN-denoising trained to reproduce full-statistic IQ, was applied to the full-statistic PET data and decimated to 30%, 10% and 5% of the original count statistics in 50 patients having ^{18}F-FDG PET (Biograph Vision, Siemens Medical Solutions, Knoxville TN). For each reconstructed dataset, we analysed the contrast-to-noise ratio (CNR) of 78 lesions, identified in the full-count images to estimate detectability, computed lung and liver signal-to-noise ratio (SNR) to assess overall IQ and performed spatial spectral analysis in the normal lung parenchyma.

Results: The mean lung/liver SNR increased by a factor 1.8/3.6, 3.2/5.1 and 4.9/6.6 in the 30%, 10% and 5% reconstructions as compared to their non-denoised counterparts. Comparing CNN-denoising improved the mean CNR by a factor 1.2, 1.5 and 1.7 in the 30%, 10% and 5% reconstructions respectively. The 30%, 10% and 5% CNN-denoised images preserved on average 96%, 89% and 74% of the full-statistic CNR respectively. We found Poisson noise and preserved spatial resolution across decimations.

Conclusion: The CNN-denoised images demonstrated IQ improvement over the non-denoised counterparts with higher lesion CNR and increased lung/liver SNR allowing activity reduction to 5-10% of normal injected activity. Spatial resolution was preserved. Additional PET datasets and application of model-observer models to better reflect the actual clinical significance of CNN denoising for lesion detectability are under investigation.

A84

Improved imaging of small lung nodules using LAFOV [18F]FDG-PET and data driven motion compensation method

C. Bregenzer[1], A. Weissensee[1], C. Mingels[1], M. Viscione[1], H. Sari[1,2], A. Rominger[3], T. Pyka[3]; [1] Inselspital – Universitätsspital Bern, Universitätsklinik für Nuklearmedizin, Bern, Switzerland, [2] Siemens Healthcare AG, ACIT – Advanced Clinical Imaging Technology, Lausanne, Switzerland, [3] Inselspital – Universitätsspital Bern, Bern, Switzerland

Purpose: Detection and characterization of lung nodules with PET has traditionally been imposed a size limit (≥ 8mm). With new long axial field of view (LAFOV) PET scanners sensitivity has been shown to be superior to traditional standard axial field of view (SAFOV) scanners. In order to improve imaging of lung lesions, data driven gating-based motion correction algorithm (DDG-MC) is available to compensate for respiratory movement.

Methods and Materials: 56 consecutive patients with a total of 100 lung lesions which had undergone [18F]FDG-PET/CT on a LAFOV PET/CT scanner (106 cm FOV) were included. Data for both LAFOV mode (600 s, maximum ring difference (MRD) 322) and sSAFOV acquisition (120 s per bed position, MRD 85) with and without data driven gating-based motion correction were reconstructed. Standard uptake values (SUV)mean/max/peak of liver, blood pool and lung background, likewise tumor volume and lesion uptake were calculated (volume of interest, 40% isocontour). SNR and CNR with lung background were calculated.

Results: Median largest lesion size was 7 mm. Lesion signal intensity above lung background was found in 31/33 small lesions (<6 mm, SUVmax 4.22±5.6; 6-8 mm in 30/30, SUVmax 8.89±11.62; ≥8 mm in 37/37, SUVmax 9.03±8.59). SNR and CNR were significantly increased in LAFOV compared to sSAFOV mode (p≤0.01; HS 2 min 29.28±30.57/26.28±30.26, HS 2 min+DDG-MC 37.98±47.14/34.98±46.80, UHS 6 min 32.78±34.66/29.00±34.18, UHS 6 min+DDG-MC 39.85±48.94/36.09±28.51). CNR in sSAVOF 2min with DDG-MC was comparable to UHS 6 minutes without motion correction (CNR: p=0.06).

Conclusion: UHS acquisition of LAFOV PET/CT with DDG-MC showed significantly higher SNR und CNR in small lung lesions. Higher detection rate compared to SAVOF could be achieved and possibly pushes the lower size limits for reliable characterization. Correlation with the final diagnosis is ongoing to determine sensitivity and specificity.

A85

Predictive value of 18F-PSMA PET/CT in mCRPC patients before 177Lu-PSMA therapy and correlation with first post-treatment scintigraphy

M. Cuzzocrea[1], G. Treglia[2,3,4,5], T. Ruberto[6], L. Ceriani[6,7], G. Paone[1,4]; [1] EOC – Ente Ospedaliero Cantonale, IIMSI – Imaging Institute of Southern Switzerland, Bellinzona, Switzerland, [2] EOC – Ente Ospedaliero Cantonale, IIMSI – Imaging Institute of Southern Switzerland, Clinic for Nuclear Medicine and Molecular Imaging, Bellinzona, Switzerland, [3] EOC – Ente Ospedaliero Cantonale, Health Technology Assessment Unit, Academic Education, Research and Innovation Area, Bellinzona, Switzerland, [4] USI – Università della Svizzera Italiana, Faculty of Biomedical Sciences, Lugano, Switzerland, [5] CHUV – Centre Hospitalier Universitaire Vaudois, Department of Nuclear Medicine and Molecular Imaging, Lausanne, Switzerland, [6] EOC – Ente Ospedaliero Cantonale, IIMSI – Imaging Institute of Southern Switzerland, Lugano, Switzerland, [7] USI – Università della Svizzera Italiana, Facoltà di Scienze Biomediche, Lugano, Switzerland

Purpose: Lutetium-177 prostate-specific membrane antigen radioligand therapy (177Lu-PSMA-RLT) is a promising targeted treatment for patients with metastatic castration resistant prostate cancer (mCRPC), but identifying who will benefit most from this therapy is still an unmet clinical need. We investigated whether quantitative parameters of 18F-PSMA-1007 PET/CT (PSMA-PET/CT) performed prior to 177Lu-PSMA-RLT can predict early biochemical recurrence within the first two cycles (EBR) and overall survival (OS). We also evaluated the concordance of PSMA-PET/CT with the first post-treatment Lu-PSMA scintigraphy.

Methods and Materials: We retrospectively collected quantitative parameters of pre-therapeutic PSMA-PET/CT including SUV-derived parameter of the reference lesion (RL-SUV) and PSMA tumor volume derived parameters (PSMA-TV). We performed a comparison between PSMA-PET/CT and Lu-PSMA scintigraphy, including lesions > 1 cm, using salivary glands as the reference organ to establish concordance of lesion uptake.

Results: 29 patients were included and 910 lesions were segmented on PSMA-PET/CT. In multivariate Cox regression, tPSMA-TV% was the only one significantly associated with EBR (0.93 [95%CI 0.87-0.99], p= 0.04). At ROC analysis, tPSMA-TV% correctly classified patients with EBR with a cut-off value of ≤55.6 (AUC 0.875 [95%CI 0.636-0.981], Sn 78.6%, Sp 100%, p< 0.001). Patients with lower tPSMA-TV% had earlier biochemical relapse (3.4 months [95%CI 2.6 - 4.2] vs 8.3 [95%CI 6.2 -10.5], p<0.0001). Patients with lower concordance between PSMA-PET/CT lesions and Lu-PSMA scintigraphy had a worse outcome.

Conclusion: These preliminary results highlight the promising role of quantitative PSMA-PET/CT parameters as potential predictors of patient outcomes. The concordance between PSMA-PET/CT and first Lu-PSMA scintigraphy also correlates with better outcome, but further studies on larger patient cohorts are needed.

A86

Impact of different PSMA PET tracers on patient selection for radioligand therapy with [¹⁷⁷Lu]Lu-PSMA-617

C. Popescu[1], B. Zhang[2], T. Sartoretti[3,4], J. Heimer[5], N. Spielhofer[1], S. Skawran[4], M. Messerli[4], A. Sauter[1,6], M. Hüllner[4], P.A. Kaufmann[4], I.A. Burger[1,4], A. Maurer[4]; [1] KSB - Kantonsspital Baden, Department of Nuclear Medicine, Baden, Switzerland, [2] ETH – Center for Radiopharmaceutical Sciences, Paul Scherrer Institute, Zurich, Switzerland, [3] ETH – Center for Radiopharmaceutical Sciences, Paul Scherrer Institute, Department of Health Sciences and Technology, Zurich, Switzerland, [4] USZ – Universitätsspital Zürich, Department of Nuclear Medicine, Zurich, Switzerland, [5] ETH – Center for Radiopharmaceutical Sciences, Paul Scherrer Institute, Department of Mathematics, Seminar for Statistics, Zurich, Switzerland, [6] Universitätsklinikum Tübingen, Department of Radiology, Tuebingen, Germany

Purpose: Liver uptake in [⁶⁸Ga]Ga-PSMA-11 PET/CT is used as internal reference in addition to clinical parameters to select patients selection for [¹⁷⁷Lu]Lu-PSMA-617 therapy. Logistical reasons led to a replacement of [⁶⁸Ga]Ga-PSMA-11 with [¹⁸F]F-PSMA-1007, a more lipophilic tracer with different biodistribution. Splenic uptake was proposed as internal reference for this tracer. We compared intra-patient tracer distribution between [⁶⁸Ga]Ga-PSMA-11 and [¹⁸F]F-PSMA-1007.

Methods and Materials: We retrospectively included fifty patients from two centers who underwent PET-examinations with both [¹⁸F]F-PSMA-1007 and [⁶⁸Ga]Ga-PSMA-11 scans within one year, between December 2018 to April 2023. Quantitative values for normal distribution (SUVmean) were obtained for liver, spleen, salivary glands, blood pool and bone. If present, primary tumor, local recurrence, lymph node, bone, or visceral metastasis were assessed (SUVmax) as well, for intra- and inter-individual comparison.

Results: Liver uptake was significantly higher on [¹⁸F]F-PSMA-1007 (SUVmean 11.7±3.9) compared to [⁶⁸Ga]Ga-PSMA-11 (SUVmean 5.4±1.7, $p < .05$), but also splenic uptake was significantly higher on [¹⁸F]F-PSMA-1007 (SUVmean 8.1±3.5, $p < .05$). Only blood pool was comparable between both scans. Malignant lesions did not show more intense uptake on [¹⁸F]F-PSMA-1007. Intra-individual comparison of liver uptake between both scans showed a linear association for hepatic uptake with SUVmean [⁶⁸Ga]Ga-PSMA-11 = 0.33 x SUVmean [¹⁸F]F-PSMA-1007 + 1.52 ($r = 0.78$, $p < .001$).

Conclusion: As expected, liver uptake on [¹⁸F]F-PSMA-1007 was significantly higher compared to [⁶⁸Ga]Ga-PSMA-11, but so was splenic uptake. The high intra-individual linearity of hepatic accumulation between both scans might allow using a conversion factor, as a base for therapy selection instead of the spleen as internal organ reference.

A102

Cyclotron production of terbium-155 via an indirect production route for its potential application in SPECT imaging

A.N. Moiseeva, C. Favaretto, Z. Talip, A. Sommerhalder, H. Zhang, N.P. van der Meulen; ETH – Center for Radiopharmaceutical Sciences, Paul Scherrer Institute, Villigen, Switzerland

Purpose: The purpose of the study is to achieve scalable production of ^{155}Tb ($T_{1/2}$=5.32 d, Eγ=87 keV (32%) 105 keV (25%)) by proton irradiation of naturally occurring ^{159}Tb for its potential application in SPECT imaging while avoiding costly enriched target material. The indirect reaction ^{159}Tb(p,5n)^{155}Dy → ^{155}Tb provides radionuclidically pure ^{155}Tb of high activity, without undesirable ^{156}Tb in the final product after chemical separation of Dy from Tb.

Methods and Materials: Initial experiments utilizing the required (p,5n) nuclear reaction were performed with the Injector 2 cyclotron at Paul Scherrer Institute. To date, 15 irradiations of Tb$_4$O$_7$ targets have been conducted to explore the production of ^{155,156}Tb at various proton energies. In order to obtain radionuclidically pure ^{155}Tb, a rapid separation of the dysprosium-155 fraction from the irradiated target (Stage I), along with subsequent purification of ^{155}Tb produced via ^{155}Dy decay (Stage II), was developed. The indirect production method was then compared to the previously established ^{156}Gd(p,2n)^{155}Tb method.

Results: The indirect production route showed comparable yields to the direct ^{156}Gd(p,2n)^{155}Tb reaction (1.2 GBq of ^{155}Tb after 8h irradiation) but superior radionuclidic purity due to the potential chemical elimination of co-produced terbium isotopes. In particular, the developed chemical separation was able to separate 10 μg Dy from 40 mg Tb$_4$O$_7$ using 0.11 M hydroxy isobutyric acid (HIBA) and Sykam resin, obtaining good chemical quality (controlled by ICP-OES). Additionally, the time to perform the initial separation would take 4 h, yielding a loss of only ~25 % of ^{155}Dy for its decay.

Conclusion: Experimental results have shown that indirect production of ^{155}Tb via ^{159}Tb(p,5n)^{155}Dy→^{155}Tb route is promising for the large-scale production of ^{155}Tb in radionuclidicly pure form for preclinical and potential clinical studies in future.

A103

Developing cyclotron based scandium-44 production towards clinical translation

P. Grundler[1], L. Gerchow[1,2], C. Favaretto[1,3], G. Dellepiane[4], C. Vigo[2], S. Braccini[4], R. Schibli[1,2], C. Müller[1,5], N. van der Meulen[1]; [1] ETH – Center for Radiopharmaceutical Sciences, Paul Scherrer Institute, Villigen, Switzerland, [2] ETH – Center for Radiopharmaceutical Sciences, Paul Scherrer Institute, Zurich, Switzerland, [3] USB – Universitätsspital Basel, Basel, Switzerland, [4] University of Bern, Bern, Switzerland, [5] ETH Zurich, Zürich, Switzerland

Purpose: The positron-emitting radionuclide ^{44}Sc decays with a half-life of 4 h, shows a coordination chemistry similar to ^{177}Lu and would enable the acquisition of PET images of a higher resolution than possible with ^{68}Ga. Therefore, it presents a promising alternative for diagnostic applications within theragnostic systems. The ability to produce this radionuclide with medical cyclotrons is an important step towards its clinical translation.

Methods and Materials: Isotopically enriched ^{44}Ca-44 (97%) was used as oxide to press solid target disks for proton irradiation. The aluminium-encapsulated targets were irradiated with ~10.3 MeV protons using appropriate degraders at solid target stations (STS) on IBA 18 MeV cyclotrons either at the University Hospital in Bern, at ETH Zürich or at the 72 MeV Injector-II cyclotron at PSI. The radiochemical separation of ^{44}Sc from the target was performed at PSI using extraction and ion exchange techniques. The radionuclidic purity was assessed by gamma-spectrometry and the radiochemical purity by test labeling of DOTATOC.

Results: Depending on irradiation duration (0.5 to 4 hours) and beam current (5 to 50 μA), activities up to 4 GBq at End of Separation (EoS) were obtained. By selecting a proton energy at ~10.3 MeV, it was possible to minimize the content (<1% at EoS) of ^{44m}Sc ($t_{1/2}$ 2.4 d) without notably affecting the yield of ^{44}Sc. Other radionuclidic impurities such as ^{47}Sc, ^{46}Sc, ^{88}Y were present at negligible levels (≤ 0.1% at EoS). The radiochemical purity of production batches ≥1 GBq was sufficient to achieve routine labeling of DOTATOC at 25 MBq/nmol. Unused ^{44}Ca can be recycled after ^{44}Sc separation.

Conclusion: ^{44}Sc can be produced in quantities and quality suitable for preclinical and clinical investigation using 18 MeV medical cyclotrons equipped with a STS. In the near future, it is envisaged to translate the labeling of ^{44}Sc to an automated production module system in a GMP setting, initiating the steps towards its clinical implementation.

A104

Tolerability of [^{161}Tb]Tb-SibuDAB in immunocompetent mice

K. Krieger[1,2], A.K. Mapanao[3], S.D. Busslinger[1], N.P. van der Meulen[1,1], U. Köster[4], R. Schibli[1,2], C. Müller[1,5]; [1] ETH – Center for Radiopharmaceutical Sciences, Paul Scherrer Institute, Villigen, Switzerland, [2] ETH – Center for Radiopharmaceutical Sciences, Paul Scherrer Institute, Department of Chemistry and Applied Biosciences, Zurich, Switzerland, [3] ETH – Center for Radiopharmaceutical Sciences, Paul Scherrer Institute, Center for Radiopharmaceutical Sciences, Villigen, Switzerland, [4] Institut Laue-Langevin, Grenoble, France, [5] ETH – Center for Radiopharmaceutical Sciences, Paul Scherrer Institute, Zurich, Switzerland

Purpose: [^{161}Tb]Tb-SibuDAB was developed with the aim to increase the efficacy of PSMA-targeted radioligand therapy in prostate cancer. The goal of this prospective study was to investigate potential undesired early adverse events in mice after application of supratherapeutic activities of [^{161}Tb]Tb-SibuDAB.

Methods and Materials: Animal experiments were ethically approved by the responsible cantonal authorities (license N_75668). Five-to-six-week-old female immunocompetent FVB mice were injected with 15, 30 or 60 MBq of [^{161}Tb]Tb-SibuDAB or vehicle control (n = 6 each). Body masses were measured thrice weekly and the mice monitored for predefined endpoint criteria. Blood cell counts were obtained from sublingual blood samples on 10, 28 and 56 days post-injection (p.i.). Plasma albumin, bilirubin, alkaline phosphatase and blood urea nitrogen were determined using retrobulbar samples on Day 56 p.i. Organ masses were obtained following necropsy on Day 56 p.i. and organ-to-brain-mass ratios calculated. Statistical analysis was performed in GraphPad Prism.

Results: Across all groups, a dose-dependent decrease in blood cell counts was observed on Day 10 p.i. relative to vehicle controls. Illustratively, decreases of red and white blood cells and platelets of 10%, 55% and 38% relative to vehicle controls, respectively, were observed in the 60 MBq group (p < 10^{-5}). Blood cell counts recovered during follow up and no significant differences were observed between groups at the study endpoint. No significant differences between the experimental groups were found in terms of plasma parameters, body mass gain, nor relative organ masses.

Conclusion: In healthy outbred mice, [^{161}Tb]Tb-SibuDAB applied at over 10-fold higher activity than required for tumor control induced transient aplasia, which fully resolved by the end of the eight-week observation period. No other adverse effects were noted. These results encourage a translation to human trials.

A105

Assessment of two gallium-68 labeled dimeric ligands for diagnostic imaging of tumors expressing FAP

A. Bilinska[1], E. Menéndez[1], E. Pilatis[1], M. Marcel[2], T. Läppchen[1], F. Rösch[2], A. Rominger[1], E. Gourni[1]; [1] Inselspital – Universitätsspital Bern, Department of Nuclear Medicine, Bern, Switzerland, [2] Johannes Gutenberg University, TRIGA site – Department of Chemistry, Mainz, Germany

Purpose: Within the tumor microenvironment, fibroblast activation protein (FAP) plays a pivotal role in tumor invasion and extracellular matrix (ECM) remodeling. With its prevalent expression in over 90% of human cancers and minimal presence in healthy tissues, FAP emerges as an attractive target for non-invasive imaging and therapy.

This study assesses the in vitro and in vivo efficacy of two gallium-68 labeled FAP-based dimers, namely DOTAGA.Glu$_2$(FAPi)2 (**1**) and DO$_3$A.Glu$_2$(FAPi)$_2$ (**2**), as potential diagnostic tools for FAP-expressing tumors.

Methods and Materials: Gallium-68 labeling was applied to (**1**) and (**2**). In vitro evaluations encompassed lipophilicity, protein binding, saturation, and internalization on cancer-associated fibroblasts with high FAP expression. In vivo studies, including biodistribution, PET imaging, and metabolic stability, were conducted on PC3 xenografts.

Results: [^{68}Ga]Ga-**1** and [^{68}Ga]Ga-**2** exhibited molar activities between 17 to 22 MBq/nmol and logD$_{octanol/PBS}$ of -2,9 ± 0,1 and -2,2 ± 0,04 respectively. Approximately 9% of the activity bound to proteins after a 30-minute incubation with human serum. Both radiotracers displayed a strong affinity for FAP, with K_d values ranging from 0.7 to 1 nM, and a substantial internalization rate peaking at about 40%. Metabolic studies 10 minutes post-injection in mice revealed that the remaining circulating activity in the blood consisted of intact radiotracer in both cases. Biodistribution studies revealed tumor uptake of 16.1±2.3 for [^{68}Ga]Ga-**1** and 19.0±2.4 for [^{68}Ga]Ga-**2** at 1h post-injection. The biodistribution data aligned well with PET imaging results.

Conclusion: The findings substantiate the potential utility of [^{68}Ga]Ga-**1** and [^{68}Ga]Ga-**2** as diagnostic radiotracers for stromal tumor imaging through FAP targeting.

A106

Evaluation of the therapeutic efficacy a lutetium-177 labeled gastrin-releasing peptide receptor (GRPR) antagonist on PC3 tumor bearing mice

A. D'Onofrio[1], E. Pilatis[1], E. Menéndez[1], E.S. Moon[2], T. Läppchen[1], F. Rösch[2], A. Rominger[1], E. Gourni[1]; [1] Inselspital – Universitätsspital Bern, Department of Nuclear Medicine, Bern, Switzerland, [2] Johannes Gutenberg University, TRIGA site – Department of Chemistry, Mainz, Germany

Purpose: The current study aimed to explore the potential of a radiolabeled peptide targeting the Gastrin-Releasing Peptide Receptor (GRPR) as a theranostic tool for various human tumors, particularly in the context of prostate cancer.

Methods and Materials: A statine-based GRPR antagonist (LF1), functionalized with AAZTA[5] via the 4-amino-1-carboxymethyl-piperidine (Pip) spacer, was labeled with lutetium-177. The research assessed the blood clearance, binding to plasma proteins, and metabolic stability of [177Lu]Lu-LF1 in healthy mice. Additionally, biodistribution studies and SPECT/CT imaging were conducted in mice with PC3 tumors.

Results: [177Lu]Lu-LF1 was successfully obtained with high radiochemical purity (>99%) and molar activities reaching up to 44 GBq/μmol. It displayed rapid blood clearance and minimal binding to plasma proteins (2–3% at 5 and 15 min post-injection). Enzymatic degradation revealed 39% intact [177Lu]Lu-LF1 in blood 15 min post-injection. The radiotracer exhibited substantial and specific tumor uptake, with values of 42±5.0 and 8.5±2.3% I.A./g at 1 and 72 h post-injection, respectively. Non-target tissues and GRPR-rich organs such as the pancreas showed fast clearance (pancreas uptake decreased from 70 to 15% I.A./g from 1 to 4 h post-injection). The favorable pharmacokinetics of [177Lu]Lu-LF1 resulted in high-contrast SPECT/CT images.

Conclusion: The exceptional in vivo performance of [177Lu]Lu-LF1, characterized by sustained high tumor uptake and low background radioactive signals, positions this radiotracer as a promising candidate for GRPR-targeted radionuclide therapies. Further studies, particularly therapeutic investigations in PC3 tumor models, are planned to validate its potential as a therapeutic agent for prostate cancer.

A95

Folate receptor α– a promising target for radionuclide therapy of ovarian cancer

B. Hunkeler[1,2], A.K. Mapanao[3], R. Schibli[1], C. Müller[1], N. Rupp[2,4]; [1] ETH – Center for Radiopharmaceutical Sciences, Paul Scherrer Institute, Zurich, Switzerland, [2] USZ – Universitätsspital Zürich, Department of Pathology and Molecular Pathology, Zurich, Switzerland, [3] ETH – Center for Radiopharmaceutical Sciences, Paul Scherrer Institute, Center for Radiopharmaceutical Sciences, Zurich, Switzerland, [4] University of Zurich, Faculty of Medicine, Zurich, Switzerland

Purpose: The folate receptor alpha (FRa) is expressed in carcinomas of diverse tissue origin, most prominently in the ovary. FR beta (FRb), another isoform, is mainly considered an immune cell marker but has recently also been described on cancer cells. The novel FRa-selective radiofolate [177Lu]Lu-6S-RedFol-1 holds promise for FRa-targeting therapy. To assess the need for a FRa-selective radioconjugate in ovarian carcinoma therapy, we investigated FRa and FRb expression in ovarian carcinoma biopsies.

Methods and Materials: Two tissue microarrays (n = 179 ovarian carcinomas, 2-3 spots per case) of diverse subtype were stained immunohistochemically for FRa (26B3.F2; Biocare Medical) and FRb (polyclonal; GeneTex). Antibody specificity was confirmed using xenografts of transfected cells exclusively expressing FRa (CHO-FRa) or FRb (CHO-FRb). Membranous FR staining intensity was semi-quantitatively evaluated (0 = negative, 1 = weak, 2 = moderate, 3 = strong) and the fraction of positive cells (in %) recorded. An immunoreactivity score (IRS) was calculated based on the intensity and fraction (IRS = intensity x fraction). An IRS ≥ 150 was considered clinically significant.

Results: FRa expression was observed in 79% of all investigated tissues, with a median IRS of 100, and 45% above an IRS of 150 (clinically significant). High-grade serous carcinoma, representing 75% of ovarian carcinoma, demonstrated significantly elevated FRa expression (median IRS = 190; 62% of IRS ≥ 150). Mucinous carcinomas displayed low FRa levels (median IRS = 0; 8% of IRS ≥ 150), while the remaining subtypes exhibited clinically significant FRa expression in 29-35% of tissues. FRb was absent in all evaluated tissues.

Conclusion: This study underscores the clinical relevance of FRa as a promising target for radionuclide therapy of ovarian cancer, particularly in high-grade serous type. Consequently, our current leading compound, the FRa-selective [177Lu]Lu-6S-RedFol-1 will be further developed for targeted radionuclide therapy.

A96

The somatostatin receptor subtype 2 antagonist DOTA-LM3 labelled with Beta- and Auger-electron emitter terbium-161: Interim results of the Phase 0 "Beta plus" Study in patients with neuroendocrine tumors

J. Fricke[1], F. Westerbergh[2], L. McDougall[3], C. Favaretto[1,4], E. Christ[5], G. Nicolas[1], S. Geistlich[4], M. Fani[6], N.P. van der Meulen[4], C. Müller[4], R. Schibli[4], P. Bernhardt[2], D. Wild[1]; [1] USB – Universitätsspital Basel, Division of Nuclear Medicine, Basel, Switzerland, [2] University of Gothenburg, Department of Radiation Medical Sciences, Gothenburg, Sweden, [3] USB – Universitätsspital Basel, Department of Nuclear Medicine, Basel, Switzerland, [4] ETH – Center for Radiopharmaceutical Sciences, Paul Scherrer Institute, Villigen, Switzerland, [5] USB – Universitätsspital Basel, Department of Endocrinology, Basel, Switzerland, [6] USB – Universitätsspital Basel, Division of Radiopharmaceutical Chemistry, Basel, Switzerland

Purpose: The goal of this Phase 0 study (NCT05359146) was the determination of absorbed doses in tumors and relevant organs together with the evaluation of [161Tb]Tb-DOTA-LM3 toxicity in comparison with [177Lu]Lu-DOTATOC in a cohort of gastroenteropancreatic tumor patients.

Methods and Materials: In this randomized, cross-over, prospective, single-center, open-label Phase 0 study, three of eight patients were evaluated to date. Patients received 1 GBq [161Tb]Tb-DOTA-LM3 followed by 1 GBq [177Lu]Lu-DOTATOC over a 4-week interval. Quantitative SPECT/CT was performed ~3, ~24, ~72 and ~168 h after infusion of both radiopharmaceuticals to calculate tumor and organ absorbed doses (3D dosimetry using Monte-Carlo-based OSEM algorithm).

Results: The median (range) of the mean tumor absorbed doses of 1 GBq [161Tb]Tb-DOTA-LM3 and 1 GBq [177Lu]Lu-DOTATOC were 57 (28 – 86) and 6.7 (3.4 – 10) Gy/GBq, respectively. The median (range) kidney and spleen absorbed doses were 3.0 (2.7 – 3.3) and 5.5 (4.1 – 6.9) Gy/GBq for [161Tb]Tb-DOTA-LM3 and 0.68 (0.66 – 0.69) and 2.9 (1.1 – 4.7) Gy/GBq for [177Lu]Lu-DOTATOC, respectively. SPECT/CT after injection of only 1 GBq [161Tb]Tb-DOTA-LM3 revealed excellent imaging quality with intense tumor uptake and a long median of the mean (range) effective tumor half-life of 120 (110 – 130) hours. According to CTCAE v5.0, there were three grade 1 adverse events (leukocytopenia, thrombocytopenia) in two of the three patients after infusion of 1 GBq [161Tb]Tb-DOTA-LM3.

Conclusion: [161Tb]Tb-DOTA-LM3 shows a 8.5-fold higher tumor absorbed dose and twice higher tumor-to-kidney absorbed dose ratio compared to [177Lu]Lu-DOTATOC. The administration of 1 GBq [161Tb]Tb-DOTA-LM3 was safe in all patients without relevant adverse events.

A97

Radiolabeled Somatostatin Receptor Antagonist versus Agonist for Peptide Receptor Radionuclide Therapy – interim analysis of a retrospective phase II study

A. Mushaweh[1], C. Eigler[1], L. McDougall[1], A. Baumann[1], E. Christ[2], G. Nicolas[1], M. Fani[1], D. Wild[1]; [1] USB – Universitätsspital Basel, Clinic for Radiology and Nuclear Medicine, Basel, Switzerland, [2] USB – Universitätsspital Basel, Department of Endocrinology, Diabetology and Metabolism, Basel, Switzerland

Purpose: Our aim was to compare tumor and organ doses as well as to measure medium progression free survival (PFS) after standard therapy with [177Lu]Lu-DOTATOC and after new [177Lu]Lu-DOTA-JR11 therapy in the same patients with therapy resistant metastatic neuroendocrine tumors (NETs).

Methods and Materials: In this retrospective, single-center, open label phase II study, 14 consecutive patients with metastatic gastroenteropancreatic NETS, NETs of the lung and pheochromocytoma were included so far: 12/14 males (age range 26-78 years). Only patients with a PFS of ≤14 months after last standard therapy with [177Lu]Lu-DOTATOC (2-4 cycles, 5.6- 7.5 GBq) were included. These patients received one cycle [177Lu]Lu-DOTATOC (5.1- 7.4 GBq) followed by 1-2 cycles [177Lu]Lu-DOTA-JR11 (2.7-4.8 GBq). Quantitative SPECT/CT was performed ~24, ~48, ~168h after injection of both radiopharmaceuticals to calculate tumor and organ doses (Olinda 3D dosimetry). Follow-up morphological imaging was done every ~3 months.

Results: The median (range) of the mean tumor and kidney doses were 101.6 (8.9-395.9) and 1.8 (1.1-3.4) Gy/cycle for [177Lu]Lu-DOTA-JR11 and 33.7 (4.2-225.1) and 1.8 (0.9-2.1) Gy/cycle for [177Lu]Lu-DOTATOC. There were 5 grade 2 adverse events (anemia, hepatic, hypokalemia) after [177Lu]Lu-DOTATOC therapy, and 4 grade 2 adverse events (anemia, hepatic) after [177Lu]Lu-DOTA-JR11 therapy. No grade 3 or higher adverse events were observed. Median PFS was 12 (95% Ci, 6-14) months after standard therapy with 2-4 cycles [177Lu]Lu-DOTATOC and 17 (95% Ci, 7-30) months after one cycle [177Lu]Lu-DOTATOC plus 1-2 cycles [177Lu]Lu-DOTA-JR11 (hazard ratio for disease progression or death with [177Lu]Lu-DOTA-JR11 vs. [177Lu]Lu-DOTATOC, 0.30; 95% Ci, 0.09-0.98; P=0.045).

Conclusion: [177Lu]Lu-DOTA-JR11 shows 1.8-5.0 times higher tumor dose per patient and cycle compared to [177Lu]Lu-DOTATOC resulting in a 5 months longer median PFS.

A98

Significance and possible utility of quantitated 177Lu-PSMA SPECT/CT-based measurements of the Molecular Tumor Volume 1h vs 24h vs 48 h pi. and its change over time to predict PSMA RLT outcome.

A. Zyrek[1], A. Chirindel[1], A. Bauman[1], M. Fani[1], E. Nitzsche[2], F. Forrer[3], A. Afshar-Oromieh[4], N. Schaefer[5], D. Wild[1], G. Nicolas[1]; [1] USB – Universitätsspital Basel, Clinic for Radiology and Nuclear Medicine, Basel, Switzerland, [2] KSA – Kantonsspital Aarau, Nuclear Medicine and PET-Center, Aarau, Switzerland, [3] KSSG – Kantonsspital St. Gallen, Department of Nuclear Medicine, St.Gallen, Switzerland, [4] Inselspital – Universitätsspital Bern, Nuclear Medicine, Bern, Switzerland, [5] CHUV – Centre Hospitalier Universitaire Vaudois, Department of Nuclear Medicine, Lausanne, Switzerland

Purpose: PSMA-targeted radionuclide therapy (PSMA-RLT) response assessment with post-therapy SPECT/CT at 24 or 48 h p.i has been proven clinically useful for predicting outcome. However, post-therapy SPECT/CT could be acquired as early as 1h p.i in a possible out-patient setting. We aim to compare the consistency and accuracy of molecular tumor volume (MTV-) change by post-therapy SPECT/CT imaging at 1h, 24h and 48h p.i, representing different therapy set-ups (out-patient vs in-patient therapy).

Methods and Materials: This is a retrospective, single centre study, based on the National PSMA-therapy Registry (BASEC ID: 2021-01271). We enrolled individuals with PSMA-expressing metastatic castration-resistant prostate cancer (mCRPC). The exclusion criteria consisted of PSMA negative (Tumor SUVmax threshold <3) or discrepant (PSMA-negative / FDG-positive) disease. ^{177}Lu-PSMA SPECT/CT was performed after the two first therapy cycles at 1h, 24h and 48h p.i. using reconstructed xQuant data. The MTV was segmented with MIMencore®, using SUV threshold ≥3. Image-based treatment evaluation (response: TTV change ≤0) was compared between each given timepoint and with PSA change between C1 and C2.

Results: The first 10 consecutive patients were screened and 8 patients fulfilled the eligibility criteria. TTV change consistently decreased in 7/8 patients for all tested timepoints. In 1 patient, TTV change was discrepant, decreasing at 1 and 24h p.i. while increasing at 48h. For this patient the PSA also increased from 289 at C1 to 350 ng/mL at C2.

Conclusion: These preliminary results indicate that MTV-based evaluation of ^{177}Lu-PSMA-therapy response status on post-therapy SPECT/CT is broadly consistent regardless of post-therapy imaging timepoint. Further enrolment is needed to assess the accuracy of imaging timepoints in comparison with established treatment outcome measures, i.e. PSA_{50} at 12 weeks and time-to-progression.

A109

Enhancing radiological anatomy learning with photorealistic volumetric rendering: insights from radiographer student education

J. Schmid[1], D.D. Rua[1], J. Perez Vasquez[1], D. Rodrigues[1], F.J. Taibo Pena[2], J.A. I. Guitián[2]; [1] HESAV/HES-SO – Haute Ecole de Santé Vaud, Geneva, Switzerland, [2] Universidade da Coruña, Coruña, Spain

Purpose: This study investigates the potential use of photorealistic volume rendering (PVR) in the Bachelor of Science (BSc) curriculum for radiography students.

Methods and Materials: We investigated the impact of PVR, a more realistic alternative to traditional volume rendering (VR) based on physically-based lighting simulation. This exploration involved both research and commercial (Siemens Cinematic Anatomy) applications. We conducted online anonymized surveys among second (n=27) and third-year (n=35) BSc radiography students, both before and after hands-on sessions with PVR. These surveys aimed to gauge the impact of PVR on learning radiological anatomy and user experience. The applications also included standard multiplanar imaging (MPR) and featured case studies, with existing anatomical annotations or the option to add them.

Results: The response rate to the surveys averaged 62%, ranging from 52% to 100%. Approximately 85% of second-year students believed that PVR could enhance their anatomical training and understanding of the impact of pathologies, and more than 92% preferred PVR over VR. Among third-year students, 73% found PVR beneficial for learning complex anatomies, and 55% preferred the combined use of PVR and MPR. The applications' interactivity and ease of use were key to user engagement, with case study annotation being a valuable learning and assessment tool, hinting at the potential of a quiz mode. Generally, PVR was seen more as a supplementary educational resource rather than a replacement for existing materials.

Conclusion: Our research indicates PVR could improve radiographers' education in radiological anatomy. Yet, the small sample size, low response rate, potential participation bias, and absence of quantitative learning metrics might restrict the broad applicability of our findings, positioning PVR as a complementary, rather than standalone, educational resource.

A110

Protocols and doses in neonatology: A Scoping Review

L. Haenggi[1], S. de Labouchere[2]; [1] CHUV – Centre Hospitalier Universitaire Vaudois, Lausanne, Switzerland, [2] HESAV/HES-SO – Haute Ecole de Santé Vaud, Lausanne, Switzerland

Purpose: Neonatal units admit newborns and premature neonate with a gestational age as low as 22 weeks and possibly, extremely low birth weights. X-rays are crucial for diagnostics and medical management, but they result in potentially harmful doses of ionizing radiation, especially for this very sensitive population who is at a higher risk of cancer. It is therefore essential to determine disparities in practices to work towards optimizing them. The aim of this scoping review is to synthesize protocols for chest X-rays and babygrams for the neonatal population.

Methods and Materials: The neonatal population and phantoms who undercame chest X-rays and babygrams in neonatology units worldwide were included. Exposure parameters, filtrations, detector placement, radiation dose, optimization proposals, and the number of radiographs were recorded. The search for these documents was limited to the year 2014, due to the transition to digital systems. Data was extracted from selected documents using an extraction table and results were presented narratively with tables and figures.

Results: The SR included 16 articles. The results showed disparities in practice between institutions and countries. Intervals between 48-75 kV and 0.32-6.3 mAs for protocols were found. Five articles reported entrance surface dose ranging from 8.11 to 2010 µGy, four dose area product ranging from 1.10 to 52.80 mGy.cm^2, and three effective dose: going up to 740 µSv. Nine out of the 16 articles identified optimization suggestions within the study.

Conclusion: The SR highlights the disparity in neonatal radiography protocols, demonstrates variability in radiation doses and the number of X-rays received by newborns, and provides optimization suggestions for future practices. Further research is needed to establish specific recommendations considering the characteristics of premature neonates, medical equipment, and available technology.

A111

A Serious game for personalized learning of MRI techniques and physics as part of the radiographer training program

C. Gaignot, M-A. Petit, G. Ismaili, J. Piguet, A. Sagne; HEdS – Geneva School of Health Sciences, Geneva, Switzerland

Purpose: We aim to assess if a serious game designed around the physical and theoretical principles of magnetic resonance imaging can boost radiographer students' motivation and improve their application of these concepts in professional settings.

Methods and Materials: Addressing challenges in physical and theoretical concepts of MRI education, this project focuses on the content of the first year of the Bachelor's degree in the MRI teaching module.This immersive game is designed to be adapted to each student's profile, allowing them to validate their skills after each success. To answer the question of motivation, we tested the "discover a radiology department" mission with first-year students to assess their satisfaction and the added value of the tool. The students' feedback was collected using online anonymized surveys.

Results: The results of the surveys and analysis show that the game is fulfilling its objective of being attractive and desirable. According to the 35 student respondents to the survey, 1st-year students gave the game a "good" satisfaction rate of 44% and a "very good" satisfaction rate of 56%. The analysis of the participants' written feedback shows that the tool could help students to take initiative during their internship.

Conclusion: The obtained preliminary results tend to support the use of this gamification platform for teaching MRI.This approach now needs to be enriched and improved in order to assess its performance in terms of anchoring knowledge retention and learning.

A112

Variation of signal intensity in post mortem MRI (PMMR) according to body temperature: Preliminary results

V. Frossard[1], C. Bruguier[1,2], V. Magnin[1], S. Grabherr[1], P. Genet[1]; [1] University Center of Legal Medicine of Lausanne-Geneva, Lausanne, Switzerland, [2] University Hospital Lausanne, Department of Radiology, Radiodiagnostic and Interventional Radiology, Lausanne, Switzerland

Purpose: Nowadays, forensic imaging methods are gaining in importance in forensic medicine, particularly the CT-scan is used routinely. However, in some medico-legal centers also PMMR-imaging is performed as a complement to forensic investigations. The same acquisition parameters as in clinical practice can be used for this purpose. However, in practice a loss of contrast on the MR-images, caused by a decrease of signal intensity related to the decrease of body temperature has been observed. Therefore the purpose of our study was to evaluate the signal intensity changes in T1 and T2 images with the decrease of the body temperature.

Methods and Materials: In this semi-quantitative retrospective study, we evaluated 40 neck PMMR examinations (1,5T, Ingenia, Philips Healthcare, Best, Netherlands) performed in cases of hanging. The evaluation was done by a radiology technician with experience in PMMR. Signal intensity was measured standardized in the subcutaneous fat, the muscle tissue, the spinal cord and a vertebral body (C6) in 2D T1, 2D T1 dixon (in phase) and 2D T2 dixon (in phase) sequences in sagittal plane. Rectal temperature was measured before each PMMR examination. A Pearsons' correlation test was used to determine the relation between signal intensity and body temperature for each defined anatomical region.

Results: Data are currently being analyzed and the final results will be presented at the congress.

Conclusion: Conclusion will depend on final results.

Exploring zero echo time and ultra-short echo time sequences in magnetic resonance imaging for the visualisation of cortical bone structures

L. Ferrari[1], T. Bianchi[1], M. Champendal[2], C. Sá dos Reis[2], S.S. Ghotra[2,3];
[1] ICH Sion – Institut Central des Hôpitaux, Department of Radiology, Sion, Switzerland, [2] HESAV/HES-SO – Haute Ecole de Santé Vaud, Lausanne, Switzerland, [3] eHnv – Hôpital of Yverdon-les-Bains, Department of Radiology, Yverdon-les-Bains, Switzerland

Purpose: To highlight the strengths, weaknesses, and technical specifications of Ultra-short Echo Time (UTE) and Zero Echo Time (ZTE) sequences for musculoskeletal system (MSK) investigations.

Methods and Materials: JBI methodology was deployed to search studies on PubMed and Embase databases published after 2005. Keywords and MeSH terms related to UTE, ZTE, magnetic resonance imaging (MRI) and the MSK were selected. Only studies involving living human participants were considered. Two independent reviewers examined eligible titles, abstracts and full texts. Disagreements were solved by consensus.

Results: 17 out of 671 studies met the inclusion criteria. UTE and ZTE sequences were mainly used for spine (6/17), lower limbs (4/17), head/neck (3/17), bones in general (3/17) and shoulder (1/17) examinations. A very short repetition time (TR) (0.425-8ms) was selected in 6 studies; 3 had a longer TR (100-1075ms), and 6 did not indicate. A very short echo time (TE) (0.00-0.34ms) was mentioned in all studies.
The short TE reached through the radial acquisition allows the acquisition of bone signal very quickly before it decreases, which improves the fracture assessment and makes these sequences comparable to other medical imaging techniques. Acquisition time has been mentioned as the main drawback, the sequence acquisition time varied between 3 to 12 minutes, with five studies indicating a time above 5 min (6-12min). The need of advanced technology has been reported as a fundamental requirement to perform UTE and ZTE.

Conclusion: The ability of UTE and ZTE to offer good contrast of bone structures, with adequate image quality was highlighted as an advantage. These sequences are an alternative method to visualize MSK. Further studies are required to assess acquisition time reduction and improve image quality, through contrast modification techniques and artificial intelligence.

Development of a free breathing in-phase and out-phase abdominal MRI sequence

A. Stöckli[1], E. Maturana[1], P-A. Poletti[1], J-P. Dillenseger[2], R. Salomir[1], M. Scheffler[1]; [1] HUG – Hôpitaux universitaires de Genève, Geneva, Switzerland, [2] Université de Strasbourg, Faculté de médecine, Strasbourg, France

Purpose: Abdominal MRI sequences requiring less than 20s are in general acquired under apnea. However, some patients are not able to perform stable or repeated breath holds, particularly in geriatric cases. Thus, motion artifacts can significantly hinder the image quality. As no commercially free-breathing T1-weighted (T1w) in-phase (IP) and out-of-phase (OP) sequence complied with the institutional quality standards on our MR system, and we did not have access to the novel generation of accelerated solutions (e.g. compressed sensing or IA-based denoising), we developed and compared in-house free-breathing strategies.

Methods and Materials: Exams were realized on a 3T MRI system (Skyra, Siemens, Erlangen, Germany) using a 30-channel surface body coil as well as a 32-channel integrated spine coil. We tested different sequence settings that allowed free-breathing IP-OP T1w acquisitions. We evaluated different strategies:
- a slice-per-slice respiration-triggered rapid gradient echo,
- radial volumetric interpolated breath-hold examination (StarVIBE),
- VIBE with the Dixon method.
- VIBE with the Dixon method and time-resolved angiography with interleaved stochastic trajectories (TWIST)
Modified parameters included echo time, bandwidth, and number of averages. Acquisition times were noted, and image quality was blind-rated by radiographers, residents, physicists, and radiologists using a five-point Likert scale.

Results: Among the different free-breathing options tested, the Dixon TWIST VIBE sequence with 35 averages required 2 min 27s acquisition time and peaked at 4.5 score, while 16 averages represented the best trade-off for clinical practice (1 min 13s acquisition time and score 4.4).

Conclusion: For geriatric patients, T1w abdominal IP and OP acquisitions can be efficiently performed using a conventional 1min 13s free-breathing TWIST VIBE sequence with Dixon method.

Brain MRI in full-term neonates: comparison between a dedicated pediatric and a standard head coil

H. El Begri Talbi, B. Delattre; HUG – Hôpitaux universitaires de Genève, Geneva, Switzerland

Purpose: In our department, we conduct brain MRIs on unstable neonates utilizing an MRI-compatible incubator, ensuring safer transfers with continuous vital sign monitoring. For these procedures, we employ a dedicated pediatric antenna, the NHC. The NHC can also be utilized outside the incubator for stable neonates. Smaller and better adapted to this age group than the standard HEAD coil, it does necessicate additional manipulations. Our study aims to assess the supplementary benefits of using the NHC outside the incubator in comparison to the HEAD coil specifically for stable, full-term neonates.

Methods and Materials: This retrospective study was performed on a Siemens Avanto 1.5T and compared the two coils performance (HEAD coil is a 20-channel Siemens coil, NHC is a 16-channel Nomag IC coil). Quantitative assessment of image quality was performed on a phantom (pig kidney) and 70 brain MRIs by calculation of the signal to noise ratio (SNR) and contrast to noise ratio (CNR). The specific absorption rate (SAR) delivered with each coil was also extracted from DICOM data. Qualitative assessments, performed by two pediatric radiologists and two MR technologists, considered motion artifacts evaluated on a Likert scale. Statistical analysis employed Student's t-Test to evaluate SNR, CNR, and SAR values for patients, while the Wilcoxon test was utilized for the phantom.

Results: Quantitative assessement on the phatom and patients showed that SNR did not differ significantly between the 2 coils (p > 0.05). No significant difference was found on the qualitative analysis of the images. However, SAR was significantly higher with the NHC compared to the HEAD coil (p < 0.05).

Conclusion: Outside the incubator, the NHC doesn't offer added advantages in terms of image quality and, in fact, escalates the energy deposited into patients. Additionally, its use poses more constraints in daily clinical practice, notably due to prolonged installation times.

Risk factors and methods to limit extravasation of contrast medium in computed tomography investigation: a scoping review

A. Meylan[1], L. Türke[1], S.S. Ghotra[1,2], S. Ding[1]; [1] HESAV/HES-SO – Haute Ecole de Santé Vaud, Lausanne, Switzerland, [2] eHnv – Hôpital of Yverdon-les-Bains, Department of Radiology, Yverdon-les-Bains, Switzerland

Purpose: The aim of this scoping review is to summarise current knowledge concerning the prevention of iodinated contrast medium extravasation in patients undergoing computed tomography (CT).

Methods and Materials: The study was conducted according to JBI methodology. Searches were performed on Pubmed and Embase, for articles published from 2018 to 2023 in French and English. Combinations of keywords and MeSH terms related to CT, contrast medium, contrast extravasation, iodine and injection site reaction were used. Two independent reviewers screened titles, abstracts, and eligible full text. Disagreements were solved through consensus

Results: A total of 580 articles were identified, with 22 meeting all criteria. In this study, the primary focus was to identify the risk factors for extravasations of contrast medium, the strategies to limit them and the indicators for evaluating the studied strategies. It appears that certain patient characteristics are among the risk factors. Concerning the strategies, prevention through communication and specific injection techniques, and the use of ultrasound guidance to insert venous lines were mentioned. In terms of indicators, the frequency and volume of extravasation have been assessed in the retrieved articles. For now, frequency seems to be studied more extensively than volume. A limitation of this review is that studies involving contrast medium extravasation with intraosseous catheters and central lines have been excluded. The results will be completed at the oral presentation, as these results are only preliminary.

Conclusion: These preliminary results already highlight that a certain number of articles have been published since the last systematic review. It would also be timely to update it.

A28

Detection of pulmonary abnormalities on chest x-rays with and without the use of bone suppression imaging software by radiographers in an emergency department

S. de Labouchere[1,2]; [1] HESAV/HES-SO – Haute Ecole de Santé Vaud, Lausanne, Switzerland, [2] CHUV – Centre Hospitalier Universitaire Vaudois, Lausanne, Switzerland

Purpose: Chest X-rays (CRX) are common for diagnosing lung and heart issues. 'Bone suppression imaging' (BSI) technic eliminates bones from CRXs, which can improve lung nodule detection. However, this has not been assessed for pneumonia. The aim of this retrospective study was to determine BSI's value in detecting pneumonia.

Methods and Materials: Adult patients that underwent erect PA CXRs in the ER, and post-processed with BSI were included in this study. Each patient had undergone a CT scan within 48 hours, and this exam was considered the reference. Two blinded radiologists assessed CXRs without and with BSI respecting an interval of >1month to reduce recall bias. Sensitivity, specificity, predictive values, and readers' certitude were calculated, and Inter-reader agreement was evaluated with the kappa statistic.

Results: This study included 99 patients. The gold standard (CT) identified 39.4% cases as pathological. The study showed a significant increase in false positives (FP) when using BSI (+251%). The use of BSI significantly ($p < 0.05$) affected one of the two readers' diagnoses and certitude. It showed a decreased in accuracy (up to 17%) and in sensitivity (up to 14%). However, specificity was increased by 66%. Inter-reader agreement was generally weak to moderate (0.113 to 0.53) and did not improve with BSI.

Conclusion: No added clinical value in the detection of pneumonia was shown when using BSI due to an important increase in false positives. Further studies are needed in order to confirm these findings and potentially adapt post-processing for CRXs in this context.

A117

Managing the AI Healthcare Revolution: Balancing Innovation, Accountability, and Privacy

F. Rijnberg; FHNW – Fachhochschule Nordwestschweiz, Olten, Switzerland

Purpose: The use of artificial intelligence (AI) in healthcare has the potential to revolutionize the industry by improving patient outcomes, reducing costs, and increasing efficiency. However, the implementation of AI in healthcare also presents significant legal, ethical, and privacy challenges that must be addressed to ensure accountability and transparency.

Methods and Materials: The paper discusses the various ways in which AI can be used in healthcare, including relieving, replacing, splitting up, and augmenting tasks performed by healthcare professionals. The paper then examines the legal and ethical challenges associated with AI in healthcare, including patient data privacy, accountability, and limitations. The author argues that healthcare organizations must take a proactive approach to addressing these challenges by implementing robust data protection policies, ensuring transparency and accountability in the use of AI, and establishing clear guidelines for the use of AI in healthcare.

Results: The paper finds that while AI has the potential to revolutionize the healthcare industry, it must be implemented in a responsible and ethical manner to ensure that patient privacy and safety are protected. The author recommends that healthcare organizations prioritize data privacy and security measures, establish clear guidelines for the use of AI in healthcare, and ensure that accountability and responsibility are clearly defined.

Conclusion: The responsible and ethical implementation of AI in healthcare requires a balance between innovation, accountability, and privacy. By taking a proactive approach to addressing legal, ethical, and privacy challenges, healthcare organizations can harness the power of AI to improve patient outcomes, reduce costs, and increase efficiency while protecting patient privacy safety.

A118

Collaborative Development of XAI Tools with Nuclear Medicine Radiographers for Improved PET Images

M. Champendal[1,2], H. Müller[3], J. Prior[2,4], C. Sá dos Reis[1]; [1] HESAV/HES-SO – Haute Ecole de Santé Vaud, Lausanne, Switzerland, [2] UNIL – University of Lausanne, Faculty of Biology and Medicine, Lausanne, Switzerland, [3] HESAV/HES-SO – Haute Ecole de Santé Vaud, Sierre, Switzerland, [4] CHUV – Centre Hospitalier Universitaire Vaudois, Nuclear Medicine and Molecular Imaging Department, Lausanne, Switzerland

Purpose: To identify the requirements of radiographers in a nuclear medicine department, aiming for a comprehensive understanding of the AI algorithm employed for improving PET/CT images.

Methods and Materials: Two Focus Groups (FG) were created to identify participants' background knowledge and perspectives on AI. An introduction to Explainable AI (XAI) was provided, followed by the exploration of specific needs and preferences through the presentation of scenarios, reflecting both accurate and inaccurate results compared to the ground truth. Questions regarding what XAI should elucidate to aid radiographers in their practice were gathered, along with key features such as output format, confidence levels, and the perceived barriers and facilitators of AI utilisation. The collected data was submitted to content analysis for further analysis.

Results: A group of ten radiographers, aged between 31 and 60, representing diverse hospital settings, presented their requirements for XAI tools. Three participants presently utilise AI tools in PET/CT but with restricted training. Their primary needs for XAI tools encompass interactivity, adaptability, accessibility/be user-friendly, minimal disruption to workflow. They identified a "trust index," visual comparisons, example-based outputs, and chatbots as valuable formats. Facilitating factors for the use of XAI included adequate training, support mechanisms, early integration, and development of "radiographer-specialists on AI". On the contrary, barriers included a lack of understanding, organisational challenges, and limitations in system capabilities.

Conclusion: The requirements for XAI tools were identified, with radiographers emphasising the need of enhancing their own knowledge and that the system is prepared for the implementation of AI without adversely affecting workflow and patient outcomes.

A119

Assessing a Blending Model Approach for Ultrasound Education in Medical Imaging

R. Teresa Ribeiro, C. Schiesser, C. Campeanu, C. Sá dos Reis; HESAV/HES-SO – Haute Ecole de Santé Vaud, Lausanne, Switzerland

Purpose: To evaluate two editions of a 4-week ultrasound (US) blended intensive programme.

Methods and Materials: A focus group was conducted to provide qualitative insights into teaching methodologies, student engagement, curriculum efficacy. Weighted average analysis of student evaluation components from the 2 editions was performed to analyse performance and compare inter-edition results regarding knowledge and skills acquisition.

The curriculum blends theory with hands-on practice, where students progress from supervised US exams to independent scanning. To pass, students must perform a practical abdominal US and critically discuss their findings and decisions. This dual approach assesses both practical skills and reflective understanding.

Results: 19 students enrolled the module across two editions (11 in 2022, 8 in 2023). They exhibited high competency in identifying anatomical structures on first attempt (84%), reflecting effective practical skill learning. Oral discussions showed high competency (96%) in justifying scans, suggesting growing proficiency and confidence. The second edition's enhancements, like abnormal anatomy studies and technical reporting, likely contributed to 78.6% reduction in assistance needed in 2023. Focus group highlighted the efficacy of the blended learning approach, combining online and hands-on learning for deeper engagement, and a collaborative environment fostering clarity in scanning techniques. Despite initial inexperience with US, students demonstrated significant growth in knowledge and skills, with one directly employed as a sonographer in a Swiss hospital.

Conclusion: This study validates the effectiveness of a blended learning approach for teaching abdominal US, producing confident and competent practitioners. Future directions focused on the expansion to radiographers and the introduction of a modular structure for personalized professional development.

A120

Assessment of tip position variability of venous catheters in the superior vena cava: comparison between projectional images and cross-sectional images

G. Gullo[1], D. Rotzinger[1,2], P. Frossard[1], A. Colin[1], G. Saliou[1,2], S. Qanadli[1]; [1] CHUV – Centre Hospitalier Universitaire Vaudois, Lausanne, Switzerland, [2] UNIL – University of Lausanne, Lausanne, Switzerland

Purpose: The assessment of central venous catheter (CVC) correct positioning is of major concern in order to avoid complications. Vascular access associations have established the cavo-atrial junction (CAJ) as the most appropriate CVC location. Among the different chest X-Ray (CXR) landmarks proposed for the assessment of tip position relative to the CAJ, only the pericardial reflection lies in the same plane as the vascular structures assessed. Although extensively used, CXR has been criticized for its difficulties in estimating catheter tip location. Our purpose was to evaluate the capability of CXR to determine tip positioning and to consider it as a reference relative to CT imaging.

Methods and Materials: 107 CT scans of patients wearing port access catheter devices realized at the Lausanne University Hospital between January and December 2021 were retrospectively analyzed. Distance from tip to cavo-atrial junction (DCAJ) was measured on topogram projectional imaging (PJ) and axial cross-sectional imaging (CS) by 2×2 observers (within and between evaluations). Observational statistics were reported using a paired t-test, repeatability coefficients (RC), and the intraclass correlation coefficient (ICC) and globally displayed using Bland-Altman plots.

Results: All ICC were >0.9, indicating excellent reliability. The mean difference between observers comparing CS and PJ was 0.13 ± 0.80cm (P = 0.10) with outer 95% confidence limits of 1.92cm and –2.17cm and an RC of 1.79cm.

Conclusion: Considering the RC range, CXR tip-position reading remains an accurate method for determining CVC localization in the context of adequate and safe placement within 1cm of the CAJ.

A121

Pain management for peripheral venous catheterization. A short scoping review.

P. Frossard, T. Cherpillod, A. Colin, G. Gullo; CHUV – Centre Hospitalier Universitaire Vaudois, Lausanne, Switzerland

Purpose: Peripheral venous catheterization (PVC) is a common procedure in radiology. Comments of patients report a lot of bad experiences with pain and fails of catheterization. Those facts may rise fear and stress and can lead to vasovagal response. These situations tend to increase anxiety and pain during subsequent venipunctures. The aim of this presentation is a scoping review of simple and non-pharmacological techniques in order to choose the best solution compatible with our practices to increase the quality of the relationship between MRTs and patients, as well as to bring an additional level of expertise through improved quality of care.
Methods and Materials: Quick scoping review related to simple and non-pharmacological techniques for pain management concerning peripheral venous catheterization using PubMed for database.
Mesh Terms: pain managment, catheterization, needle
Title/abstract: pain management, catheterization, venipuncture, needle
Results: We retrieve a total of 39 articles including 4 systematic reviews. These articles covered 5 easily applicable techniques: reflexive question, inspirium (and Valsalva), cough-trick, aural or visual distraction, thermos-coolant spray or pad (and/or vibrating pad). Among them one is of particular interest due to its simplicity to use in practice even for allophone patients. Breathing technique with Valsalva maneuver entails no additional cost and is highly compatible with aseptic standards and respect for the individual, whether child or adult.
Conclusion: We would like to share this knowledge with our colleagues to reduce anxiety and pain in patients requiring a venous catheter at no extra cost, while increasing the level of MRTs expertise and confidence between us and our patients.

A122

Radiology Deep Vein Team: Management of challenging venous access in radiology

T. Cherpillod, A. Colin, P. Frossard, G. Gullo; CHUV – Centre Hospitalier Universitaire Vaudois, Lausanne, Switzerland

Purpose: The actual PIVC practice at ground level (BSc / ES graduate TRM level) usually consists of blind insertions. In case of repeated unsuccessful procedure, referral to other practitioners' specialists (nurse anesthetists) is made. In our institution, we modified this practice into a three-level system. 1. Ground PIVC level (blind guided procedures). 2. US PIVC general level (with specific short training formation in ultrasound). 3. US PIVC expert level (with extended US and vascular training formation inserting long PIVC (>6cm)). The purpose of this study was to evaluate our practice of US guided peripheral intravenous catheter (PIVC) insertion for CT exams and compare it to published literature regarding contrast media extravasation rates.
Methods and Materials We retrospectively analyzed injected CT scans performed in our institution from October 2022 to July 2023. The number of extravasation as well as the number of long PIVC inserted were retrieved from our quality insurance database. Descriptive statistics were used as well as chi square for comparisons.
Results: In a 10-month period, 18'024 CT were injected, with a total of 28 extravasation. Thus, the total rate of extravasation was 1.6‰. Among them, 66 long PIVC were inserted at the expert level with 2 extravasations. These data were compared with a systematic review by Behzadi et al. (Medicine (2018) 97:9) accounting for 17 studies (1979 extravasation/759047 CT exams/2‰). There was a statistically significant difference in extravasation rate ($p<0.01$)
Conclusion: Our results suggest the possibility of changing the existing PIVC paradigms in challenging venous access. A 3-level process can mitigate delays linked to challenging venous access and avoid workflow disruptions. Both allowing better efficiency of diagnostic and patient care.

A123

Renal function evaluation before contrast media administration in medical imaging departments

M-R. Alfred[1], N. Chun[2], S.S. Ghotra[3,4], S. Ding[3]; [1] CHUV – Centre Hospitalier Universitaire Vaudois, Lausanne, Switzerland, [2] Hirslanden Clinique Cecil, Department of Radiology, Lausanne, Switzerland, [3] HESAV/HES-SO – Haute Ecole de Santé Vaud, Lausanne, Switzerland, [4] eHnv – Hôpital of Yverdon-les-Bains, Department of Radiology, Yverdon-les-Bains, Switzerland

Purpose: The aim of this scoping review is to summarise knowledge on the renal function analysis prior injection of iodine or gadolinium-based contrast medium (CM) in CT and MRI patients.
Methods and Materials: The scoping review was conducted in accordance with the JBI methodology based on guidelines from professional societies'. The guidelines were searched in PubMed and on websites using several keywords and were limited to the last ten years and the French and English languages. The number of documents studied is six.
Results: For iodine-based CM, most guidelines advise assessing renal function only in specific patients with risk factors that could generate Post-Contrast Acute Renal Failure (PC-IRA). An estimated Glomerular Filtration Rate (eGFR) below 30 mL/min/1.73m² is considered an increased risk of developing PC-IRA. For gadolinium-based CM, the renal function evaluation is less recommended except for certain products (linear gadoline CM). Indeed, some guidelines have established a classification of gadolinium-based CM into several groups according to their level of risk of causing Nephrogenic Systemic Fibrosis (NSF) or according to the number of NSF cases with which they have been associated. Most guidelines considered that patients are at increased risk of NSF if eGFR is below 30 mL/min/1.73m². Various guidelines recommend using the CKD-EPI or MDRD formula to evaluate adult renal function. For children, the revised Schwartz formula is recommending
Conclusion: The guidelines studied indicate that renal function can be analysed according to risk factors or the type of CM. This analysis can be done using different formulas and the thresholds presented in the guidelines are similar. This study would allow radiographers to broaden their knowledge of the diversity of practices. Further investigations should be carried out to implement evidence-based-practice in clinical settings.

A124

Pedagogy and simulation in the delivery room

A. Tanari[1,2], L. Gaucher[2,3], C. Gaignot[2], A. Cooper[2]; [1] HESAV/HES-SO – Haute Ecole de Santé Vaud, Lausanne, Switzerland, [2] HEdS – Geneva School of Health Sciences, Geneva, Switzerland, [3] HCL – Hôpital Louis Pradel, Lyon, France

Purpose:
Overall objective: Evaluation of the impact of a low-fidelity prototype enabling a bimodal examination (ultrasound and digital) on students' acquisition of competence in determining the orientation of the fetal cephalic pole
Specific objectives:
a) Identify 3D printing materials with echogenicity qualities that most closely resemble the cortex of a fetal skull, according to a panel of sonographers
b) Produce a bimodal prototype using a specific 3D printer technique, based on the results obtained
Methods and Materials: We collected 14 samples of 2*5cm 3D printing material with a thickness of 3mm. To be able to take ultrasound images of these samples, we created a posage to guarantee reproducibility of the images. We took 14 images with the same ultrasound parameters for each sample, using a low-frequency "Philips Lumify" probe and a "Lenovo" tablet. We made an initial selection with the aim of keeping just 5 samples to be evaluated by sonographers through a quantitative self-questionnaire survey. In parallel, we retrieved DICOM data from a pelvimetry scan of a pregnant woman, segmented the fetal skull and extracted it as an STL file.
Results: Of the 61 participants, only 36 provided complete answers. We chose to retain only midwives and gyn-obs, representing a total of 26 individuals. Thanks to the participants' responses, as well as the constraints related to encapsulation, we were able to conclude which samples are most similar to the cortex of a fetal skull. The complexity of the skull's structure means that it can only be printed using a resin bath. The skull was printed in SLA resin at HEPIA. Arion Laboratories were able to encapsulate the skull in an anechogenic liquid.
Conclusion: This pilot study aims to improve the initial and continuing training of midwives and radiographers in ultrasound, both in the interests of public health and to reinforce the independence of healthcare professionals in Switzerland. The prototype will then be tested, HEdS and HESAV with students in initial training.

A125

Virtual monochromatic spectral imaging with Dual-Energy CT for contrast enhancement optimization and reduced contrast media dosage

M. Gulizia, M. Jreige, Y. Marro, C. Chevallier, A. Viry, C. Dromain, N. Vietti-Violi; CHUV - Centre Hospitalier Universitaire Vaudois, Lausanne, Switzerland

Purpose: The aim of this study is to define the best virtual monochromatic spectral imaging (VMI) level providing the best image quality for thoraco-abdominopelvic CT in portal phase.

The second objective is to compare image quality and radiation dose of SECT protocol with the new DECT protocol with reduced iodinated contrast media injection.

Methods and Materials: TWe retrospectively included 44 adult patients requiring thoraco-abdomino-pelvic (TAP) in portal phase for an oncologic indication. SECT protocol and DECT protocol with reduced contrast volume were compared. For SECT protocol, contrast volume was calculated as body weight + 30 in mL and only to body weight for DECT protocol.

VMI sets from 40 to 80 keV at 5 keV intervals were reconstructed. Quantitative analysis were done measuring enhancement and calculating both CNR and SNR. A subjective analysis were done to assess the best VMI reconstruction in term of enhancement, noise and overall image quality.

Results: Contrast enahncement (HU), CNR, SNR in liver parenchyma and portal vein were significantly higher in DECT protocol at 60 keV than the SECT protocol (p<0.001). Both raters assessed significantly higher the contrast enhancement and noise at 60 keV (p > 0.01). However, the overall quality was not significantly different between both protocol (p=0.29). Higher rate for overall image quality was observed with 60 keV monoenergetic images. DECT protocol presented mean CTDIvol was 34.7% higher than SECT protocol.

Mean CTDI, DLP and effective dose were significantly higher than in SECT protocol (p<0.05).

Conclusion: 60 keV provided the optimal image quality between noise and enhancement.

GSI protocol allows to save a significant amount of contrast media providing higher image quality. Radiation exposure with DECT protocol remains lower than the target value provided by the diagnostic reference level.

A126

Hamartomas from head to toe in paediatric patients and young adults – Overview of clinicoradiological features

L. Kozma[1,2], _L. Pittet_[1,3], M. Champendal[1], L. Flaction[1], C. Sá dos Reis[1];
[1] HESAV/HES-SO – Haute Ecole de Santé Vaud, Lausanne, Switzerland,
[2] EHC-vd – Hôpital de Morges, Morges, Switzerland, [3] CHUV – Centre Hospitalier Universitaire Vaudois, Lausanne, Switzerland

Purpose: This study synthesises optimised CTPA protocols, aiming to enhance radiation protection, contrast media (CM) utilisation, image quality (IQ).

Methods and Materials: Utilising the JBI method, optimised CTPA protocols tailored for adult patients, including pregnant women and high BMI individuals were identified. The emphasis was on radiation protection, optimising the iodinated CM, improving IQ, achieving a high exam success rate. Explorations were conducted across PubMed, Embase. The search criteria incorporated studies published in French/English after 2018. Various keywords and MeSH terms related to topic and having more than 100 patients participating in the studies were considered. Abstracts and titles were screened, and all eligible full-text publications were independently reviewed by 2 assessors. Data extraction and categorisation were conducted.

Results: Twenty-eight articles, including participants ranging from 100 to 3998, unveiled diverse optimisation techniques categorised into 5 groups: acquisition, injection, breathing, reconstruction parameters, and adaptations for specific populations. Strategies such as reducing scan length with a 37 to 48% dose reduction, employing high-pitch, dose modulation (auto-mA, ODOM), lowering kV, using auto kVp, applying dual-energy methods were proposed to minimise dose and improve patient outcomes. For pregnant women, recommendations included 100 kVp beam, free breathing, increased injection rate.

Conclusion: Optimising CTPA protocols proves to be an intricate mission due to the multitude of parameters that necessitate consideration. It demands dedicated studies for each specific variable to accumulate dependable data. Routine protocol reviews play a pivotal role in achieving effective optimisation, incorporating all pertinent technical updates. Radiographers are central to this optimisation process, blending their technical proficiency with expertise in patient-centered care.

A127

Failure of cerebral venous sinus opacification in post-mortem CT-angiography: an artifact linked to circumstances of death?

M. Angulo Santander[1], V. Corno[1], J. Schmid[2], C. Egger[3]; [1] HESAV/HES-SO – Haute Ecole de Santé Vaud, Lausanne, Switzerland, [2] HESAV/HES-SO – Haute Ecole de Santé Vaud, Geneva, Switzerland, [3] CHUV – Centre Hospitalier Universitaire Vaudois, Unit of Forensic Medicine and Imaging, University Center of Legal Medicine Lausanne, Geneva, Switzerland

Purpose: To investigate a potential correlation between the failure of cerebral venous sinus opacification in multi-phase post-mortem CT-angiography (MPMCTA) and the circumstances of death.

Methods and Materials: We gathered data from 414 cases at a Swiss forensic medicine center, such as causes of death, cardiopulmonary resuscitation, hospitalization or antiplatelet medication prior to death, based on autopsy and radiological reports. Additionally, we examined the opacification of cerebral venous sinuses in MPMCTA images. Data's collection trustworthiness was tested by measuring the inter-rater reliability on 30 cases. Logistic regression was used to investigate which variables had a relation with the opacity failures of the sinuses. The study was approved by the Cantonal Ethics Committee.

Results: Over 73% of our dataset was composed of natural causes of death, which were mostly heart failure causes (n=213). Only 18% percent of the cases had a hospitalization and 21% had an antiplatelet medication prior to death, whereas 54% benefitted from a cardiopulmonary resuscitation attempt. Layering artifact were observed in 71% of all cases and blood clot in 34%. Reliability of data collection was considered as fair for artifact variables such as blood clot, layering artifact or contrast extravasation. Otherwise, the reliability ranged from moderate to perfect (Cohen's Kappa: [0.49-1]). Preliminary results of the logistic regression seem to show that hospitalization and cardiopulmonary resuscitation variables have an important impact on the opacification of the cerebral venous sinuses.

Conclusion: Our preliminary findings suggest that hospitalization or cardiopulmonary resuscitation prior to death play an important role in the opacification of the venous sinuses with the MPMCTA imaging technique.

A128

CT reconstruction by artificial intelligence: What is the real gain?

D. Delarbre[1], E. Maturana[1], M. Scheffler[1], D. Racine[2], H. Zaidi[1];
[1] HUG – Hôpitaux universitaires de Genève, Geneva, Switzerland, [2] CHUV – Centre Hospitalier Universitaire Vaudois, L'Institut de radiophysique, Lausanne, Switzerland

Purpose: To evaluate the image quality obtained by using a commercially available deep learning (DL)-based CT reconstruction algorithm, as well as its potential for dose reduction in abdominal CT, compared to an iterative reconstruction method.

Methods and Materials: Raw data of CT scans with different dose levels (Aquilion Prime SP, Canon, Tokyo, Japan) of a low-contrast abdominal phantom were reconstructed with a DL-based algorithm (Advanced intelligent Clear-lQ Engine) as well as a second-generation iterative algorithm (Adaptive Iterative Dose Reduction 3D) commercially offered by the manufacturer. Evaluation by blinded readers will be made for signal-to-noise ratio and contrast resolution.

Results: Evaluations are still ongoing. The results will be compared with indicators obtained from other scanners of the same type that are already monitored by the Institute of Radiophysics in Lausanne.

Conclusion: Following the multi-site comparison, we hope to be able to confirm preferability of DL-based CT image reconstruction, following the current trend, while evaluating for further potential in dose reduction capacities.

A129

Adjustments of iodinated contrast media using lean body weight for abdominopelvic Computed Tomography: a systematic review and meta-analysis

M. Gulizia[1], S. Ding2, C. Jaques[1], C. Sá dos Reis[2], C. Dromain[1];
[1] CHUV – Centre Hospitalier Universitaire Vaudois, Lausanne, Switzerland,
[2] HESAV/HES-SO – Haute Ecole de Santé Vaud, Lausanne, Switzerland

Purpose: This systematic review aimed to compare the performance of injection protocols based on Lean-Body-Weight (LBW) in contrast with other protocols for abdominopelvic CT examination on portal phase.
Methods and Materials: A systematic review including randomized controlled trials (RCT) and quasi-RCT was performed. PubMed, Embase, MEDLINE, CINAHL, Cochrane were searched for studies published from 2002 to 2021 with no language limitation. Participants of these studies are adults undergoing an abdominopelvic CT protocol with single contrast media injectionfor oncologic follow-up and acute disease. The quantitative component of the review will consider studies that evaluate effectiveness of volume calculation based on LBW for diagnostic enhancement. The comparator of intervention is the effectiveness of other type of dose calculation: total body weight, fixed dose, body mass index, body surface area, and blood volume. Titles, abstracts and then full texts were screened independently by two researchers.
Results: The meta-analysis reveals lower significant contrast volume injected with LBW protocol compared to TBW protocol (p=0.003). However, contrast enhancement in liver parenchyma and aorta were not significantly different (p= 0.07, p=0.06, respectively).
Conclusion: Injection protocol based on LBW allows to reduce iodinated contrast media injected for abdominopelvic CT in portal phase without significant difference in terms of contrast enhancement between with TBW protocol.

A130

Standardisation and optimisation of computed tomography protocols in a multi-site hospital

F. Magoga[1], M. Merli[1], G. Cadei[1], S. Ferrari[2], E. Rezzonico[2]; [1] EOC – Ente Ospedaliero Cantonale, IIMSI – Imaging Institute of Southern Switzerland, Lugano, Switzerland, [2] EOC – Ente Ospedaliero Cantonale, IIMSI – Imaging Institute of Southern Switzerland, Locarno, Switzerland

Purpose: In the context of a multi-site hospital, we describe our experience in managing CT protocols through the creation of a multidisciplinary dose-team, composed of medical radiographers, medical physicists and radiologists, with the aid of software which allows to simulate and optimise the dosimetry in diagnostic and interventional CT examinations. The purpose is to raise awareness among medical imaging professionals about the importance of controlling and managing CT radiation dose within a multi-site hospital.
Methods and Materials: The unification and optimisation of study protocols on dissimilar CT scanners, the use of dosimetry management software, the creation and update of departmental directives, compliance with federal DRLs, such as the creation of internal DRLs, carry out internal clinical audits and continuous staff training are part of the project that the multidisciplinary dose-team develops constantly in the various hospital sites of the institute.
Results: The use of increasingly standardised CT protocols for specific clinical cases, continuous staff training, compliance with federal and internal DRLs have made it possible, in less of 20 years, to lower the absorbed dose by 70% on the chest and by 60% on the abdomen, maintaining the quality of the radiological images unchanged. Since the birth of the institute, in the context of the radiology subspecialties, the dosimetric values of each individual CT examination are constantly standardised at each hospital site through the optimisation of the study protocols.
Conclusion: The creation of a multidisciplinary dose-team, compliance with the federal directives and departmental guidelines, the use of dose management software and the standardisation of CT protocols have made it possible to align, lower and monitor radiation doses throughout the institute. The role of the medical radiographer allows, also in the context of the dosimetric values management, to standardise the quality and safety in a complex reality such as the multi-site hospital.

A131

Impact of Time Constraints and Workload on Radiographer Well-being and Patient Safety in the Computed Tomography Department

N. Yoganathan[1], C. Sá dos Reis[2], F. Serranheira[3]; [1] eHnv – Hôpital of Yverdon-les-Bains, Yverdon-les-Bains, Switzerland, [2] HESAV/HES-SO – Haute Ecole de Santé Vaud, Lausanne, Switzerland, [3] Universidade Nova de Lisboa, Lisbon, Portugal

Purpose: This study seeks to evaluate how organizational, spatial, and temporal factors influence procedures and workload within a CT unit, with a specific focus on promoting patient safety & enhancing radiographer well-being.
Methods and Materials: This research was carried out at a CT unit within a Swiss university hospital, utilizing the Systems Engineering Initiative for Patient Safety (SEIPS) model to examine the workflow and time constraints experienced by radiographers. Data collection involved employing observations and task analysis to capture details such as the timing and location of tasks performed by radiographers. Questionnaires were applied to collect evidence about real work performance and descriptive analyses was conducted.
Results: The workflow of radiographers in the CT department is intricate, involving numerous tasks. The entire process extends from 26 to 41 min, with Machine-Time (time spent in the CT room) varying between 10 to 16 min. Inefficiencies in the workflow were identified, notably significant time allocated to patient preparation and an unsuitable machine-time rate. The department's layout presents limited space in the preparation area, contributed to ergonomic challenges for radiographers. Organizational factors regarding scheduling had an impact on workflow. Examination durations varied based on scan type and patient, introducing time pressure and potential safety concerns.
Conclusion: The research underscored the importance of revising time allocation practices in CT examinations for enhanced patient and radiographer safety. Proposed recommendations encompass extending the machine-time rate, tailoring examination durations according to CT type, designating a dedicated radiographer for order review. Additionally, improving the working environment to meet ergonomic needs is crucial. Addressing these considerations has the potential to elevate the efficiency and safety of CT departments, benefiting both patients and radiographers.

A132

Création d'une filière de radiographies anticipées aux urgences dans le but de diminuer le temps de prise en charge patient

J. Baechler[1], E. Tavares Alves[2], H. Thoeny[1], V. Ribordy[2]; [1] HFR – Hôpital fribourgeois, Fribourg, Switzerland, [2] HFR – Hôpital fribourgeois, Service des urgences, Fribourg, Switzerland

Learning objectives: Comment un service de radiologie et un service d'urgence peut mettre en commun leur compétences afin de diminuer le temps d'attente aux urgences.
Background: Les urgences ont mis en place des stratégies afin de diminuer l'engorgement de leur unité. Malgré cela, la situation n'est toujours pas optimale et leur fréquentation ne fait qu'augmenter en entrainant des temps d'attente. Dans ce contexte, il s'agit de trouver des solutions innovantes permettant de diminuer la durée de prise en charge tout en utilisant les compétences et les ressources existantes. Nous avons évalué l'impact d'une filière rapide faisant collaborer l'équipe infirmière et l'équipe de techniciens en radiologie médicale afin de décharger le staff médical. L'infirmier fournissant une anamnèse détaillée et le TRM participant au choix éclairé de la radiographie, nous supprimons l'étape de la première consultation médicale qui devient un acte médical délégué aux soignants.
Imaging findings or procedure details: Le patient est trié selon des critères d'inclusion et d'exclusion clairs. Le TRM prend connaissance de l'anamnèse, échange avec le patient et décide des radiographies à effectuer. Finalement, le patient est mis en attente de consultation médicale. En cas de doute, le médecin responsable de tri est atteignable.
Conclusion: La mise en place de cette filière n'a eu aucun impact significatif sur la durée de prise en charge des patients. Elle a néanmoins permis d'associer des ressources soignantes existantes afin de libérer des ressources médicales. Finalement, ce projet a donné naissance à une délégation médicale novatrice qui pourrait être appliquer à plus large échelle au niveau Suisse.

A133

A Comprehensive Review of Explainable Artificial Intelligence in Medical Imaging

M. Champendal[1,2], H. Müller[3], J. Prior[2,4], C. Sá dos Reis[1]; [1] HESAV/HES-SO – Haute Ecole de Santé Vaud, Lausanne, Switzerland, [2] UNIL – University of Lausanne, Faculty of Biology and Medicine, Lausanne, Switzerland, [3] HESAV/HES-SO – Haute Ecole de Santé Vaud, Sierre, Switzerland, [4] CHUV – Centre Hospitalier Universitaire Vaudois, Nuclear Medicine and Molecular Imaging Department, Lausanne, Switzerland

Purpose: To review Explainable Artificial Intelligence(XAI) methodologies in medical imaging(MI).

Methods and Materials: In compliance with the Joanna Briggs Institute methodology, a scoping review was conducted on PubMed, Embase, CI-NAHL, Web of Science, BioRxiv, MedRxiv, Google Scholar. The search criteria included studies published after 2017 in French and English. Combinations of keywords and MeSH terms related to explainability, and medical imaging modalities/fields were applied. Abstracts and titles, eligible full-text publications, underwent screening by two independent reviewers. Discrepancies between the reviewers were resolved through consensus.

Results: Out of 1258 publications, 229 studies met all criteria. XAI related publications increased from 2018 to 2022, particularly between 2020 and 2021. MRI, CT and X-ray imaging are the main modalities where XAI tools act to explain lung(n=82) and brain(n=74) pathologies, such as Covid-19(n=48), Alzheimer's(n=25), brain tumors(n=15). Explanations were presented through visual(n=187), numerical(n=68), rule-based(n=11), textual(n=11), and example-based(n=6) formats. Classification(n=90), prediction(n=47), diagnosis(n=39), detection(n=29), segmentation(n=13) and image quality improvement(n=6) were the main explained tasks. The majority of explanations provided were local (77.7%: n=178/229), global (5.7%: n=13/229) or both types (16.6%: n=38/229). Various terms were interchangeably used, such as *explainable* (n=208), *interpretable* (n=188), *understandable* (n=112), *transparent* (n=61), *reliable* (n=31) and *intelligible* (n=3) being interchangeably used.

Conclusion: XAI techniques explain locally lung and brain pathologies using visual and numerical formats. Currently, there is a scarcity of explanations addressing the improvement of image quality across various imaging modalities. In the literature, the terms "explainable" and "interpretable" are often used synonymously.

A134

Bridging Knowledge to Clinical Practice in the Evolving Role of Radiographers with AI Integration

R. Teresa Ribeiro, M. Champendal, C. Sá dos Reis; HESAV/HES-SO – Haute Ecole de Santé Vaud, Lausanne, Switzerland

Purpose: Envisioning a future where Artificial Intelligence (AI) transforms radiography, this study explores the intersection of evidence-based healthcare principles and AI technologies, aiming to define their collective impact on health outcomes and radiographer practice.

Methods and Materials: JBI model of Evidence-based healthcare was applied to identify how the integration of AI in radiography is being conducted in Scopus and IEEE databases. It explores 4 components: healthcare evidence generation, evidence synthesis, evidence transfer, and evidence utilisation. The review also addresses the critical translational gaps in AI-driven radiography, tracing the journey from initial knowledge need to discovery, and from discovery through to clinical application and subsequent actions

Results: 387 studies were included. AI integration in radiography starts with the Healthcare Evidence Generation phase, where R&D entities develop algorithms compatible with equipment and procedures, setting the groundwork. Evidence Synthesis phase involves independent reviews and meta-analyses, requiring collaboration among AI developers, radiology departments, and third-party evaluators. Such collaboration is essential to ensure objectivity and reliability of the tool. The Evidence Transfer phase, defines the commercial roll-out process, highlighting the importance of marketing, training, and certification, ensuring radiologists and radiographers are proficient in using these AI tools. Evidence Utilisation phase involves deploying these tools in clinical settings, emphasising the necessity for radiographers' continuous monitoring and effectiveness evaluation of the applications.

Conclusion: The integration of AI into radiology's translational cycle needs an approach ranging from development to application. A successful integration of AI in practice hinges on a collaborative, multi-faceted approach that aligns technological innovation with clinical context, enhancing the capabilities of radiographers.

A135

Exploring Perspectives from Radiographers Working in European French-Speaking Countries About Profession and Professional Identify Changes Promoted by Artificial Intelligence

G. Walsh[1], N. Stogiannos[1,2], M. Champendal[3], R. Teresa Ribeiro[3], Y. Kyratsis[4], M. McEntee[5], C. Malamateniou[6], C. Sá dos Reis[3]; [1] University of London, Division of Midwifery & Radiography, School of Health and Psychological Sciences, London, United Kingdom, [2] General Hospital of Corfu – Agia Eirini, Medical Imaging Department, Corfu, Greece, [3] HESAV/HES-SO – Haute Ecole de Santé Vaud, Lausanne, Switzerland, [4] Vrije Universiteit Amsterdam, Amsterdam, Netherlands, [5] UCC – University College Cork, Cork, Ireland, [6] School of Health and Psychological Sciences, Division of Midwifery & Radiography, London, United Kingdom

Purpose: To map radiographers' experiences and perspectives on the integration of AI in the radiographer profession and future impacts in European French-Speaking Countries.

Methods and Materials: An exploratory online survey (Qualtrics) with 36 questions, 9 'open-ended' and 28 'close-ended' questions, was sent to radiographers working in academia and clinical settings, as well as radiography students. Quantitative data were analysed using descriptive statistics and qualitative responses using thematic content analysis. Ethical approval was obtained.

Results: 241 radiographers working in Switzerland (135), France (103) and Belgium (3) answered to the questionnaire. Four of them are experts in AI, 11 have advance knowledge, 69 intermediate and 151 basics, 12 never heard about AI. 52% of the participants did not have any training about AI, while 48% had specific training on AI during undergraduate studies, continuous training by a company or by ASTRM. Most of the participants (64%) use AI tools at least occasionally, while 32% never used it. The majority of participants (72%) agree or strongly agree that "Radiographers (…) roles and professional identity may be quite different from today", while 38% thinks that "With time, AI will ultimately replace radiographers". Needs of specific training and knowledge was highlighted by 43% of the participants.

Conclusion: Radiographers foresee major changes in the identity and role of the profession due to the integration of AI in daily practice. AI and digital health literacy were identified as critical, embedded in specific education and training, to fully exploit potential benefits, and risk mitigation, of AI usage in clinical practice, enabling radiographers to provide a better patient-centered care.

A136

Is remote scanning a commercial innovation or evidence-based practice for radiographers?

R. Teresa Ribeiro, I. Gremion, C. Sá dos Reis; HESAV/HES-SO – Haute Ecole de Santé Vaud, Lausanne, Switzerland

Purpose: This study aims to identify and characterise research on remote scanning in radiology/medical imaging, a practice implemented in several European countries, focusing on its impact on the radiographer's profession and person-centred care.

Methods and Materials: A bibliometric analysis was conducted on PubMed, Scopus and Google Scholar. MeSH terms related to teleworking and remote scanning were identified applied to identify studies from 2000 to 2023 on the topic. Data was analysed using Python libraries for behaviour and magnitude trends (Mann-Kendall test and Sen's Slope Estimate, p<0.05). Articles with specific remote scanning keywords in radiology/medical imaging were extracted for content analysis to identify the opportunities and challenges of remote scanning.

Results: MeSH term telemedicine (n=62580) showed the sharpest trend and magnitude (0.93, p<0.05) and Teleradiology displayed a negative trend (-0.29, p>0.05). In Scopus, only 0.3% of telemedicine research involved medical imaging terms like CT, MRI or ultrasound. No studies were found on radiographers in remote scanning, with ultrasound focused on robotic developments. Remote scanning, searched in Scopus (65 articles) and Google Scholar (85 articles), revealed 4 articles directly related with radiographers, which emphasise the need for carefully consideration of practical issues (loss of person-centred care), professional (lack of regulation, non-qualified staff, identity deterioration) and safety aspects (system responsiveness, procedures and education, governance and legal implications).

Conclusion: The lack of research evidence on remote scanning technology suggests that it is primarily driven by commercial innovation and market interests. Radiographers need to ensure that new procedures are not only innovative but also evidence-base, regulatory and legally recognised, safe and ethical for adequate person-centred care and professional development.

A137

FRadiographers' eco-friendly practices for sustainable medical imaging departments

S.S. Ghotra[1,2], M. Champendal1, L. Flaction[1], C. Sá dos Reis[1];
[1] HESAV/HES-SO – Haute Ecole de Santé Vaud, Lausanne, Switzerland,
[2] eHnv – Hôpital of Yverdon-les-Bains, Department of Radiology, Yverdon-les-Bains, Switzerland

Purpose: To explore key approaches to minimize the environmental impact of medical imaging departments (MID).
Methods and Materials: JBI methodology was applied to identify sustainable practices in MID through keywords and mesh term combinations on PubMed, Embase, and CINAHL from 2013 onward in French and English. Abstracts, titles, and full texts were reviewed by three independent assessors and disagreements were resolved via consensus.
Results: Of 4630 studies, 38 met the criteria providing insights about MID environmental impact. 32 studies focused on developed countries, 6 on non-developed nations. One-third was published post-2022. The main imaging modalities covered were CT (9/38), MRI (6/38), IR (4/38), CR (4/38), US (2/38), mix (9/38). The findings revealed 7 categories to reduce impact in MID: 1) justification, 2) energy consumption, 3) waste production, 4) recycling, 5) local resources usage, 6) pollution, 7) education. The studies showed a need of integrating sustainability analysis into the QA programs of the MIDs.
Conclusion: To mitigate the environmental impact of MID, a multifaceted approach is imperative. This involves the education of healthcare professionals, ensuring proper justification for examinations, exerting control over consumption, and simultaneously striving to enhance health outcomes. Further research is essential to prioritise and evaluate the effectiveness of these strategies, to offer valuable support for decision-making among both managers and MI professionals in adopting sustainable practices.

A138

Communication between patients and radiographers to improve well-being during mammography: a scoping review.

A. Dällenbach, M. Dias Arroja, S. Ding, T. Fontaine; HESAV/HES-SO – Haute Ecole de Santé Vaud, Lausanne, Switzerland

Purpose: The aim of this scoping review is to find and summarize communication tools to increase patient well-being during a mammography.
Methods and Materials: This study was conducted in accordance with the JBI methodology for scoping reviews. The documents published between 1985 and 2023 were searched in the Pubmed and Cinahl databases. The inclusion criteria were as follows: 1) Participants: women, men, transgender and non-binary people of all ages and nationalities; 2) Concept: radiographers interpersonal skills, including verbal and non-verbal communication; 3) Context: diagnostic or screening mammography.
Results: Our search equations yielded 105 articles. Following a first selection based on title and abstract, 76 articles were eliminated. A second selection was made based on the full text of the remaining 29 articles. We thus obtained 9 articles corresponding to our inclusion criteria. Our search equations led to studies that considered communication between the medical radiology technician and the patient in the context of a diagnostic or screening mammography examination. Various means of communication were presented in the included studies. The results of this study will be developed during the oral presentation.
Conclusion: The preliminary results of this scoping review indicate the existence of a few articles that have studied the importance of communication between patients and radiographers in the context of mammography.

A139

Investigating the Use of Communication Tools to Improve Radiographer-Patient Communication

S. Quirke[1,2], C. Sá dos Reis[3], M. McEntee[4], N. Moore[1]; [1] UCC – University College Cork, Medical Imaging and Radiation Therapy, School of Medicine, UGF ASSERT, Brookfield Health Sciences, Cork, Ireland, [2] Bons Secours Hospital, Cork, Ireland, [3] HESAV/HES-SO – Haute Ecole de Santé Vaud, Lausanne, Switzerland, [4] UCC – University College Cork, Cork, Ireland

Purpose: To evaluate radiographers' experiences communicating with patients and their willingness to accept further training and utilise recognised communication tools, i.e. AIDET.
Methods and Materials: An exploratory online survey (MS-Forms platform) with 43 questions, 13 qualitative 'open-ended' and 30 'close-ended' quantitative questions, was sent to radiographers working in clinical settings. Quantitative data were analysed using descriptive statistics and qualitative responses using thematic content analysis. Cross distribution analysis, basic percentages, and graphic bar charts were used for quantitative data analysis. Ethical approval was obtained.
Results: One hundred and nine radiographers completed the questionnaire. Quantitative analysis found that 83.6% (n=88) of radiographers had not received additional training in patient communication post-qualification. Communication skills were considered as "very good" or "excellent" by the participants when explaining the procedure to the adult patients, while with patients with an Intellectual Disability, Cognitive impairment, or Additional needs were considered mainly "good". Five themes emerged from the thematic analysis: (1) Expectations, (2) Education, (3) Improvements, (4) Errors and (5) Communication Tools. Rushing was recognised as a common error among their colleagues by 26% of responders AIDET, according to 88.5% (n=93) of respondents, could be helpful in their interactions with patients.
Conclusion: Radiographers express a lack of updated training for patient communication and express a desire for further education in this area. They view AIDET as a valuable communication tool, especially for student radiographers or those for whom English is not their first language and suggest its implementation as a starting step.

A140

Comparative analysis of breast lesion classification with deep learning in dynamic MRI using different types of regions of interest

B. Lokaj[1], V. Durand De Gevigney[1], K. Kinkel[2], D-A. Djema[3], C. Lovis[4], J. Schmid[1]; [1] HESAV/HES-SO – Haute Ecole de Santé Vaud, Geneva, Switzerland, [2] RHNe – Réseau Hospitalier Neuchâtelois, Neuchâtel, Switzerland, [3] Hirslanden Clinique des Grangettes, Geneva, Switzerland, [4] HUG – Hôpitaux universitaires de Genève, Division of Medical Information Sciences, Geneva, Switzerland

Purpose: To assess the influence of lesion region of interest (ROI) selection on the performances of deep learning models for lesion classification in breast MRI.
Methods and Materials: An expert radiologist annotated breast ultrafast (UF) dynamic MRI examinations collected from a swiss clinical center. 987 lesions including 280 benign, 586 lymph nodes, and 121 malignant lesions were segmented. Lesion characteristics, such as volume, size, and position in the breast, were calculated from the segmentations. From the last phase of the UF MR sequence, two types of 3D ROI patches were generated: tight ROI (tightly enclosing the lesion) and non-tight ROI (with a fixed cubic dimension of 5cm). A densenet121 convolutional neural network model was trained and tested for lesion classification with a five-fold cross-validation scheme, in 2-classes (benign and lymph nodes versus malignant) and 3-classes (benign versus lymph nodes versus malignant) classification scenarios. Standard performance metrics were used to compare each method. The study was approved by the Geneva Cantonal Ethics Committee (CCER), and written informed consent was obtained.
Results: In our dataset, malignant lesions were significantly larger than benign ones (p<0.05). Position in the breast also differed according to the type of lesion. Results were consistently better with non-tight ROI (2-classes: mean area under the ROC curve (mAUC)=0.84, Accuracy (Acc)=0.89; 3-classes: mAUC=0.84, Acc=0.70) than with tight regions (2-classes: mAUC=0.73, Acc=0.87; 3-classes: mAUC=0.73, Acc=0.62).
Conclusion: Our findings showed that malignant lesions are typically larger than benign ones. Lesion location is relevant, particularly for identifying lymph nodes from other lesions. Using non-tight lesion data improves classification outcomes, emphasizing the significance of lesion size and surrounding information for diagnosis.

PO26

Automated Pancreas Segmentation in MRI: Validation with Radiologist Annotations in a Mixed Cohort

D. Counter[1], V.Jain[1], A. Triay Bagur[1], H. Thomaides Brears[1], M. Brady[1], P. Aljabar[1], M. Pansini[2,3]; [1] Perspectum Ltd, Oxford, United Kingdom, [2] EOC – Ente Ospedaliero Cantonale, IIMSI – Imaging Institute of Southern Switzerland, Lugano, Switzerland, [3] John Radcliffe Hospital, Department of Radiology, Oxford, United Kingdom

Purpose: Pancreatic volume is an important biomarker that varies in response to many different pancreatic diseases such as diabetes and chronic pancreatitis. However, pancreas delineation is challenging and manually involved. This study aims to validate automated deep learning-based pancreas segmentation in MRI against radiologist annotations.

Methods and Materials: A 3D U-Net model was trained on a cohort (319 training, 41 hold-out validation) of volumetric scans of healthy and pancreatobiliary disease subjects, acquired on scanners from three major MRI vendors, at 1.5T and 3T field strengths. 24 datasets were reserved for evaluation and annotated independently by a radiologist and a researcher. Inter-operator agreement was compared against model vs radiologist agreement. Segmentation performance was evaluated using Dice similarity coefficient (DSC), 95th percentile Hausdorff distance (HD95), and volume agreement.

Results: Model agreement with radiologist (mean±STD: DSC=0.74±0.05, HD95=9.13±4.79 mm) was comparable to inter-operator agreement (DSC=0.73±0.09, HD95=15.1±18.36 mm) (paired t-test: p=0.30 DSC, p=0.09 HD95). Two cases with diffuse fat infiltration showed DSC below 0.5. Volume differences in inter-operator (bias=-12.4 mL, LoA=[-49.0, 24.0] mL) and model vs radiologist (bias=-3.14 mL, LoA=[-51.0, 44.0] mL) were above the suggested 30% diagnostic threshold.

Conclusion: The model shows promising accuracy and robustness across scanner models and field strengths. Our results suggest that processes like fat infiltration create a lobular appearance that complicates segmentation. Differences in annotation protocols contributed to inter-operator variability and will be addressed.

PO27

Differentiating urinary stone composition with photon-counting detector CT: First in-vivo experience

D. Nakhostin, K. Higashigaito, H. Alkadhi; USZ – Universitätsspital Zürich, Institut für diagnostische und interventionelle Radiologie, Zurich, Switzerland

Purpose: To determine whether urinary stones can be differentiated with photon-counting detector CT in-vivo.

Methods and Materials: Between May 2021 and April 2022, consecutive patients with suspected urinary stones were scanned on a clinical, photon-counting detector CT (PCD-CT) scanner (tube voltage 140 kV, automated exposure control). CT scans with urinary stones were measured and analyzed with commercially available software which allows for color-coded differentiation between uric acid and non-uric acid containing stones. Patients were followed-up and electronic records were checked for chemical urinary analysis.

Results: A total of 37 patients (6 female, 31 male, mean age 47 +/- 16 years) with urinary stones (mean stone size 4.64 mm) were included. Chemical analysis yielded 34 non-uric acid stones (majority whewellite) and 3 uric acid stones. The software accurately detected and characterized 30/37 stones. The additional 7 stones had to be manually marked and also yielded a correct dual-energy ratio for differentiation.

Conclusion: To our knowledge, this is the first patient study evaluating the feasibility of PCD-CT for characterizing urinary stone composition, demonstrating that the inherent spectral capabilities of the scanner allow for an accurate differentiation between uric acid and non-uric acid containing stones. The automated workflow using commercially available software was accurate, however, required manual interaction in mostly small-sized stones.

PO28

Prostate cancer staging: radio-pathologic correlation

J. Matthey-des-Bornels[1], S. Schaer[1], M. Valério[2], A. Richemond[3], J. Dagher[1], A. Rakauskas[1], C. Dromain[1], M. Jreige[1], N. Vietti-Violi[1]; [1] CHUV – Centre Hospitalier Universitaire Vaudois, Lausanne, Switzerland, [2] HUG – Hôpitaux universitaires de Genève, Geneva, Switzerland, [3] UNIL – University of Lausanne, Lausanne, Switzerland

Purpose: To perform a radio-pathologic correlation of prostate cancer in terms of lesion detection and cancer volume correlation.

Methods and Materials This retrospective study included 64 consecutive patients (mean age: 64 ± 9yo) with radical prostatectomy for biopsy-proven prostate adenocarcinoma between 2018 and 2020. All patients underwent prostate MRI within 6 months before surgery. One radiologist performed 3D prostate cancer lesion segmentation using Mint Lesion™ software, for all detected lesions (up to 3 lesions), allowing volume measurements. Segmentations were performed on T2 weighted imaging (WI), diffusion weighted imaging (DWI), apparent coefficient diffusion (ADC) and perfusion. Two pathologists viewed the prostate specimens and measured the volume of each lesion. Radio-pathologic correlation of each lesion considering ≥ grade group 2 and volume ≥ 0.5ml was tested for detectability and for volume correlation using Pearson's correlation, Bland-Altman limit-of-agreement and Lin's concordance correlation.

Results: In total 63 lesions (grade group 2 or higher and volume ≥ 0.5 ml) were identified on pathology. 41 patients had one lesion on pathology, 9 had 2 lesions and 1 had 3 lesions. When considering lesion detection detectability diagnostic performance, the sensitivity and specificity were 91.8% and 97.8% for T2WI, 85.2% and 98.5% for DWI, 90.2% and 98.5% for ADC, and 86.9% and 97.1% for perfusion, respectively. The mean lesion volume was 5.8±7.9ml on pathology and 5±7.6ml on perfusion MR (p=0.569). Perfusion showed the best correlation with lesion volume derived from pathology compared to T2WI, DWI, and ADC (ρc= 0.934, ρc= 0.571, ρc= 0.418, and ρc= 0.485, respectively).

Conclusion: Prostate MRI allows detection of prostate cancer with high sensitivity and specificity. Perfusion is the most accurate sequence for cancer volume measurement, highlighting the added value of multi-parametric MRI for prostate cancer staging and treatment planning.

Noninvasive assessment of liver segmental volumes and its relationship with 5-year prognostication

D. Catucci[1], J. Hrycyk[2], N.F. Lange[3], V.C. Obmann[1], A. Berzigotti[3], L. Ebner[1,4], J.T. Heverhagen[5], A. Christe[1], A.T. Huber[1,4]; [1] Inselspital – Universitätsspital Bern, Department of Diagnostic, Interventional and Pediatric Radiology, Bern, Switzerland, [2] Inselspital – Universitätsspital Bern, Institute for Diagnostic and Interventional Neuroradiology, Bern, Switzerland, [3] Inselspital – Universitätsspital Bern, Hepatology, Department of Visceral Surgery and Medicine, Bern, Switzerland, [4] LUKS – Luzerner Kantonsspital, Department of Radiology and Nuclear Medicine, Lucerne, Switzerland, [5] Inselspital – Universitätsspital Bern, Department of Diagnostic, Interventional and Paediatric Radiology, Bern, Switzerland

Purpose: This study aimed to analyze the predictive value of liver segmental volume and attenuation ratio (LSVR / LSVAR), and caudate to right lobe ratio (CRL-R) for chronic liver disease (CLD) on routine abdominal CT scans and to predict the 5-year probability of transplant-free survival and first hepatic decompensation.

Methods and Materials: This retrospective study included 108 patients without CLD (noCLD-group; n=108), as well as 98 patients with biopsy-proven CLD. All patients underwent abdominal CT scans between 03/2015 and 08/2017. Patients with CLD were divided into three groups: early CLD (F0-F2; eCLD; n=40), advanced CLD (F3-F4; aCLD; n=20), and aCLD with clinically significant portal hypertension according to the BAVENO VII consensus (aCLDPH; n=38). CRL-R, LSVR, and LSVAR were compared between groups using Kruskal-Wallis test and ROC analysis was used to determine cut-off-values. 5-year transplant-free survival and first hepatic decompensation were assessed by Kaplan-Meier curve analysis.

Results: CRL-R, LSVR and LSVAR differed significantly between all groups (p<0.001). A CRL-R cutoff-value of >0.93 predicted aCLD with a sensitivity of 69% and a specificity of 78%, while LSVR >0.37 had a sensitivity of 68% and a specificity of 80%. Patients with both CRL-R >0.99 and LSVR >0.37 had the lowest probability of 5-year transplant-free survival (46%) and the lowest probability of a decompensation-free 5-year course (75%). In comparison, patients with both CRL-R <0.99 and LSVR <0.37 showed a higher probability of 5-year transplant-free survival (86%) and a higher probability of a decompensation-free 5-year course (98%).

Conclusion: ILSVR, LSVAR and CRL-R, measured on routine abdominal CT scans, show a high predictive value for CLD and 5-year outcome prognostication and are helpful in detecting chronic liver disease and predicting liver disease progression.

MRI liver segmentation protocol enables high quality segmentation for radiomics and machine learning analysis

P. Jeltsch, K. Monnin, M. Jreige, L. Fernandes-mendes, J. Richiardi, C. Dromain, N. Vietti-Violi; CHUV – Centre Hospitalier Universitaire Vaudois, Lausanne, Switzerland

Purpose: Establishing a liver MRI segmentation protocol and evaluate its potential to enhance quality and inter-reader agreement of annotations.

Methods and Materials: Retrospective single-center study included 20 patients (M/F:15/5, mean age: 54 y.o.) randomly selected from a database of patients with chronic liver disease. Liver segmentations were performed manually using Mint Lesion™ software by a radiologist and a radiology technician on Fat Saturated T2 weighted imaging (wi) and T1wi at the portal venous phase. The first segmentation set was performed with minimal instructions to the annotators. Based on the inter-reader discrepancies, a segmentation protocol was established. The second set was performed adhering to the protocol. Dice Similarity Coefficient (DSC) assessed inter-reader agreement pre- and post-protocol implementation on a per-patient (volume) and per-slice basis, with a Wilcoxon signed-rank test. McNemar test evaluated the number of patients with a non-annotated slice by at least one annotator at the extreme cranial or caudal slice of the liver between the first and second set.

Results: Per-patient DSC increased from 0.944 ±0.013 to 0.957 ±0.008 in T2wi (p=0.03) and from 0.953 ±0.011 to 0.957 ±0.009 in T1wi (p<0.01) between the first and second set. Per-slice DSC increased from 0.885 ±0.208 to 0.924 ±0.134 in T2wi (p<0.01) and from 0.918 ±0.145 to 0.925 ±0.125 in T1wi (p<0.01). The number of patients with a non-annotated slice by at least one annotator reduced from 20/20 to 12/20 in T1wi (p=0.04), but the change was not significant on T2wi (from 17/20 to 11/20 (p=0.16)).

Conclusion: Establishing a liver MRI segmentation protocol enhances quality and inter-reader agreement of annotations. This protocol could be used in future studies to enhance automatic segmentation quality, thereby expanding the potential applications of radiomics and machine learning.

Value of virtual monochromatic versus polychromatic conventional CT for detecting acute bowel ischemia.

K. Rothenbühler, R. Troxler, A. Sayadi, C. Sempoux, D. Rotzinger, S. Schmidt Kobbe; CHUV – Centre Hospitalier Universitaire Vaudois, Lausanne, Switzerland

Purpose: To qualitatively compare 40keV virtual monochromatic images (VMI) with conventionally acquired, polychromatic CT images (CONV) to detect acute bowel ischemia (ABI).

Methods and Materials: We retrospectively included 47 patients with pathologically proven ABI consecutively admitted urgently between 1st January 2018 and 30 April 2021. They underwent contrast-enhanced abdominal CT followed by surgery within <48h. 18 CT examinations were acquired with dual-energy CT (DECT), and 29 in the conventional polychromatic mode. After dividing the small and large bowel into 10 segments, 3 radiologists read CONV and DECT (virtual unenhanced and 40keV virtual monochromatic images in the venous phase) examinations separately and blinded to the exact localization of ABI.

Interobserver agreement and differences in the detection of ABI between the two patients' groups were determined, considering a p-value <0.05 as significant.

Results: Qualitative analysis showed good sensitivity (72-86%) and specificity (82-89%) for detecting ABI per bowel segment for all readers on both CONV and VMI without significant differences between the two techniques. The inter-observer agreement, calculated per bowel segment, was important or near perfect, with a kappa ranging from 0.61 to 0.83.

VMI exhibited significantly lower sensitivity (p : 0.07), and CONV images had lower specificity (p : 0.08) for colonic analysis than small bowel assessment.

Conclusion: Preliminary results comparing VMI with CONV CT images for detecting ABI revealed good diagnostic value and substantial or near-perfect inter-reader agreement among all radiologists for both techniques, without any significant difference.

Our preliminary qualitative analyses suggest a lower diagnostic performance for the analysis of the colon compared with the small bowel for both VMI and CONV modalities.

MRI and CT radiomics for the diagnosis of acute pancreatitis

C. Tartari[1], F. Porões[2], S. S. Schmidt Kobbe[1], D. Abler[1], A. Depeursinge[1], C. Dromain[1], N. Vietti Violi[1], M. Jreige[1]; [1] CHUV – Centre Hospitalier Universitaire Vaudois, Lausanne, Switzerland, [2] HFR – Hôpital fribourgeois, Fribourg, Switzerland

Purpose: To evaluate the respective and combined diagnostic performances of CT and MRI radiomic features for the diagnosis of acute pancreatitis (AP).

Methods and Materials: This monocentric prospective study included 79 patients diagnosed with AP between 2020 and 2022 who underwent contrast-enhanced CT (CECT) and MRI within 48-72 hours of the onset of symptoms. A matched control group (n = 77) of subjects with a normal pancreas was used to assess radiomic features of normal pancreatic parenchyma. The entire pancreatic gland was manually segmented in consensus by two operators using MintTM Software and radiomic features were extracted from CECT images on portal venous phase and from MRI on T2-weighted (WI) sequence HASTE, and on native and portal venous T1FS-WI phases using the QuantImage v2 platform. The dataset was split into training (80%) and test (20%) sets and various classification algorithms were explored. Receiver operating characteristic (ROC) curve analysis was performed to predict the performance of the obtained models.

Results: The T2WI model showed the highest overall performance compared to T1WI and CECT, with a sensitivity, specificity and AUC of 86% (95% CI: 85–88), 46% (43–47), 0.887 (0.874–0.897) for T2WI, 72% (67–74), 63% (64–68), 0.675 (0.662–0.694) for T1WI native, 69% (68–71), 70% (67–72), 0.702 (0.676–0.714) for T1WI venous, and 69% (67–71), 50% (47–53), 0.617 (0.593–0.639) for CECT. Compared to the T2WI model alone, the models using the three MRI sequences combined with CECT revealed a higher diagnostic performance, with a sensitivity, specificity and AUC of 93% (92-93), 73% (70-75) and 0.906 (0.896–0.915), respectively.

Conclusion: The radiomics model based on MRI and CECT showed a good performance in predicting the diagnosis of AP. The translation of multimodal radiomic models into routine clinical practice may improve the detection of AP and should be investigated for the prediction of AP severity and complications.

Cost-effectiveness analysis of different imaging modalities for the staging of oesophageal cancer in Switzerland

N. Guignard[1], K. Moschetti[1], M. Jreige[1], L. Brunner[2], L. Haefliger[1], V. Levy[1], N. Vietti Violi[1], C. Dromain[1]; [1] CHUV – Centre Hospitalier Universitaire Vaudois, Lausanne, Switzerland, [2] Unisanté, Lausanne, Switzerland

Purpose: To compare the diagnostic performance and cost of 4 different imaging strategies, including MRI, for the initial staging of oesophageal cancer (EC).

Methods and Materials: The cost-effectiveness of 4 TNM staging strategies (EUS + PET-CT, EUS + PET-CT+ CECT, EUS + PET-CT + IRM and IRM + PET-CT) was prospectively analyzed in 62 patients. Patients were classified into 3 groups based on each imaging strategy: (1) upfront surgery (T1/T2/N0/M0), (2) neoadjuvant therapy (T3/T4a/N+/M0) and (3) palliative treatment (T4b/M+). The diagnostic performance was defined as the agreement between the classification made by each strategy compared to the multidisciplinary consensus. A dichotomized analysis (groups 1 vs 2+3 and 1+2 vs 3) was employed to identify the most effective and accurate staging strategy.

Results: The cost (CHF) of the staging strategies were 2694 for EUS + PET-CT, 3291 for EUS + PET-CT + CECT, 3292 for EUS + PET-CT + IRM and 2718 for IRM + PET-CT. Diagnostic performances for differentiating group 1 vs 2+3 were: 0.944 for EUS + PET-CT, 0.935 for EUS + PET-CT + CECT, 0.932 for EUS + PET-CT + IRM and 0.915 for IRM + PET CT. Diagnostic performances for differentiating group 1+2 vs 3 were: 0.944 for EUS + PET-CT, 0.952 for EUS + PET-CT + CECT, 0.949 for EUS + PET-CT + IRM and 0.966 for IRM + PET-CT.

Conclusion: The combination of MRI + PET-CT demonstrates non inferiority and lower cost when compared to the current strategy of EUS + PET-CT + CECT used in Switzerland. Consequently, this study advocates for replacing the current invasive staging strategy of EUS + PET-CT + CECT with the combination of MRI + PET-CT, asserting it as a diagnostically accurate, cost effective and non-invasive approach for EC staging.

Comparing AI-Assisted Liver Lesion Segmentation: Non-Expert Technicians vs. Expert Radiologists in Liver Cancer Resection Planning

L. Núñez[1], C. Ferreira[1], A. Mojtahed[2], H. Lamb[3], _M. Pansini_[1,4,5], J. Connell[1]; [1] Perspectum Ltd, Oxford, United Kingdom, [2] Harvard Medical School, Department of Abdominal Imaging, Massachusetts General Hospital, Boston, United States, [3] University of Leiden, Department of Radiology, Leiden, Netherlands, [4] EOC – Ente Ospedaliero Cantonale, IIMSI – Imaging Institute of Southern Switzerland, Lugano, Switzerland, 5 John Radcliffe Hospital, Department of Radiology, Oxford, United Kingdom

Purpose: Detection and delineation of lesions in the liver is an important radiological task that allows for characterization and informs clinical decision making and surgical planning. This task is time-consuming and requires expert training. Also, studies found marked variability in scores of the same lesions between radiologists. Artificial Intelligence (AI) assisted solutions have already shown great promise in reducing variability between readers in liver volumetry. This study evaluates the accuracy of non-expert technicians vs radiologists in performing whole liver and liver lesion delineation in the context of colorectal liver metastases resection planning when technicians are assisted using an AI-enabled decision support tool (Hepatica).

Methods and Materials: Non-contrast T1w MRI scans from 18 patients with colorectal liver metastasis were retrospectively analyzed. Hepatica automatically delineated the liver and detected and outlined potential liver lesions. Masks generated by Hepatica were given to three technicians and three radiologists to guide them in finishing the delineation. Size metrics were automatically measured from the final delineation. Agreement between technicians+AI and radiologists in measuring liver parameters was assessed using ICC.

Results: The 41 lesions detected by all radiologists, with volume ranged from 1.3-43.4ml and diameter from 11.4-51.0mm, were detected by all technicians. ICC of mean of technicians vs mean of radiologists for liver volume, lesion diameter and lesion volume were 0.999, 0.981 and 0.987, respectively.

Conclusion: The performance of the AI-assisted technicians and expert radiologists was comparable for detection and measurement of liver lesions. These findings suggest that delegating certain time-consuming manual radiologists' tasks to less qualified personnel, can deliver comparable results when supported by AI. This shows AI-assisting tools like Hepatica for decision support can enhance the overall efficiency of radiology departments for decision support.

CT-derived quantitative image features predict neoadjuvant treatment response in adenocarcinoma of the esophagogastric junction with high accuracy

M. Graf[1], S. Ziegelmayer[1], S. Reischl[1], J. Gawlitza[1], F. Gassert[1], A. Marka[1], J. Bachmann[2], M. Makowski[1], D. Reim[2], F. Lohöfer[1], R. Braren[1], E. Burian[3]; [1] MRI TUM – School of Medicine & Klinikum rechts der Isar, Department of Diagnostic and Interventional Radiology, Munich, Germany, [2] MRI TUM – School of Medicine & Klinikum rechts der Isar, Department of Surgery, Munich, Germany, [3] Kantonsspital Frauenfeld, Department of Nuclear Medicine, Frauenfeld, Switzerland

Purpose: The purpose of this retrospective study was to evaluate the value of contrast enhanced-computed tomography (CE-CT) image features in predicting histopathological response in patients with an adenocarcinoma of the esophagogastric junction (AEG) under neoadjuvant chemotherapy.

Methods and Materials: 105 patients with the diagnosis of AEG were examined by CE-CT at baseline and preoperatively after neoadjuvant chemotherapy. All patients underwent surgical resection. Histopathological parameters and tumor regression grading according to Becker et al. were collected in 93 patients. Line profiles of the primary tumor area in baseline and preoperative CE-CT were generated using ImageJ. Maximum tumor density and tumor-to-wall density delta were calculated and correlated with the histopathologic tumor response. In addition, tumor response was assessed according to standard RECIST measurements in all patients and by endoscopy in 72 patients.

Conclusion: Baseline and change of baseline to preoperative CE-CT parameters showed no significant differences between responders (Becker grade 1a, 1b) and non-responders (Becker grade 2, 3). After neoadjuvant therapy, responders and non-responders showed significant differences in maximum density and tumor-to-wall density delta values. Line profile measurements showed excellent inter-rater agreement. In comparison, neither RECIST nor endoscopy showed significant differences between these groups.

Conclusion: CE-CT can predict histopathological therapy response to neoadjuvant treatment in AEG patients with high accuracy and thus may improve patient management.

Abbreviated MRI for the abdomen: Optimized protocols and current clinical applications

J. Ferrari, C. Dromain, M. Fraga Christinet, P. Jeltsch, L. Fernandes Mendes, N. Vietti-Violi; CHUV – Centre Hospitalier Universitaire Vaudois, Lausanne, Switzerland

Learning objectives: Explore the potential indications of AMRI in abdominal imaging.

Examine different AMRI protocols in the abdomen.

Highlight the potential impact of AMRI on current MRI workflows efficiency and resource utilization.

Background: Traditional MRI application has greatly expanded but its complexity, timing and high cost are limiting, driving a shift toward AMRI protocols to address more efficiently each clinical question without compromising diagnostic performance.

Imaging findings or procedure details: AMRI protocols, built on necessary sequences allow reduced acquisition times and cost, while keeping high diagnostic performance for a specific question, such as:

- Characterizing diffuse liver diseases with rapid, non-contrast AMRI, which precisely quantify hepatic stiffness and fat/iron content with the same power of conventional MRI, emerging as a key alternative in chronic liver diseases monitoring.
- AMRI in the context of hepatocellular screening, particularly when coupled with blood tests, achieve higher diagnostic performance than ultrasound, the established technique for screening, similarly to full MRI protocol. These shortened protocols can then be completed by full sequence acquisition only when needed.
- AMRI can potentially be applied for the follow up of pancreatic cystic lesions, small renal masses, hepatic metastases and for the characterization of adrenal incidentalomas, with reduced acquisition and reading times, and, often, without the risks related to contrast injection. AMRI is already used in prostate MRI when performing bi-parametric MRI.

Conclusion: AMRI is a pivotal advancement in radiology, improving MRI workflows by reducing examination and interpretation times and cost while offering high diagnostic performance for specific clinical questions. This educational poster will discuss the added value of implementation of AMRI in the clinical practice, the proposed protocols, as well as their clinical indication in abdominal imaging.

Imaging of Gynaecological Emergencies

F. Orthmann, K. Mandralis, S. Schmidt Kobbe; CHUV – Centre Hospitalier Universitaire Vaudois, Lausanne, Switzerland

Learning objectives: To review the diagnostic workup for the most common gynecological emergencies using different imaging modalities, such as US, CT and MRI.

Background: Gynecological emergencies often have a non-specific clinical presentation; for example, lower abdominal pain, nausea and vomiting may be present in acute gynecological, urologic and gastrointestinal diseases. Physical examination may also be difficult, especially in pregnant woman. This is why imaging plays such a central role in the management of gynecological emergencies.

Ultrasonography (transvaginal or transabdominal) should be the initial examination of choice but has technical and clinical limitations. Certain patients may need further imaging by CT or MRI for subsequent evaluation. However, CT is invariably associated with radiation exposure to these, very often, young women, and the MRI is not always available in emergency conditions.

Imaging findings or procedure details: We will present the radiological features of the most common gynecological emergencies and demonstrate the diagnoses made using different imaging modalities (US, CT and MRI). The images of our selected cases of adnexal and uterine emergencies come from our institution.
- Adnexal emergencies
- Hemorrhagic ovarian cysts
- Ectopic pregnancy
- Adnexal torsion
- Tubo-ovarian abscess
- Uterine emergencies
- Acute fibroid complications
- Uterine rupture
- Acute uterine bleeding

Conclusion: Due to their non-specific clinical presentation gynecological emergencies are a diagnostic challenge. Radiologists play a key role, having to choose between different imaging modalities in order to make an accurate diagnosis and therefore ensure appropriate medical or surgical treatment.

The Biliary Labyrinth: Navigating Non-Stone Obstructions

F. De Lucia[1], M. Ben Salah[1], H. Thoeny[1,2], L. Widmer[1,2]; [1] HFR – Hôpital fribourgeois, Fribourg, Switzerland, [2] University of Fribourg, Fribourg, Switzerland

Learning objectives:
1. To expose etiologies of non-stone biliary obstructions, through radiological imaging and clinical correlation.
2. To illustrate diagnostic steps, enabling accurate differentiation between various obstruction types and facilitating timely intervention.
3. To enhance treatment decision-making by providing a comprehensive overview of endoscopic, surgical, and medical management approaches.

Background: Biliary obstruction, typically associated with gallstones, is a well-known condition. However, non-stone etiologies of bile duct blockage, often overlooked, can pose life-threatening risks when late or misdiagnosed. Clinicobiological findings, along with first-line imaging ones, play a key-role in guiding radiologists towards recommending appropriate supplementary work-up. MRI is a reliable modality for comprehensive biliary duct mapping, precise localization, and diagnostic orientation, facilitating subsequent examination or biopsy techniques if warranted.

Imaging findings or procedure details: Non-stone biliary obstructions include sludge, tumors, casts, foreign bodies, parasitic infections and biofilms. Even if they present with a common clinicobiological manifestation of cholestasis, they may exhibit unique clinical, biological and radiological findings. This poster outlines a standardized MRI protocol for comprehensive biliary investigation, detailing sequences used and emphasizing cholangiographic ones. We propose a management algorithm highlighting clinicoradiological traits, aiding precise and minimally invasive diagnosis. Primary care involves biliary drainage aiming to overcome life-threatening complications. The choice between endoscopic and/or percutaneous procedures depends on the etiology, location, and local expertise.

Conclusion: Non-stone biliary obstruction is an overlooked condition, poorly documented in the literature. We propose an algorithm serving as a guide for precise diagnosis and therapeutic management, empowering radiologists to navigate the complexities of the biliary tree.

The role of standardized report in the assessment of peritoneal carcinomatosis.

L. Ghosn, R. Hajri, L. Haefliger, M. Jreige, N. Vietti Violi, C. Dromain; CHUV – Centre Hospitalier Universitaire Vaudois, Lausanne, Switzerland

Learning objectives: Familiarize radiologists with the importance of detecting peritoneal carcinomatosis (PC) through its various forms.

Enumerate essential features to be documented for the selection of patients who will benefit from surgery.

Establish a standardized radiological report for the preoperative assessment of PC.

Background: Despite significant advances in imaging technology, the assessment of PC remains challenging, particularly for untrained radiologists. Since cytoreductive surgery and Hyperthermic Intraperitoneal Chemotherapy (HIPEC) has become the standard treatment for PC, the role of imaging has gained considerable importance in the preoperative assessment of patients with suspected PC.

Imaging findings or procedure details: A dedicated reading of the peritoneum as a distinct organ allows producing a quantitative and qualitative evaluation of PC extension to better assist surgeons in the selection of candidates for curative surgery.

The analysis should include the distribution of ascites, its appearance and abundance, the Computed Tomography-calculated Peritoneal Cancer Index (CT-PCI), the identification of lesions associated with a low probability of complete surgical resection (such as portal hepatis infiltration, plurifocal bowel obstruction or mesentery involvement), lesions requiring specific surgical interventions and the identification of extraperitoneal metastases. These elements enable the creation of a standardized report, which is a key component for the communication between radiologists and surgeons.

Conclusion: Standardized radiological report for PC provides a powerful tool to identify patients likely to benefit from cytoreduction and assist in surgical planning.

MRI ZTE deep learning augmented sequences enhance diagnostic confidence of hand and feet protocols

C. Obermüller, K. Pawlus, M. Kaniewska, R. Guggenberger;
USZ – Universitätsspital Zürich, Zurich, Switzerland

Purpose: To assess the potential benefit of integrating ZTE (zero echo time) deep learning augmented sequences into a standard musculoskeletal MRI protocol for the comprehensive evaluation of joint pathologies in hand and feet.

Methods and Materials: This prospective cohort encompassed both hands and feet, with 26 datasets in total, and five specific regions evaluated individually. Six musculoskeletal features were assessed: subcortical sclerosis (yes/no), erosions/ganglia (yes/no), osteophytes (yes/no), joint space narrowing (yes/no), fractures (yes/no), and ossicles/soft tissue calcifications (on a scale: 0 = none, <3 = 1, 3-6 = 2, >6 = 3) with each a diagnostic confidence scale of 1 (low confidence) to 3 (high confidence). In the hands, the five regions were the radioulnocarpal joints and proximal Gilula arc, carpometacarpal joints and distal Gilula arcs, the thumb saddle joint, the metacarpophalangeal joints, and the interphalangeal joints. In the feet, the five regions were defined as Chopart joints, Lisfranc joints, the first metatarsophalangeal joint, the metatarsophalangeal joints II-V, and the interphalangeal joint.

Results: The integration of ZTE deep learning augmented sequences demonstrated consistently higher diagnostic confidence across all categories (subcortical sclerosis, erosions/ganglia, osteophytes, joint space narrowing, fractures, and ossicles/soft tissue calcifications) compared to the standard musculoskeletal protocol (n = 26, $p < 0.05$ Holm-corrected). Interreader agreement showed robust values (n = 2, average kappa of 0.62 for significant Holm-corrected p-values, interquartile range of these average kappa values: 0.58-0.68).

Conclusion: Incorporating ZTE deep learning augmented sequences into a standard musculoskeletal MRI protocol of hands and feet enhances the diagnostic confidence of bone and joint pathologies.

Most Patients with Increased Femoral Torsion and Ischiofemoral Impingement Have Symmetrical Femoral Torsion and Ischiofemoral Distance on CT

T. Kaim[1], F. Schmaranzer1, M. Hanke[2], S. Steppacher[2], M. Tannast[3], T. Lerch[1]; [1] Inselspital – Universitätsspital Bern, Department of Diagnostic, Interventional and Paediatric Radiology, Bern, Switzerland, [2] Inselspital – Universitätsspital Bern, Department of Orthopaedic Surgery, Bern, Switzerland, [3] HFR – Hôpital fribourgeois, Department of Orthopaedic Surgery, Fribourg, Switzerland

Purpose: Ischiofemoral hip impingement is a hip disease affecting mainly female patients and was associated with increased femoral version(FV). It is unknown, if these patients have bilateral or unilateral increased FV. Therefore, we report(1) mean FV, (2) side-to-side difference and frequency of >10° FV side-to-side difference and (3) ischiofemoral distance for patients with increased FV and ischiofemoral impingement.

Methods and Materials: A retrospective CT analysis involving 64 hips(32 patients, 01/2013-03/2019) was performed. Inclusion criteria were symptomatic ischiofemoral hip impingement and increased femoral version>25° and treatment with femoral derotation osteotomy (30 female patients, mean age 27 years).
We evaluated FV using the Murphy method and ischiofemoral distance on CT. FV was compared to the contralateral side.
We evaluated FV of a control group of 19 asymptomatic volunteers (mean age was 27±3, range 21–33years) on rapid MRI sequences: bilateral T1 VIBE Dixon MRI sequence (AT 32-40 seconds) of the pelvis and knee.

Results: (1)Mean FV of the symptomatic side (46±11°) was significantly (p<0.001) higher compared to control group(28±16°) and not different compared to contralateral side(43±11°).
(2)Side-to-side difference of FV was slightly decreased for the patients(6±6°) compared to control group(7±5°) and >10° FV was prevalent in 8 patients (25%), and in 5 volunteers(26%).
(3)Ischiofemoral distance of the symptomatic side (19mm) was not different to asymptomatic side (20 mm).

Conclusion: Most of the patients with ischiofemoral impingement undergoing surgical treatment showed symmetric deformity, but 25% of patients showed asymmetrical deformity of increased FV. Therefore, routine bilateral CT/MRI evaluation is recommended for these patients to assess rotational profile and search for torsional malalignment.

How much does the labrum and cartilage contribute to joint contact surface in different hip deformities? – An automatic deep learning based 3D MRI analysis

M. Meier[1], J. Roshardt[1], A. Ruckli[2], N. Gerber[2], T.D. Lerch[3], M. Tannast[4], S.D. Steppacher[1], F. Schmaranzer[3]; [1] Inselspital – Universitätsspital Bern, Department of Orthopaedic Surgery and Traumatology, Bern, Switzerland, [2] University of Bern, Bern, Switzerland, [3] Inselspital – Universitätsspital Bern, Department of Diagnostic, Interventional and Paediatric Radiology, Bern, Switzerland, [4] HFR – Hôpital fribourgeois, Department of Orthopaedic Surgery and Traumatology, Fribourg, Switzerland

Purpose: Using a deep learning based approach for automatic 3D segmentation of MRI we asked: What are the differences in labrum contribution to joint contact surface among different hip deformities and which radiographic parameters influence labral contribution to joint contact surface?

Methods and Materials: This retrospective study was approved by the local ethics committee with waiver for informed consent. 100 patients with symptomatic hip deformities undergoing direct hip MR arthrography (large flexible body coil, 3T) between January 2020-October 2021 were consecutively selected (mean age = 30±9; 64% female). Standard imaging protocol included multiplanar PD-w TSE images and an axial-oblique 3D T1 MP2RAGE sequence. According to acetabular morphology, patients were divided into subgroups: dysplasia (LCE<23°), normal coverage (LCE 23-33°), overcoverage (LCE 33-39°), severe overcoverage (LCE>39°) and retroversion (retroversion index>30% and all 3 retroversion signs positive). A previously validated deep learning approach for automatic segmentation and software for calculation of joint contact surface were used. Labral contribution to joint contact surface was defined as: labrum surface area/(labrum surface area+cartilage surface area). One-way ANOVA with Tukey's correction for multiple comparison and linear regression analysis was performed.

Results: Labral contribution to joint contact surface differed among hip deformities (p<0.001). Mean labral contribution of joint contact surface of dysplastic hips was 26±5 (17–33)% and higher compared to all other hip deformities (p from 0.001 to 0.036).
Linear regression analysis showed linear relationship between labral contribution to joint contact surface and LCE (b = -0.002, p < 0.001) and femoral torsion (b = 0.001, p = 0.008) with a goodness of fit of $R2= 0.35$.

Conclusion: Labral contribution to joint contact surface differs among hip deformities and is influenced by lateral acetabular coverage and femoral torsion.

The missed chapter on midfoot: Chopart injuries

B. Abs, H. Bouredoucen, M. Buzzi Amillano, A. Platon, P-A. Poletti, D. Ferreira Branco, S. Boudabbous; HUG – Hôpitaux universitaires de Genève, Geneva, Switzerland

Purpose: Assessment of mid tarsal bone injuries with emphasis on Chopart on Cone Beam CT and comparison to radiograph's accuracy for missed lesions.

Methods and Materials: All cases of CBCT performed for traumatic ankle and foot were retrospectively analysed during a period of five years. Cases with Chopart and Lisfranc were retrieved. Association with ankle injuries was reported. A second look to prior radiographs was as well performed. Accuracy for midtarsal injuries of later imaging was calculated and results were compared to the litterature.

Results: 754 traumatic cases of CBCT were analysed. Lisfranc and Chopart injuries were detected in 142 (18.8%) and 146 (19.3%) patients respectively. Regarding Chopart, 84 patients (57.5%) have talonavicular avulsion, 113 patients (77.3%) have calcaneonavicular avulsion and 69 patients (47.2%) have calcaneocuboid injuries. Association of Lisfranc and Chopart injuries was visible only in 33 cases (11.4%) if one feature was considered and only in 2.25% if all features of Chopart were grouped. Malleolar injuries were detected respectively in 26 and 42 cases for medial and lateral sides without significant association with Lisfranc nor chopart injuries (0.66% and 1.32% respectively). No case of associated dislocation was detected. Further findings will be detailed in the presentation. Blinded retrospective analysis of prior radiographs shows a sensitivity of 0.590, 0.946 of specificity and 0.893 accuracy of this modality for detection of Lisfranc and Chopart avulsions.

Conclusion: This study highlights the missed injuries of Chopart on XR, the low association with Lisfranc avulsions. It emphasis that calcaneo-navicular avulsions are the most frequent pattern of Chopart lesions to be investigated with caution on XR. Cross sectional imaging is mandatory to specify traumatic injuries with higher confidence and to guide treatment. We propose CBCT as a reliable tool for the diagnosis.

PO66

High-resolution mapping of hand innervation: Novel approaches at 7T MRI

P. Guillemin[1], D. Ferreira Branco[2], Y. M'rad[1], L.Mattera[3], O. Lorton[1], P-A. Poletti[4], G.-F. Piredda[5,6], A. Klauser[5,6], R. Martuzzi[3], R. Salomir[7], S. Boudabbous[8]; [1] University of Geneva, Faculty of medicine, Geneva, Switzerland, [2] USZ – Universitätsspital Zürich, Department of Radiology, Geneva, Switzerland, [3] FCBG – Fondation Campus Biotech, Geneva, Switzerland, [4] HUG - Hôpitaux universitaires de Genève, Geneva, Switzerland, [5] Siemens Healthineers, ACIT – Advanced Clinical Imaging Technology, Lausanne, Switzerland, [6] CIBM – Center for Biomedical Imaging, Geneva, Switzerland, [7] HUG – Hôpitaux universitaires de Genève, Radiology department, Geneva, Switzerland, [8] HUG – Hôpitaux universitaires de Genève, Department of Radiology, Geneva, Switzerland

Purpose: Visualizing the complex nerve network of the human hand with conventional clinical MRI proves challenging due to the multiplanar nature of nerve pathways. For this purpose, the emergence of ultra-high field MRI offers the potential to explore fine anatomical structures, thus our aim is to assess the sensory and motor nerve structures of the hand in adults.

Methods and Materials: Three volunteers were recruited for bilateral hand imaging and were examined using a 7T MRI (MAGNETOM Terra.X, Siemens, Germany). A 3D T2 DESS optimized sequence was performed (TE:5.22ms ,TR:11.06ms,R:0.4x0.4x0.5mm). For the three volunteers, the four nerves of each long finger were manually tracked using Osirix's 3D Curved MPR function (Osirix, Switzerland), which locally unfolds the nerve's tortuosity, used to take several measurements to characterize the nerve. Additionally, Pacinians corpuscles were semi-automatically segmented in 3D using 3DSlicer. **Results:** Using the T2 DESS sequence, it was possible to accurately reconstruct all the digital nerves and provide further anatomic description. Sharp delineation of nerve fascicles was demonstrated with the perineurium of each fascicle distinctly identified. For all the volunteers digital nerves were found, on average, between 2 and 3 mm deep, except within flexion folds, where the nerve was approximately 1.5 mm from the skin. Pacinian corpuscle segmented for the six cases are most tightly grouped in the metacarpals zone, located on the palmar side and on the surface of the tendinous, muscular and bone structures. The diameters of the Pacinian corpuscles ranged from 1 to 5 mm.

Conclusion: Our study demonstrated the feasibility of high-resolution 7T MRI imaging for examining nerve fascicles. This advancement is expected to enable the visualization of microstructural distal traumatic lesions in the peripheral nervous system, with improvements in anatomical and tractographic sequences.

PO67

Accelerated MRI-Acquisition using Deep-Learning Image Reconstruction and Edge Sharpening, and Standard Acquisition Protocol in Evaluating Patients after Rotator Cuff Repair – A Comparison

R. Marcus[1], G. Feuerriegel[1], C. Baum[2], A. Marth[1], D. Nanz[1], R. Sutter[1]; [1] Balgrist University Hospital, Zurich, Switzerland, [2] USB – Universitätsspital Basel, Basel, Switzerland

Purpose: To assess the diagnostic performance of accelerated MRI acquisition with deep-learning reconstruction and edge sharpening in patients after rotator cuff repair.

Methods and Materials: This prospective study was approved by the local IRB. Unenhanced MRI scans of the operated shoulder were performed on 116 patients using a 3 Tesla (T) scanner (MAGNETOM Prisma, Siemens Healthineers, Erlangen, Germany). Standard and accelerated protocols were used during the same scanning session acquiring three sequences in coronal plane (TIRM, PD TSE and PD FS), two sequences in sagittal plane (TIRM and T1 TSE) and one sequence in axial plane (PD FS) with a slice thickness of 3 mm each. The acquisition times of the standard and the accelerated protocols were recorded. Two experienced radiologists, blinded to the acquisition protocol, evaluated postsurgical changes of the tendons as per Sugaya classification (1: sufficient thickness, 2: sufficient thickness with partial high intensity, 3: insufficient thickness, 4: minor discontinuity, 5: major discontinuity).

Results: Inter-rater and intra-rater reliabilities of the evaluated 207 operated tendons were strong (k = 0.824 – 0.863). The accelerated protocol reduced the acquisition time by 80% (3.7 minutes [2.5 – 6.3] vs. 18.4 minutes [17 – 33.7] for accelerated vs. standard protocol, p <0.001). A total of four intra-rater disagreements were observed (2%), due to motion artifact in the standard acquisition or slightly different acquisition planes. No motion artifact was recorded during the accelerated protocol.

Conclusion: Accelerated MRI acquisition with deep - learning reconstruction and edge sharpening significantly shorten the acquisition time while maintaining a high diagnostic accuracy of evaluating the condition of the shoulder after rotator cuff repair.

PO68

Dorsal ganglion: Update on epidemiologic data, anatomic and clinic correlation based on high filed MRI in tertiary center

D. Ferreira Branco, P. Botti; HUG – Hôpitaux universitaires de Genève, Department of Radiology, Geneva, Switzerland

Purpose: Ganglia are the most common soft tissue tumor of hand and those on dorsal surface of wrist represent between 57 and 70% of wrist cysts, always at the expense of dorsal scapholunate (SL) region. They are reported as a cause of chronic dorsal wrist pain. The aim of this study is to determine prevalence of incidental ganglion of dorsal SL region and an update of epidemiologic data for this entity based on 3 Tesla (3T) MRI for anatomic and clinic study

Methods and Materials: In this retrospective study, we analyzed all consecutive 3T MRI performed for post traumatic wrist in patients aged from 18 to 75 years (mean age-38.7 years), between January 2019 to October 2023 in University Hospital. Images were evaluated independently by two musculoskeletal radiologists on 3D proton density (3DPD) sequence and correlated to symptoms (dorsal pain), epidemiologic data (age, sex, traumatic event) as well as relationship with extrinsic ligaments and posterior interosseous nerve (PIN). Statistics were performed on Graphpad Prism software.

Results: Dorsal wrist ganglia were identified in 152 out of 295 wrists with a mean volume of 68.79 mm3 (range 0.52-1683). Agreement between readers was almost perfect for epidemiologic parameters (ICC>0.81). 73% percent of patients have a history of acute trauma and although 27% of patients reported dorsal SL pain on clinical examination, only 5% had an associated lesion of dorsal SL ligament. Inter-observer reliability for ganglion volumetry, assessment of distance to PIN and staging according to Guerini's classification are moderate to substantial(0.41-0.60). Finally assessment of relationship with joint capsular reflection (DCSS) was challenging even using 3D sequence.

Conclusion: Dorsal SL ganglia are common even in absence of correlation with dorsal pain. Furthermore, relationship with extrinsic ligaments and PIN was not correlated with her. MRI with 3D sequence is accurate on assessment of SL ganglia and association with ligament injury, however it still lacks precision for DCSS analysis

PO69

Spectral Topograms from Photon Counting Detector CT: Bone Mineral Density Assessment

L.J. Moser[1], J. Pitteloud[2], V. Mergen[1], D. Frey[3], O. Distler[3], M. Eberhard[1,4], H. Alkadhi[1]; [1] USZ – Universitätsspital Zürich, Department of Diagnostic and Interventional Radiology, Zurich, Switzerland, [2] USZ – Universitätsspital Zürich, Department of Diagnostic and Interventional Paediatric Radiology, Zurich, Switzerland, [3] USZ – Universitätsspital Zürich, Department of Rheumatology, Zurich, Switzerland, [4] Spitäler fmi AG – Spital Interlaken, Department of Radiology, Unterseen, Switzerland

Purpose: To evaluate the feasibility and accuracy of bone mineral density (BMD) quantification from spectrally acquired topograms with photon-counting detector (PCD)-CT, in comparison with DXA.

Methods and Materials: For this experimental study, spectrally-resolved topograms on a clinical dual-source PCD-CT scanner (NEAOTOM Alpha, Siemens) acquired with 140kVp and with four different tube currents (10mA, 20mA, 30mA and 40mA) of the European Spine Phantom were obtained. Scans were repeated three times. We used two setups: (A) the phantom placed directly on the CT table and (B) the phantom submerged in water with an anterior-posterior diameter of 30 cm simulating a slightly overweight patient. Corresponding DXA scans were acquired. Assessment of aBMD in spectral topograms was enabled by leveraging the spectral information with material decomposition maps for hydroxyapatite and water. The spine phantom-supplied values were used as the reference standard.

Results: The mean absolute error (MAE) in setup A for spectral topogram derived aBMD across all tube currents and vertebrae was 0.003g/cm2 with a relative difference of ΔaBMD ranging from -0.6% to +0.6%. Coefficients of variance (CV) were below 1% stratified for tube current in setup A. In setup B, the MAE was 0.018g/cm2, and the ΔaBMD ranged from +0.6% to +3.7%. CV was below 3% for all tube currents and below 2% excluding 10mA. The absolute error of DXA scans in both setups (-0.041g/cm2 for setup A, -0.06g/cm2 for setup B) was higher than corresponding MAEs from PCD-CT.

Conclusion: Our phantom study indicates that spectral topograms obtained with PCD-CT enable the calculation of BMD with high accuracy.

PO70

Enhanced bone assessment of the shoulder using zero-echo time MRI with deep-learning image reconstruction

F. Ensle[1], M. Kaniewska[1], M. Lohezic[2], R. Guggenberger[1]; [1] USZ – Universitätsspital Zürich, Department of Diagnostic and Interventional Radiology, Zurich, Switzerland, [2] GE HealthCare, Zurich, Switzerland

Purpose: To assess a deep learning-based reconstruction algorithm (DL-Recon) in zero echo-time (ZTE) MRI of the shoulder at 1.5 Tesla for improved delineation of osseous findings.

Methods and Materials: In this retrospective study, 64 consecutive exams of 52 patients (28 female) undergoing shoulder MRI at 1.5 Tesla in clinical routine were included. Coronal 3D isotropic radial ZTE pulse sequences were acquired in the standard MR shoulder protocol. In addition to standard-of-care (SOC) image reconstruction, the same raw data was reconstructed with a vendor-supplied prototype DLRecon algorithm. Exams were classified in three subgroups according to the written radiology report: no pathological findings, degenerative changes and posttraumatic changes, respectively. Two blinded readers performed bone assessment on a 4-point scale by qualitatively grading image quality features and delineation of osseous pathologies including diagnostic confidence in the respective subgroups. Quantitatively, signal-to-noise ratio (SNR) and contrast-to-noise ratio (CNR) of bone were measured. Comparative analyses were conducted to assess the differences between the reconstruction methods. Interreader agreement was evaluated with Cohen's kappa.

Results: DLRecon scored significantly higher than SOC in all image quality features ($p < 0.03$), except in the artifact category ($p = 0.37$). DLRecon also received superior scores for delineation of osseous pathologies and diagnostic confidence ($p ≤ 0.03$). Quantitatively, DLRecon achieved superior CNR and SNR of bone than SOC ($p < 0.001$). Interreader agreement ranged from moderate to substantial ($κ = 0.46 - 0.78$).

Conclusion: ODLRecon enhanced image quality in ZTE MRI and improved delineation of osseous pathologies, allowing for increased diagnostic confidence in bone assessment of the shoulder.

PO71

Rheumatoid Arthritis in the Wrists and Hands – What the Radiologist Should Know

J. Evers[1], C. Guessoum[1], N. Antil[2], K. Stevens[2], G. Andreisek[3,1], A. Lutz[2,1]; [1] Kantonsspital Münsterlingen, Team Radiologie Plus, Münsterlingen, Switzerland, [2] Stanford University School of Medicine, Department of Radiology, Stanford, United States, [3] University of Zurich, Medical Faculty, Zurich, Switzerland

Learning objectives

- To understand the pivotal role of imaging in the early detection and management of Rheumatoid Arthritis (RA)
- To recognize the roles of various imaging modalities and specific findings in RA
- To understand the impact of disease modifying drugs on classic RA imaging findings

Background: Rheumatoid Arthritis is a prevalent autoimmune disorder characterized by symmetrical polyarthritis, predominantly affecting small joints. Untreated, the disease progression often leads to joint destruction and disability, making early detection and treatment essential. Radiologists play a crucial role in diagnosing and monitoring RA through various imaging techniques, each with unique findings and indications.

Imaging findings or procedure details: Conventional radiography, although commonly used, has limitations in detecting early disease stages. Ultrasound (US) and Magnetic Resonance Imaging (MRI) are more sensitive, revealing early signs like synovitis and bone marrow edema. US is particularly useful in assessing soft tissue changes and joint effusions. MRI excels in detailed joint evaluation, especially in detecting bone erosions and cartilage damage. Novel techniques like Dynamic Contrast-Enhanced MRI and Diffusion-Weighted Imaging provide additional insight into disease activity. Advanced molecular imaging has emerged as a potential tool in early diagnosis, offering cellular and molecular level information.

Conclusion: Effective management of RA relies heavily on imaging for early diagnosis, differentiation from other arthritides, and monitoring of treatment response. Radiologists must be familiar with the spectrum of imaging findings specific to RA across various modalities as well as the appropriate disease classification.

Not All Erosions Are Created Equal – Arthritides Beyond Rheumatoid Arthritis

C.I. Guessoum[1], I. Evers[1], N. Antil[2], K. Stevens[2], G. Andreisek[3,1], A. Lutz[1,2];
[1] Kantonsspital Münsterlingen, Team Radiologie Plus, Münsterlingen, Switzerland, [2] Stanford University School of Medicine, Department of Radiology, Stanford, United States, [3] University of Zurich, Medical Faculty, Zurich, Switzerland

Learning objectives
- to review arthropathies affecting wrist and hand joints beside rheumatoid arthritis (RA)
- to recognize the imaging features and specific key features of each arthropathy
- to emphasize the significance of radiologic imaging in early detection and differentiation of the various arthritides from RA.

Background: Arthritic conditions affecting the wrist and hand are numerous, and clinical differentiation from RA is often difficult. This poster highlights several arthritic entities, including psoriatic arthritis (PsA), crystalline arthritis, various types of infectious arthritis, systemic rheumatic arthritis (e.g. sarcoidosis) and inflammatory osteoarthritis. Each condition shows unique imaging characteristics, which are crucial for an accurate diagnosis.

Imaging findings or procedure details: PsA often shows a combination of osteo-proliferative and osteo-destructive changes and favors the distal interphalangeal joints. Crystalline arthropathies like gout and pseudogout involve para- and intra-articular tissue and show different patterns of crystal deposition. Systemic rheumatic diseases present with a spectrum of joint and soft tissue abnormalities, often requiring MRI for detailed assessment. Infectious arthritides such as septic arthritis can exhibit rapid joint destruction, but certain entities demonstrate slow smoldering disease courses. Here, MRI plays an important role in the early stages of diagnosis when plain radiographs may remain negative. Central erosions and osteophyte formation in the interphalangeal joints characterize erosive osteoarthritis.

Conclusion: Differentiating RA from other arthropathies in the wrist and hand is crucial for suitable treatment and to minimize long term sequelae. Radiological evaluation plays a central role in this differentiation. Recognizing the specific imaging features of each condition allows the initiating of a targeted therapy, thus improving patient outcome.

Flexor retinaculum injury: an overlooked diagnosis yet easy on standard ankle MRI

S. Richard, M. Nguyen; RHNe – Réseau Hospitalier Neuchâtelois, Neuchâtel, Switzerland

Learning objectives: Learn the normal anatomy and imaging appearance of the flexor retinaculum. Recognize flexor retinaculum injuries using MRI.

Background: The flexor retinaculum extends to the periosteum of the medial malleolus and to the origin of the superficial deltoid ligament, collectively forming the "fascial sleeve of the medial malleolus". It provides dynamic stability and smooth gliding surface during ankle joint movements, retaining and protecting tendons, nerves and vessels as they pass through the tarsal tunnel. Due to their connections, the flexor retinaculum injuries are often associated with tears of the origin of the superficial deltoid ligament and can be overlooked on MRI.

Imaging findings or procedure details: The normal flexor retinaculum is visible on MRI as a thin and regular fibrous band attaching tightly on the periosteum of the medial malleolus.

A spectrum of injuries can be seen, from subtle thickening of the attachment of the flexor retinaculum to the complete detachment of the flexor retinaculum, superficial deltoid ligament and medial malleolus periosteum, leading to tibialis posterior dislocation. Any fluid signal depicted on a fluid-sensitive sequence axial plane between the attachment of the flexor retinaculum and the periosteum of the medial malleolus is considered pathological.

Conclusion: This poster serves as a resource for understanding and identifying retinaculum flexor injuries in the ankle. We highlight the importance of specific anatomical knowledge and emphasize the utility of fluid-sensitive sequence axial plane in standard MRI protocols for accurate diagnosis.

Performance of Ultra-Low Dose CT in confirmed T1-Tumors of the Lung: Evaluation of Virtual Ultra-Low Dose CT Protocols

A. Peters[1], *J. Munz*[1], *J. Klaus*[1], *A. Macek*[1], *A. Huber*[1], *N. Alsaihati*[2], *E. Samei*[2], *W. Valenzuela*[1], *A. Christe*[1], *J. Heverhagen*[1], *J. Solomon*[2], *L. Ebner*[1];
[1] *Inselspital – Universitätsspital Bern, Bern, Switzerland,* [2] *Duke University Medical Center, Carl E. Ravin Advanced Imaging Laboratories, Durham, United States*

Purpose: To determine the diagnostic performance of simulated reduced-dose chest CT scans regarding pulmonary T1 tumors and assess the potential impact on patient management.

Methods and Materials: A repository containing 218 patients with histologically proven pulmonary T1 tumors was the primary database. Virtual reduced-dose images were created simulating 50%-, 25%-, 10%- and 5%-dose levels. In a pilot study, the differences in signal-to-noise ratio and contrast-to-noise ratio between the different dose levels were elaborated. Size category, tumor attenuation and localization were scored by two experienced chest radiologists. The impact on patient management was assessed by comparing the hypothetical LungRADS scores of the simulations.

Results: In total, 210 patients (41% females, mean age 64.5 ± 9.2 years) with 250 T1 tumors could be included into the study. Following the results of the pilot study, the 10%- and 50%-dose simulations were excluded from further analysis. There were no differences between the original dose and the 25%-dose simulations regarding any endpoint. The sensitivity of reader 1 was significantly lower using the 5%-dose vs. 25%-dose vs. original dose for size categorization (0.80 vs. 0.85 vs. 0.84; p=0.007) and segmental localization (0.81 vs. 0.86 vs. 0.83; p=0.018). The sensitivity of reader 2 was not affected by dose reduction for any endpoint. There were differences in the LungRADS scores between the simulations; there was no clear tendency towards malignancy risk over- or underestimation.

Conclusion: CT dose reduction may affect the correct categorization and localization of pulmonary T1 tumors and has a potential impact on patient management.

A Radiomics-based approach for predicting EGFR- and ALK-mutational status in advanced NSCLC

T.L Ngo[1,2], *C. Heidt*[1,2], *J. Kroschke*[3,1,2], *O. von Stackelberg*[1,2], *J. Bohn*[4], *T. Nonnenmacher*[1,2], *P. Christopoulos*[5,2], *C.P. Heußel*[6,2], *H-U. Kauczor*[6,2];
[1] *Universitätsklinikum Heidelberg, Department of Diagnostic and Interventional Radiology, Heidelberg, Germany,* [2] *TLRC – Translational Lung Research Center Heidelberg, DZL – German Center for Lung Research, Heidelberg, Germany,* [3] *Spital Thurgau AG, Institute for Radiology, Münsterlingen, Switzerland,* [4] *DKFZ – German Cancer Research Center, Department of Medical Imaging Computing, Heidelberg, Germany,* [5] *Universitätsklinikum Heidelberg, Department of Thoracic Oncology, Thoraxklinik and National Center for Tumor Diseases (NCT), Heidelberg, Germany,* [6] *Universitätsklinikum Heidelberg, Department of Diagnostic and Interventional Radiology with Nuclear Medicine, Heidelberg, Germany*

Purpose: Several studies have shown that the use of radiomics-based approaches could be feasible in predicting the mutational status in non-small cell lung cancer (NSCLC). Radiomics, the analysis of imaging data using classification algorithms, has been used for the identification of imaging biomarkers in different settings, however, in advanced lung cancer its use has been limited. In NSCLC patients, identifying tumor mutational status is crucial for individual targeted treatment. Tumor heterogeneity, especially in advanced NSCLC cases, reduces the validity of conventional biopsy methods. This study aims to build predictive radiomics models to assess for EGFR- or ALK-mutational status in advanced NSCLC compared to "wildtype" tumors as a basis for future development of a "virtual biopsy" model.

Methods and Materials: This study included 392 patients with NSCLC, carrying EGFR (n=268), ALK (n=47) or no known tumor mutation (="wildtype", n=77). Radiomics features were extracted from CT images, together with clinical features and trained using Random Forest, XGBoost and SVM algorithms to predict tumor mutational status.

Results: The classification models had AUC values ranging from 0,49 to 0,77 when implementing radiomics features only. When implementing clinical data in addition to radiomics features, the AUC values ranged from 0,53 to 0,78.

Conclusion: In this pilot study, a solely image based Radiomics-approach for prediction of tumor mutational status in advanced NSCLC did not yield convincing results as proposed by previous studies, possibly due to the sometimes complex tumor anatomy with difficulties in discriminating tumor volume from adjacent/infiltrated structures. However, an improvement in classification performance was observed by implementing clinical data into the model building as a multiparametric approach. Further studies using large, multicenter-multiparameter datasets are required to investigate and improve the robustness of imaging biomarkers.

Mosaic attenuation patterns on CT-scan

C. Bettaieb, R. Troxler, D. Rotzinger, G. Fahrni; CHUV – Centre Hospitalier Universitaire Vaudois, Lausanne, Switzerland

Learning objectives:
- To give the radiologist the means to distinguish abnormal white or black lung in mosaic attenuation
- To provide an overview of mosaic attenuation patterns and their etiologies
- To help distinguish them and set up a decisional tree
- To raise awareness of common diagnostic traps and emphasize the importance of making the difference between subgroups

Background: Mosaic attenuation results from an imbalance of attenuation components, generating a patchwork of hyper and hypodense parenchymal areas.

We identify three distinct entities associated with different pathophysiology, etiology, and semiology. Major patterns include mosaic perfusion from vascular or bronchiolar causes, patchy ground-glass changes, and mixed causes (three-density pattern).

This educational poster aims to describe the different mosaic attenuation patterns, underlying pathophysiology and related differential diagnoses while focusing on tools supporting radiologists in distinguishing them.

Imaging findings or procedure details: We will expose and discuss the method to distinguish between hyper or hypodense lung parenchyma abnormality based on the size and uniformity of vessels.

We will discuss the different hyperattenuating components, (microcirculation, interstitium, alveoli) and hypoattenuating components (air or vasoconstriction).

We will discuss three groups of mosaic attenuation patterns: mosaic perfusion of vascular or bronchiolar origin, mosaic ground-glass, and mixed causes called "three density pattern".

We will propose a strategy to distinguish the different patterns and avoid falling into diagnostic traps, discuss each subgroup's semiology and differential diagnoses.

Multiple cases illustrate each pattern. Diagnoses are summed up in a table.

Conclusion: Mosaic attenuation includes different patterns with many differential diagnoses. This poster will help radiologists to distinguish between them and to be able to make a relevant diagnosis for the patient.

Chronic thromboembolic pulmonary hypertension (CTEPH) and its CT diagnosis

N. Al Amar, G. Fahrni, D. Rotzinger; CHUV – Centre Hospitalier Universitaire Vaudois, Lausanne, Switzerland

Learning objectives:
- Remind the definition of pulmonary hypertension (PH), and focusing on the pathophysiology, the diagnostic evaluation and the treatment of CTEPH, which is the only potentially curable form of PH.
- To gather and explain the radiologic signs of PH and especially to distinguish the signs that are specific to CTEPH on CT scan.

Background: PH definition has recently been updated in 2022, and is now defined as as an elevated mean pulmonary pressure higher than 20mmHg at rest. Imaging helps to confirm PH and identify the cause, especially to distinguish between pre and post capillary PH. CTEPH is due to an incomplete resolution of pulmonary emboli for unclear reasons, still this is the only curable form with better outcome when diagnosed early.

Thus, it is important for radiologists to recognize CTEPH specific signs on CT. Plus, CT pulmonary angiography is capital to predict the responsiveness to thromboendarteriectomy, main treatment of CTEPH.

The aim of this educational poster is to gather PH signs on CT and emphasize the ones that help distinguish CTEPH, through illustrations and explanations.

Imaging findings or procedure details: We discuss first non specifics signs of PH, for example: enlargement of the main pulmonary artery, ratio hypertrophy, tortuous and wall calcification of pulmonary vessels.

Then, we show the specific or more frequent signs of CTEPH, divided into vascular signs (complete obstruction of pulmonary arteries and their dilatation post stenosis, partial filling defects due to chronic thrombi, collateral systemic supply, perfusion defects (on available spectral CT)) and parenchymal signs (scars of old pulmonary infarcts, mosaic pattern, air trapping signs, cylindrical bronchial airway dilatation).

Conclusion: There are many signs of PH, that can be identified on a CT scan, some of them are specific or more frequent in CTEPH, the only potentially curable form. Therefore, being able to recognize them is critical. This poster helps radiologists to understand changes related to PH and to distinguish those due to CTEPH.

Cystic Lung Disease: Diagnostic Approach and Imaging Findings

A. Touray, R. Troxler, C. Pozzessere, D.C. Rotzinger, G. Fahrni; CHUV – Centre Hospitalier Universitaire Vaudois, Lausanne, Switzerland

Learning objectives:
· Distinguish true lung cysts from their mimics.
· Provide a stepwise approach to pulmonary cystic syndromes.
· Emphasize the importance of considering clinical context for improved diagnostic accuracy.

Background: Cystic lung disease (CLD) refers to a heterogenous group of congenital or acquired lung disorders characterized by the presence of multiple air-filled lucencies surrounded by thin walls. Because of the widespread use of high-resolution computed tomography (HRCT), they are increasingly identified and represent a considerable diagnostic challenge for radiologists. However, a stepwise approach using HRCT combined with knowledge of patients' history can lead to a rightful diagnosis in a majority of cases.

Imaging findings or procedure details: Our aim is to present HRCT diagnostic findings and features of CLD and their main mimics. We will mainly discuss pulmonary Langerhans cell histiocytosis (PLCH), lymphangioleiomyomatosis (LAM), Birt-Hogg-Dubé syndrome (BHD), lymphocytic interstitial pneumonia (LIP), and light chain deposition disease (LCCD). Congenital cysts, including cystic adenomatoid malformation (CAM), are part of the imaging spectrum but will not be discussed in detail. For each diagnosis, we will provide a brief summary of main discriminating features and clinical information that can help reaching an accurate diagnosis. Furthermore, each pathology will be illustrated by a typical case. Radiologic features and clinical context will be summarized in a didactic differential diagnosis table.

Conclusion: HRCT stands as a noninvasive diagnostic tool for evaluating diffuse CLD. A stepwise approach combining HRCT with patients' history facilitates accurate diagnoses, potentially obviating the need for invasive procedures like surgical lung biopsy. Radiologists should know how to approach cystic structures using radiologic features and clinical information when available. Employing a systematic approach provides a straightforward means to achieve precise diagnosis, which is pivotal for optimal patient management.

False negative and false positive cases after implementation of an automated breast ultrasound system for breast cancer screening in an academic radiology department: A retrospective study in 1219 women

E. Nikolova, J. Weber, G. Zanetti, J. Wieler, T. Frauenfelder, M. Marcon; USZ – Universitätsspital Zürich, Zurich, Switzerland

Purpose: To investigate the false positive(FP) and false negative(FN) rate over 3 years after implementation of an automated breast ultrasound (ABUS) system.

Methods and Materials: : In this IRB-approved retrospective study all women undergoing ABUS examination in our department between Oct2015-Oct2018 have been revised (total 1995 women; mean age ±SD,48.9±13 years). We included all women who have undergone a follow-up of at least 24 months after ABUS examination or with BI-RADS category 4 or 5, who have undergone histological evaluation.FP cases were defined as cases classified BI-RADS 3,4 or 5 in ABUS who have shown to be benign lesions during follow-up or after biopsy.FN cases were defined as all cases of cancer diagnosed during follow-up and that were retrospectively already visible in the ABUS examination.Descriptive statistics was used

Results: 1219 women (51.9±11.0 years) were included and classification after ABUS examination was: BI-RADS 1 n=136 (11.1%), BI-RADS 2 n=890 (73.0%), BI-RADS 3 n=161 (13.2%), BI-RADS 4 n=15 (1.2%) and BI-RADS 5 n=17 (1.4%). Patients had a mean follow-up ±SD of 54.3±16.7 months. A woman was diagnosed with an invasive carcinoma 14 months and another 24 months after ABUS examination classified BI-RADS 2; both lesions were already visible in previous ABUS and mammography and the "retraction phenomenon sign"was visible in the ABUS-coronal reconstruction. A malignancy was also diagnosed in 3/161 (1.9%) BI-RADS 3 lesions, 7/15 (46.6%) BI-RADS 4 lesions and 17/17 lesions (100%) BI-RADS 5. The FN rate was 6.9% (2/29 cases). The FP rate was 13.9% (166/1190 cases). Among the 14 malignant lesions, in one case the lesion was only visible in ABUS and not in mammography (7.1%); in 3 cases lesion was visible in both but multifocality only in ABUS (21.4%)

Conclusion: We found a FN rate of 6.9% and a FP rate of 13.9%. To avoid false negative cases ABUS coronal reconstruction should be accurately evaluated

Prevalence of extremely dense breasts in women in screening age in Switzerland: Preliminary results of a single center experience

A. Vitorio Kaiser[1], D. Zanolin-Purin[1], N. Chuck[2], D. Wruk[2]; [1] UFL – Private University in the Principality of Liechtenstein, Triesen, Liechtenstein, [2] KSSG – Kantonsspital St. Gallen, Netzwerk Radiologie, St. Gallen, Switzerland

Purpose: To determine the prevalence of mammographic extremely dense breasts in a cohort of women in breast screening age.

Methods and Materials: Retrospective analysis was conducted of consecutive mammographic images from women aged between 50 years and 69 years old, who underwent a diagnostic mammography exam and opportunistic mammography screening at the Breast Centre facility in the east of Switzerland, from January 1th 2009 to May 31th 2014. A commercial software (b-box by b-rayZ v 1.1.0) analyzed the mammography images and assigned the breast density in compliance with the ACR BIRADS 5th edition. This study was approved by the Ethics Committee. Descriptive statistics were used to summarize and describe the variables for the sample of categorical data. P-values < 0.05 were considered statistically significant and reported as a two-sided confidence interval. The Strengthening the Reporting of Observational Studies in Epidemiology (STROBE) Guidelines were used to report this study.

Results: A total of 2810 mammography examinations from women aged 50 to 69 years old (59 ± 5.6 years) were included in this study. Overall, the prevalence of extremely breast density category was 20%. The prevalence of extremely dense breasts depended on the age. For women aged between 50 and 69 years old, the prevalence of extremely breast density category decreased significantly from 31.5% to 12.3% respectively (p≤0.001).

Conclusion: The preliminary results presented in this study showed a prevalence of 20% extremely dense breasts in women at the screening age of 50 to 69 years in the evaluated local population and a significant dependency on the distribution from the age of the population. Those findings could be used to help planing the allocation of human and financial resources to cover supplemental screening in women with extremely dense breasts and a higher risk of developing breast cancer.

Potential of non-contrast breast dedicated CT to exploit lesion density and favor breast cancer detection: a proof-of-concept study

J.K. Weber, G. Zanetti, E. Nikolova, T. Frauenfelder, M. Marcon, J. Wieler; USZ – Universitätsspital Zürich, Zurich, Switzerland

Purpose: To investigate the potential of non-contrast breast dedicated CT (BCT) to exploit lesion density and favor breast cancer detection.

Methods and Materials: In this IRB-approved prospective study we consecutively included all women undergoing BCT examination between April 2023 and October 2023 with: histologically proved breast cancer; fibroadenoma with histologic confirmation or stable size > 24 months retrospective; cysts > 10 mm with ultrasound correlation and clearly detectable in BCT; and women with extremely dense breast tissue (EDBT) and no sonographic findings. Three regions of interest (ROIs) were placed on three different slices of each lesion and 3 different area of the breast in women with EDBT. Evaluation was performed independently by two readers with different level of breast imaging experience (more than 4 years and 3 months). Kruskal-Wallis test and intraclass correlation (ICC) were used. A p-value of <0.01 was considered statistically significant.

Results: 10 malignant lesions (median diameter 13.5 mm, IQR 9.2-17.5 mm), 6 fibroadenoma (10 mm, IQR 10-13.7 mm), 4 cysts (11 mm, IQR 10-12.5 mm) and 9 women with EDBT (median ROI 10 mm, IQR 10-12 mm) were included. Density of malignant lesion (61,7 HU, IQR 54.9-69.7) was significantly higher than EDBT (32 HU, IQR 28.2-34.2) (p<.001). There was no statistically significant difference between density of fibroadenoma (43 HU, IQR 38.5-54.5) and cysts (40.7 HU, IQR 31.3-46.8) (p=.254) or glandular tissue (p=.007) as well as between fibroadenoma, cysts and malignant lesions (p=.031 and p=.002, respectively). The agreement between the two readers was almost perfect (ICC 0.961, p<.001).

Conclusion: Malignant lesions are more dense than glandular tissue whereas benign lesions show similar density, therefore non-contrast BCT has potential for breast cancer detection in women with dense breast tissue.

Wire preoperative ultrasound localization of clip-marked axillary lymph nodes in breast cancer: Does the delay between localization and intervention influence the success rate of lymph nodes excision?

I. Holzmann[1], *A. Astarita*[2,3], *R. Hajri*[1,4], *E. Tenisch*[4], *D. Hastir*[4,5], *L. Lelièvre*[4,6], *J-Y. Meuwly*[4]; [1] *UNIL – University of Lausanne, Lausanne, Switzerland,* [2] *HUG – Hôpitaux universitaires de Genève, Lausanne, Switzerland,* [3] *CHUV – Centre Hospitalier Universitaire Vaudois, Department of Radiology, Lausanne, Switzerland,* [4] *CHUV – Centre Hospitalier Universitaire Vaudois, Lausanne, Switzerland,* [5] *CHUV – Centre Hospitalier Universitaire Vaudois, Department of Pathology, Lausanne, Switzerland,* [6] *CHUV – Centre Hospitalier Universitaire Vaudois, Department of Gynecology, Lausanne, Switzerland*

Purpose: Breast cancer is the most common malignancy in women. The presence of metastatic lymphadenopathy in the axillary fossa is an important prognostic factor in deciding on locoregional or systemic therapy. In case of positive axillary fossa, neoadjuvant chemotherapy (NACT) can make axillary metastases disappear in 40% to 75% of cases. This success has challenged traditional management that required axillary dissection (ALND), and its replacement with a targeted exploration of the axilla (TAD). One of the key points of TAD is therefore the identification of the biopsied lymph node before the onset of NACT. The aim of this retrospective work was to determine the success rate of the excision of the clipped node, measure the time delay between the wire localization and intervention, and to identify the causes of possible failures.

Methods and Materials: We performed a retrospective analysis of cases of preoperative axillary lymph node wire localization from January 2020 to September 2023. In order to observe an eventual displacement of the wire, the cases of lymph node wire localization without clip were also included. The presence of the targeted lymph node in the resected material was observed. We measured the time delay between the localization and the intervention.

Results: Eighty-one patients were included, with a median age of 51 years old (range 26-90). Eighty-four lymph nodes were localized, seventy with a clip, fourteen without clip. The median time delay between the localization and excision was one day, three hours and 20 minutes (range 4 h-2 days, 4 hours and 45 minutes). Eighty-tree targeted nodes were present in the resected material (98.8%).

Conclusion: The localization of the axillary lymph node with a wire made it possible to find it with almost 100% success. The time delay between the localization and the excision has no influence on the success of the procedure.

Accuracy of artificial intelligence (AI) for detection and BIRADS characterization of mass lesions on digital mammography (DM) compared to radiologists

S.C. Sautter[1], *S. Kyathanahally*[2], *C. Ruppert*[2], *A. Ciritsis*[2], *M. Meier*[2], *J. Roos*[3], *A. Boss*[4], *S. Schrading*[3]; [1] *LUKS – Luzerner Kantonsspital, Lucerne, Switzerland,* [2] *USZ – Universitätsspital Zürich, Zurich, Switzerland,* [3] *LUKS – Luzerner Kantonsspital, Department of Radiology, Lucerne, Switzerland,* [4] *GZO – Spital Wetzikon, Wetzikon, Switzerland*

Purpose: In this prospective observational study, the performance of an AI model in the detection of breast mass lesions and categorization into BIRADS categories on DM was compared to different general radiologists. While the use of AI has been thoroughly evaluated for calcifications on DM, there are only few studies assessing its performance for mass lesions. As the employment of AI in mass lesion detection is significantly more demanding, especially in low contrast lesions, technical improvements in AI methods are necessary to achieve adequate accuracy of AI.

Methods and Materials: The dataset consisted of 5978 images, from multiple centers and public repositories. It served to train and validate the YOLO (You Only Look Once) model, for AI-based mass lesion detection. After training, the AI model and three radiologists with 3, 8 and 17 years of experience in reading DM, evaluated independently the same clinical DM cases. All readers marked any mass lesion in the DM and classified these according to BIRADS. BIRADS 2 and 3 were considered as benign, BIRADS 4 and 5 malignant. Additionally, BIRADS 3, 4, and 5 were classified as suspicious, BIRADS 2 as unsuspicious. The evaluation metrics focused on combining sensitivity and specificity in f1-score to determine malignancy and suspicion.

Results: The AI YOLO model achieved f1-scores of 0.48 (sensitivity 0.65, specificity 0.71) for detecting malignant, and 0.56 (0.58 and 0.74) for suspicious mass lesions. In comparison, depending on their level of experience, radiologists reached f1-scores of 0.55-0.68 (0.6-0.65 and 0.75-0.9) for malignant, and 0.48-0.68 (0.5-0.75 and 0.42-0.72) for suspicious mass lesions compared to the reference standard.

Conclusion: The trained YOLO model demonstrated comparable performance to experienced, as well as less experienced breast radiologists in detecting benign and malignant breast mass lesions.

Assessment of Histopathological Correlation between Two Synchronous, Ipsilateral Groups of Calcifications in light of Imaging Features

C. Theodoropoulos, A. Triantafyllou, A. Marneri, D. Koulocheri, G. Skountzos, M. Alafaki, G. Zografos, N. Michalopoulos; Hippokration Hospital, Athens, Greece

Purpose: To inquire whether mammographic features of synchronous, ipsilateral, suspicious microcalcification groups correlate with their pathological diagnosis.

Methods and Materials: This is a retrospective analysis of prospectively collected data regarding 82 patients who underwent stereotactic breast biopsy of two distinct groups of suspicious calcifications in the same breast during a single biopsy session. Digital mammograms were examined and radiologic findings were assessed with regard to pathology results.

Results: Most patients (59.8%) were diagnosed with benign lesions, whereas invasive carcinoma was found in 11 women (13.4%). Mammographic lesions were classified as BI-RADS 4 or 5, the majority of them being BI-RADS 4a (77.4%). The average in-between distance for the target pairs was 46.2 ±20.5 mm (range 20 – 130). Histopathological concordance of the two targets regarding disorder's biological behavior (benign or malignant) was found in 71 cases (86.6%). A significant (p=0.003) regression equation was found according to which concordance probability rate decreases by 0.6% for each millimeter increase in the distance between the mammographic targets assessed. Hormone receptor (ER, PR) and HER2/neu status demonstrated very high concordance levels among patients diagnosed with two carcinomas.

Conclusion: Our findings support that histopathological agreement between two distinct, mammographic findings (e.g. calcifications) correlates with their relative distance. When biological behavior is considered, a concordance rate greater than 90% is to be expected for in-between distances less than 31mm.

B3 lesions treated with vacuum-assisted excision (VAE): A systematic review and meta-analysis

A. Cozzi[1], M. Cao[2], N. Sharma[3], F. Del Grande[1,4], S. Schiaffino[1]; [1] EOC – Ente Ospedaliero Cantonale, IIMSI – Imaging Institute of Southern Switzerland, Lugano, Switzerland, [2] Università degli Studi di Milano Statale, Milan, Italy, [3] Leeds Teaching Hospitals NHS Trust, Leeds, United Kingdom, [4] USI – Università della Svizzera Italiana, Facoltà di Scienze Biomediche, Lugano, Switzerland

Purpose: To perform a systematic review and meta-analysis of the upgrade rates to malignancy and the surgical excision rates of B3 lesions treated with vacuum-assisted excision (VAE) after core-needle biopsy (CNB), also analyzing the procedural complication rate of VAE.

Methods and Materials: After protocol registration on PROSPERO (CRD42023396663), PubMed and EMBASE were searched for articles published up to 15/04/2023 reporting the use of VAE on B3 lesions diagnosed at CNB, taking surgical pathology and/or follow-up as reference standard. Three readers independently performed article selection and extracted data for the following endpoints: immediate upgrade rate, rate of complications, rates of immediate and long-term surgical excision, upgrade rates after immediate surgical excision and during follow-up. Random-effects meta-analyses of single proportions were performed for each endpoint.

Results: Sixteen studies (3941 patients, 3975 VAE procedures) from 6 countries, published between 2008 and 2023, were included in quantitative synthesis. The summary immediate upgrade rate at VAE was 4.0% (95% CI 1.4–7.6%). A total of 81 complications were found among 854 patients and the overall summary complication rate was 6.6% (95% CI 1.3–14.6%): 79 (97.5%) were minor complications whereas only 2 (2.5%) were major complications. Immediate surgical excision was performed in 214 cases, with a 1.5% immediate surgical excision summary rate (95% CI 0.1–3.6%) and a corresponding 25.4% summary upgrade rate (95% CI 11.0–42.4%). Among 1375 patients in follow-up, surgical excision was performed in 39 cases, with a 1.4% summary rate of surgical excision during follow-up (95% CI 0.1–3.4%) and a summary upgrade rate during follow-up of 0.01% (95% CI 0.0–0.6%).

Conclusion: VAE of B3 lesions has low rates of procedural complications and of immediate upgrade after VAE, with similar rates of immediate and long-term surgical excision, highlighting its promising role as first-line treatment of B3 lesions.

Breast ultrasound: key elements in performing, interpreting and reporting

W. Santner[1], B. Amort[2], M. Daniaux[2]; [1] Radiologie Südost, Team Radiologie Plus, Chur, Switzerland, [2] Tirol Kliniken, Innsbruck, Austria

Learning objectives: Understanding the important indications, appropriate positioning of the patient, accurate coupling and guidance of the transducer, the required examination procedures, precise lesion localization, and comprehensive description of focal findings. The learning objectives correspond to the SGUM/ÖGUM/DEGUM guidelines.

Background: Ultrasound is a crucial diagnostic tool for detecting and interpreting breast abnormalities in both screening and routine clinical work-up, following mammography. Its significance to the medical field is paramount, reiterated by its widespread use and scientific endorsement.

Imaging findings or procedure details: Example images showing the positioning of the patient, successful transfer of mammography findings to ultrasound localisation, and typical image features of benign and malignant findings in B-mode, Doppler-ultrasound, and Elastography are presented.

Conclusion: Knowing how to perform and interpret ultrasound is important in diagnosing breast lesions as either benign or malignant, ultimately leading to improved early detection of breast cancer.

Solid components in ovarian cysts – to worry or not to worry?

C. Chong, N. Nini, M. Amini, M.V. Fortier; KK Women's and Children's Hospital, Singapore, Singapore

Learning objectives: To demonstrate ultrasound features useful in distinguishing benign from malignant ovarian cysts. To outline the strengths and limitations of ultrasound in the diagnosis of ovarian tumors.

Background: Ovarian cysts in both pre- and post-menopausal women may represent benign or malignant tumours. On ultrasound, one of the key imaging features is to detect and characterise solid components within the cyst. Despite technological advancements in ultrasound, determining whether a solid component within an ovarian cyst represents malignancy remains challenging. In many cases ultrasound assessment is inconclusive necessitating further evaluation with MRI and clinical correlation with tumor markers such as CA-125.

Imaging findings or procedure details: A wide spectrum of ovarian cysts with solid components in both pre- and post-menopausal women is reviewed. Using the ACR O-RADS US lexicon, the cysts with solid components were pre-operatively classified from Categories 1 to 5. The corresponding MRI findings were also evaluated. Histopathological confirmation was achieved in all of Categories 4 and 5 cases. We also highlight those ovarian cysts that were pre-operatively assessed as likely malignant (Categories 4-5) but histologically proven to be otherwise thus exemplifying the limitations of ultrasound.

Conclusion: Ultrasound plays a pivotal role in the evaluation of ovarian cysts. We will delineate those sonographic features that help distinguish benign from malignant cysts. However, radiologists and sonographers should be aware of the limitations of ultrasound and know when to suspect malignancy.

Comparison of Late Gadolinium Enhancement Assessment Techniques for Monitoring Fibrotic Transformation After Acute Myocarditis

M. Károlyi[1], M. Polacin[1], J.M. Sokolska[1,2], I. Matziris[1], L. Weber[3], H. Alkadhi[1], R. Manka[1]; [1] USZ – Universitätsspital Zürich, Zurich, Switzerland, [2] Wroclaw Medical University, Wroclaw, Poland, [3] KSW – Kantonsspital Winterthur, Winterthur, Switzerland

Purpose: Persistent late gadolinium enhancement (LGE) after acute myocarditis is associated with myocardial fibrosis and adverse outcomes. However, there is no consensus on the optimal LGE follow-up technique post-myocarditis in cardiac magnetic resonance imaging (CMR). We compared the reproducibility and interrelationships of LGE assessment methods for monitoring fibrotic changes post-myocarditis.

Methods and Materials: Patients with acute myocarditis underwent baseline and 3-month follow-up CMR. LGE extent was assessed with common quantitative techniques (FWHM, SD5, SD6, VAT, FM) and semi-quantitatively with visual-presence-score (VPS) and visual-transmurality-score (VCS) at baseline and at follow-up. In addition, we directly compared the two CMRs using a simplified visual-score (VCS). Reproducibility was evaluated using the Intra-class Correlation Coefficient (ICC), and methods were compared with Spearman's correlation.

Results: 47 patients met inclusion criteria. LGE extent (%) at baseline and follow-up differed among quantitative techniques ($p<0.01$). The proportion of patients with LGE changes varied among techniques (FWHM: 62%, SD5: 74%, SD6: 66%, VAT: 43%, FM: 60%, VPS: 53%, VTS: 77%, VCS: 89%). Reproducibility was highest with FWHM (ICC: 0.97) and lowest with SD5 (ICC: 0.89). Slightly lower values were observed for semi-quantitative scoring (VPS ICC: 0.81, VTS ICC: 0.71). Reproducibility of VCS was excellent (ICC: 0.93). VPS and VTS correlated with quantitative LGE techniques (r between 0.31-0.73, $p<0.05$ all). VCS was positively associated with VPS (r=0.68), VTS (r=0.60), VAT (r=0.35), and FM (r=0.03) ($p<0.05$ all), but not with FHWM, SD5, and SD6.

Conclusion: FWHM is least observer-dependent for LGE change evaluation in myocarditis follow-up. VPS and VTS, along with VCS, offer reliable alternatives for assessing LGE alterations in longitudinal myocarditis studies. Categorizing patients with stable or changing LGE is technique-dependent and warrants further evaluation in prognostic investigations.

Virtual Calcium Removal in Calcified Coronary Arteries with Photon-Counting Detector CT

V. Mergen[1], S. Rusek[2], F. Civaia[2], R. Rajagopal[1,3], E. Bättig[1,4], R. Manka[1,5], A. Candreva[5], M. Eberhard[1,6], H. Alkadhi[1]; [1] USZ – Universitätsspital Zürich, Department of Diagnostic and Interventional Radiology, Zurich, Switzerland, [2] Monaco Cardiothoracic Center, Monaco, Monaco, [3] All India Institute of Medical Sciences, Department of Diagnostic and Interventional Radiology, Jodhpur, India, [4] La Fe – Hospital Universitari i Politècnic, Department of Radiology, Valencia, Spain, [5] USZ – Universitätsspital Zürich, Department of Cardiology, University Heart Center, Zurich, Switzerland, [6] Spitäler fmi AG – Spital Interlaken, Department of Radiology, Unterseen, Switzerland

Purpose: To evaluate, in patients with known or suspected coronary artery disease, the feasibility and accuracy of quantification of calcified coronary stenoses using virtual non-calcium (VNCa) images in coronary CT angiography (CCTA) with photon-counting detector (PCD) CT compared with quantitative coronary angiography (QCA).

Methods and Materials: This retrospective, institutional-review board approved study included consecutive patients with calcified coronary artery plaques undergoing CCTA with PCD-CT and invasive coronary angiography between July and December 2022. Virtual monoenergetic images (VMI) and VNCa images were reconstructed. Diameter stenoses were quantified on VMI and VNCa images by two readers. 3D-QCA served as the standard of reference. Measurements were compared using Bland-Altman analyses, Wilcoxon tests, and intraclass correlation coefficients (ICC).

Results: Thirty patients (mean age, 64 years ± 8 [standard deviation]; 26 men) with 81 coronary stenoses from calcified plaques were included. Ten of the 81 stenoses (12%) had to be excluded because of erroneous plaque subtraction on VNCa images. Median diameter stenosis determined on 3D-QCA was 22% (interquartile range, 11-35%; total range, 4-88%). As compared with 3D-QCA, VMI overestimated diameter stenoses (mean differences -7%, $p<.001$, ICC:.84 and -10%, $p<.001$, ICC:.87 for reader 1 and 2, respectively), whereas VNCa images showed similar diameter stenoses (mean differences 1%, $p=.07$, ICC:.93 and 0%, $p=.68$, ICC:.94 for reader 1 and 2, respectively).

Conclusion: Preliminary evidence in mainly minimal to moderate stenoses suggests that virtual calcium removal in CCTA with PCD-CT, when feasible, has the potential to improve the quantification of calcified stenoses.

Automatic Segmentations of Cardiovascular Structures on Chest CT Data Sets: An Update of the TotalSegmentator

D. Hinck, M. Segeroth, J. Bremerich, J. Wasserthal, M. Pradella; USB – Universitätsspital Basel, Basel, Switzerland

Purpose: Regarding cardiovascular (CV) structures, segmentations play an important role in quantifying changes such as volume increase or in case of aneurysms diameter assessment. The TotalSegmentator is an open source, free-to-use deep learning (DL) tool, which provides segmentations of 104 structures on CT datasets including some CV structures. We intended to add new and enhance previously included CV structures.

Methods and Materials: Using the TotalSegmentator dataset of 1648 cases (training: 1502; validation: 57; testing: 89), segmentations were performed in a dedicated software (NORA Imaging) by a trainee supervised by a CV radiologist (6 years of experience). Two sets of segmentation tasks were performed: enhancement of previously included CV structures (aorta, left/right atrium (LA/RA), pulmonary trunk (PT), and central pulmonary arteries) and de-novo segmentations (superior vena cava (SVC), bilateral brachiocephalic veins (LBCV/RBCV), brachiocephalic trunk (BCT), bilateral subclavian (LSCA/RSCA) and common carotid arteries (LCCA/RCCA), left atrial appendage (LAA), right and left pulmonary veins (LPV/RPV, ostia till first branching)). For faster progress, we used an iterative learning approach: First, 20 cases were manually segmented to train a preliminary nnU-Net. Second, it was applied to 100 cases for correction, review and retraining. We repeated this approach for all 1502 training cases. To assess segmentation quality, we calculated the Dice similarity score (DICE) on the test dataset.

Results: The mean (±SD) DICE of all structures was 0.955±0.025. The DL tool achieved the best DICE result for the aorta (0.981±0.025), 2nd best RA (0.971±0.021) and 3rd LBCV (0.963±0.029). Lowest DICE were found in the RCCA (0.932±0.038), 2nd RBCV (0.935±0.057) and 3rd pulmonary veins (0.948±0.072).

Conclusion: TotalSegmentator has been enriched by robust and highly accurate segmentation of additional CV structures.

Stress-induced aortic hemodynamics by rapid 2D MR flow imaging using an in-house developed MR-compatible ergometer

N. L'Abate[1], F. Haupt[2], G. Cereghetti[1], A. Aksoez[3], A. Razmi[4], D. Becker[5], B. Jung[2], H. von Tengg-Kobligk[2]; [1] Inselspital – Universitätsspital Bern, Department of Diagnostic, Interventional and Pediatric Radiology, Bern, Switzerland, [2] Inselspital – Universitätsspital Bern, DIPR – Department of Diagnostic, Interventional and Pediatric Radiology, Bern, Switzerland, [3] HuCE – Institute for Human Centred Engineering, Department of Mechatronics and Systems Engineering School of Engineering and Information Technology, Bern, Switzerland, [4] Skan AG EPFL, Lausanne, Switzerland, [5] Inselspital – Universitätsspital Bern, Clinic of Vascular Surgery, Bern, Switzerland

Purpose: To investigate the feasibility of an MR-compatible ergometer for the application of exercise induced aortic wall and flow characteristics. Aim is to establish an MR setting for the abdominal aorta enabling the extraction of vascular parameters under stress-conditions, since resting conditions do not reflect potential risk conditions in aortic pathologies.Drug induced cardiac stress-MRI has been well established but the method has inherent limitations to assess the abdominal aorta and certain individuals could not be assessed.

Methods and Materials: 31 male participants (median age 67yrs) were analysed in a prospective study. MRI of the infrarenal aorta was performed using a clinical 3T scanner acquiring 2D flow at rest and immediately after exercise. Physical exercise was accomplished by an in-house developed MR compatible pneumatic stepper. Stress was applied in gradual increase up to 50% of the max. load capacity, which was previously determined during spiroergometry (gold standard). Peak flow (PF) was measured at both conditions. In addition, blood pressure (BP) and heart rate (HR) were measured before and during stress. Additional hemodynamic parameters like pulse wave velocity were extracted.

Results: Mean peak power of the ergometer was 172W (219W at Spiroergometrie). Mean HR was significantly higher after stress (66.0±11.2 vs 74.6±15.0 bpm,p=.001). BP was also significantly elevated after stress (90.2±10.8 vs 104.0±13.1 mmHg,p<.001). PF showed a significant increase (156.2±38.4 vs 179.2±55.2 ml/s,p=0.019).

Conclusion: Physical stress application using a hydraulic MR-compatible ergometer is feasible for studies of the abdominal aorta. We expect that MR protocol and exercise optimizations should be able to further increase the effect of the ergometer.

Automated versus Manual Planning of Cardiac MR Imaging: A Comparative Study

C. Glessgen, L. Crowe, J-P. Vallée, J-F. Deux; HUG – Hôpitaux universitaires de Genève, Geneva, Switzerland

Purpose: To evaluate the accuracy, robustness and impact on scanning times of a fully automatic AI-based software dedicated to the acquisition of cardiac MR (cMR) studies.

Methods and Materials: 48 patients (15 female, mean age 52.5y) were enrolled in this prospective study. 25 patients underwent an AI-planned cMR examination (AI Cardiac Scan Companion, Siemens Healthineers AG, Erlangen, Germany) and 23 patients a manually planned, standard cMR study, all on the same 1.5T MRI scanner. The same cMR protocol with contrast administration was used in both groups to warrant comparison. The number of planning errors and quality of cardiac plane placement (1-low to 5-excellent) were recorded by the supervising radiologist. Overall scan times, acquisition times and proportion of non-acquisition time (dead time) between sequences were also recorded.

Results: All examinations (48/48) were complete. There were fewer planning errors using the automatic scheme than the manual one (error per scan: 0.5 ± 0.8 vs. 1.2 ± 1.2, p<0.05, respectively) and similar quality of plane placement (4.4 ± 0.8 vs. 4.2 ± 0.9, p=0.45, respectively). Overall scan time was similar between automatic and manual acquisitions (40.2 ± 8.1 min vs. 43.2 ± 6.1 min, respectively, p=0.14). The proportion of dead time was lower in AI acquisitions compared to manual ones (0.44 ± 0.1 vs. 0.50 ± 0.1%, p<0.01, respectively). Of note, the AI software tended to plan more short-axis slices compared to manual positioning (15.9 ± 1.8 slices vs. 15.0 ± 1.4, p=0.07, respectively), despite similar patient size between groups.

Conclusion: PA fully automatic AI-based software was able to reliably plan cMR examinations. Less planning errors occurred in comparison to manual acquisitions, while both plane placement quality and acquisition times remained similar. Overall scan time remained similar despite a significantly reduced dead time in automatic examinations.

Occurrence of a transient interruption of contrast (TIC) in pulmonary CT angiography (CTPA): Assessment of patient characteristics and technical parameters with impact on the quality of CTPA

M. Frenzel[1], A. Spirig[1], A. Gutzeit[2], Z. Szucs-Farkas[3], T. Schnitzler[1], F. Burn[4], S. Schindera[1], H. Zaytoun[1]; [1] KSA – Kantonsspital Aarau, Department of Radiology, Aarau, Switzerland, [2] Kantonsspital Schaffhausen, Department of Radiology, Schaffhausen, Switzerland, [3] Spitalzentrum Biel – Centre hospitalier Bienne, Department of Radiology, Biel, Switzerland, [4] KSA – Kantonsspital Aarau, AI & Data Science CoE, Aarau, Switzerland

Purpose: This study aims to identify patient characteristics and technical parameters in patients who have a risk to develop transient interruption of contrast (TIC) in CTPA to identify patient groups needing protocol optimization.

Methods and Materials: This retrospective, monocentric, IRB-approved study included 1762 patients (18-97 years (y); mean 65.6 ± 15.9y) who underwent CTPA. The patients were separated in groups by age and BMI. Attenuation values, measured in Hounsfield units, were assessed at 5 locations in the central and peripheral pulmonary arteries, ascending aorta (AA) and superior vena cava (SVC) of each patient. Additional factors such as contrast medium reflux into the inferior vena cava/hepatic veins and cardiomegaly were extracted. A subjective quality assessment (QA) of pulmonary arteries (good, acceptable, not diagnostic) was made by two radiology residents (2 und 4y of experience). Respiratory motion artifact in the CTPA was also assessed by the QA. TIC was considered present when the density in the pulmonary trunk was less than in the AA and SVC. Measurements and factors were compared by using the Mann-Whitney U test (MWUT) and Spearman`s rank test (SRT).

Results: A total of 104 (5.9%) TIC cases were identified. Density in the pulmonary trunk and TIC occurrence was significantly associated with age and BMI groups (p < 0.05). Higher density and less TIC cases were observed in groups of patients with age > 70y and with BMI < 25 and accordingly lower vessel attenuation and more TIC cases in patients with age < 20y and BMI > 25. SRT (R: 0.116) and MWUT (U: 6114.5 and Z: -4.58) showed a significant correlation between a TIC and the QA (p < 0.001). 369 (20.9%) patients showed a respiratory motion artifact.

Conclusion: Age and BMI has a significant impact on the quality of CTPA and the occurrence of a TIC phenomenon. In individual cases, the improvement of CTPA quality can thus hopefully be achieved by optimizing the protocol accordingly and eventually using breathing maneuvers.

<div style="text-align: right">PO18</div>

Effect of Temporal Resolution on Calcium Scoring: Insights from Photon-Counting Detector CT

T. Sartoretti, V. Mergen, A. Dzaferi, R. Manka, H. Alkadhi, M. Eberhard;
USZ - Universitätsspital Zürich, Zurich, Switzerland

Purpose: To intra-individually investigate the variation of coronary artery calcium (CAC), aortic valve calcium (AVC), and mitral annular calcium (MAC) scores and the presence of blur artifacts as a function of temporal resolution in patients undergoing non-contrast cardiac CT on a dual-source photon counting detector (PCD) CT.

Methods and Materials: 70 patients (30 women, 40 men, mean age 78 ± 9 years) who underwent ECG-gated cardiac non-contrast CT with PCD-CT (gantry rotation time 0.25 s) prior to transcatheter aortic valve replacement were retrospectively included. Each scan was reconstructed at a temporal resolution of 66 ms using the dual-source information and at 125 ms using the single-source information. Average heart rate and heart rate variability were calculated from the recorded ECG. CAC, AVC, and MAC were quantified according to the Agatston method on both image types. Two readers assessed blur artifacts using a 4-point visual grading scale.

Results: Mean heart rate and heart rate variability during data acquisition were 76±17 beats per minute (bpm) and 4±6 bpm, respectively. CAC scores were smaller on 66 ms (median, 511; interquartile range, 220-978) than on 125 ms reconstructions (538; 203-1050, p<0.001). Median AVC scores [2809 (2009-3952) versus 3177 (2158-4273)] and median MAC scores [226 (0-1284) versus 251 (0-1574)] were also significantly smaller on 66ms than on 125ms reconstructions (p<0.001). Reclassification of CAC and AVC risk categories occurred in 4% and 11% of cases, respectively, whereby the risk category was always overestimated on 125ms reconstructions. Image blur artifacts were significantly less on 66ms as opposed to 125 ms reconstructions (p<0.001).

Conclusion: Intra-individual analyses indicate that temporal resolution significantly impacts on calcium scoring with cardiac CT, with CAC, MAC, and AVC being overestimated at lower temporal resolution because of increased motion artifacts eventually leading to an overestimation of patient risk.

<div style="text-align: right">PO19</div>

Validation of Splenic Switch-Off Against Fractional Flow Reserve for Assessing Stress Adequacy in Adenosine Stress CMR

M. Károlyi[1], S. Plein[2], I. Paetsch[3], C. Jahnke[3], M. Frick[4], H. Alkadhi[1],
S. Kozerke[5], R. Manka[1]; [1] USZ – Universitätsspital Zürich, Zurich,
Switzerland, [2]University of Leeds, Leeds, United Kingdom, [3] University of
Leipzig, Leipzig, Germany, [4] RWTH Uniklinik Aachen, Aachen, Germany,
[5] ETH – Center for Radiopharmaceutical Sciences, Paul Scherrer Institute,
Zurich, Switzerland

Purpose: Splenic switch-off (SSO) during cardiac magnetic resonance imaging (CMR) stress-perfusion with adenosine is often used as a quality marker for stress adequacy. Yet, the reliability of SSO against gold standard fractional flow reserve (FFR) remains unknown.

Methods and Materials: Patients with suspected coronary artery disease underwent 3D CMR stress-perfusion with adenosine and invasive coronary angiography with FFR. SSO was assessed visually. In addition, signal intensities (SI) of the spleen between rest and stress were compared, as SI_{SSO} (%) = $[(SI_{rest\ spleen} - SI_{test\ spleen}) - (SI_{stress\ spleen} - SI_{test\ spleen})]$ / $(SI_{rest\ spleen} - SI_{test\ spleen})$ * 100. The association between true negative and false negative CMR studies, and the presence or absence or SSO was tested with chi-square test. Receiver Operating Characteristic (ROC) analysis was used to assess the accuracy of SISSO to predict visual SSO and false negative CMR.

Results: 179 patients were included. SSO was present in 73% of the patients. SSO was more frequent in patients with true negative CMR, as compared to false negative CMR results (80.6% vs. 36.8%, p<0.001). In concordance, absent SSO was more frequent when CMR was false negative, as compared to true negative results (63.2% vs. 19.4%, p<0.001). ROC analysis AUC for SISSO for predicting SSO was 0.947 (95%CI: 0.915-0.980). AUC of SISSO for predicting false-negative CMR was 0.709 (95%CI: 0.593-0.826). Optimal SISSO cut-offs were ≥73.5% for SSO (Sensitivity: 82.9% and Specificity: 90.9%) and ≤68.6% for false-negative CMR (Sensitivity: 69.5% and Specificity: 72.2%).

Conclusion: Our study is the first to validate SSO against FFR for myocardial ischemia testing with CMR adenosine stress-perfusion. SSO effectively identifies patients with inadequate adenosine stress. Quantitative spleen signal intensity difference between rest and stress is a valuable predictor of visual SSO and false-negative CMR results.

<div style="text-align: right">PO20</div>

Complications following ECMO placement detected by imaging

G. Ilanjian, Z. Ltaief, A. Denys, K. Mandralis, S. Schmidt Kobbe;
CHUV – Centre Hospitalier Universitaire Vaudois, Lausanne, Switzerland

Learning objectives To discuss and demonstrate main cerebral and thoraco-abdominal complications occurring after ECMO placement and detected by imaging.

Background: ECMO provides cardio-respiratory support and is available in two main versions : veno-venous circuit (ECMO-VV) for severe respiratory failure, and arteriovenous circuit (ECMO-VA) in refractory cardiogenic shock, possibly accompanied by respiratory failure. The growing use of this device puts patients at high risk of complications, due to their frailty and the need to introduce anticoagulant therapy.

Imaging findings or procedure details: The main complications encountered following ECMO are hemorrhagic, thromboembolic, infectious, and iatrogenic.

Hemorrhagic complications are the most frequent and can have a multi-systemic effect, with an estimated incidence of intracranial bleeding of 3%, abdominal hemorrhage of 3% and thoracic hemorrhage of 14%.

Then, there are also thromboembolic complications, with an estimated 7% incidence of cerebral ischemic events, 7.5% of deep vein thrombosis, 2% of pulmonary embolism and 9% of ECMO cannula thrombosis. Moreover, infectious complications under ECMO, whether acquired or nosocomial, depend on the type of ECMO used, the duration of its use, and the presence or not of concomitant immunosuppression. These are, most frequently, ventilator associated pneumonia, bacteremia and ECMO cannula infections. Eventually, iatrogenic complications have an estimated of 10%, consisting mainly of cannulation site aneurysms/pseudo-aneurysms. Thus, radiology, particularly angio-CT, plays a major role in the search for complications, enabling us to assess their nature and degree of severity and to guide medical and surgical management.

Conclusion: Given the need for anticoagulation and the fragility of ECMO patients, the occurrence of complications is relatively frequent and often requires early management, which is why radiology plays a key role in detecting them.

PO80

Selective Internal Radiation Therapy: Main applications and importance of personalized dosimetry

G. Xhepa, A. Gleyzolle, J. Grossmann, P. Faerber, E. El Ghoul, J. Kohler, I. Constantinescu, A. Ricoeur; HUG – Hôpitaux universitaires de Genève, Geneva, Switzerland

Learning objectives To understand the application of Selective Internal Radiation Therapy (SIRT) in liver malignancies and metastases.
To understand the importance of the personalized dosimetry.
To recognize the importance of appropriate patient selection in order to achieve good clinical outcomes and reduce the complication rate.

Background: Liver malignancies and metastases pose significant risks to cancer patients, often precluding surgery. Selective Internal Radiation Therapy (SIRT) serve as local alternative therapies. SIRT, utilizing mainly yttrium-90 (Y90), delivers focalized radiation to tumors. However, understanding contraindications, and conducting arterial liver anatomy mapping using technetium-99m-labeled macroaggregated albumin (Tc-99m MAA), is crucial.

Imaging findings or procedure details: The rationale behind intra-arterial delivery of Y90 microspheres to hepatic tumors capitalizes on the tumors' predominant blood supply from the hepatic artery (90%). Once the Y90 microspheres are within the tumor's microvasculature, the emission of pure β-particles, with a limited tissue penetration of 2 to 3 mm, predominantly affects the tumor tissue. Evaluating eligibility for repeated radioembolization is essential after each treatment session. Pretreatment planning aims to reduce uncertainty in radiation dosimetry models and expected oncological outcomes. Angiographic evaluation aims for adequate catheter positioning to ensure optimal and reproducible microsphere delivery. Current practice uses Tc-99m MAA to predict distribution into the lesion. Pre-treatment 99mTc-MAA deposition activity predicts Y90 absorbed doses, leading to personalized dosimetry and optimized treatment planning.

Conclusion: This presentation aims to emphasize a careful patient selection, the importance of personalized dosimetry and a demonstration of the broad spectrum of SIRT applications, which is constantly evolving.

Assessing Auricular Dimensions in CT: Unveiling the Relationship Be-tween Ear Dimensions, Age, and Gender Using 3D Volume Rendering Reconstructions.

B. Schulz[1,2], R. Kubik[1], M. Thali[2], T. Niemann[1]; [1] KSB – Kantonsspital Baden, Baden, Switzerland, [2] University of Zurich, Institut für Rechtsmedizin Zürich, Zurich, Switzerland

Purpose: Retrospective assessment of the auricles using CT volumetric datasets aimed to correlate various measurements and observations with sex and age.

Methods and Materials: To investigate the relationship between sex, age, and auricle measurements using CT volumetric datasets, 652 head CT scans of patients aged 18-97 (mean age = 60 ± 19; 331 females and 321 males) were included in this study. Two lengths, two widths, and the circumference of the auricle were measured in each case.

Results: In our study of 671 participants aged 18-97, we found that ear measurements increased with age, with perimeter showing the strongest correlation in both men (Pearson correlation coefficient right/left = 0.49/0.48) and women (Pearson correlation coefficient 0.53/0.54). Notably, one width measurement showed weaker correlations and left-right differences, possibly due to variability in landmark identification. By assessing vertical lines, we identified the gender-specific mean age at which these lines typically develop, providing insights into age-related changes. Vertical lines develop at a minimum/mean age of 48/66 years in men and 45/70 years in women.

Conclusion: Our pioneering approach sheds new light on auricle morphology and the development of the vertical line, highlighting the interplay of age, gender, and ear dimensions. Further research will deepen our understanding of these dynamics.

Edema in teeth – using a water sensitive short tau inversion recovery (STIR) sequence for caries imaging

E. Burian[1], M. Probst[2], A. Lutz[3], M. Folwaczny[4], G. Andreisek[3]; [1] Kantonsspital Frauenfeld, Department of Nuclear Medicine, Frauenfeld, Switzerland, [2] MRI TUM – School of Medicine & Klinikum rechts der Isar, Munich, Germany, [3] Kantonsspital Frauenfeld, Department of Radiology, Frauenfeld, Switzerland, [4] LMU München, Department of Restorative Dentistry and Periodontology, Munich, Germany

Purpose: In clinical practice, diagnosis of suspected carious lesions is verified by using conventional dental radiography (DR), including panoramic radiography (OPT), bitewing imaging, and dental X-ray. The aim of this study was to evaluate the use of magnetic resonance imaging (MRI) for caries visualization.

Methods and Materials: Fourteen patients with clinically suspected carious lesions, verified by standardized dental examination including DR and OPT, were imaged with 3D isotropic T2-weighted STIR (short tau inversion recovery) and T1 FFE Black bone sequences. Intensities of dental caries, hard tissue and pulp were measured and calculated as aSNR (apparent signal to noise ratio) and aHTMCNR (apparent hard tissue to muscle contrast to noise ratio) in both sequences. Imaging findings were then correlated to clinical examination results.

Results: In STIR as well as in T1 FFE black bone images, aSNR and aHTMCNR was significantly higher in carious lesions than in healthy hard tissue (p < 0.001). Using water-sensitive STIR sequence allowed for detecting significantly lower aSNR and aHTMCNR in carious teeth compared to healthy teeth (p = 0.01).

Conclusion: The use of MRI for the detection of caries is a promising imaging technique that may complement clinical exams and traditional imaging.

The XAI Orchestrator: Combining Multimodal and Longitudinal Data for Explainable Artificial Intelligence (XAI) in Medical Imaging – an Outlook.

A. Pahud de Mortanges[1], Z. Shu[1], A. Kamath[1], Y. Suter[1,2], M. Shelan[2], A. Pöllinger[3], M. Reyes[1,2]; [1] ARTORG Center for Biomedical Engineering Research, University of Bern, Bern, Switzerland, [2] Inselspital – Universitätsspital Bern, Department of Radiation Oncology, Bern, Switzerland, [3] Inselspital – Universitätsspital Bern, Department of Diagnostic, Interventional and Pediatric Radiology, Bern, Switzerland

Purpose: The limitations arising from the black-box nature of AI are aggravated when multimodal and longitudinal data increase model complexity. We postulate that explainable AI (XAI) needs to be leveraged to analyze medical image data jointly with other data types, such as report texts or laboratory results. LLMs are well-suited to fuse and convey these explanations in a user-friendly manner due to their strong semantic capabilities. We envision an instance that orchestrates XAI systems in radiology and may serve as a virtual assistant with dialogical abilities.

Methods and Materials: Multimodal and longitudinal data are processed to predict an outcome, and the results are interpreted by modality- and time-point-specific explainable AI (XAI) systems. Everything is assembled by the superordinate XAI orchestrator, which considers the input data, the prediction, and the explainability output to produce an overall explanation. The XAI orchestrator should have the following key properties: 1) It should be adaptive to variable data input types and appropriately handle missingness. 2) It should be interactive and provide further explanations upon request. 3) It should be aware of uncertainties in the data and the prediction. 4) It should be aware of causal dependencies between the data. 5) Privacy preservation should be ensured, for example, through federated learning. 6) Time-effectiveness is key to successful translation to clinical routine.

Results: We are looking to implement the first version of the proposed XAI orchestrator for disease assessment of brain tumors from multimodal and longitudinal imaging using the LUMIERE dataset and Alzheimer's classification using the ADNI dataset. In both cases, we aim at handling modality-specific explanations via embeddings to an LLM (e.g. MedBERT), fine-tuned on disease-specific text corpora to summarize multimodal explanations.

Conclusion: In the future, the XAI orchestrator may serve as a virtual assistant to radiologists when dealing with multimodal and longitudinal data.

Non-traumatic "Do Not Touch" (DNT) Skull Based Lesions

V. Chua[1], Q. Lu[1], C. Long Ho[1,2,3,4]; [1] Sengkang General Hospital, Singapore, Singapore, [2] Duke-NUS Medical School, Singapore, Singapore, [3] NUS – National University of Singapore, Singapore, Singapore, [4] Lee Kong Chian School of Medicine, Singapore, Singapore

Learning objectives: To present imaging characteristics of various non-aggressive skull-based lesions.

Background: Skull-based lesions often pose diagnostic challenges due to their anatomical complexity. With accurate image interpretation, radiologists play a major role in patient management. This pictorial review showcases imaging characteristics of various skull-based "do not touch"(DNT) lesions, differentiating them from infiltrative masses.

Imaging findings or procedure details: Skull-based DNT lesions:
- Anatomical variants: Arachnoid granulations often mimic lytic lesions; parasagittal, protruding into superior sagittal sinuses.
- Brown tumours, or osteoclastomas: rare manifestation of secondary hyperparathyroidism, can mimic infiltrative lytic lesions.
- Craniofacial fibrous dysplasia, or 'Leontiasis Ossea': developmental benign fibro-osseous process with facial deformity by arresting bone growth in woven bone.
- Ecchordosis physaliphora: arises from ectopic notochordal remnant in the midline craniospinal axis.
- Epidermoid cysts: may be congenital, arise from ectodermal inclusion during neural tube closure.
- Hemangioma: benign vascular tumour with "corduroy sign" on CT, show abnormal signal on MRI due to high fat content.
- Osteoid osteoma: benign bone tumour with specific 'double density sign' on bone scintigraphy.
- Neurofibromatosis type 1: neurocutaneous tumour syndrome with sphenoid wing dysplasia. Slow expansion of middle cranial fossa with herniation of temporal lobe into the orbit, giving 'bare orbit sign' on CT.
- Myelodysplastic/myeloproliferative bone marrow disorders.
- Osteoradionecrosis: occurs post-irradiation of naso/oro-pharyngeal carcinoma.
- Paget's disease: skeletal growth disorder from excessive bone remodelling. Often shows bony trabeculae coarsening, cortical thickening and diploic widening.

Conclusion: Accurate radiological diagnosis of skull-based DNT lesions is essential in guiding patient management and avoiding unnecessary biopsy/surgery.

Pictorial review of infiltrative skull lesions

Q. Lyu[1], V. Chua[1], C. Long Ho[1,2,3,4]; [1] Sengkang General Hospital, Singapore, Singapore, [2] Duke-NUS Medical School, Singapore, Singapore, [3] NUS – National University of Singapore, Singapore, Singapore, [4] Lee Kong Chian School of Medicine, Singapore, Singapore

Learning objectives:
1. To identify infiltrative skull lesions based on specific imaging features
2. Differentiating primary from secondary infiltrative skull lesions

Background: Primary infiltrative skull lesions are rarely encountered and often pose a diagnostic challenge for clinicians. Imaging plays an increasing and pivotal role in the diagnosis and surveillance of skull lesions. Besides conventional radiographs and computed tomography, magnetic resonance imaging and proton emission tomographic scans can aid in the diagnostic process. In this pictorial review, we present the radiological features of various infiltrative skull lesions, subcategorizing them into primary and secondary infiltrative lesions based on specific imaging features.

Imaging findings or procedure details: Primary infiltrative skull lesions are often locally aggressive tumours:
- Most common malignant bone neoplasm: Multiple myeloma (punched-out lucent lesions).
- Intraosseous meningioma and solitary fibrous tumour: Locally aggressive tumours originate from the meninges and mesenchymal tissues, respectively.
- Osteosarcoma: Aggressive periosteal reaction in sunburst pattern or lamellated/'onion-skin' reaction
- Chondrosarcoma: Rings and arcs configuration of tumour calcification.
- Infiltrative bone marrow lesions include Langerhans Cell Histiocytosis, chordoma and lymphoma.

Secondary infiltrative skull lesions are more variable in imaging features:
- Direct extension from neoplastic process involving adjacent structures such as nasopharyngeal carcinoma, glomus tumor or neuroblastoma.
- Metastases from known primary carcinomas (lungs, liver and breast).
- Large white epidermoid cyst scalloping the skull with mass effect on the underlying brain.

Conclusion: Besides anatomic localization of these lesions, imaging can assess their locoregional involvement including brain invasion. When combined with different imaging modalities, most skull lesions can be diagnosed accurately and help guide appropriate patient management.

Imaging in Rapid Progressive Dementia: Tips and tricks on how to "not lose your mind"

E. Radew[1], R. Srikantharajah[1], J. Evers[1], A. Lutz[1,2], G. Andreisek[1,3], A. Péporté[1];
[1] Kantonsspital Frauenfeld, Team Radiologie Plus, Frauenfeld, Switzerland,
[2] Stanford University School of Medicine, Department of Radiology, Stanford, United States, [3] University of Zurich, Medical Faculty, Zurich, Switzerland

Learning objectives:
- To investigate multimodal imaging findings in potentially 'reversible' causes of rapid progressive dementia (RPD)
- To emphasize the importance of early diagnosis of secondary diseases in improving patient outcomes
- To recognize the pivotal role of the radiologist in securing the diagnosis of RPD

Background: RPDs are neurological conditions that progress subacutely over a period of weeks to months, or in rare instances, acutely over days. Unlike most neurodegenerative conditions, which can take years to progress to death, RPD can be fatal quickly. It is imperative to promptly evaluate the RPD patient, typically in a hospital setting, as they may possess a condition that can be treated. In this pictorial review, we discuss a differential diagnostic approach to RPD, emphasizing vascular, toxic/metabolic, infectious, autoimmune, neoplastic, and other conditions to consider.

Imaging findings or procedure details: As many types of conditions can cause RPD and they can progress quickly, it is important to take an organized and systematic approach to diagnosis. Some of the major categories of etiologies for RPDs can be summarized with the mnemonic "VITAMINS". RPDs that present with space occupying brain lesions can be readily identified by means of a CT or MR scan. Vascular lesions need additional angiography. We emphasize the RPDs that are most difficult to diagnose or least likely to be recognized and highlight some diagnostic pearls and pitfalls.

Conclusion: Radiologists should be aware of the most important and frequent differential diagnoses that are treatable and potentially reversible when assessing RPD patients' scans.

PO07

An "eye-opening" approach to imaging in Horner syndrome

R. Srikantharajah[1], J. Evers[1], A. Lutz[1,2], G. Andreisek[1,3], A. Péporté[1]; [1] Kantonsspital Frauenfeld, Team Radiologie Plus, Frauenfeld, Switzerland, [2] Stanford University School of Medicine, Department of Radiology, Stanford, United States, [3] University of Zurich, Medical Faculty, Zurich, Switzerland

Learning objectives:
· To understand how the anatomical location of sympathic pathway disruption can influence the clinical presentation
· To recognize the critical role of specific imaging modalities in assessing the anatomical position of the lesion
· To highlight the importance of precise radiological evaluation for this rare disease

Background: Disruption of the oculosympathetic pathway (OSP) results in Horner syndrome. This rare neuro-opthalmic condition is characterized by ptosis, miosis, anhidrosis and (pseudo-)enopthalmus. The clinical presentation can reveal the anatomical location of the lesion. The most common cause of Horner syndrome remains iatrogenic manipulations, as well as tumors and vasculopathies. This educational exhibit highlights the significance of Horner syndrome and its radiological findings.

Imaging findings or procedure details: The myriad of possible etiologies for the same pathology, prevents the establishment of a single recommended imaging strategy. Presence and location of anhidrosis suggests whether the lesions affect the central, preganglionic or postganglionic structures. In case of a central lesion and accompanying brain (stem) symptoms (e.g. Wallenberg-syndrome) a brain-MRI (with angiography) is recommended. Without brain (stem) symptoms a MR of the cervical and upper thoracic spine is proposed. In preganglionic disruption, CT or MR (C2 – T2 level) is recommended depending on the type of pathology. An angiographic scan can reveal the underlying cause of postganglionic damage, since the majority of the sections are vasculopathies.

Conclusion: Horner syndrome encompasses both benign and malignant processes. The presence of this secondary disease is not always the sole clinical finding, and it may be accompanied by other signs and symptoms, which aid in establishing the diagnosis and the appropriate imaging protocol for identifying the lesions without causing unnecessary delay.

PO08

Imaging evaluation of Cavernous Sinus Thrombosis as a complication of Paranasal Sinusitis in Children

S.Y. Ooi, T.S. E. Tan, E.L.H.J. Teo; KK Women's and Children's Hospital, Singapore, Singapore

Learning objectives:
· To review the anatomy and drainage pathways of the cavernous sinuses
· To familiarize with the radiological features and management of cavernous sinus thrombosis (CST) resulting from paranasal sinusitis

Background: Paranasal sinusitis is common in children. Severe sinusitis may cause phlebitis of the veins draining the central portion of the face towards the cavernous sinuses, resulting in septic CST. As the cavernous sinuses communicate with one another, the thrombophlebitis often becomes bilateral. CST may lead to orbital and intracranial abscesses or empyema, meningitis, cerebral infarction, septicemia and death. The diagnosis of CST is usually clinical with presentation of unilateral periorbital edema, photophobia, proptosis, opthalmoplegia, visual loss and headache. Emergent imaging studies are often necessitated to evaluate for complications in pediatric patients with symptoms persist and/or if there is clinical suspicion for intracranial or orbital complications. Early diagnosis and prompt intervention with intravenous antimicrobial therapy or surgical procedure is essential for a favorable clinical outcome.

Imaging findings or procedure details: Contrast enhanced computed tomography (CT) is excellent in determining intraorbital extension of paranasal sinusitis. A contrast enhanced magnetic resonance imaging (MRI) study is indicated to assess for intracranial/cavernous sinus spread. CST signs can be divided into direct and indirect signs. Direct signs for CST include filling defects in the cavernous sinus and convexity of the lateral sinus wall. Indirect signs for CST include extensive paranasal sinusitis, proptosis, dilatation of the superior ophthalmic vein and narrowing of the internal carotid artery cavernous segment.

Conclusion: Cavernous sinus thrombosis is an uncommon but serious complication of untreated infections, primarily involving the paranasal sinuses, facial and orbital regions. Close interval follow up imaging is often required to assess the treatment response and to evaluate for further complications.

PO09

Red flags in MRI of salivary gland tumors

A. Steorobaneanu, S. Neveu, M. Becker; HUG – Hôpitaux universitaires de Genève, Geneva, Switzerland

Learning objectives: The aim of this poster is to illustrate key features that improve the diagnostic performance of multiparametric MRI in salivary gland tumors.

Background: MRI characterization of salivary gland tumors is challenging even for experienced radiologists because of many overlapping characteristics between malignant and benign tumors. In clinical routine, the diagnosis is done either by MRI or ultrasound-guided fine-needle aspiration cytology (USFNAC). As each modality alone can be misleading, we illustrate pitfalls of multiparametric MRI and the advantages of a combined MRI – USFNAC approach.

Imaging findings or procedure details: Important parameters to consider in each MRI exam are location, morphology, diffusion and perfusion patterns. The probability of malignancy is inversely proportional to salivary gland size. On T1 and T2 weighted sequences, certain morphological features should immediately raise suspicion of malignancy, such as irregular margins, extra-capsular extension or signs of perineural spread. Multiparametric sequences have limitations. While type C and A perfusion curves demonstrate acceptable specificity, type B curves remain nonspecific. Even if type B curves suggest Warthin tumor, the concordance with morphological sequences is primordial in order not to miss a malignant tumor. It is commonly accepted that mean ADC values of benign lesions are significantly higher than those of malignant lesions. Nevertheless, diffusion weighted imaging can be misleading in salivary gland tumors because of an important overlap in ADC values between benign and malignant tumor.

Conclusion: Radiologists must be aware of and actively search for the "red flags" of salivary gland tumors on MRI in order to not miss signs of malignancy, which drastically change the therapeutic approach.

PO10

Diving into Detail: 7T MRI in Clinical Neuroradiology

I. Hutuca, D. Botta, A. Fitsiori, J. Boto, S. Boudabbous, P-A. Poletti, K-O. Lovblad; HUG – Hôpitaux universitaires de Genève, Geneva, Switzerland

Learning objectives: The goal of this educational exhibit is to show the current neuroradiology applications of 7T MRI in clinical practice.

Background: Regulatory approval for seven-tesla (7T) MRI was granted in both the European Union and the USA in 2017. In our institution we started using 7T MRI for clinical purpose as of November 2023. With increased signal-to-noise ratio, spatial resolution, and contrast-to-noise ratio, 7T MRI can produce high-resolution images that have the potential to enhance diagnostic accuracy for neurological diseases compared to 3T or 1.5T MRI. Two of the most promising clinical applications to show improved diagnostic accuracy with 7T MRI are epilepsy and multiple sclerosis (MS). The visualisation of hippocampi microstructure and of the cerebral cortex increases the detection of lesions in patients with epilepsy, having an important impact on the surgical management. 7T MRI helps in differentiating MS lesions from mimics by detecting the central vein sign and the iron rims on susceptibility weighted imaging (SWI). Additionally, it has a higher diagnostic accuracy in detecting cortical lesions compared to 3TMRI. SWI at 7 Tesla MRI offers enhanced sensitivity to paramagnetic substances, enabling precise detection of cerebral microbleeds, detailed imaging of venous structures, and valuable insights into brain iron distribution.

Imaging findings or procedure details: This educational poster illustrates the use of 7T MRI in neuroradiology, with a focus on lesion detection in MS and in epilepsy. A secondary goal is to exemplify the great detail of anatomical structures and how this impacts lesion detection.

Conclusion: The integration of seven-tesla MRI into clinical neuroimaging practices proves valuable, enabling precise diagnoses where conventional field strength MRI falls short.

Radiological Assessment of Complications in Extreme Premature Newborns: Prevalence, Patterns, and Clinical Correlations

E. Katirtzidou, M. Laurent, S. Toso, F. Barcos Muniz, M. Rebollo Polo; HUG – Hôpitaux universitaires de Genève, Geneva, Switzerland

Purpose: Extreme prematurity (birth before 28weeks of gestational age) leads to complications due to the immaturity of various organ systems. This study aims to evaluate the prevalence and distribution of specific complications in extremely premature newborns: intraventricular hemorrhage (IVH), surfactant deficiency disorder (SDD) and necrotizing enterocolitis (NEC).
Methods and Materials: This retrospective monocentric study analyzed a cohort of 175 extreme premature newborns (mean GA 24.6weeks ± 1week) admitted to the neonatal intensive care unit of Geneva University Hospitals between November 2016 and November 2023. The mean duration of hospitalization was 71 ± 34 days. Imaging studies performed during that time (cerebral and abdominal ultrasound, abdominal et chest X-ray and cerebral MRI) were reviewed. Emphasis was placed on the prevalence, radiological semiology and correlation with short-term clinical outcomes of IVH, SDD and NEC.
Results: The preliminary findings involved 60 out of 175 premature newborns, showed a prevalence of 23.3% for IVH, 100% for SDD and 16.7% for NEC. Mean appearance time for each complication was 19 ± 25 days for IVH, at birth for SDD, and 32 ± 23.6 days for NEC. In this group, 8/60 newborns (13.3%) were deceased. Among the affected newborns for each system, 14% of those with IVH developed hydrocephalus and 75% of newborns with SDD developed bronchopulmonary dysplasia (BPD). Surgical intervention was necessary for 60% of premature newborns with NEC, the remainder were conservatively managed.
Conclusion: The prevalence rates and associated outcomes of IVH, SDD and NEC highlights the significance of early detection and management, as they are associated with high mortality rate. These preliminary findings show the critical role of radiological imaging in diagnosing and monitoring potential complications, facilitating timely interventions and improved outcomes.

Photon-Counting CT in Pediatrics: A Systematic Review of Applications and Clinical Implications

M. Ndengera, J. Namorado Stoffel Feria, M. Laurent, S. Toso; HUG – Hôpitaux universitaires de Genève, Geneva, Switzerland

Purpose: Photon-counting CT allows for imaging with lower radiation doses, a crucial consideration in pediatrics. Information specific to its pediatric applications remains limited. We perform a systematic review of the literature to identify the current status of photon counting CT in pediatrics.
Methods and Materials: Our systematic literature review was conducted using a targeted search in PubMed on the 15 of October, employing the query: ("Photon-counting CT" OR "Photon-counting computed tomography") AND ("Pediatric imaging" OR "Pediatrics" OR "Pediatric radiology" OR "Low-dose CT" OR "Radiation dose"). We focused on peer-reviewed articles that discuss photon-counting CT in pediatric imaging. Initial screening of titles and abstracts was followed by a full-text review, culminating in a qualitative data synthesis that emphasizes the technology's potential benefits and limitations in pediatric radiology.
Results: Our systematic search yielded 92 articles, from which 6 were potentially relevant based on their titles and abstracts. Two studies were excluded (not accessible and not in English). The four remaining studies were selected for analysis. All focused on thoracic applications in pediatrics with significant dose reduction from photon-counting CT (PCD-CT) compared to traditional energy-integrating detector CT (EID-CT). Improvements in spatial resolution and image quality were also noted.
Conclusion: The current literature, while indicative of the potential benefits, is constrained both in scope and quantity, with all selected studies concentrated on thoracic imaging. This highlights a critical need for broader and more diverse research to fully understand and leverage the capabilities of PCD-CT across various pediatric applications.

Global Review of Current Practices in Pediatric Radiology Fellowship Training: Identifying Gaps and Enhancing Educational Quality

C-M. Bitter, E. Katirtzidou, B.M. Cipullo, M. Rebollo Polo, M. Laurent, S. Toso; HUG – Hôpitaux universitaires de Genève, Geneva, Switzerland

Purpose: Specialized training in Pediatric Radiology is crucial, yet significant variations in training delivery persist. We evaluate the current global landscape of fellowship training curricula in Paediatric Radiology, aiming to identify existing gaps in these curricula.
Methods and Materials: Institutions across North America, Europe, Africa, and Asia were selected. Inclusion criteria targeted centres recognized for training fellows in Paediatric Radiology. A questionnaire was distributed to institutions about their specialized training programs. Inquiries regarding certification structures, program duration, examination methods, teaching methodologies, and access to educational resources were included. Responses were collected anonymously.
Results: Seven centres participated (response rate of 58.3%). Findings revealed diverse certification structures: 42.9% federal diplomas, 25% secondary institution certifications (e.g., radiological societies), 50% institution-specific certificates, and 25% no specialty certification. Training duration: 57.2% 1-year, 28.6% 2-years, and 14.3% beyond 2 years. Subspecialty examinations were undertaken by 71.4% of centres--oral exams (40%), written assessments (20%), or both (40%). Notably, 42.9% had benchmarks for specific examination quantities. While 57.1% had structured syllabi, none included training in AI and computer programming. Teaching averaged 6 hours/week (SD +- 4.5 hours) and was predominantly delivered by radiologists (100%) and by non-radiologist physicians (28.6%), physicists (14.3%), and technologists (28.6%). Furthermore, 85.7% reported fellows publishing articles and presenting at conferences.
Conclusion: Paediatric Radiology fellowship training varies particularly in certification structure, structured teaching, and new technologies in AI, across the globe, highlighting a potential gap in preparing future paediatric radiologists for the evolving technological landscape. Addressing these gaps is pivotal in enhancing the quality of fellowship training programs.

Clinical application of an AI-based 3D segmentation tool for pediatric MR urography

N.M. Kocher, C. Kellenberger, F. Callaghan; Kinderspital Zürich, Eleonore Foundation, Zurich, Switzerland

Purpose: T1-weighted dynamic excretory MR urography after intravenous gadolinium injection is an important but also demanding diagnostic tool for the anatomic and functional assessment of congenital abnormalities of the urinary system in pediatric patients. So far, the postprocessing of the MR data and the functional evaluation is complex and time-consuming. To accelerate the process an artificial intelligence (AI)-algorithm was developed to automatically segment the different kidney compartments in one dynamic sequence to determine volume and function based on the 3D data. This study intends to evaluate the performance of this AI-based workflow in the clinical setting in comparison to a standard manually conducted postprocessing of the MR urography (ImageJ).
Methods and Materials: n=8 diseased and n=8 non-diseased kidneys from 8 patients (n=4 female, n=4 male, age range from 10 months to 16 years) were segmented both manually and with the help of the previously trained AI-algorithm. The accuracy of the segmentation was assessed using a 5-point-scale. The segmented volume of the kidneys as well as the Slope of the Patlak plot as functional parameters were compared by Bland-Altman analysis.
Results: The accuracy of the segmentation for the AI-algorithm was rated with a mean of 4.0 for the non-diseased kidneys and with 2.9 for the diseased kidneys. The differences of the measured volumes and slopes, plotted in a Bland-Altman diagram, scattered around zero for the non-diseased kidneys, thus no consistent bias of both methods could be seen for this group.
Conclusion: The AI-based segmentation is reliable for non-diseased kidneys. In diseased kidneys more manual corrections of the segmentation are needed so far. The functional analysis based on the 3D volume is comparable to a standard post-processing tool. The work-up in one compact software is an outstanding advantage of the AI-based method.

PO54

High prevalence of asymptomatic carotid artery narrowing in paediatric retro- and parapharyngeal space infection.

M.B. Cipullo, M. Becker, C-M. Bitter, H. Cao Van, M. Rebollo Polo; HUG – Hôpitaux universitaires de Genève, Geneva, Switzerland

Purpose: Infection of the parapharyngeal space (PPS) and retropharyngeal space (RPS) is common in the paediatric population. It can be associated with moderate-to-severe narrowing of the carotid arteries (CA). However, it is not clear from the existing literature whether the prevalence of CA narrowing differs among the two spaces and whether CA narrowing as detected at CT is associated with neurologic symptoms. The aim of this study was to answer these questions based on a retrospective study performed in our hospital.
Methods and Materials: A total of 136 consecutive Computed Tomography (CT) examinations were obtained during the past 5 years for suspected paediatric neck infection. The clinical and CT data of 60 children (boys: 28/60; girls: 32/60; mean age=7.97 y) with PPS or RPS infection formed the basis of this study. The lumen area of the internal and common CA was measured at several neck levels on both neck sides, and the mean narrowing ratio (MSR) between the left and right side was calculated. CA narrowing was also assessed visually using a 3-point scale (slight/moderate/severe).
Results: Abscesses, cellulitis and suppurative lymphadenopathy were found in 28/60 (46.6%) patients in the PPS, and in 32/60 (53.3%) in the RPS, respectively. Slight, moderate, and severe CA narrowing was identified in 8, 15 and 9 of the RPS lesions, and in 12, 13 and 3 of PPS lesions, respectively. The MSR in the PPS and RPS was 55% and 60.3%, respectively with a significant difference between the two neck sides in the RPS only (p<0.01). Only one out of 60 children developed transient neurologic symptoms.
Conclusion: Narrowing of the CAs was found in all children with infectious RPS and PPS lesions. As only one child had transient neurologic manifestations, there appears to be no clinical implication of CA narrowing as seen at CT in RPS and PPS paediatric infection.

PO55

Imaging Paediatric Metabolic Bone Disease

E.L.H.J. Teo[1], S.Y. Ooi[2], S.E.T. Tan[1]; [1] KK Women's and Children's Hospital, Singapore, Singapore, [2] Changi General Hospital, Singapore, Singapore

Learning objectives: To familiarise the reader with the imaging findings of important metabolic diseases in children
Upon familiarisation with these findings, the reader will be able to provide a differential diagnosis regarding the aetiology.
Background: Metabolic bone diseases comprise a wide range of conditions that may be inherited or acquired, eg secondary to nutritional deficiencies or chronic disorders, or treatment with drugs. If unrecognised and left untreated, these conditions may cause weakening of the underlying bone resulting in stunted growth, pathological fractures, deformations, deterioration of motor development and disability. It is therefore important for clinicians and radiologists to recognise the imaging features of these conditions so that the patient can undergo early treatment and prevent long-term disability.
Imaging findings or procedure details: The pathophysiology and imaging features of diseases such as primary and secondary osteoporosis, rickets, osteomalacia, renal osteodystrophy, sclerosing bony disorders, scurvy and inherited disorders such as but not limited to, hypophosphatasia, Wilson's disease and osteogenesis imperfecta, will be shown. The subtle differences in the imaging findings between these entities will be highlighted.
Conclusion: Childhood diseases, both inherited and acquired, may affect the underlying bone. It is important for clinicians and radiologists to be able to recognise and diagnose these conditions early before long term complications occur. This poster highlights the important radiological features of many of these conditions and will help the reader come to an early diagnosis and hence early treatment for the patient.

PO56

Scurvy – How to recognise this forgotten disease

A. Mürset[1], J. Busch[1], A. Felser[2]; [1] Inselspital – Universitätsspital Bern, Universitätsinstitut für Diagnostische, Interventionelle und Pädiatrische Radiologie, Bern, Switzerland, [2] Inselspital – Universitätsspital Bern, Universitätsinstitut für Kinderheilkunde, Bern, Switzerland

Learning objectives: Scurvy, caused by Vitamin C deficiency, were less frequently seen these past years in the developed world. It is however still important, especially for recently qualified Radiologists, to know and recognise the Imaging findings of this forgotten disease as increased cases might present with immigration and in the first world spectrum.The clinical findings which raise the suspicion of this condition should aslo be recognised.
Background: Vitamin C is an essential nutrient in humans, that need to be aquired by adeqaute intake. Animals produces it themselves. It acts as an antioxidant and cofactor in tissue growth and repair, as well as maintain functioning of certain neurotransmitters and proper immune function. Historically it is known as early as Ancient Egypt times and mostly as a historical disease within ancient sailors with nutritional restrictions in long distance sea travel. Today it is mostly seen in developing countries due to malnutrition. One should however be aware of this in the developed world in patient populations with classic predisposing factors such as psychiatric conditions or malabsorption - but also in the healthy child who is a picky eater.
Imaging findings or procedure details: The clinical signs and symptoms, together with the imaging findings, of 3 patients who presented to our institute within the past 5 years with the confirmed diagnosis of Scurvy, will be presented. IThe typical Imaging findings will be desribed and discussed with the relevant Xrays and MRI pictures of these 3 patients. Vitamin C-levels will be added to it, as well as a short description of the improvement after treatment.
Conclusion: Radiologists would have been made aware of the typical clinical and imaging findings in this forgotten disease, who is making a slow comeback due to reasons desribed, and taking into consideration the possible increase in cases due to the recent increase in immigration from developing countries.

PO57

Pediatric Imaging of the Elbow: Variants, Pitfalls and pathological findings

P. Bleus, A. Dhouib, K. Minkner, A. Stolz; RHNe – Réseau Hospitalier Neuchâtelois, Neuchâtel, Switzerland

Learning objectives: To review the developmental normal anatomy, diagnostic pitfalls that result from normal elbow growth in children and present most common pathological conditions.
Background: Imaging of the pediatric elbow is challenging giving the complex maturation of the elbow. Appearance of secondary ossification centers occurs in a predictable sequence according to age. Recognizing this natural progression is key to accurate radiological interpretation and effective management of elbow injuries.
Imaging findings or procedure details: The pediatric elbow, being a complex joint, is prone to a wide spectrum of issues, including traumatic, inflammatory, metabolic, and neoplastic conditions.
This pictorial review aims to provide an in-depth visual insight into pediatric elbow imaging, showcasing various conditions unique to this demographic. Imaging pitfalls specific to children are described.
Conclusion: Pediatric elbow imaging highlights distinct anatomical differences in children compared to adults. On both Radiography and MRI, understanding physeal and apophyseal development is of paramount importance in interpreting elbow pathological conditions, as several physiological elbow entities can be mistaken for pathology.

PO58

Radiological Assessment of Complications of Sickle Cell Disease in Pediatric Patients

T. Sartoretti, E. Tenisch, L. Alamo, J-Y. Meuwly; CHUV – Centre Hospitalier Universitaire Vaudois, Lausanne, Switzerland

Learning objectives: Understand the crucial role of medical imaging in diagnosing, surveilling, and managing complications of Sickle Cell Disease (SCD) in pediatric patients.
Recognize the significance of specific imaging modalities in evaluating frequent complications in pediatric SCD, such as acute chest syndrome (ACS), musculo-skeletal and abdominal manifestations.
Background: SCD, characterized by hemoglobin S (HbS) formation, may cause complications affecting multiples organs and systems. This abstract focuses on the role of medical imaging in the diagnosis and evaluation of SCD-related complications in pediatric patients (apart from neurological).
Imaging findings or procedure details: *Musculo-skeletal complications:* Erythrocyte-endothelium adhesion produces vaso-occlusion and avascular necrosis that lead to acute pain crises. MRI allows identifications and evaluation of the extensions of osseous ischemic changes and superinfection.
Acute chest syndrome: While being essentially a clinic diagnosis, both chest X-rays and chest-CT remain necessary to evaluate extent and recognize potential complications.
Abdominal Manifestations: Abdominal ultrasonography and CT scans are essential in identifying complications like cholelithiasis, splenic sequestration or ileus secondary to intestinal vaso-occlusion. Early recognition of these complications is crucial in mitigating severe morbidity in pediatric SCD.
Conclusion: The outlined imaging findings provide a comprehensive approach to navigating the diverse landscape of SCD-related complications in the pediatric population.

PO59

Calculator for Paediatric Polytrauma Split-Bolus Protocol

A.C. Rocha, C. Chavallier, N. Ostojic, L. Alamo, E. Tenisch; CHUV – Centre Hospitalier Universitaire Vaudois, Lausanne, Switzerland

Learning objectives: The purpose of this study was to build an easy-to-use calculator to set the contrast media injector parameters when performing a split-bolus CT acquisition, in the context of a paediatric polytraumatic event.
Background: The split-bolus CT acquisition consists of a single CT acquisition following an initial contrast media injection for parenchymal impregnation and venous opacification, and a second injection for arterial opacification.
Success in obtaining a split-bolus CT acquisition with optimal opacification is a challenge, especially in such a heterogeneous group. Its preparation is a source of stress and delay in image acquisition as well as susceptible to error.
Imaging findings or procedure details: The acquisition time was set to 50 s up to 30kg and 65s for those above 30kg.
The total contrast volume was 2ml/kg for weight up to 30kg. In children >30kg weight, we added 30ml to the weight of the patient up to a maximum of 80 ml. The volume was split, with two-thirds in the first injection and the remaining third in the second injection.
Contrast media volume, saline volume, flow rate, injection time and pause time were calculated based on five weight categories.
The calculator was built in Excel following the previous described rules, with a similar design to the display of the dual-headed injector used in our department.
The calculation method is accessible by a QR code link.
Conclusion: We built an Excel-based easy-to-use calculator to set a dual-headed injector, with a single input (weight of patient) that gives automatically all the required information to perform an optimal split-bolus CT acquisition (volume, flow rate, injection time and pause time), reducing imaging delay and risk of error during a stressful event. We share it with a QR code link.

PO60

Soft tissue fatty lesions in children: a pragmatic approach

B.M. Cipullo, E. Katirtzidou, M. Laurent, S. Toso; HUG – Hôpitaux universitaires de Genève, Geneva, Switzerland

Learning objectives: Fatty lesions of soft tissues are often found in routine paediatric practice and can pose difficulties in the diagnostic work-up and management. We provide an algorithmic-based approach to diagnostic work-up based on imaging characteristics for the training radiologist.
Background: Many different aetiologies can be hypothesized in the case of a soft tissue mass with fatty content, opening a wide spectrum of differential diagnosis. A classical and widely diffuse approach is based on clinical differences, separating these lesions based on benign vs malignant criteria. This may not necessarily be the most useful approach for radiologists, who are usually confronted with imaging characteristics.
Imaging findings or procedure details: We present some key imaging features of the different soft tissue lesions, as depicted in ultrasound (US) and Magnetic Resonance Imaging (MRI). We offer an algorithm-based evaluation of these features. Some lesions could immediately be classified based on the US solely. For all the others, we provide MRI characteristics to help distinguish lesions that require no further follow-up, follow-up or histologic confirmation.
Conclusion: The aim of this poster is to provide a more practical approach based algorithms on an imaging to help radiologists work-up paediatric fat containing lesions in soft tissue.

PO61

Imaging of congenital ear malformations in children: A pictorial essay.

C-M. Bitter, E. Katirtzidou, M.B. Cipullo, M. Rebollo Polo; HUG – Hôpitaux universitaires de Genève, Geneva, Switzerland

Learning objectives: To illustrate the imaging findings of congenital ear malformations in children and to learn which imaging technique is indicated according to the clinical context.
Background: In Switzerland, widespread newborn hearing screenings are reliably conducted. Additionnally, associated malformations, such as aural atresia or syndromic features prompt the search for temporal bone malformation. Congenital ear malformations cover a wide range of anomalies affecting the external, middle, and inner ear structures. Early and precise diagnosis is crucial for therapeutic decisions as hearing impairment can significantly impact language development. Radiological imaging plays a key role in assessing these malformations, providing detailed insights into their complex anatomy. It also helps tailor management approaches, including determining the need/suitability for cochlear implants, where early intervention often leads to better outcomes.
Imaging findings or procedure details: This pictorial essay showcases various congenital ear malformations through a collection of imaging studies, including computed tomography (CT), Cone-Beam CT, and magnetic resonance imaging. Middle ear anomalies, such as ossicular malformations, can contribute to conductive hearing loss, while inner ear abnormalities, such as cochlear dysplasia, labyrinthine dysplasia, and enlarged vestibular aqueduct, often lead to sensorineural hearing loss. Emphasis is placed on detailing the radiological characteristics for accurate identification and classification of these malformations, with visual aids and flowchart illustrating pro and cons of each imaging technique in the pediatric population.
Conclusion: For radiologists, enhanced familiarity with the main features of the most frequent congenital ear malformations is crucial to enhance collaboration with clinicians: making precise diagnosis, evaluating eligibility for cochlear implants, and tailoring treatment plans in order to facilitate timely interventions that benefit both language development and hearing rehabilitation.

Assessment of Ultrasound Image Quality in a Reference Phantom Using Gel and Liquid Standoff Pads

C. Paverd[1], A. Martin[1], M. Rominger[1], L. Ruby[1,2]; [1] USZ – Universitätsspital Zürich, Zurich, Switzerland, [2] Memorial Sloan Kettering, New York, United States

Purpose: Ultrasound standoff pads have been used historically in clinical settings to improve ultrasound image quality when imaging superficial targets. Recently, a liquid standoff pad, "aiSon™ Focus" (aiSon Technologies AG) has been created to address the issue of non-adaptability of traditional gel pads. This new type of standoff pad has not been assessed for the effect it may have on image quality. Additionally, the benefit of standoff pads in general has not been re-evaluated in light of modern ultrasound systems. The goal of this study was to compare standoff pads (traditional gel and new liquid types) with no standoff pad images in a standard reference phantom using a modern ultrasound system.

Methods and Materials: Measurements were made with a Canon Aplio i800 ultrasound system on a standardized ultrasound phantom (Computerized Imaging Reference Systems, Inc.). Images with and without standoff pads at different heights the phantom were acquired in order to assess and compare lateral resolution, nearfield target intensity, and contrast to noise ratio of echogenicity targets. Two cases are examined: when the ultrasound images are taken with the probe at different heights above the phantom (the normal clinical use-case for standoff pads); and when the ultrasound probe is artificially always placed at the same height above the phantom (allowing for direct image comparison).

Results: The main differences in the standard clinical use-case were observed in nearfield image intensity, with a mean difference of 22.4 ± 11.1% between highest and lowest positions. Investigation of probes at the same height above the phantom shows that differences appear to be due primarily due to the height of the probe above the phantom, rather than the pads themselves.

Conclusion: Image quality does not improve or degrade directly due to standoff pads, but rather image intensity changes with height of the probe above the target.

In vitro blood sample assessment: Investigating Correlation of Hemoglobin and Dual Energy CT Measurements (Rho/Z)

B. Schulz[1,2], M. Thali[2], A. Euler[1], L. Hefermehl[1], R. Kubik[1], H-R. Schmid[1], T. Niemann[1]; [1] KSB – Kantonsspital Baden, Baden, Switzerland, [2] University of Zurich, Institut für Rechtsmedizin Zürich, Zurich, Switzerland

Purpose: Our study comprised a single-center retrospective in vitro correlation between ρ/Z values derived from scanning blood samples using DECT with the corresponding Hb/Hct levels to assess the potential utility of these parameters in detecting anemia compared with CT attenuation values.

Methods and Materials: Six hundred blood samples were scanned using a single-source dual-energy CT system with a standardized scan protocol (80/Sn150 kV and 158/321 mAs; Au/Sn140 kV and 320 mAs). Electron density relative to water (ρe or Rho), effective atomic number (Zeff), and CT attenuation (HU) were measured by placing a freehand region of interest (ROI) in the blood samples.

Results: In this study the blood samples of 347 women and 253 men were scanned and attenuation values were correlated with hemoglobin/hematocrit values in both genders (r-values from 0.6 to 0.89). Similar correlations were observed between Rho and hemoglobin/hematocrit values (r-values from 0.35 to 0.57). No correlation was observed for Z-values. Attenuation values were significantly different between blood samples with and without anemia in both genders (p-value < 0.005). ROC analysis showed sufficient discrimination with an AUC of 0.93 for women and 0.96 for men. Cutoff values of 39 HU for women and 42 HU for men for indicating the presence of anemia (hemoglobin < 12 g/dl in women and < 13 g/dl in men) were determined.

Conclusion: Dual-energy computed tomography (DECT) can be used to measure CT attenuation, Rho values, and Z values in blood samples. Rho values and attenuation values are correlated with hemoglobin and hematocrit levels, which can be used to detect anemia. However, the cutoff values for detecting anemia are only valid for non-contrast DECT.

Impact of COVID-19 on the number of emergency CT scans at a maximum care provider in Switzerland

D. Jäschke, J. Vosshenrich, B. Ceresa, F. Kempter, T. Heye;
USB – Universitätsspital Basel, Basel, Switzerland

Purpose: To measure the impact of the COVID-19 pandemic on emergency CT examination counts.

Methods and Materials: 54944 CT scans of selected body regions ordered by the emergency department at our university hospital from 01/2018-08/2023 were retrospectively analyzed with approval of the local ethics committee. Data was divided into three time periods: pre-pandemic (01/2018-01/2020, n=17796), pandemic (02/2020-10/2022, n=29057) and post-pandemic (11/2022-06/2023, n=8091). A focus was put on night shifts (10pm-8am; n=16659), as these hours are most representative for emergency exam counts. For comparison, 7100 chest radiographs performed at night were included. Analysis was done by using a two-sided, unpaired t-test.

Results: Mean overall monthly CT counts during night shifts were highest during the pandemic (mean: 327±44) and increased (p<0.001) from the pre- (262±22) to the post-pandemic era (309±32). The proportion and absolute number per month of chest CTs increased from 12%±2% (32±7, pre) to 22%±4% (71±15) during the pandemic and remained (p<0.001) higher post-pandemic with 16%±4% (50±15). Simultaneously, chest radiograph counts decreased (p<0.001) during the pandemic and remained lower (p<0.001)(pre: 142±17; pandemic: 75±29; post: 105±25).The number of chest-abdomen-pelvis CTs increased both in absolute number and relative share (p<0.001) (pre: 4%±1%, 10±3; pandemic: 7%±1%, 23±5; post: 6%±1%, 20±4), while abdomen-pelvis CT share of total decreased (p=0.05) (pre: 21%±3%, 56±9; pandemic: 17%±1%, 55±11; post: 19%±2%, 59±4).

Conclusion: Following the COVID-19 pandemic, more chest CTs and combined scans, rather than chest radiographs and simple abdomen-pelvis CTs are performed in the emergency setting. These trends suggest an increase in workload, healthcare expenses and patient radiation exposure.

Energy-optimized scheduling of CT examinations through mathematic modelling

M. Segeroth[1], A. Nurkanović[2], J. Vosshenrich[1], M. Diehl2, T. Heye[1];
[1] USB – Universitätsspital Basel, Basel, Switzerland, [2] University of Freiburg, Freiburg, Germany

Purpose: Radiology departments and medical imaging devices in particular are major energy consumers within a hospital. The aim of this study was to calculate possible energy savings by optimally scheduling CT examinations.

Methods and Materials: Data of all CT examinations performed in our tertiary care radiology department in 2015 on three CT scanners was retrospectively included. Data consisted of examination timestamps and power consumption in kilowatts. The optimal scheduling problem was formulated using linear constraints, a linear objective function and only binary decision variables as an integer linear programming (ILP) problem. This formulation allowed rigorous modelling of a non-convex and non-differentiable objective function and offers the possibility to compute the optimal solution even for very large models.

Results: In total 261 workdays were analyzed, with 15'072 CT examinations scheduled on the three CT scanners. The duration to solve the ILP for every workday was 10.14 s (9.46-10.80 s). The model yielded a 34.9% reduction in the scanners' combined daily energy consumption through optimal examination scheduling. In absolute values, daily energy consumption could be decreased by 42.2 kWh from 121.0 kWh (120.6-121.4 kWh) to 78.8 kWh (77.8-79.8 kWh; p<.001). Energy savings are primarily attributed to examination shifting, allowing for increased system off times. Overall, 10'930.6 kWh in energy, \$2'864 in cost, and 1'399.1 kgCO$_2$eq in carbon emissions could theoretically be saved in our setting.

Conclusion: Optimized CT examination scheduling through automatic modelling has substantial sustainability and cost benefits for radiology departments. Feasibility of model implementation in clinical routine needs further investigation.

Fetal and Gonadal Shielding: An Analysis of Online Social Media Perceptions

A.N. Sahin[1], M. McInnes[2], M. Sampaio[3]; [1] The Ottawa Hospital, Senior Radiology Resident-Physician, Ottawa, Canada, [2] The Ottawa Hospital, Professor of Radiology and Epidemiology, Abdominal Radiologist, Ottawa, Canada, [3] The Ottawa Hospital, Musculoskeletal Imaging Section Head, Assistant Professor of Radiology, Department Lead for X-ray Modality and Digital Imaging, recent Radiation Protection Officer, Musculoskeletal Radiologist, Ottawa, Canada

Purpose: Several societies released statements to recommend discontinuation of gonadal and fetal shielding. However, patients' and medical professionals' understanding of radiation risks remains limited. Many jurisdictions, notably in Canada, continue to mandate use of shielding, adding to confusion. The objective of this study was to describe social media perceptions on the discontinuation of fetal and gonadal shielding in diagnostic imaging.

Methods and Materials: Three major social media platforms were queried using eHealth informatics search strategies. Videos and posts were retrieved. Content in English, French or Spanish pertaining to the topic was included. Textual/visual thematic and bivariate/contingency analyses were performed after recording dates, view counts, likes, location and user authoritativeness.

Results: 122 posts and 26 YouTube videos were included. 85% of authoritative posts agreed with shielding discontinuation, in contrast to 64% for others (p<0.01). 21% of posts from non-authoritative or unidentified users expressed concern about radiation without shielding, versus 4% of authoritative users (p=0.04). The proportion of posts in favor of discontinuation when comparing before and after mid-2021 remained stable, around two-thirds. Posts suggesting shielding is protective had fewer likes, on average 2.9 versus 7.2 (p<0.01). 21 posts and 5 videos raised concerns about ongoing regulatory issues. Five posts and five videos with sensationalist misinformation on radiation were identified.

Conclusion: Many users are ambivalent about or in disagreement with shielding discontinuation. Agreement is higher within authoritative users. The release of the position statements has not proportionally increased support for shielding discontinuation on social media over the last two years. Ongoing regulatory issues, such as outdated policies or practice standards and professional liability, were frequently noted.

PO74

3D of patient contact shielding: discuss, decide, and dispose

N. Saltybaeva, E. Samara, J. Ekeberg, C. Waschkies, A. Stüssi;
USZ – Universitätsspital Zürich, Zurich, Switzerland

Purpose: It has been recently shown that the usage of patient contact shielding in X-ray imaging procedures provides negligible or no benefit and even carries a risk of increasing patient dose and compromising the diagnostic efficacy. The newest Swiss recommendation (valid since 2022) suggests abandoning the use of patient contact shielding in most of the X-ray examinations. The implementation of these recommendations may however strongly depend on the local practice and historical training in a particular radiological department. The aim of this study was to investigate how the situation in Switzerland has evolved since the first survey in 2020.
Methods and Materials: To evaluate the practice in Switzerland, a questionnaire was sent to radiation protection experts in several public hospitals and private healthcare centers. The participants were asked on the availability and usage (routinely, partially or not at all) of patient contact shielding, and where applicable, the date of abandoning the shielding.
Results: Although the results of 2020 showed a significant difference between the French- and German-speaking parts in Switzerland, this difference after the new recommendations in 2022 is less evident. Contact shielding is still available and employed in some radiological departments, while contact shielding is no longer used in the university hospitals. The reasons for not disposing the protective garments will be presented and discussed.
Conclusion: Discontinuing the use of patient contact shielding for the patients requires continuous education and training for practitioners, a high level of trust, as well as clear communication between caregivers and patients. In order to make the implied changes to the working processes, active support from the radiologists and radiographers is essential.

PO75

Quality control of radiation protection equipment: Methodology and organization at the University Hospitals of Geneva

J.A. Garcia, M. Patonnier, M. Sans Merce; HUG – Hôpitaux universitaires de Genève, Geneva, Switzerland

Purpose: The new Radiological Protection Ordinance came into force in 2018 requiring the radiation protection equipment (RPE) to be checked at least annually for its proper performance and to ensure optimal safety conditions for personnel working with ionizing radiation.
Methods and Materials: The project is made up of 4 axes: updating institutional inventory; identification of imaging modality, measurement protocol and sorting criteria for control; carrying out quality control (QC) of inventory; analysing results and optimizing the method. Self-adhesive labels were used to identify 670 RPE and gathered the information into the management database system. Then, RPE were checked using two methods: first visually and tactically (VT) by 3 inspectors and then radiographically (XR). For the XR method, EOS® system was chosen. A score, according to detected defects' location, is provided and the result qualifies the RPE condition.
Results: A large part of the RPE (394) were checked during first QC'21 with both methods (VT and XR) and then compared. The results indicate that the VT control agrees with the corresponding XR control in 84.2% of cases. Despite this high result, reached with optimal conditions during VT control, the XR method is essential. In total, 27 items were withdrawn, 13 should be changed quickly. Quality controls are time-consuming, requiring extensive logistics. To optimize the method, we tried the Flow D® system, an x-ray self-shielded mobile detector during our QC'23 campaign, checking 394 RPE. An intercomparative analysis is going on between imaging systems.
Conclusion: VT checks are insufficient to guarantee RPE's integrity, imaging is therefore necessary. Solutions were found to be compliant with the legislation. Different elements must be considered and add to our study, such as RPE's lifespan, depending on their use and storage.

PO76

Efficiency of a prototype of leaded protection in interventional cardiology

N. Ryckx[1], J. Garré[2], R. Bonvini[3], F. Rigamonti[3], J-C. Stauffer[1]; [1] Hirslanden Klinik, Zurich, Switzerland, [2] Hirslanden Clinique des Grangettes, Geneva, Switzerland, [3] Hirslanden Clinique des Grangettes, Centre Cardiovasculaire, Geneva, Switzerland

Purpose: The number of procedures performed under fluoroscopic guidance is constantly increasing. A leaded acrylic screen supported by a ceiling-mounted mechanical arm offers upper-body protection. To ensure continuity of protection, this screen is fitted with a series of leaded lamellae. However, the design of the latter sometimes creates physical discontinuities through which scattered radiation can lead to increased operator exposure in the event of inadequate positioning. To overcome this problem, we developed a prototype of leaded lamellae attached to the bottom of the leaded glass and resting on the patient.
Methods and Materials: The prototype was first tested under controlled conditions using an anthropomorphic phantom simulating an adult patient, using the main beam orientations used for cardiac vascular procedures. Scattered radiation intensity was measured using a solid-state detector. The prototype was then tested in a single centre, with two operators, in a prospective non-randomized pilot study involving 140 non-consecutive patients. Operator exposure was measured using a real-time electronic dosimetry system at chest level, outside the lead apron. Scattered radiation doses were normalized by the dose-surface product recorded on the angiography system.
Results: Measurements under controlled conditions showed a reduction in the exposure factor of the first operator by an average factor of 33 between combinations without and with the prototype. In clinical use, the reduction in scatter factor for operators without and with the prototype was lower, respectively by a factor of 6 and 2.5 for the two operators respectively. There was no significant difference in patient irradiation between the two combinations of radiation protection methods.
Conclusion: Our prototype shows significant potential for optimizing the exposure of interventional cardiology operators, without any significant change in the way the available means of protection are used, and without any noticeable impact on patient care.

PO77

Patient eye lens radiation exposure during interventional neuroradiology procedures

E. Samara, A. Stüssi, S. Tanadini-Lang, M. Guckenberger, Z. Kulcsar; USZ – Universitätsspital Zürich, Zurich, Switzerland

Purpose: Neuroradiological interventions are minimally invasive procedures that can provide diagnostic information and offer treatment for diseases such as an ischemic stroke or cerebral aneurysm. These procedures have several advantages for the patient, such as fewer complications than open operations and shorter recovery times. However, they are accompanied by radiation exposure. Aim of this study was to measure eye lens doses during different neuro-interventional procedures.
Methods and Materials: Real-time measurements were performed on patients who underwent diagnostic or therapeutic neurointerventional procedures. Gafchromic™ XR-RV3 films were placed for radiation dose measurements close to the patients' eyes.
Results: The dose-area product, fluoroscopy time and cumulative air-kerma were collected for every patient. The median eye dose during neuro-interventional procedures was 150 mGy, as measured with the Gafchromic films, with a maximum of 1007 mGy in a single procedure. The mean dose for the left eye (located toward the lateral C-arm X-ray source) was 1.5 times higher than the mean dose for the right one. Doses to the left eye showed better correlation with the air-kerma (r2=0.7) for diagnostics procedures than for therapeutic (r2=0.4), probably because of the complexity of the latter (primary beam, multiple beam projection, etc.).
Conclusion: Some patients may receive eye doses exceeding the threshold of tissue reaction, especially on the left side. High eye dose are mainly related to therapeutic procedures. A careful optimization of the procedures and follow-up of these patients to evaluate potential lens opacities should be considered.

PO84

The Monocle Sign on 18F-FDG-PET Indicates Contralateral Peripheral Facial Nerve Palsy

F. Dana; USZ – Universitätsspital Zürich, Zurich, Switzerland

Purpose: To analyse FDG-PET/CT data in patients with facial nerve palsy (FNP) for the presence of the monocle sign.

Methods and Materials: This retrospective study received approval from the local ethics committee, and all enrolled patients provided written consent for the use of their medical data for research purposes. A total of 85 patients with unilateral FNP were included into our study, thereof 73 with peripheral FNP, and 12 with central FNP. A population of 33 patients without FNP served as standard of reference. The data is from the period 05/2015 to 11/2021 and the age of the patients ranged from 21 to 94 years old with a median age of 67 ± 16.8. FDG uptake (SUV_{max}, total lesion glycolysis (TLG)) was measured in both orbicularis oculi muscles (OOM). FDG uptake of paralytic and non-paralytic muscles was compared in patients with FNP (Wilcoxon test and Mann-Whitney test), and was also compared to FDG uptake in patients without FNP (Mann-Whitney test). The relationship between age, sex and PET parameters of paralytic and non-paralytic muscles in patients with peripheral FNP was also analyzed using Spearman correlation.

Results: In patients with peripheral FNP, non-paralytic eye muscles had significantly higher FDG uptake than paralytic muscles (SUVmax: 4.7 ± 2.6 vs. 2.9 ± 0.8, respectively; $p < 0.001$). Patients with peripheral FNP had significantly higher FDG uptake in their non-paralytic OOM compared to the OOM of patients without FNP ($p < 0.001$). In Patients with central FNP, there was no significant difference in FDG uptake of non-paralytic and paralytic OOM. Correlation analysis yielded no relationship of age, sex and PET parameters of paralytic and non-paralytic muscles in patients with peripheral FNP.

Conclusion: Asymmetrically increased FDG uptake of the orbicularis oculi muscle (the "monocle sign") indicates contralateral peripheral facial nerve palsy.

PO85

Feasibility of 99mTc-MIP-1404 PSMA Radioguided Surgery in a Patient with Lymph Node Metastases in Recurrent Prostate Cancer

H. Geiger, O. Maas, D. Engeler, C. Babst, F. Forrer; KSSG – Kantonsspital St. Gallen, St. Gallen, Switzerland

Learning objectives: 99mTc-MIP-1404 enables radioguided surgery (RGS) in metastatic prostate cancer (PCa). To demonstrate its feasibility, we report on its first implementation in Switzerland.

Background: After histological confirmation of PCa in a 61-year-old, radical prostatectomy with lymphadenectomy was performed in October 2019. With rising PSA levels, a salvage radiotherapy of the prostate region was performed from August to September 2020. As PSA levels continued to rise, imaging without evidence of local recurrence was performed in October 2021 (PSMA-PET/CT), in July 2022 (Choline-PET/CT) and in January 2023 (Choline-PET/CT). Only in April 2023, a PET/CT detected two pelvic PSMA-positive lymph node metastases. As curatively intended radiotherapy could not be realized due to previous radiotherapy, the indication for surgical salvage lymphadenectomy was set. To enable less invasive and successful laparoscopic dissection of the two lymph nodes, radiolabeling of the target was requested. We used 99mTc-MIP-1404 (ROTOP Pharmaka GmbH), a 99mTc-labelled PSMA-radioligand for preoperative labelling of the metastatic lymph nodes. 740 MBq 99mTc-MIP-1404 was administered preoperatively. 18 hours p.i. a preoperative SPECT/CT demonstrated activity only in one (of two) PET/CT-positive lesions.

Imaging findings or procedure details: Regardless of visualization on SPECT/CT, intraoperatively both lymph nodes could be reliably detected using a laparoscopic gamma probe. Histopathological work-up of the resected specimens confirmed metastases of the known adenocarcinoma of the prostate. Six weeks after PSMA-RGS, serum PSA decreased from 4.22ng/ml to 0.02ng/ml (complete biochemical response).

Visualization rates are expected to be lower for SPECT than for PET because of the inferior spatial resolution of SPECT.

Conclusion: 99mTc-MIP-1404 represents a promising radiotracer for RGS and further use in selected cases is encouraged in the future.

PO86

Predictive Metabolic Radiogenomics Modeling of Driver Gene Mutations in Non-Small Cell Lung Cancer

R. Stolzmann-Hinzpeter[1,2], R. Kulanthaivelu[3], A. Kohan[4], V. Murad[2], S.A. Mirshahvalad[2], L. Avery[5], C. Ortega[2], U. Metser[2], A. Hope[6], J. Yeung[7], M. McInnis[2], P. Veit-Haibach[2]; [1] USZ – Universitätsspital Zürich, Institute for Diagnostic and Interventional Radiology, Zurich, Switzerland, [2] University Health Network Toronto, University Medical Imaging Toronto, Toronto, Canada, [3] University Health Network, University Medical Imaging Toronto, Toronto, Canada, [4] Toronto General Hospital Medical Imaging, Toronto, Canada, 5 University Health Network Toronto, Department of Biostatistics, Toronto, Canada, 6 University Health Network, Department of Radiation Oncology, Toronto, Canada, 7 University Health Network Toronto, Division of Thoracic Surgery, Toronto, Canada

Purpose: To investigate whether [18F]-FDG PET/CT-derived radiomics may correlate with driver gene mutations in patients with non-small cell lung cancer (NSCLC).

Methods and Materials: In this IRB-approved retrospective study, 203 patients with surgically treated NSCLC and who underwent subsequent genomic analysis of the primary tumor at our institution between December 2004 and January 2014 were identified. Of those, 128 patients (mean age 62.4±10.8 years; range: 35-84 years) received preoperative [18F]-FDG PET/CT as part of their initial staging and thus were included in the study. PET and CT image segmentation and feature extraction were performed semi-automatically with a commonly used open-source software platform (LIFEx, Version 6.30, lifexsoft.org). Molecular profiles using different next-generation sequencing (NGS) panels were collected from a web-based resource (cBioPortal.ca for Cancer genomics). Two statistical models were then built, to evaluate the predictive ability of [18F]-FDG PET/CT-derived radiomics features for driver gene mutations in NSCLC.

Results: More than half (68/128, 53%) of all tumor samples harbored three or more gene mutations. Overall, 55% of tumor samples demonstrated a mutation in TP53, 26% of samples had alterations in KRAS and 17% in EGFR. Extensive statistical analysis resulted in moderate to good predictive ability. The highest Youden Index for TP53 was achieved using combined PET/CT features (0.70), for KRAS using PET features only (0.57) and for EGFR using CT features only (0.60).

Conclusion: Our study demonstrates a moderate to good correlation between radiomics features and driver gene mutations in NSCLC, indicating increased predictive ability of genomic profiles using combined [18F]-FDG PET/CT -derived radiomics features.

FDG PET/CT in neurodegenerative diseases: Are 2 minutes of acquisition time sufficient?

M. Kulgawczuk[1], T. Meyer-Heim[2], T. Oblasser[2], V. Garibotto[3], M. Wissmeyer[2,3];
[1] Stadtspital Zürich Waid, Zurich, Switzerland, [2] USZ – Universitätsspital Zürich, Zurich, Switzerland, [3] HUG – Hôpitaux universitaires de Genève, Geneva, Switzerland

Learning objectives: To know the usual acquisition parameters of FDG PET/CT in diagnosis of neurodegenerative diseases. To identify regions of cerebral hypometabolism by visual and standardized statistical analysis in FDG PET/CT brain scans.

To interrogate standard acquisition parameters in FDG PET/CT of the brain.

Background: A 57 year old patient with history of an autistic disease was referred for a 18F-FDG PET/CT due to new mnestic impairment and suspicion of additional frontotemporal dementia (FTLD). After i.v. injection of 101 MBq 18F-FDG, the patient remained in a dark and silent uptake room for 50 minutes. Following the CT-scout and the AC-CT scan, a standard PET-acquisition of the brain (20 minutes) was started on a GE Discovery MI 2nd generation PET/CT scanner. However, the anxious patient interrupted the scan after only two minutes of data acquisition. After calming down the patient, the PET-scan was repeated and carried out for the whole 20 minutes acquisition time.

Imaging findings or procedure details: We performed visual analysis as well as a standardized quantitative analysis using the GE CortexID-Suite(R). The latter comprised cerebral cortex/pons ratios (CPR) as well as comparison with an age matched reference population (Z-scores) . Visual as well as quantitative analysis showed significant and partially asymmetric hypometabolism in the frontal and temporal cortex as well as in the precuneus, anterior and posterior cingulum. Less significant hypometabolism was found in the parietal cortex. Statistical analysis showed excellent correlation in regional cortical glucose metabolism between the two PET acquisitions (CPR: r=0.83; p=0.66; Z-scores: r=0.99; p=0.002).

Conclusion: In this particular case of a patient with suspicion of neurodegenerative disorder in addition to an autistic disease, no visual and statistical difference in regional cortical glucose metabolism was found between a 2-minute and a 20-minute FDG PET scan. Systemic analysis of this finding in a greater cohort is subject of an ongoing study.

M. Kulgawczuk[1], T. Meyer-Heim[2], T. Oblasser[2], V. Garibotto[3], M. Wissmeyer[2,3];
[1] Stadtspital Zürich Waid, Zurich, Switzerland, [2] USZ – Universitätsspital Zürich, Zurich, Switzerland, [3] HUG – Hôpitaux universitaires de Genève, Geneva, Switzerland

PO88

Thyroid scintigraphy in congenital hypothyroidism

K. Auf der Springe, R. Dias Correia, N. Schaefer, J. Prior, M. Nicod-Lalonde;
CHUV – Centre Hospitalier Universitaire Vaudois, Lausanne, Switzerland

Learning objectives: Planification and procedure of thyroid scintigraphy in the newborn with congenital hypothyroidism.
Identify scintigraphic patterns in congenital hypothyroidism.
Differentiate between structural anomalies and functional deficiencies through scintigraphy.
Understand the treatment implications of the findings.

Background: Newborn screening identifies congenital hypothyroidism on the third day of life. Thyroid scintigraphy with technecium-99m pertechnetate helps identify the underlying pathology. To ensure best patient outcome, scintigraphy must not delay the beginning of hormone substitution and can be done up until two days after the beginning of the treatment.

Imaging findings or procedure details: The objective of thyroid scintigraphy in congenital hypothyroidism is to identify the underlying etiology, differentiate between dysgenesis and dyshormonogenesis, and guide appropriate therapeutic interventions. Dysgenesis refers to abnormal thyroid gland development, such as agenesis or ectopic location, while dyshormonogenesis involves impaired hormone synthesis within a structurally normal gland.
By obtaining scintigraphic images, clinicians can ascertain the severity of thyroid dysfunction and underling pathology, allowing personalized treatment plans. The ability to distinguish between dysgenesis and dyshormonogenesis has implications for long-term management, including the duration of hormone replacement therapy.
Additionally, thyroid scintigraphy facilitates the localization of ectopic thyroid tissue, and allows to distinguish athyreosis from lingual thyroid. This information ensures comprehensive care for patients with congenital hypothyroidism.

Conclusion: Thyroid scintigraphy in congenital hypothyroidism is an important diagnostic and therapeutic tool that provides valuable insights into thyroid gland morphology, function, and localization, guiding clinicians in tailoring treatment strategies for improved patient outcomes.

PO89

Pratique avancée en radiologie: la mise en place des Picc-line par le technicien en radiologie médicale (TRM)

M. Tavares, A. Magnin; HFR – Hôpital fribourgeois, Fribourg, Switzerland

Learning objectives: Il s'agit de présenter les étapes, le processus qui a permis de mettre en place une pratique avancée en radiologie plus précisément la mise en place, par les techniciens en radiologie médicale, des cathéters Picc-line.

Background: Nous avons réalisé l'état des lieux de la pratique du service et constaté une marge d'amélioration dans la réalisation de ce geste technique. Suite à de la formation continue et une formation en interne, la délégation du geste technique a pu être implémentée en clinique. L'officialisation de la délégation a permis de certifier les TRM et un processus de qualité permet de garantir la réalisation optimale du geste.

Imaging findings or procedure details: Un bilan organisationnel et qualitatif positif apporté par la délégation de ce geste technique aux TRM a été constaté. Un taux de réussite élevé a permis de démontrer les compétences des TRM dans cette pratique.

Conclusion: Les compétences du TRM sont en constantes évolution dans le paysage médicale actuel. La délégation de la pose de cathéters Picc-Line est une réussite et cela prouve que la formation continue des TRM et leurs compétences leurs permettent de mettre en avant leurs capacités à réaliser des tâches médico-déléguées.

PO90

Noise Reduction in Cerebral CT Images Using Artificial Intelligence Algorithm

F. Mattiussi; EOC – Ente Ospedaliero Cantonale, Lugano, Switzerland

Purpose: The study aims to develop and implement a deep learning algorithm using the Python programming language. The main objective is to reduce noise in cerebral CT images through the use of a specially designed Neural Network. This advanced approach allows for effective separation of the useful signal from unwanted noise, thereby improving the clarity and interpretation of cerebral CT images.

Methods and Materials:
· Collection of a dataset composed of 150 low-quality cerebral CT images (acquired at low dose) and 150 high-quality cerebral CT images (acquired at high dose).
· Image preprocessing, including correct tilt, centering on the anatomical area of interest, and resizing to 400x400 pixels.
· Development of a Deep Neural Network model in Python, trained on each image.
· Validation of the resulting images through the analysis of "Loss", Mean Squared Error (MSE), contrast value, noise via standard deviation, and a student's t-test to assess statistical significance.

Results: The 5-layer convolutional Neural Network model exhibited a final Loss of 450, an average MSE of 163.17, unchanged contrast value (1.0), and an average noise reduction (standard deviation) of 15%. The student's t-test yielded a T-statistic average of 31.48 and a P-value of 0.0009, indicating that the differences in the results obtained are statistically significant.

Conclusion: The detected Mean Squared Error (MSE) of 163.17 signifies a significant reduction in noise in the resulting images, while the unchanged contrast value indicates that the Neural Network does not alter the contrast, the computation of the standard deviation demonstrated the overall reduction in noise. The T-statistic of 31.48 and the low P-value of 0.0009 confirm the effectiveness of the proposed algorithm in noise reduction in cerebral CT images

PO91

Hypnose en Médecine Nucléaire : Un an d'expérience

S. Erismann, P. Leite Ferreira, J. Prior, G. Saliou; CHUV – Centre Hospitalier Universitaire Vaudois, Lausanne, Switzerland

Learning objectives: Réduire l'anxiété générée par les examens en médecine nucléaire et limiter les douleurs des injections, nous avons en 2023 un soutien en hypnose par un TRM, chez les patients demandant un accompagnement.

Methods and Materials: Utilisation de techniques hypnotiques lors de prise en charge des patients en médecine nucléaire, par un TRM étudiant au CAS en Art et technique hypnotiques. Observations directes des patients par le praticien et feedback en fin d'examen. Feedback de l'équipe TRM. Un tableau relevant la traçabilité des prises en charges en hypnose a été établi.

Imaging findings or procedure details: Réalisation de 39 examens avec des techniques hypnotique, dont 1 conclu par un échec nécessitant une sédation pour les images. Notre expérience montre que l'utilisation de l'hypnose lors de la réalisation des images présente plusieurs avantages: (1) réduction de l'anxiété et du stress ressentis. Amélioration du confort des patient et augmentation des chances de réussite; (2) réduction de la douleur associée aux injections et diminution du ressenti négatif des effets secondaires; (3) réalisation de certains examens voués à un échec sur claustrophobie. Meilleure relaxation de patients lors de l'acquisition des images et limitation des mouvements relatifs à un mal-être.

Conclusion: L'hypnose est prometteuse, et améliore l'expérience patient et la qualité des examens des patients. Notre expérience est positive et les feed-back des patients encourageants. L'utilisation de technique hypnotiques permet la réalisation d'images de plusieurs patients pour lesquels nous nous attendions à un échec. Une augmentation des demandes nous pousse à former un deuxième TRM.